

**Faculty of Science and Engineering  
School of Civil and Mechanical Engineering**

**Durability Properties of High Volume Slag and Slag-Fly  
Ash Blended Concrete Containing Nano materials**

**Md Anwar Hosan**

**This thesis is presented for the Degree of  
Doctor of Philosophy  
Of  
Curtin University**

**December 2020**

*Dedicated*

*To my late dad who always inspired me to make a better world*

*&*

*My mom who was always there for me*

*&*

*My wife for her patience and sacrifices during the pregnancy of our  
first child*

# DECLARATION

---

To the best of my knowledge and belief this thesis contains no material previously published by any other person except where due acknowledgement has been made.

This thesis contains no material that has been accepted for the award of any other degree or diploma in any university or institute.

Signature: \_\_\_\_\_

Date: 15/12/2020

# ACKNOWLEDGEMENT

---

Firstly, I would like to express my sincere gratitude to The Almighty Allah for the opportunity of this research and good health without any major injuries of sickness during last three and half years. I am thankful for all this accomplishment of life, knowledge and all the opportunities of my life.

My deep gratitude goes first to Associate Professor Faiz Uddin Ahmed Shaikh, who expertly supervised me through my research. I am appreciative to him for his endless support, dynamic guidance, thoughtful advice, and unwavering enthusiasm for research which helped and kept me constantly engaged with my doctoral program. I am greatly indebted to him for his proper direction and assistance, kind co-operation to finish this doctoral research on time. I have learned a lot throughout this research to face challenges and overcome them.

My endless thanks to both of Professor Abhijit Mukherjee as a chairperson and Associate Professor Prabir Sarkar as co-supervisor for their keen support, precious advice and valuable time whenever I needed in order to improve the research quality and myself to be a better researcher.

I acknowledge the financial support of Australian Government Research Training Program (RTP) Scholarship for this research. I would like to express my thanks toward the Technical Operations co-ordinator Mr Mark Whittaker, Senior Technical Officer Darren Isaac, Technical Officers Mr Kevin Reilly, Mr Ashley Hughes, Mr Leon Forgas, Mr Gary Woodward and all other technical staffs for their assistance and kind support to successfully complete my all expected experimental works on time in the Concrete laboratory at Curtin University. I would like to thank Ms Elaine Miller of Microscopy and Microanalysis Facility, John deLaeter Centre, Curtin University for her training and support during the microstructural and phase identification analysis. I would also like to acknowledge the use of laboratory equipment, materials and technical support of that facility. I would also like to acknowledge the assistance of Dr Arne Bredin and Dr Dipok Sarker during the nano indentation data collection.

I would like to express my eternal appreciation towards my family for their unconditional supports and patience. I am really thankful for their understanding and never ending motivations. I am also thankful to my friends, colleagues and fellow researchers for their kind support during my study and life at Curtin University.

# ABSTRACT

---

Environmental and economic considerations played a great role to develop a sustainable concrete by replacing cement with more sustainable materials such as blast furnace slag (BFS) and fly ash (FA) to produce a greener and sustainable concrete composites. The fractional replacement of Ordinary Portland Cement (OPC) with slag and fly ash improve the engineering properties and performance of concrete. Due to the huge challenges of using BFS and FA or their blended mix with high volume replacement, a small amount of nano silica (NS) and nano calcium carbonate (NC) added to improve those challenges. This study conducted a series of experimental works and analysis to evaluate the optimum content of NS and NC into the high volume slag (HVS) and high volume slag-fly ash blended composites to achieve a sustainable concrete with superior mechanical and durability properties compared to ordinary concrete.

This study was divided in two parts. In first part, an optimum combination of nano materials (NS or NC), BFS and FA along with OPC were determined based on the 28 days compressive strengths of HVS and HVS-FA paste and their microstructural changes. In this part, 1-4% of NS and NC were replaced into 60-90% BFS and BFS-FA blended paste and their 28 days compressive strengths were determined. Based on their compressive strengths, few samples were selected for further microstructural investigations and carbon di-oxide (CO<sub>2</sub>) emission analysis. Results show that the addition of 1-4% NS improves the compressive strength of high volume BFS paste containing 70% slag by about 9-24%. However, at higher BFS contents such as 80% and 90% containing BFS, this improvement is even higher e.g., 11-29% and 17-41%, respectively due to the addition of 1-4% NS. The NS addition also significantly improves the compressive strength of high volume BFS-FA pastes. Similarly, addition of 1-4% NC improved the compressive strengths by 8-24%, 1-16% and 2-20% of HVS pastes containing 70%, 80% and 90%, respectively slag compared to their reference paste without NC inclusion. The compressive strength of HVSFA paste containing combined slag and fly ash content of 70% is also increased significantly by 16-24% than the reference control paste due to addition of 1-4% NC and maintained higher compressive strength than OPC paste after 28 days of curing. The addition of 1% NC reduced the large capillary pores of HVS paste containing 70% slag and addition of 4% and 1% NC reduced the cumulative pore volume of HVS paste with 80% BFS and HVSFA paste containing combined slag and fly ash content of 70% respectively. The addition of NS also significantly reduced the pore volume of high volume BFS and

combined BFS-FA pastes. The thermogravimetric analysis (TGA) results confirm the reduction of calcium hydroxide (CH) in high volume BFS and combined BFS-FA pastes containing both NS and NC indicating the formation of additional calcium silicate hydrate (C-S-H) gels in the system. The X-ray diffraction (XRD) analysis also confirms the reduction of intensity of CH peaks indicating its consumption in pozzolanic reaction. A denser microstructure with fewer internal micro-cracks and more hydrated products are also revealed in scanning electron microscopic (SEM) images and EDS trace analysis in all HVS and HVSFA pastes due to the addition of NS or NC compared to those without nano addition. HVS and HVSFA paste with significantly lower carbon footprint and similar or even higher compressive strength than control cement paste can be achievable with the inclusion of small amount of NS or NC.

Second part of this study evaluated the compressive strengths of HVS and HVS-FA concrete samples after 3, 7, 28, 56, 90, and 180 days of age and durability properties after 28 and 90 days of wet curing due to the addition of optimum content of NS and NC determined in the first part of this study. The results showed that addition of NS improved the early age (3 days) compressive strength of HVS and HVS-FA concretes significantly by 34% and 45%. In addition, the HVS concrete containing 78% BFS (blast furnace slag) gained considerable compressive strengths at later age due to the addition of 2% NS than the control HVS concrete with 80% BFS and showed comparable compressive strengths to OPC concrete. On the other hand, the compressive strengths of HVS-FA concrete containing 67% BFS-FA blend and 3% NS surpassed OPC concrete at 28 days and exhibited superior strengths at later ages than the OPC concrete. Significant reduction in sorptivity of both HVS and HVS-FA concretes is observed at 28 and 91 days due to the addition of NS. It is also found that that the addition of 1% NC improved the compressive strengths of HVS and HVS-FA concretes significantly by 43% and 28%, respectively at 3 days compared to the control HVS and HVS-FA concretes without NC and exceeded the compressive strengths of control OPC concrete at later ages. Superior performance against chloride permeability, chloride diffusion and chloride induced corrosion are also observed in both HVS and HVS-FA concretes due to the addition of both nano materials. Among NS and NC, the concretes containing NC performed much better than the concrete mixes with NS. Significant extension of service life is also observed in both HVS and HVS-FA concretes by the inclusion of both nano materials. Significant reduction in sorptivity of both HVS and HVS-FA concretes is observed at 28 and 91 days due to the addition of NS. Similar substantial reduction of drying shrinkage, chloride ion permeability and volume

of permeable voids are also witnessed in both HVS and HVS-FA concrete due to the inclusion of NS than their respective control concretes without NS and exhibited better performance than control OPC concrete in most occasions. It is also found that 1% NC inclusion reduced the water sorptivity of HVS and HVS-FA concretes reasonably after 28 days of curing and reduction is greater after 90 days of curing exhibited comparable water sorptivity to OPC concrete. Significant improvement is also observed in reducing the volume of permeable voids and controlling the drying shrinkage strain at early age as well as later ages of both HVS and HVS-FA concretes due to 1% NC inclusion. Outstanding resistance against chloride ion penetration is also observed in HVS and HVS-FA concretes due to addition of 1% NC. It is also investigated that the addition of NC and NS improved the modulus and hardness of hydration products in the ITZ area of matrix of HVS and HVS-FA concretes. The thickness of ITZ is also reduced in those concretes due to addition of NS and NC. SEM and EDS analysis also confirm the above observation where dense microstructure with less voids and micro cracks and higher peaks of Ca, Si and Al were observed. The observed improvement of 28 days compressive strengths of the HVS and HVS-FA concretes due to addition of NC and NS also correlated well with the improvement of microstructures of ITZ area.

Overall, using a small amount of NS or NC into the HVS and HVS-FA composites was found very favourable to overcome the challenges of replacing OPC with high volume by BFS and FA and hence, produce a sustainable environment friendly green concrete.

# LIST OF PUBLICATIONS

---

## Journals:

1. Shaikh, F.U.A. and A. Hosan, Effect of nano silica on compressive strength and microstructures of high volume blast furnace slag and high volume blast furnace slag-fly ash blended pastes. *Sustainable Materials and Technologies*, 2019. **20**: p. e00111.
2. Hosan, A. and F.U.A. Shaikh, Influence of nano-CaCO<sub>3</sub> addition on the compressive strength and microstructure of high volume slag and high volume slag-fly ash blended pastes. *Journal of Building Engineering*, 2020. **27**: p. 100929.
3. Hosan, A., Shaikh, F.U.A., Sarker, P. and Aslani, F., Nano- and micro-scale characterisation of interfacial transition zone (ITZ) of high volume slag and slag-fly ash blended concretes containing nano SiO<sub>2</sub> and nano CaCO<sub>3</sub>. *Construction and Building Materials*, 2020: p. 121311.
4. Hosan, A. and F.U.A. Shaikh, Influence of nano silica on compressive strength, durability, and microstructure of high-volume slag and high-volume slag-fly ash blended concretes. *Structural Concrete*. <https://doi.org/10.1002/suco.202000251>.
5. Hosan, A. and F.U.A. Shaikh, Compressive strength development and durability properties of high volume slag and slag-fly ash blended concretes containing nano-CaCO<sub>3</sub>. *Journal of Materials Research and Technology*. <https://doi.org/10.1016/j.jmrt.2021.01.001>
6. Hosan, A. and F.U.A. Shaikh, Effect of nano materials on chloride induced corrosion and service life of high volume slag and high volume slag-fly ash blended concretes. *Journal of Materials in Civil Engineering*. (Under review).

## Conferences:

1. Shaikh, F. U. A., & Hosan, A. (2019). High Volume Slag and Slag-Fly Ash Blended Cement Pastes Containing Nano Silica. *Materials Science Forum*, 967, 205–213. <https://doi.org/10.4028/www.scientific.net/msf.967.205>
2. Hosan, A. and F.U.A. Shaikh (2019). Durability properties and compressive strength of high volume slag and high volume slag-fly ash blended concretes containing nano silica. In proceedings of International conference on “Durable Concrete for Infrastructure under Severe Conditions – smart admixtures, self-responsiveness and nano-additions. Held on 10-11 September 2019, Ghent University, Belgium.



# TABLE OF CONTENTS

---

	Page
DECLARATION	iii
ACKNOWLEDGEMENT	iv
ABSTRACT	v
LIST OF PUBLICATION	viii
TABLE OF CONTENTS	ix
LIST OF FIGURES	xvii
LIST OF TABLES	xxii
ABBREVIATIONS	xxiii
LIST OF NOTATIONS	xxv

## **PART I: INTRODUCTION AND LITERATURE REVIEW**

<b>Chapter 1: Introduction</b>	1
1.1 Background	1
1.2 Research significance	5
1.3 Research objectives	6
1.4 Research approach	6
1.5 Thesis structure	7
1.6 References	8
<b>Chapter 2: Literature Review</b>	12
2.1 Nano Technology	12
2.2 Nano materials and cementitious materials	13
2.3 Effect of nano materials on high volume fly ash (HVFA) composites	14
2.3.1 Hydration properties	14

2.3.2 Fresh properties	16
2.3.3 Mechanical properties	17
2.3.4 Durability properties	21
2.3.5 Microstructural properties	23
2.4 Effect of nano materials on high volume slag (HVS) composites	26
2.4.1 Hydration properties	26
2.4.2 Fresh properties	27
2.4.3 Mechanical properties	27
2.4.4 Durability properties	29
2.4.5 Microstructural properties	31
2.5 Effect of nano materials on high volume slag-fly (HVS-FA) composites	32
2.6 Limitations and scopes	33
2.7 References	34

## **PART II: MECHANICAL AND MICROSTRUCTURAL PROPERTIES**

### **Chapter 3: High volume slag and high volume slag-fly ash blended paste containing nano silica**

3.1 Overview	40
3.2 Experimental program	42
3.3 Materials, mix proportions and casting	42
3.4 Testing methods	45
3.5 Results and Discussion	48
3.5.1 Compressive strengths	48
3.5.1.1 Effects of high volume blast furnace slag and high volume blast furnace slag-fly ash	48

3.5.1.2 Effect of nano silica in high volume blast furnace slag and high volume blast furnace slag-fly ash	49
3.5.2 Microstructure	51
3.5.2.1 Mercury intrusion porosimetry (MIP)	52
3.5.2.2 Thermogravimetric (TGA) analysis	55
3.5.2.3 X-ray diffraction (XRD) analysis	57
3.5.2.4 Scanning electron microscopy (SEM) and energy dispersive X-ray spectroscopy (EDS) analysis	59
3.5.3 CO <sub>2</sub> emission analysis	62
3.6 Summary	64
3.7 References	66
<b>Chapter 4: High volume slag and high volume slag-fly ash blended paste containing nano calcium carbonate</b>	<b>68</b>
4.1 Overview	68
4.2 Experimental details	70
4.3 Materials	71
4.4 Mix proportions	73
4.5 Specimen preparation and curing	74
4.6 Testing methods	75
4.7 Results and discussion	77
4.7.1 Compressive strength development	77
4.7.1.1 Effect of high volume slag and high volume slag-fly ash blend	77
4.7.1.2 Effect of nano-CaCO <sub>3</sub>	78
4.7.2 Microstructure	79
4.7.2.1 Mercury intrusion porosimetry (MIP)	81
4.7.2.2 Thermogravimetric analysis (TGA)	83
4.7.2.3 X-ray diffraction (XRD) analysis	84

4.7.2.4 Scanning electron microscopy (SEM) and energy dispersive X-ray spectroscopy (EDS) analysis	86
4.7.3 CO <sub>2</sub> emission analysis	91
4.8 Summary	93
4.9 References	95
<b>Chapter 5: Nano characterisation of ITZ of HVS and HVS-FA concretes containing nano silica and nano calcium carbonate</b>	<b>97</b>
5.1 Overview	97
5.2 Experimental program	99
5.2.1 Materials	99
5.2.2 Mix design and sample preparation	100
5.2.3 Experimental methods	102
5.2.3.1 Nano indentation test	102
5.2.3.2 Scanning electron microscopy (SEM) and energy dispersive X-ray spectroscopy (EDS)	105
5.2.3.3 Compressive strength	106
5.3 Results and discussions	106
5.3.1 Interfacial transition zone (ITZ) based on nanoindentation	106
5.3.1.1 Effect of nano calcium carbonate on ITZ	108
5.3.1.2 Effect of nano silica on ITZ	109
5.3.2 ITZ based on SEM and EDS analysis	115
5.4 Summary	121
5.5 References	122

## **PART III: DURABILITY PROPERTIES**

### **Chapter 6: Mechanical and durability properties of HVS and HVS-FA concretes containing nano silica** 125

6.1 Overview	125
6.2 Experimental procedure	127
6.2.1 Materials	127
6.2.2 Concrete mix design	128
6.2.3 Casting concrete specimens	129
6.2.4 Testing procedure	130
6.2.4.1 Compressive strengths	130
6.2.4.2 Sorptivity test	130
6.2.4.3 Drying shrinkage	130
6.2.4.4 Volume of permeable voids (VPV)	130
6.2.4.5 Rapid chloride permeability test (RCPT)	131
6.2.4.6 Scanning electron microscope (SEM) and energy-dispersive X-ray spectroscopy (EDS)	131
6.3 Results and Discussions	133
6.3.1 Compressive strengths	133
6.3.2 Water sorptivity	135
6.3.3 Drying shrinkage	136
6.3.4 Volume of permeable voids (VPV)	138
6.3.5 Rapid chloride permeability test (RCPT)	139
6.3.6 Microstructural modification through SEM images and EDS spectrum	142
6.4 Summary	143
6.5 References	145

**Chapter 7: Mechanical and durability properties of HVS and HVS-FA concretes containing nano calcium carbonate** 147

7.1 Overview	147
7.2 Outline of the Experiments	149
7.2.1 Materials	149
7.2.2 Mix proportions	150
7.2.3 Sample preparation	150
7.2.4 Testing methods	151
7.3 Results and discussions	154
7.3.1 Compressive strengths	154
7.3.2 Durability properties	158
7.3.3 Microstructural modifications	162
7.4 Summary	165
7.5 References	167

**Chapter 8: Chloride induced corrosion and chloride diffusion of HVS and HVS-FA concretes containing nano silica and nano calcium carbonate** 171

8.1 Overview	171
8.2 Experimental program	174
8.2.1 Materials	174
8.2.2 Mix design and sample preparation	174
8.2.3 Experimental methods	176
8.2.3.1 Compressive strengths	176
8.2.3.2 Accelerated chloride induced corrosion	179
8.2.3.3 Chloride diffusion	180
8.2.3.4 Service life assessment	180
8.3 Results and discussions	183

8.3.1 Compressive strengths	183
8.3.1.1 Effect of nano calcium carbonate	183
8.3.1.2 Effect of nano silica	184
8.3.1.3 Comparison of concretes with nano materials	184
8.3.2 Chloride induced corrosion	187
8.3.2.1 Effect of nano calcium carbonate	187
8.3.2.2 Effect of nano silica	190
8.3.2.3 Performance against corrosion of concretes containing nano materials	192
8.3.2.4 Visual observations	193
8.3.2.4.1 Corrosion induced cracking	193
8.3.2.4.2 Chloride penetration depth and cracks width	195
8.3.2.4.3 Corrosion of reinforcement	196
8.3.3 Chloride diffusion	199
8.3.3.1 Effect of nano calcium carbonate	199
8.3.3.2 Effect of nano silica	201
8.3.3.3 Comparison of concretes containing nano materials	201
8.3.4 Service Life	202
8.3.4.1 Influence of nano calcium carbonate	202
8.3.4.2 Influence of nano silica	204
8.3.4.3 Influence comparison between nano materials	204
8.4 Summary	205
8.5 References	207

## **PART IV: CONCLUSIONS AND RECOMMENDATIONS**

<b>Chapter 9: Research findings and future recommendations</b>	211
9.1 Review of the study	211
9.2 Main research findings	211
9.2.1 Effect of nano materials on HVS and HVS-FA paste	211
9.2.2 Effect of nano materials on durability properties and compressive strength development of HVS and HVS-FA concretes	213
9.3 Recommendations for future study	215
<b>APPENDICES</b>	217
<b>APPENDIX A: Experimental images</b>	218
<b>APPENDIX B: Test results analysis</b>	223
<b>APPENDIX C: Attribution of research outputs</b>	260
<b>APPENDIX D: Copyright permission</b>	262



# LIST OF FIGURES

---

- 2.1** Particle size and specific surface area related to concrete materials
- 2.2** Effects of 2% NS on compressive strength of mortars containing HVFA
- 2.3** Effects of 2% NS on compressive strength of HVFA concretes containing 40% and 60% fly ash
- 2.4** Backscattered electron (BSE) images of polished surface of paste samples
- 2.5** SEM images of 50% FA containing paste with and without NS addition
- 2.6** Effect of the nano-silica dosage on the compressive strength development of mortars
- 2.7** Typical micro-structural characteristics of reference concrete with 50% slag
- 2.8** Typical micro-structural characteristics of 2% NS added slag concrete
- 3.1** XRD analysis of class F fly ash and blast furnace slag
- 3.2** XRD analysis of nano silica
- 3.3** Ultrasonic mixing of nano silica in water containing superplasticizer
- 3.4** Compressive strength of high volume BFS pastes and combined BFS-FA pastes measured at 28 days
- 3.5** Effect of various nano silica contents on compressive strength of high volume BFS pastes and combined high volume BFS-FA pastes measured at 28 days
- 3.6** Cumulative pore volume and distribution of pore sizes of high volume BFS pastes and combined BFS-FA pastes measured at 28 days
- 3.7** Cumulative pore volume and distribution of pore sizes of high volume BFS pastes and combined BFS-FA pastes containing nano silica measured at 28 days
- 3.8** (a) Mass loss and (b) calculated calcium hydroxide of high volume BFS pastes and combined BFS-FA pastes with and without nano silica
- 3.9** XRD patterns of (a) high volume BFS pastes and combined BFS-FA pastes and (b) those containing nano silica
- 3.10** Backscattered scanning electron microscopic (SEM) images and EDS spectra of HVS and HVSFA pastes with and without nano silica

- 3.11** CO<sub>2</sub> emission analysis of HVS and HVSFA pastes with and without nano silica
- 4.1** XRD analysis of Cement, Blast furnace slag and fly ash
- 4.2** XRD analysis of nano calcium carbonate
- 4.3** Ultrasonic mixing of nano calcium carbonate
- 4.4** Effect of high volume slag and slag-fly ash blend mixes on the compressive strengths of cement paste at 28 days of age
- 4.5** Effect of Nano calcium carbonate on the compressive strengths of high volume slag and slag-fly ash blended paste at 28 days of age
- 4.6** Effect of nano-CaCO<sub>3</sub> on the a) cumulative pore volume and b) pore size distribution of HVS and HVSFA pastes
- 4.7** TGA analysis a) High volume slag and High volume slag-fly ash blended pastes with and without nano-CaCO<sub>3</sub> and b) Ca(OH)<sub>2</sub> contents
- 4.8** XRD patterns of a) HVS and HVSFA paste b) HVS and HVSFA paste containing nano-CaCO<sub>3</sub>
- 4.9** Backscattered electron images of a) OPC b) 70BFS c) 69BFS1NC d) 80BFS e) 76BFS4NC f) 49BFS21FA g) 49BFS20FA1NC pastes at lower magnification
- 4.10** Backscattered electron images and EDS spectra of different HVS and HVSFA pastes with and without NC
- 4.11** CO<sub>2</sub> emission and CO<sub>2</sub> intensity indicator analysis of HVS and HVSFA pastes with and without nano-CaCO<sub>3</sub>
- 5.1** Nanoindentation test setup in Agilent Nano Indenter G200
- 5.2** (a) Typical indent area and (b) Indent plan (total 9x12=108 indents)
- 5.3** Nano indentation principle (a) a typical load-displacement curve (b) a typical indenter with three-sided pyramidal diamond
- 5.4** Typical load-depth diagram of different zones in concrete
- 5.5** (a) Modulus distribution (b) hardness distribution and contour map of (c) indentation modulus (d) hardness distribution in ITZ of OPC concrete mix
- 5.6** (a) Modulus distribution (b) hardness distribution and contour map of (c) indentation modulus (d) hardness distribution in ITZ of 70BFS concrete mix

- 5.7** (a) Modulus distribution (b) hardness distribution and contour map of (c) indentation modulus (d) hardness distribution in ITZ of 69BFS.1NC concrete mix
- 5.8** (a) Modulus distribution (b) hardness distribution and contour map of (c) indentation modulus (d) hardness distribution in ITZ of 70BFS-FA concrete mix
- 5.9** (a) Modulus distribution (b) hardness distribution and contour map of (c) indentation modulus (d) hardness distribution in ITZ of 69BFS-FA.1NC concrete mix
- 5.10** (a) Modulus distribution (b) hardness distribution and contour map of (c) indentation modulus (d) hardness distribution in ITZ of 80BFS concrete mix.
- 5.11** (a) Modulus distribution (b) hardness distribution and contour map of (c) indentation modulus (d) hardness distribution in ITZ of 78BFS.2NS concrete mix.
- 5.12** (a) Modulus distribution (b) hardness distribution and contour map of (c) indentation modulus (d) hardness distribution in ITZ of 67BFS-FA.3NS concrete mix.
- 5.13** SEM images of different concrete mixes after 28 days of curing with and without nano materials addition
- 5.14** EDS spectras of different concrete mixes containing (a) NC and (b) NS
- 5.15** Compressive strength of HVS and HVS-FA concretes containing NS and NC
- 6.1** Compressive strengths of different HVS and HVS-FA mixes with and without NS
- 6.2** Gaining of compressive strengths of HVS and HVS-FA concrete due to the addition of NS
- 6.3** Water absorption of different concrete mixes with and without NS at a) 28 days b) 90 days
- 6.4** Sorptivity of different concrete mixes with and without NS after 28 days and 90 days
- 6.5** Shrinkage strain of different concrete mixes with and without NS at different age of concrete
- 6.6** Average volume of permeable voids of concrete mixes with and without NS
- 6.7** Average charge passed through concrete mixes with and without NS after 28 and 90 days of curing
- 6.8** Improvement of different properties of concrete samples containing NS
- 6.9a-f** BSE images and comparison of EDS traces at ITZ of different concrete mixes with and without nano-SiO<sub>2</sub> after 28 days of curing

- 7.1** Average compressive strengths of different types concretes with and without NC at various ages of concrete
- 7.2** Benchmarking of compressive strength of HVS and HVS-FA concretes with control OPC concrete
- 7.3** Improvement of compressive strengths of HVS and HVS-FA concretes containing 1% NC
- 7.4** Water absorption of different type concrete with and without NC at a) 28 and b) 90 days of age
- 7.5** Sorptivity of different concrete mixes at 28 and 90 days
- 7.6** Average volume of permeable voids of concrete mixes with and without NC at 28 and 90 days
- 7.7** Chloride ion penetration of different concretes with and without NC at 28 and 90 days
- 7.8** Improvement comparison of different properties due to NC addition
- 7.9** Drying shrinkage strain of control OPC, HVS and HVS-FA with and without NC at various ages of concrete mixes
- 7.10** SEM images and EDS spectrum of different concrete mixes with and without nano-CaCO<sub>3</sub> addition after 28 days of curing
- 8.1** Slump test of a concrete mix
- 8.2** Chloride induced accelerated corrosion test of concrete mixes (a) test setup (b) applied voltage (c) typical data collection (d) schematic diagram
- 8.3** Average compressive strengths of different concrete mixes at various ages with and without nano materials
- 8.4** Corrosion rate and concrete resistivity of OPC, HVS and HVS-FA concrete with and without nano-CaCO<sub>3</sub> addition
- 8.5** Corrosion rate and concrete resistivity of different concrete mixes with and without nano-SiO<sub>2</sub>
- 8.6** Comparison of corrosion rates of HVS and HVS-FA concrete mixes with nano materials
- 8.7** Comparison of concrete resistivity of OPC, HVS and HVS-FA concrete with nano materials
- 8.8** Concrete samples after (a) 26 weeks and (b) 52 weeks of accelerated corrosion test

**8.9** Chloride penetration of OPC, HVS and HVS-FA concrete mixes with and without nano materials addition

**8.10** Deterioration of rebars of control OPC concrete and HVS and HVS-FA concrete with and without (a) nano-CaCO<sub>3</sub> (b) nano-SiO<sub>2</sub> inclusion

**8.11** (a) Acid soluble chloride content and (b) chloride diffusion coefficient of control OPC and HVS, HVS-FA concrete with and without nano-CaCO<sub>3</sub> inclusion

**8.12** (a) Acid soluble chloride content and (b) chloride diffusion coefficient of different concrete mixes with and without nano-SiO<sub>2</sub> addition

**8.13** Comparison of chloride diffusion coefficient of control OPC and HVS, HVS-FA concretes containing nano-CaCO<sub>3</sub> and nano-SiO<sub>2</sub>

**8.14** Estimated service life span of different concrete mixtures with and without nano-CaCO<sub>3</sub> when (a) C<sub>t</sub> = 0.05% (b) C<sub>t</sub> = 0.1%

**8.15** Estimated service life span of different concrete mixtures with and without nano-SiO<sub>2</sub> when (a) C<sub>t</sub> = 0.05% (b) C<sub>t</sub> = 0.1%

**8.16** Comparison of service life span of different concrete mixtures with the addition of nano-CaCO<sub>3</sub> and nano-SiO<sub>2</sub> along with control OPC concrete when (a) C<sub>t</sub> = 0.05% (b) C<sub>t</sub> = 0.1%

# LIST OF TABLES

---

- 3.1** Chemical analysis and physical properties of OPC, fly ash, blast furnace slag and nano silica
- 3.2** Mix proportions of high volume slag and high volume slag-fly ash blend cement pastes
- 3.3** Mix proportions of high volume slag and high volume slag-fly ash blend cement pastes containing nano silica
- 4.1** Physical properties and chemical compositions of Ordinary Portland Cement (OPC), Blast Furnace Slag (BFS), Class F Fly Ash (FA) and Nano-Calcium Carbonate (NC)
- 4.2** Mix proportions of cement paste containing high volume blast furnace slag (BFS) and slag-fly ash blend
- 4.3** Mix proportions of high volume slag and slag-fly ash blended cement pastes incorporation of nano-calcium carbonate (NC)
- 5.1** Physical properties and chemical compositions of Ordinary Portland Cement (OPC), Blast Furnace Slag (BFS), Class F Fly Ash (FA), Nano Calcium Carbonate (NC) and Nano Silica (NS)
- 5.2** Mixing proportions of concretes ( $\text{Kg/m}^3$ ) and measured slump
- 5.3** Modulus, hardness and length of ITZ of different concrete mixes with and without nano materials
- 6.1** Mixing proportions of different concrete mixes ( $\text{Kg/m}^3$ ) and measured slump
- 7.1** Mixing proportions of different concrete mixes ( $\text{Kg/m}^3$ )
- 8.1** Mass loss of rebar of different concrete mixes after 52 weeks of accelerated corrosion test
- 8.2** Chloride diffusion coefficient and service life of different concrete mixes

# ABBREVIATIONS

---

AgNO <sub>3</sub>	Silver Nitrate
AS	Australian Standards
ASTM	American Society of Testing Materials
BFS	Blast Furnace Slag
BFS-FA	Blast Furnace Slag-Fly Ash
BSE	Backscattered Electron
C <sub>3</sub> A	Tricalcium Aluminate
C <sub>3</sub> S	Tricalcium Silicate
CAH	Calcium Aluminate Hydrate
CH	Calcium Hydroxide
CNB	Colloidal Nano Boehmite
CNF	Carbon Nano Fibre
CNS	Colloidal Nano Silica
CNT	Carbon Nano Tube
CO <sub>2</sub>	Carbon Dioxide
CSH	Calcium Silicate Hydrate
EDS	Energy-dispersive X-ray Spectroscopy
FA	Fly Ash
GGBFS	Ground Granulated Blast Furnace Slag
GPa	Giga Pascal
HVFA	High Volume Fly Ash
HVFA-HL	High Volume Fly Ash-Hydrated Lime
HVS	High Volume Slag

HVS-FA	High Volume Slag Fly Ash
ITZ	Interfacial Transition Zone
MIP	Mercury Intrusion Porosimetry
MPa	Mega Pascal
NA	Nano Alumina
NaCl	Sodium Chloride
NC	Nano Calcium Carbonate
NS	Nano Silica
NT	Nano Titanium
OPC	Ordinary Portland Cement
RCPT	Rapid Chloride Permeable Test
SCC	Self-compacting Concrete
SCM	Supplementary Cementitious Materials
SD	Standard Deviation
SEM	Scanning Electron Microscope
SF	Silica Fume
SP	Super Plasticizer
SSD	Saturated Surface Dry
TGA	Thermogravimetric Analysis
VPV	Volume of Permeable Voids
XRD	X-ray Diffraction



# LIST OF NOTATIONS

---

- $A_c$  = contact area of indenter at maximum load
- $C(x, t)$  = the chloride concentration at a depth  $x$  and exposure time  $t$  (mass %)
- $C_i$  = initial chloride concentration of the concrete prior to the submersion in the exposure liquid (mass %)
- $C_s$  = the chloride concentration at the surface of the samples (mass %)
- $D$  = diameter of the rebar (cm)
- $d$  = the pore diameter ( $\mu\text{m}$ )
- $D_{28}$  = chloride diffusion coefficient at 28 days ( $\text{m}^2/\text{s}$ )
- $D_{28}$  = the early age chloride diffusion coefficient calculated by using Fick's second law
- $D_a$  = the chloride diffusion coefficient ( $\text{m}^2/\text{s}$ )
- $D_t$  = chloride diffusion coefficient ( $\text{m}^2/\text{s}$ ) at time  $t$  (days)
- $D_{ult}$  = ultimate chloride diffusion coefficient ( $\text{m}^2/\text{s}$ )
- $E$  = indentation modulus, GPa
- $E_r$  = reduced modulus
- $erf$  = the error function
- FA = percentage of fly ash
- $h$  = indentation depth (nm)
- $H$  = hardness, GPa
- $L$  = length of the rebar sample (cm)
- $m$  = diffusion decay constant
- $M_{ac}$  = actual mass of rust per unit surface area of the bar ( $\text{g}/\text{cm}^2$ ),
- $MW_{\text{H}_2\text{O}}$  = the molecular weight of  $\text{H}_2\text{O}$

- $P$  = the net pressure across the mercury meniscus at the time of the cumulative intrusion measurement (MPa)
- $P_{max}$  = maximum load during indentation (mN)
- $S$  = stiffness of the unloading curve
- SG = percentage of slag of the total cementitious materials in the mix
- $t$  = the exposure time (seconds).
- $W_f$  = weight after corrosion (g) for a given duration of induced corrosion (T)
- $W_i$  = initial weight of the bar before corrosion (g)
- $WL_{CH}$  = the weight loss during the dehydration of CH as percentage of the ignited weight (%)
- $MW_{CH}$  = the molecular weight of CH
- $x$  = depth below the exposure surface (m)
- $\theta$  = the contact angle between mercury and the pore wall ( $^{\circ}$ )
- $\gamma$  = the surface tension (mN/m)
- $\nu$  = Poisson's ratio of specimen

# Chapter 1: Introduction

---

## 1.1 Background

Rapid urbanisation due to increase in population caused the demand of concrete production in last few decades. Ordinary Portland cement (OPC) is used as the binding material of concrete which is extremely energy intensive and every single tonne of OPC manufacture releases roughly one tonne of carbon dioxide (CO<sub>2</sub>) into the atmosphere during the calcination process (Malhotra, 2002; Mehta, 2001). Another study reported that only cement production contributes approximately 7% of global carbon dioxide emission per year which has a crucial effect on global warming (Tharakan et al., 2013). In response to global warming, the use of several industrial waste materials, commonly known as supplementary cementitious materials (SCM), such as ground granulated blast furnace slag (GGBFS), fly ash (FA), silica fume (SF), metakaolin etc. as partial replacement of OPC in the concrete to produce an eco-friendly concrete is used in the construction industry. Among various SCM, blast furnace slag (BFS) is a by-product of the steel production process, which has been widely used in concrete for several years to substitute the OPC in concrete to further enhance the workability, mechanical and durability properties and the reduction of carbon footprint (Hooton, 2000). However, the BFS replacement typically lies between 30-60% by the mass of the cement even though there is a strong demand for the higher volume of BFS replacement from the perspective of CO<sub>2</sub> reduction but is rarely used due to the challenges of low early strength, noteworthy autogenous and/or drying shrinkage, large scale of bleeding, and tendency for carbonation (Duran & Bilim, 2007; Güneyisi & Gesoğlu, 2008; Oner & Akyuz, 2007). Commercially available blast-furnace cement class B which is commonly used in the construction industry contains only 40% BFS powder as partial replacement of OPC and high volume (>50%) BFS concrete is usually used in severe condition such as marine environment and water with high sulphate contents mentioned in different studies. Several studies have investigated the use of high volume slag (HVS) as the partial replacement of OPC in concretes.

Duran and Bilim (2007) investigated the compressive strengths of concretes containing BFS under dry and wet curing conditions. It is concluded that compressive strength of wet cured concretes containing 20% and 40% BFS as partial replacement of OPC was higher than the control concrete at 28 days. However, the compressive strengths of 80% BFS containing concrete was found satisfactory compared to OPC concrete for wet curing

conditions. On the other hand, the compressive strengths of dry cured concretes containing 20% and 40% BFS as partial replacement of OPC were equivalent of control and satisfactory at 60% replacement level while the compressive strength at 80% replacement level was much lower than the control at 28 days and after three months. Similarly, Güneyisi and Gesoğlu (2008) found that there is a systematic decrease of compressive and splitting tensile strengths with the increase in slag content and is more pronounced with the air curing conditions especially for the early age. However, the strengths are increased with OPC replacement by slag up to 60% for 90 days wet cured specimens. The results also reflected the outcome by Bilim et al. (2009) while an artificial neural network (ANN) study was implemented to predict the compressive strengths of BFS concrete.

Oner and Akyuz (2007) examined the optimum level usage of BFS for the compressive strength and observed that early ages strengths of BFS concrete were lowered than the control mixes. However, the strengths are increased with the curing periods and exceeded the control after one year of curing and compressive strengths were maximum when BFS addition was around 55% of total binder content. Similarly, Wainwright and Rey (2000) had performed the bleed tests and demonstrated that the 55% slag addition amplified the bleed capacity by 30% with compared to plain OPC concrete but had a slight influence on the bleed rate. Hashimoto et al. (2016) also found that the compressive strength, carbonation resistance, setting time, durability and surface layer air permeability coefficients with water-binder ratio of 0.5 are equivalent to those of concrete using commercial blast furnace cement type B (containing 40% BFS) with water binder ratio of 0.55. Surprisingly, Elchalakani et al. (2014) concluded that a mix with 80% BFS and 20% OPC can make an economical concrete with low carbon foot print with compressive strength about 36 MPa at 3 days and about 68 MPa at 28 days and also meet the durability, setting times, water absorption and workability requirements of a sustainable concrete.

Hill and Sharp (2002) concluded that sound cement paste can be obtained with 90% BFS, though the compressive strengths of pastes samples were reduced contrasting to the study by Aghaeipour & Madhkhan (2017) which showed that concrete containing 40% slag reduced porosity, lowered water absorption, and concrete permeability while mix designs containing 60% slag led to enhanced penetration depth thus less water absorbed. While it is demonstrated that the total porosity is increased with the increasing content of BFS in the specimens at early ages, whereas porosity is decreased at later ages (Choi et al., 2017). They also found that the initial and final setting times are increased with the BFS contents.

Furthermore, it is found that the smaller grain size of slag produced higher compressive strengths than the samples without slag and finer particle size slag exhibits positive behaviour against the sulphate attack (López et al., 2015).

A number of studies have also been conducted to study different mechanical and durability properties of mortar and concretes prepared with blended mix of high volume slags, fly ash, silica fume and limestone filler. A combination of 40% OPC, 40% BFS and 20% FA (4:4:2) have been broadly used for concrete construction in South Korea and Jeong et al. (2015) demonstrated that concrete containing 30% OPC, 50% BFS, 20% FA exhibits adequate mechanical properties and presented superior performance of 14% lower adiabatic temperature increase. In addition, Demirboga et al. (2004) found that the compressive strength and ultrasonic pulse velocity (UPV) of concretes containing 25% BFS+25% FA, 30% BFS+30% FA and 35% BFS+35% FA were very low for all mixes at early ages especially for the samples with FA and increase at the later ages for all mixes. Gesoğlu and Özbay (2007) reported that the compressive strength and electrical resistivity of the concretes with BFS and SF were much higher than control and ternary blends of BFS (45%) and SF (15%) had as high as 87 MPa compressive strength at the age of 28 days. Kuder et al. (2012) studied the early and long-term compressive strength, elastic modulus and creep behaviour of high volumes of fly ash and slag concrete replacing 60-90% of the OPC in the control mix and noted that the early age strengths were lower than the control in all mixes as expected. Moreover, El-Chabib and Syed (2013) found that the addition of 10% SF in ternary and quaternary mixes of BFS and FA increased the compressive strength but lowered the workability significantly. In another study, Alonso et al. (2012) concluded that the ternary mix of blast furnace slag, fly ash and limestone filler showed better compressive strength than other binary mixes and use of appropriate contents of mineral components will allow binders to fulfil the expected mechanical requirements.

Nowadays, a very few studies have conducted relating to the influence of nano silica (NS) and nano calcium carbonate (NC) on the mechanical properties, durability properties and microstructure of high volume slag (HVS) and high volume fly ash (HVFA) composites. For instance, Zhang et al. (2012) studied the use of NS to reduce the setting time and increase the early strength of concrete with high volume of slag (HVS) and found that addition of 2% NS increased the compressive strength of HVS concrete by 22% and 18% at 3 and 7 days, respectively and reduced initial and final setting times by 95 and 105

minutes compared to the reference concrete of 50% slag with no NS. The hydration rate of cement and slag were accelerated and span of dormant phase was shortened due to the addition of NS and also densified the paste-aggregate interface compared to the control concrete without NS. In another study, Liu et al. (2016) evaluated the interaction between nano silica and blast furnace slag where 3% NS is added into cement along with 10%, 20%, 30% and 40% dosage of BFS. It is summarized that the compressive strength of the mortar specimens increased by 21.71%, 17.17% and 10.67% at 3, 7 and 28 days respectively compared to the mortar without NS inclusion and the highest compressive strength (59.42 MPa) was found with 30% BFS and 3% NS. The degree of heat generation was increased with the addition of NS and induction period was shortened. Similarly, Nazari and Riahi (2011) also reported that the addition of up to 3% NS increased the split tensile strength of concrete specimens as a result of formation of crystalline  $\text{Ca}(\text{OH})_2$  amount in the early age of hydration while examined the splitting tensile strength of concrete using 45% BFS as the replacement of cement. It is also noted that any further increase of NS dosage caused the reduction of splitting tensile strength.

On the other hand, Sato and Beaudoin (2011) concluded that the addition of nano- $\text{CaCO}_3$  (NC) as the replacement of cement accelerated the hydration of OPC and the acceleration was greater with the higher amount of NC when added with 50% slag or 50% FA containing paste. It is also found that the microhardness and modulus of elasticity at early age of hydration products were significantly improved and increased with increasing content of NC. Furthermore, 5% addition of NC significantly reduced the initial and final setting times of pastes samples containing 50% FA compared to OPC paste and exhibited the same setting times when sonication process was applied for the mixing of NC (Kawashima & Shah, 2013). It is reported that 1% replacement of FA by NC in a concrete containing 40% FA improved the compressive strengths by 46% and 54% at 3 days and 28 days, respectively compared to control concrete containing 40% FA only. However, no such great improvement is noticed in the compressive strengths of concrete containing 59% FA and 1% NC (Shaikh & Supit, 2014). This study also reported significant improvement of durability properties due to inclusion of 1% NC in HVFA concretes.

In a very recent study, It is showed that the inclusion of NS into high volume fly ash-hydrated lime blended (HVFA-HL) paste can serve as nucleation sites, hence, increased the early age hydration and resulted to a considerably higher peak of heat flow curve compared to HVFA-HL paste without NS (Gunasekara et al., 2020). It is also concluded that 3% NS inclusion in to

HVFA-HL pastes containing 65% and 80% FA and HL achieved about 50% and 98.6% of 7 days compressive strengths and about 10.3% and 35.9% of 28 days compressive strength of control pastes without NS inclusion.

## **1.2 Research significance**

In numerous researches discussed above, different types of nano materials have been used to enhance the early age strength and reduce the setting time of high volume slag (HVS) and high volume fly ash (HVFA) concretes. Though there is sufficient evidence that nano materials such as nano silica (NS) and nano  $\text{CaCO}_3$  (NC) enhanced the strength of concrete especially in the early age and improve other properties by densifying the pores in the concrete, the study of using nano materials with the high volume slag (60-90%) as partial replacement of OPC in concrete is still lacking. Moreover, the effect of using two or more supplementary cementitious materials such as high volume slag-fly ash blend (HVS-FA) containing nano materials was also not investigated. Despite the fact of using NS and NC to improve the early strengths of HVS and HVFA concrete, no durability properties such as, drying shrinkage, sorptivity, volume of permeable voids (VPV), rapid chloride penetration test (RCPT), chloride induced corrosion, chloride diffusion etc. of HVS and HVS-FA have yet investigated. Therefore, it would be highly beneficial to investigate the effects of addition of NS and NC on the early age compressive strength as well as later ages compressive strength development and durability properties of HVS and HVS-FA concretes. This research aimed to investigate the compressive strengths and durability properties of high volume slag (HVS) concrete and high volume slag-fly ash blended (HVS-FA) concrete incorporating NS and NC. Microstructural investigation and slag reactivity through scanning electron microscope (SEM), x-ray diffraction (XRD), mercury intrusion porosimetry (MIP), thermogravimetric (TGA) analysis, nano indentation etc. of HVS and HVS-FA composites were also aimed to be investigated in this study.

The outcome of this study will definitely help to provide a clear understanding of using nano materials on the high volume slag (HVS) and high volume slag-fly ash (HVS-FA) concretes to improve their durability properties and compressive strength development consequently to produce a highly beneficial and economic HVS and HVS-FA concretes. The development of HVS and HVS-FA concretes will also be useful to the environment by hugely reducing the  $\text{CO}_2$  emission into the atmosphere compared to the OPC concrete.

### **1.3 Research objectives**

The main aim of this research is to expand the understanding of using nano silica and nano calcium carbonate to develop an environment friendly and economical HVS and HVS-FA concretes. To achieve this aim, the specific objectives are as follows.

- Evaluate the optimum combination of slag, fly ash and nano materials based on the compressive strengths and microstructural investigation of high volume slag and high volume slag-fly ash blended pastes.
- Evaluate the effect of optimum content of nano materials on the development of early and long term compressive strength of high volume slag (HVS) and high volume slag-fly ash (HVS-FA) blended concretes.
- Study the effects of optimum contents of nano materials on the durability properties such as drying shrinkage, sorptivity, volume of permeable voids, rapid chloride penetration, chloride induced corrosion and chloride diffusion of HVS and HVS-FA concretes.
- Study the interfacial transition zone around coarse aggregates and microstructure of matrix of HVS and HVS-FA concretes due to the addition of optimum content of nano materials.

### **1.4 Research approach**

This study was divided into two parts. In first part, different contents of nano silica (NS) and nano calcium carbonate (NC) were added into the pastes containing 60-90% by wt. slag and slag-fly ash blend to determine the optimum content based on their 28 days compressive strength. Among number of paste samples containing NS and NC, few of them were selected for further microstructural investigation to know the microstructural changes due to the addition of NS and NC and optimum content of slag, fly ash and nano materials were found.

In the second part of this investigation, the effects of optimum content of NS and NC on the compressive strengths of HVS and HVS-FA concretes containing 70% and 80% slag and 70% slag-fly ash blended mix were evaluated at 3, 7, 28, 56, 90 and 180 days. Drying shrinkage of those HVS and HVS-FA concretes were measured and analysed at 7, 14, 28, 35, 56, 91, 120, 150, 180, 270, 330 and 365 days after initial curing. The durability of HVS and HVS-FA concretes containing NS and NC were investigated through sorptivity, VPV, RCPT after 28 and 90 days of wet curing. Chloride induced corrosion and chloride



diffusion of HVS and HVS-FA concretes containing NS and NC were also investigated after 28 days of wet curing following ASTM standards. The micro- and nano- structural changes of interfacial transition zone (ITZ) of HVS and HVS-FA concretes were also studied by nano indentation, scanning electron microscopy (SEM) images and energy-dispersive X-ray spectroscopy (EDS) analysis.

## **1.5 Thesis structure**

The thesis is composed of four parts containing nine chapters and outlined as follows:

There are two chapters in Part I, Chapter 1 contains the background, significance, objectives and approach of the study. Chapter 2 focuses on the literature review of the past study related to the use of nano materials on the HVS and HVFA concretes.

Part II presents the effect of NS and NC on the HVS and high volume slag-fly ash (HVS-FA) blended pastes. It consists of three chapters in which Chapter 3 investigates the effect of different dosages of nano silica (NS) on the compressive strengths of the HVS and HVS-FA paste containing 60-90% of slag and slag-fly ash blend while Chapter 4 explored the effects of different dosages of NC. These chapters also clarify the microstructural evaluation of HVS and HVS-FA pastes containing NS and NC. In chapter 5, a comparative investigation of effect of NS and NC on the ITZ of HVS and HVS-FA concretes is demonstrated. In this chapter, nano- and micro-scale investigation of ITZ are conducted and comparison of two nano materials on the structural changes are made.

Part III of this research presents the effect of NS and NC on the HVS and HVS-FA concretes. This part consists of three chapters. Chapter 6 presents the effect of NS on the compressive strengths and durability properties of HVS and HVS-FA concretes while chapter 7 describes the effect of NC on the same properties. Chapter 8 evaluates the effect of NS and NC on the chloride induced corrosion and chloride diffusion of the HVS and HVS-FA concretes. This chapter also evaluates the effect of NS and NC on the service live of those HVS and HVS-FA concretes.

Finally, in Part IV which has only one chapter, the outcome of this research and its beneficial role in these field of construction materials and future recommendation are included in the Chapter 9.

## 1.6 References

- Aghaeipour, A., & Madhkhan, M. (2017). Effect of ground granulated blast furnace slag (GGBFS) on RCCP durability. *Construction and Building Materials*, 141, 533-541.
- Alonso, M. C., Garcia Calvo, J. L., Sanchez, M., & Fernandez, A. (2012). Ternary mixes with high mineral additions contents and corrosion related properties. *Materials and Corrosion*, 63(12), 1078-1086.
- Bilim, C., Atiş, C. D., Tanyildizi, H., & Karahan, O. (2009). Predicting the compressive strength of ground granulated blast furnace slag concrete using artificial neural network. *Advances in Engineering Software*, 40(5), 334-340.
- Choi, Y. C., Kim, J., & Choi, S. (2017). Mercury intrusion porosimetry characterization of micropore structures of high-strength cement pastes incorporating high volume ground granulated blast-furnace slag. *Construction and Building Materials*, 137, 96-103.
- Demirboğa, R., Türkmen, İ., & Karakoç, M. B. (2004). Relationship between ultrasonic velocity and compressive strength for high-volume mineral-admixed concrete. *Cement and Concrete Research*, 34(12), 2329-2336.
- Duran Atiş, C., & Bilim, C. (2007). Wet and dry cured compressive strength of concrete containing ground granulated blast-furnace slag. *Building and Environment*, 42(8), 3060-3065.
- El-Chabib, H., & Syed, A. (2013). Properties of Self-Consolidating Concrete made with High volume of Supplementary Cementitious Materials. *Materials in Civil Engineering*, 25(11), 1579-1586.
- Elchalakani, M., Aly, T., & Abu-Aisheh, E. (2014). Sustainable concrete with high volume GGBFS to build Masdar City in the UAE. *Case Studies in Construction Materials*, 1, 10-24.
- Gesoğlu, M., & Özbay, E. (2007). Effects of mineral admixtures on fresh and hardened properties of self-compacting concretes: binary, ternary and quaternary systems. *Materials and Structures*, 40(9), 923-937.
- Gunasekara, C., Sandanayake, M., Zhou, Z., Law, D. W., & Setunge, S. (2020). Effect of nano-silica addition into high volume fly ash-hydrated lime blended concrete. *Construction and Building Materials*, 253, 119205.

- Güneyisi, E., & Gesoğlu, M. (2008). A study on durability properties of high-performance concretes incorporating high replacement levels of slag. *Materials and Structures*, 41(3), 479-493.
- Hashimoto, M., Sakata, N., Sakai, E., Yonezawa, T., Hayashi, D., & Muronoi, T. (2016). Study on Concrete for Civil Engineering Structure Using High Volume Blast Furnace Slag Cement. *Advance Concrete Technology*, 14, 163-171.
- Hill, J., & Sharp, J. H. (2002). The mineralogy and microstructure of three composite cements with high replacement levels. *Cement and Concrete Composites*, 24(2), 191-199.
- Hooton, R. D. (2000). Canadian use of ground granulated blast-furnace slag as a supplementary cementing material for enhanced performance of concrete. *Canadian Journal of Civil Engineering*, 27(4), 754-760.
- Jeong, Y., Park, H., Jun, Y., Jeong, J.-H., & Oh, J. E. (2015). Microstructural verification of the strength performance of ternary blended cement systems with high volumes of fly ash and GGBFS. *Construction and Building Materials*, 95, 96-107.
- Jo, B.-W., Kim, C.-H., Tae, G.-h., & Park, J.-B. (2007). Characteristics of cement mortar with nano-SiO<sub>2</sub> particles. *Construction and Building Materials*, 21(6), 1351-1355.
- Kawashima, S., et al., Modification of cement-based materials with nanoparticles. *Cement and Concrete Composites*, 2013. 36(Supplement C): p. 8-15.
- Kuder, K., Lehman, D., Berman, J., Hannesson, G., & Shogren, R. (2012). Mechanical properties of self consolidating concrete blended with high volumes of fly ash and slag. *Construction and Building Materials*, 34, 285-295.
- Land, G., & Stephan, D. (2012). The influence of nano-silica on the hydration of ordinary Portland cement. *Journal of Materials Science*, 47(2), 1011-1017.
- Li, Z., Wang, H., He, S., Lu, Y., & Wang, M. (2006). Investigations on the preparation and mechanical properties of the nano-alumina reinforced cement composite. *Materials Letters*, 60(3), 356-359.
- Liu, M., Zhou, Z., Zhang, X., Yang, X., & Cheng, X. (2016). The synergistic effect of nano-silica with blast furnace slag in cement based materials. *Construction and Building Materials*, 126, 624-631.

López, M. M., Pineda, Y., & Gutiérrez, O. (2015). Evaluation of Durability and Mechanical Properties of the Cement Mortar Added with Slag Blast Furnace. *Procedia Materials Science*, 9, 367-376.

Malhotra, V. M. (2002). Introduction: Sustainable development and concrete technology, ACI Board Group on Sustainable Development. *ACI Concrete International*, 24(7), 22.

Mehta, P. K. (2001). Reducing the environmental impact of concrete. *ACI Concrete International*, 23(10), 61-66.

Nazari, A., & Riahi, S. (2011). Splitting tensile strength of concrete using ground granulated blast furnace slag and SiO<sub>2</sub> nanoparticles as binder. *Energy and Buildings*, 43(4), 864-872.

Oner, A., & Akyuz, S. (2007). An experimental study on optimum usage of GGBS for the compressive strength of concrete. *Cement and Concrete Composites*, 29(6), 505-514.

Sato, T., & Beaudoin, J. J. (2011). Effect of nano-CaCO<sub>3</sub> on hydration of cement containing supplementary cementitious materials *Advances in Cement Research*, 23, 33-43.

Shaikh, F.U.A. and S.W.M. Supit, Chloride induced corrosion durability of high volume fly ash concretes containing nano particles. *Construction and Building Materials*, 2015. 99: p. 208-225.

Shaikh, F.U.A. and S.W.M. Supit, Mechanical and durability properties of high volume fly ash (HVFA) concrete containing calcium carbonate (CaCO<sub>3</sub>) nanoparticles. *Construction and Building Materials*, 2014. 70(Supplement C): p. 309-321.

Tharakan, J. L. P., Macdonald, D., & Liang, X. (2013). Technological, economic and financial prospects of carbon dioxide capture in the cement industry. . *Energy Policy*, 61, 1377-1387.

Thomas, J. J., Jennings, H. M., & Chen, J. J. (2009). Influence of Nucleation Seeding on the Hydration Mechanisms of Tricalcium Silicate and Cement. *The Journal of Physical Chemistry C*, 113(11), 4327-4334.

Wainwright, P. J., & Rey, N. (2000). The influence of ground granulated blastfurnace slag (GGBS) additions and time delay on the bleeding of concrete. *Cement and Concrete Composites*, 22(4), 253-257.

Zhang, M.-H., & Islam, J. (2012). Use of nano-silica to reduce setting time and increase early strength of concretes with high volume of fly ash or slag. *Construction and Building Materials*, 29, 573-580.

Zhang, M.-H., Islam, J., & Peethamparan, S. (2012). Use of nano-silica to increase early strength and reduce setting time of concretes with high volumes of slag. *Cement and Concrete Composites*, 34(5), 650-662.

*All reasonable efforts have been made to acknowledge the authors of the copyright material. It would be highly appreciated if I can hear from any authors has been ignored or incorrectly acknowledged.*

## Chapter 2: Literature Review

This chapter provides a preview of past studies on the effects of nano materials on various properties and microstructure of high volume fly ash (HVFA), high volume slag (HVS) and high volume slag-fly ash (HVS-FA) blended composites.

### 2.1 Nano technology

In 1959, the concept of nanotechnology was introduced by Noble prize winner physicist Richard P. Feynman in his famous lecture “There’s Plenty of Room at the Bottom” at a meeting of the American Physical Society and explored the ideas of manipulating material at an extremely small scale of individual atoms and molecules, i.e., the nanoscale (Feynman, 1960). Nanotechnology has been defined by Drexler et al. (Drexler et al.,1991) “the control of the structure of matter based on molecule-by-molecule control of products and by-products”. The meaning of “nanotechnology” can varies from field to field. For construction sector, nanotechnology can be termed as the controller of properties at nanometre scale can make significant changes in the performance of the bulk materials. The dimensions of the nano materials ranged from 100 nm down to approximately 0.1 nm (**Fig. 2.1**).

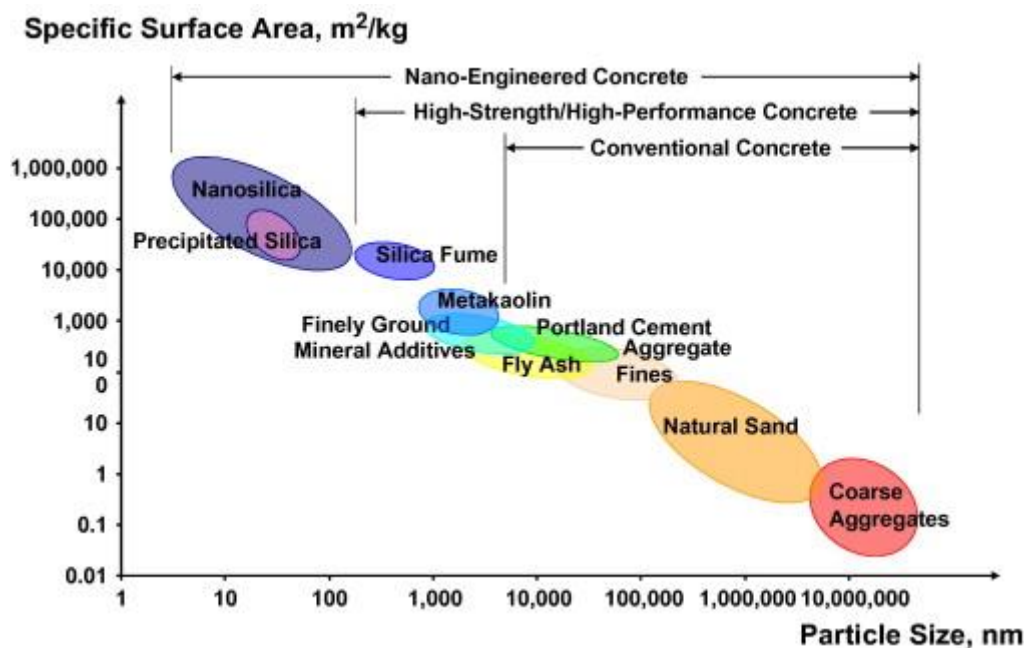
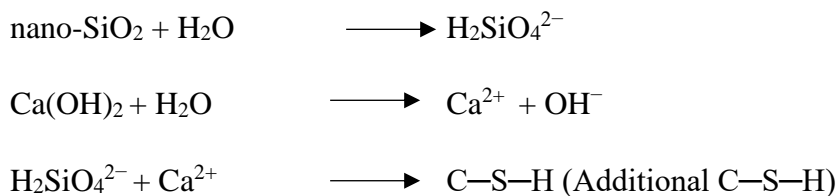


**Fig. 2.1** Particle size and specific surface area related to concrete materials (Sobolev & Ferrada-Gutiérrez, 2005)

## 2.2 Nano materials and cementitious composites

Using a small amount of nano materials along with cementitious composites has gained popularity due to their huge specific surface area and tiny particle size which has the ability to influence the acceleration of hydration of cementitious materials. By accelerating the hydration, nano materials have an outstanding impact to boost the early compressive strengths and durability properties of cement paste, mortar and concrete.

Quite a few studies reported the effect of nano-SiO<sub>2</sub> (NS) on cementitious materials such as, Thomas et al. (2009) showed that the addition of NS accelerated the amount of early hydration by first reacting with calcium ions released by tricalcium silicate (C<sub>3</sub>S) to form calcium silicate hydrate (C–S–H), which seeds the hydration process by filling the capillary pore space away from the C<sub>3</sub>S surfaces. Land and Stephan (2012) described that surface of the NS act as a nucleation site which accelerate the hydration of cement. Addition of NS accelerated the consumption of tricalcium silicate (C<sub>3</sub>S), the development of portlandite (small sized CH) crystals and homogenous groups of C–S–H composition that are created on the silica surface. Jo et al. (2007) concluded that the addition of NS increased the amount of heat evolved during hydration reaction of the cement which is crucial to accelerate the early hydration and pozzolanic reactions. It was found that the NS acted as an activator to promote pozzolanic reactions and improved the microstructure. SEM micrograph showed that C–S–H gels existed in an isolation form and enclosed and linked with many needle-hydrates hands while the microstructure of the mixture with NS exposed a dense and compact formation of hydration products with a lower amount of Ca(OH)<sub>2</sub> crystals. It has also been found that the NS improved concrete workability and strength (Li et al.,2004; Said et al.,Tian, 2012; Sobolev & Ferrada-Gutiérrez, 2005; Sobolev et al., 2009; Zhu et al., 2015). NS is also found to improve the strength of concrete much better than the silica fume (Qing et al., 2007). The reaction between nano-SiO<sub>2</sub> and CH to generate additional C-S-H gel is shown in the following equation (Qing et al., 2006)



Nano-CaCO<sub>3</sub> (NC) was being used as a filler materials initially as a replacement of cement and gypsum. Some studies have found that it can be used as an economically beneficial material to

improve early strengths, accelerating hydration of cementitious materials and concrete (Bentz, 2014; Bentz et al., 2012; De Weerd et al., 2011; Georgescu & Saca, 2009; Pera et al., 1999; Sato & Diallo, 2010; Vishwakarma et al., 2016). Sato and Beaudoin (2011) concluded that the addition of NC as partial replacement of cement accelerated the hydration of OPC and the acceleration was greater with higher amount of NC. It is also found that microhardness and modulus of elasticity at early age of hydration products are significantly improved with increase in NC contents.

There are few other nano materials such as, nano- $\text{Al}_2\text{O}_3$  (NA) which showed improvement in various properties of cementitious materials. Many studies reported that NA improved the modulus of elasticity significantly but showed little improvement on the compressive and split tensile strengths. NA also accelerated the pozzolanic reaction and improved the filler effect (Agarkar & Joshi, 2012; Arefi et al., 2011; Li et al., 2006; Nazari & Riahi, 2011a, 2011b, 2011c; Nazari et al., 2010). Few studies have found that nano- $\text{TiO}_2$  (NT) improved the early age hydration of cementitious materials and consequently improved the compressive strengths, flexural strengths and other durability properties (Jayapalan & Kurtis, 2009; Mohseni et al., 2015; Nazari & Riahi, 2011d, 2011f; Rao et al., 2015; Vishwakarma et al., 2016). It is also found that the addition of NT in concrete exhibited self-cleaning properties which made concretes to perform on the mechanism of photocatalytic degradation and decomposes the environmental pollutants such as carbon monoxide,  $\text{NO}_x$ , VOCs, chlorophenols etc. emitted from different polluting sources (Murata, Tawara, Obata, & Takeuchi, 1999; Vallee F et al., 2004). Several researches have studied the use of carbon nanotubes/ carbon nanofibers (CNTs/CNFs) in cementitious materials and observed extraordinary increase in modulus of elasticity and tensile strengths in the range of TPa and GPa, respectively. It is also reported that the CNTs can influence early age hydration and thus a strong bond is likely between cement paste and CNTs (Makar et al., 2005; Salvetat J-P et al., 1999; Srivastava et al., 2003).

## **2.3 Effect of nano materials on high volume fly ash (HVFA) composites**

### **2.3.1 Hydration properties**

High volume fly ash (HVFA) concrete delays the hydration heat and it happens at around 30-40h, while inclusion of NS accelerates the hydration and is similar to that of ordinary concrete which occurs at around 15-25h. It has also been reported that a little addition of NS accelerated the pozzolanic reaction of fly ash. About 19% increase in hydration heat due to 4% addition of NS in concrete containing 50% FA as partial replacement of cement is observed compared to



the control concrete (G. Li, 2004). On the other hand, Sato and Beaudoin (2011) concluded that the addition of nano- $\text{CaCO}_3$  (NC) as partial replacement of cement accelerated the hydration of OPC and the acceleration was greater with higher amount of NC. In this study, 10% and 20% micro- $\text{CaCO}_3$  and NC, respectively were added to the binder along with 50% fly ash as the cement replacement. Zhang and Islam (2012) concluded that 1% addition of NS accelerated the cement and fly ash hydration more significantly and shortened the dormant period when added with 49% cement replaced paste. Likewise, it is reported that 3% NS addition into a mortar containing 30% FA decreased the first peak value of hydration exothermic as an indication of decreased quantity of tricalcium aluminate mineral ( $\text{C}_3\text{A}$ ) (Wang et al., 2020). It is also found that the NS inclusion generated large amount of heat rapidly and accelerated the hydration reaction at the early stage. Another study (Zaidi et al., 2019) found that NS addition into a 50% FA containing mortar decreased the thermal insulation value and increased the thermal conductivity by 20% through filling micro voids due to its tiny particle size and 3% NS addition considered to be the optimum content of NS addition with varying curing conditions.

Effects of colloidal nano- $\text{SiO}_2$  (CNS) on the hydration properties of mortar containing 50% FA was characterised by the calcium hydroxide (CH) peak in XRD analysis and it is established that the addition of CNS reduced the CH peaks and found relatively more lower peaks with the increasing dosage of CNS. However, the CNS addition did not show any noticeable change in the peaks of calcium silicate ( $\text{C}_3\text{S}$  and  $\text{C}_2\text{S}$ ) (Liu et al., 2019). Similar reduction of CH contents due to the addition of 0.5% CNS in a 30% FA containing paste is also observed in another study (Liu et al., 2020) and it is also demonstrated that the reduction was significant when NS content is increased to 4% and produced more C-S-H gels. This study also found that the addition of CNS reduced the average Ca/Si ratio and the reduction was higher with higher amount of CNS inclusion. Similar to the other studies, CNS addition reduced the calcium hydroxide peak significantly in the samples before exposure to the elevated temperature (Ibrahim et al., 2012). After exposure to the elevated temperature to  $700^\circ\text{C}$ , it is found that the CH peaks are decreased in the control cement paste and these peaks are disappeared in the samples with CNS addition. It is also believed that the decrease in calcium silicate and silica peaks in the samples with CNS and FA formed a new silicate compounds due to the reaction from these two materials resulted a higher residual strengths after exposure to  $700^\circ\text{C}$ . Hydration rate and temperature peak were increased due to the addition of CNS and colloidal nano-Boehmite (CNB) individually and in combination. Increment of hydration rate and temperature

peak appeared earlier with the higher dosage of CNS and CNB in both individual and combined addition reported in the study (Zhu et al., 2015). It is also found that addition of NT can promote the early hydration rate of OPC-FA blend paste in which FA prolonged the initial hydration (Ma et al., 2016).

### **2.3.2 Fresh properties**

Zhang and Islam (2012) reported significant reduction in both initial and final setting times of concrete containing 50% fly ash as partial replacement of OPC. With the incorporation of 2% NS, the initial and final setting times are reduced by 28.1% and 22.1%, respectively when compared to that of the reference concrete with no NS. It is also found that the NS acted as a reactive filler which reduced the bleeding and increased the density of the concrete. Another study also reported that 1% addition of NS reduced the initial and final setting times by 60 and 100 minutes, respectively of paste samples containing 30% FA compared to the control samples without NS addition (Lin et al., 2008). High volume replacement of cement with fly ash increased the workability and caused the bleeding, while addition of NS and NC reduced the workability especially for the concrete containing 40% fly ash (Shaikh & Supit, 2015). Fresh properties such as slump flow diameter,  $T_{50}$  slump flow time, V-funnel flow time and L-box height ratio of self-compacting concrete containing 50% and 70% FA were aggravated with the addition of 2%, 4% and 6% NS which were enhanced by the replacement of FA (Güneyisi et al., 2015). This result is also consistent with the findings of another investigation (Kawashima et al., 2013), which concluded that the workability of a HVFA mortar containing 60% FA decreased with the addition of CNS and greater reduction is found with the increasing amount of CNS such as when 6% CNS was added into the mortars. On the other hand, a recent study (Siang et al., 2020) demonstrated that up to 3% addition of NS, nano-TiO<sub>2</sub> (NT) and nano-Fe<sub>2</sub>O<sub>3</sub> (NF) does not impact the workability of mortars containing 30% FA. However, any further addition of NS and NT reduced the workability by 42.6% and 10.9%, respectively compared to the control mortar. Surprisingly, 5% dosage of NF exhibited an improved workability by 11% compared to the control sample. Similar workability outcome is also showed in another study when 3% NT is added into a mortar containing 30% FA (Ma et al., 2016). This study also revealed that 3% NT addition into a paste containing 30% FA reduced the initial setting time by 9.8% and the final setting time by 7.9% compared to the control OPC paste. Increasing content of FA prolonged the setting times and NT addition accelerated the settings of paste specimens because of its larger specific surface area reported in the study. On the other hand, 5% addition of NC significantly reduced the initial and final

setting times of paste samples with a 50% replacement of cement by fly ash compared to the ordinary cement paste and exhibited the same setting times when sonication process is applied for the mixing of NC reported in that study.

### 2.3.3 Mechanical properties

Addition of 4% NS increased the early age compressive strengths of HVFA concrete significantly as well as the long term compressive strengths. It is reported that 4% NS inclusion into the concrete containing 50% FA enhanced the compressive strengths by 80.35% at 3 days and 68.57% at 7 days with respect to control HVFA concrete without NS (G. Li, 2004). It is found that microhardness and modulus of elasticity at early age of hydration products were significantly improved and increase with increase in NC contents (Sato & Beaudoin, 2011). Compressive strengths of mortars containing 50% FA is increased by 62.16%, 24.31%, 17.10%, 6.86% and 4.35% at 1, 3, 7, 28 and 91 days, respectively when 1% FA is replaced with NS and the strengths were higher for the mortars prepared by the ultra-sonication process than those of mechanical mixing (Zhang & Islam, 2012). Shaikh et al. (2014) observed a slight (5%~9%) improvement of compressive strengths of mortars containing 40% and 50% FA at 7 and 28 days. On the other hand, about 33% and 48% improvement is reported in the mortars containing 60% and 70% FA respectively at age of 28 days (**Fig. 2.2**). In this study, 2% NS was added as a fly ash replacement in the mortars containing 40%, 50%, 60% and 70% FA as replacement of cement. This study concluded that the addition of 2% NS improved the 7 days compressive strengths of mortars containing up to 50% fly ash and 28 days compressive strengths of mortars containing more than 50% fly ash. Authors also conducted the 2% NS significantly improved the 3 days compressive strengths of HVFA concretes containing 40% and 60% FA and is more pronounced about 95% improvement with concrete containing 60% fly ash but no such improvements are observed at ages of 7, 28, 56 and 90 days (**Fig. 2.3**). Mei et al. (2018) studied the combined effect of 1 to 4% inclusion of NS and steam curing of 40% OPC replaced mortars by FA on the compressive strengths after 3 days. It is established that NS inclusion increased the compressive strengths up to 3% NS addition by weight and then any further addition of NS resulted a slight reduction of compressive strengths regardless of the curing conditions. However, the increments were always higher with the 12 h steam curing followed by 60 hours standard curing than the 3 days of standard curing. It is also demonstrated that 3% NS addition exhibited the highest improvement of compressive strengths by 31.7% and 44.3% under standard curing and steam curing process, respectively. A recent study (Ng et al., 2020) investigated the effect of NS, NT and NF on the compressive and flexural strengths

of mortar containing 30% FA and compared their improvement. This study showed that the addition of 3% dosage of NS, NT and NF improved the compressive strength by 38%, 36% and 35%, respectively after 28 days and 3% dosage of all nano materials exhibited the maximum increase of the compressive strength. Similar development is observed on the flexural strength of a mortar containing 30% FA after 28 days compared to control mortar mix and the NS addition always resulted the higher improvement of compression and flexural strength than both NT and NF addition.

Güneysi et al. (2015) reported the compressive strengths of self-compacting concrete (SCC) concretes were significantly decreased due to the 50% and 75% replacement of OPC by FA while NS addition up to 4% enhanced the compressive strengths by 27.1% and 71.1% of concrete containing 50% and 75% FA, respectively at 28 days. Any further addition of NS experienced a reduction of compressive strengths reported in this study. A very recent study (Wang et al., 2020) reported that 3% NS inclusion improved the compressive strengths of 30% and 40% FA containing mortars by 30.55% and 27.55%, respectively at 7 days providing the evidence of accelerated hydration of FA at early age and hence more gels are generated. It is also stated that addition of 3% NS increased the compressive strengths of those mortars by 6.96% and 22.72%, respectively at 28 days compared to the control mortar without NS. Contrasting to the above results, Zaidi et al. (2019) concluded that NS addition did not affect the compressive strength and even affects negatively when mortar samples containing 50% FA cured without water. Hence, it is believed that NS needed additional water to react faster and thus lower amount of C-S-H produced when cured without water.

The effect of CNS on the compressive strengths of cement mortar containing 50% FA was studied and demonstrated that the early age compressive strengths could be greatly improved by the inclusion of CNS and the improvement is more pronounced with the higher amount of addition. However, the CNS is unfavourable to the strength gain at later ages and observed a reduction in strengths gain with the higher dosages of CNS (Hou et al., 2013). Significant improvement of the compressive strengths was found after 7 days and 28 days of curing when 1%, 3% and 5% CNS were added into the 50% FA containing paste specimens (Huang et al., 2021). It is reported that about 20.3%, 45.3% and 63.5% increment of compressive strengths are observed compared to the reference HVFA paste due to the addition of 1%, 3% and 5% CNS, respectively after 7 days of curing, while the improvements were 15.5%, 36.1% and 45.2% after 28 days of curing suggested an early hydration due to the CNS addition. Moreover, the addition of 1% to 4% CNS into mortar containing 50% FA increased the compressive

strengths and flexural strengths significantly after 9 hours of steam curing and it is increased with the increasing dosage of CNS reported in other study (Liu et al., 2019). Another study also reported that the addition of 0.5% CNS into a 30% FA containing paste amplified the compressive strength by 2.77%, 11.46% and 6.66% at 7, 28 and 90 days, respectively while the improvement were by 24.68%, 37.15% and 30.80% at 7, 28 and 90 days, respectively due to the addition of 4% CNS (Liu et al., 2020). Fire resistance of 25%, 35% and 45% FA containing mortar with 2.5%, 5% and 7.5% CNS inclusion were investigated (Ibrahim et al., 2012) and it is concluded that the specimens containing CNS had the higher residual compressive strengths and flexural strengths than the control specimens after exposure to 700°C after any stage of curing period of 3, 7 and 28 days. It is also demonstrated that mortar samples containing 7.5% CNS and 37.5% FA exhibited comparable strengths to control mortar specimens at ambient temperature after 3, 7 and 28 days of curing.

The individual and combined effect of CNS and CNB with an average particle size of 30 nm into the 30% OPC replaced mortars by FA investigated by Zhu et al. (2015). It is illustrated that both CNS and CNB contributed the enhancement of compressive strengths significantly at the early ages with a lower percentage of dosage up to 2.5%. Any further individual addition of CNS and CNB showed a downward trend than the control mortar. Similar results were also observed when CNS and CNB added combined, and 0.1% addition of combined CNB-CNS resulted considerable improvement of the compressive strengths at early and later ages up to 180 days.

On the other hand, it is reported that 1% replacement of FA by NC in a 60% FA containing mortars improved the compressive strengths by around 133% and 106.25% at ages 7 days and 28 days, respectively compared to 60% FA mortars with no NC while no such great improvement is noticed in the compressive strengths of concrete containing 39% FA and 1% NC (Shaikh & Supit, 2014). In addition (Harilal et al., 2019), a study investigated a combined effect of 1% NT and 1% NC of a concrete containing 40% FA and reported a 50% and 36% increase in compressive strengths at 3 days and 7 days, respectively compared to the composites without nano addition. However, the compressive strengths remained lower than the ordinary control concrete in both ages. Surprisingly, the addition of 2% NaNO<sub>2</sub> (NN) along with NC and NT in the same 40% FA containing composites showed significant improvement in the compressive strength and exhibited similar strength of ordinary concrete after 7 days of curing. Moreover, after 28 days of curing samples with NC, NT and NN showed 13% higher strength and samples containing only NC and NT displayed similar strength to that of control

concrete. Similar outcome is also found in the results of split tensile strength test and flexural strength test after 28 days of curing.

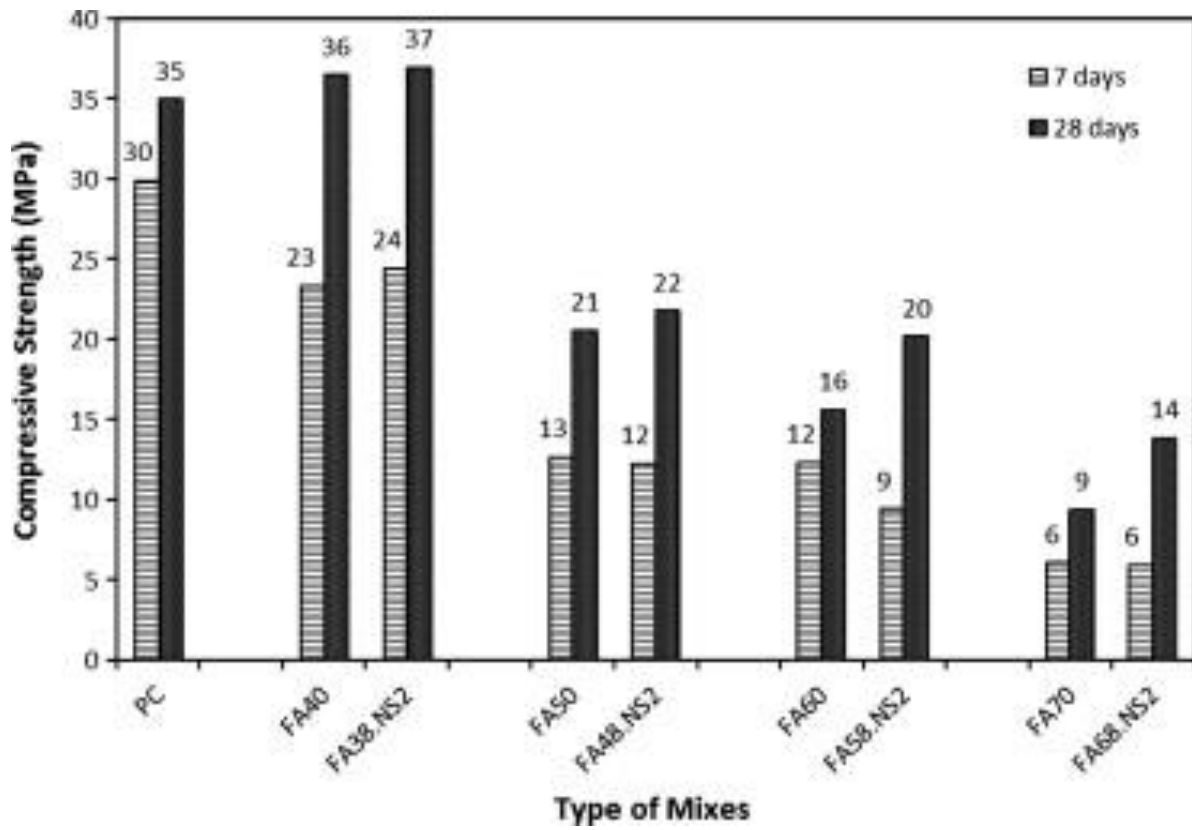


**Fig. 2.2** Effects of 2% NS on compressive strength of mortars containing HVFA adopted from (Shaikh et al., 2014).

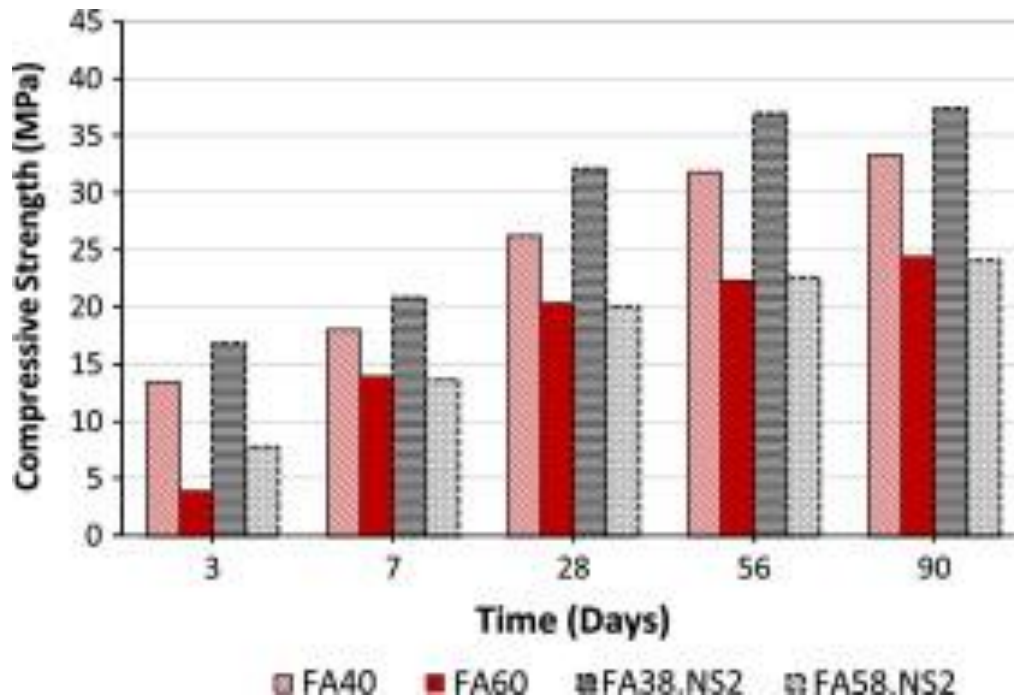


**Fig. 2.3** Effects of 2% NS on compressive strength of HVFA concretes containing 40% and 60% fly ash adopted from (Shaikh et al., 2014).

### 2.3.4 Durability properties

Incorporation of NS makes HVFA concrete a compact structures by reducing the porosity and pore size even after a short period of curing (Li, 2004). The chloride-ion permeability resistance of concretes is increased due to the addition of 2% NS in comparison to that of reference concrete containing 50% FA with no NS inclusion. It is reported that the charge passed is reduced by 25.64% at age of 28 days (Zhang & Islam, 2012) while another study (Shaikh & Supit, 2015) reported about 38% reduction at 28 days of concrete containing 38% FA and 2% NS and the reduction were about 9% and 20% at 28 days and 90 days respectively, in the HVFA concrete containing 58% FA and 2% NS. The water sorptivity values of HVFA concretes containing 38% FA and 2% NS were about 27-32% lower than that of concretes with no NS. In addition, it is also found that NS is more active in reducing water absorption of concrete containing 58% FA and 2% NS. Replacing 2% FA with NS lowered the chloride diffusion coefficient about 21% and 14% of the concrete containing 40% FA and 60% FA, respectively compared to that of no NS and the resistance of concrete against corrosion is improved by the incorporation of NS reported in that study (Shaikh & Supit, 2015). Addition

of 0.5% CNS into a cement paste containing 30% FA enhanced the chloride immobilization by 10.86% at 28 days and reduced the pore volume significantly. However, any further increment of CNS dosage reduced the chloride immobility and an additional drop of pore volume reported in a very recent study (Liu et al., 2020).

Furthermore, it is found that 1% addition of NC into a HVFA concrete containing 59% FA reduced the water sorptivity by 19% and 60% than ordinary concrete at 28 days and 90 days, respectively due to the formation of additional CSH gel (Shaikh & Supit, 2014). This study also reported about 7% and 21% reduction of the volume of permeable voids after 28 and 90 days curing, respectively. It is also showed that the chloride ion permeability resistance of concretes is increased with the inclusion of 1% NC which was about 11% and 8% reduction of charge passed at the age of 28 days and 90 days, respectively. The chloride diffusion of HVFA concrete containing 59% FA and 1% NC were 32% lower than that of HVFA concrete without NC. In another study, it is concluded that addition of 2% combined NT and NC reduced the water sorptivity by 26-28% compared to their control concrete without nano materials addition (Harilal et al., 2019). Moreover, a further 2 % addition of NN in the combined 2% NC and NT resulted a further 21% reduction of sortivity in this study. It is also reported that a significant reduction of charge passing is observed during the rapid chloride permeability test and reduction of CO<sub>2</sub> ingress in carbonation test. Overall investigation of the previous studies have established that the addition of NS in HVFA concrete performed better than the addition of NC in terms of improvement of durability properties of HVFA concretes.



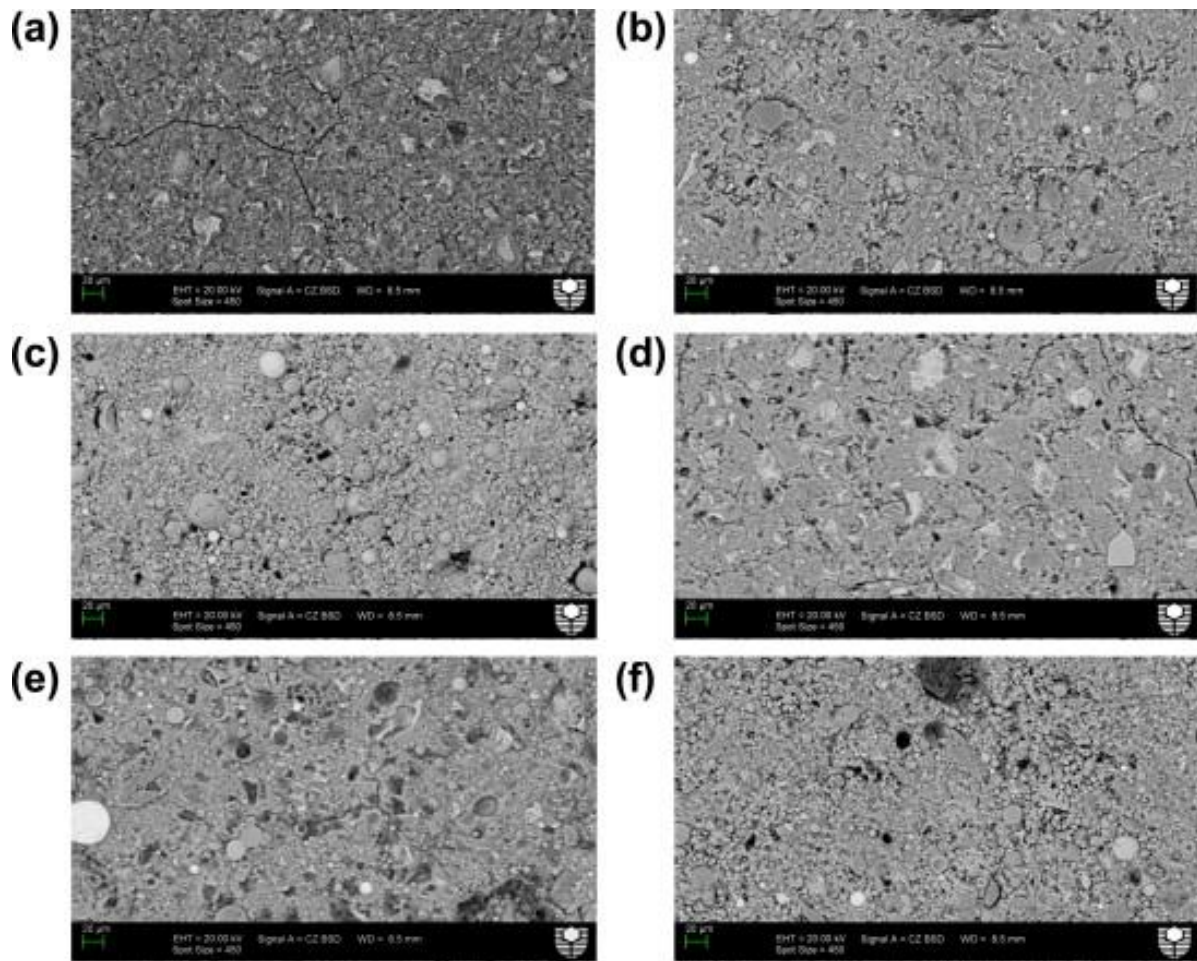


**Fig. 2.4** Backscattered electron (BSE) images of polished surface of paste samples after 28 days of curing: (a) cement paste, (b) paste containing 40% fly ash, (c) paste containing 60% fly ash, (d) paste containing 2% NS, (e) paste containing 38% fly ash and 2% NS and (f) paste containing 58% fly ash and 2% NS adopted from (Shaikh et al., 2014).

### 2.3.5 Microstructural properties

Shaikh et al. (2014) evaluated the microstructural properties of HVFA pastes containing 2% NS through scanning electron microscopy (SEM) images (**Fig. 2.4**) and X-ray diffraction (XRD) analysis. It is demonstrated that the presence of 2% NS significantly improved the microstructure of the matrix and reduced the calcium hydroxide by about 10% and 30% of HVFA pastes containing 38% and 58% fly ash, respectively. It is also evaluated that the 3% NS inclusion in 30% FA containing mortar reduced total porosity by 3.44% while less harmless pores ranges from 0.02 to 0.05  $\mu\text{m}$  are decreased significantly by 17.60% and harmful pores are decreased by around 4% (Wang et al., 2020). Another study (Mei et al., 2018) investigated

the combined effect of NS dosage and steam curing on the pore volume and pore size distribution through mercury intrusion porosimetry (MIP) tests. It is found that NS and steam curing increased the harmless pores (<20 nm) by promoting the hydration process of OPC and further enhanced the pozzolanic activity of fly ash in the early days and produce more amount of hydrated C<sub>3</sub>S and C<sub>3</sub>A gels. This study also found that the combined effect of NS and steam curing reduced the intensity of CH peaks and believed to be decreased more significantly by increasing the temperature of steam curing. It is also found that higher consumption of CH due to the NS addition and steam curing increased the polymerization of C-S-H gels which directed to the compact and denser microstructure of ITZ.

Scanning electron microscopy (SEM) analysis (Siang et al., 2020) of 30% FA containing mortar with the inclusion of NS, NT and NF found more compact microstructure compared to the reference mortar and the addition of optimum content (3% by weight) of NS, NT and NF resulted a most homogenous microstructure with the lowest porosity. Further addition of NS, NT and NF caused an agglomeration of nano particles and formed a weak microstructure with higher percentage of porosity. It is also concluded that the addition of nano materials (NS, NT and NF) improved the micromechanical properties such as modulus and hardness of ITZ and with the increasing content of nano particles indicated the higher rate of hydration of OPC and FA particles in the ITZ.

X-ray Diffraction (XRD) analysis of a 50% FA containing paste specimens exhibited consumption of Portlandite (CH) due to the addition of CNS and attributed that Portlandite consumption led to the formation of additional C-S-H gel (Huang et al., 2021). Significant improvement of microstructural properties with new C-S-H gel (needle-like element) production due to the addition of CNS was observed through SEM images (**Fig.2.5**) of paste specimens containing 50% FA. It is also believed that formation of new C-S-H gel was more prominent with the higher amount of CNS inclusion (Liu et al., 2019) and more compact and dense interfacial transition zone (ITZ) was established. It is also found that 1% and 3% CNS addition considerably lowered the total porosity by 18.7% and 25.50%, respectively of a 50% FA containing paste. Furthermore, larger and medium capillary pores of paste containing 50% FA reduced significantly and were lower than the control OPC paste due to the NS addition demonstrated in this study. After exposure to elevated temperature such as 700°C, samples with CNS appeared to have more stable calcium silicate hydrate than the control samples without CNS and it is believed that fire resistance of HVFA concretes with CNS addition are much higher than the samples without CNS addition (Ibrahim et al., 2012). Moreover, pore size

distribution investigation before and after elevated temperature exposure showed that the samples incorporated with CNS and FA exhibited better pore refinement and lower volume of smaller size pores than the control specimens. Another study noted that the addition of CNS and CNB in 30% FA containing mortar resulted a compact ITZ with fewer micro holes and micro fracture which was believed to lead the compressive strengths increment concluded by the SEM image analysis (Zhu et al., 2015).

On the other hand, MIP results showed that the inclusion of 1% NC had significant influence in decreasing total capillary porosities and pore diameters of HVFA composites (Shaikh & Supit, 2014). In addition, the XRD analysis results of HVFA pastes containing 1% NC exhibited reduction of CH and CS and increase in C-S-H gel which are also confirmed through thermogravimetric (TGA) analysis (Shaikh & Supit, 2014). Similar reduction of CH and formation of new C-S-H are observed in another study when 1% NC, 1% NT and 2% NN are added in a concrete containing 40% FA (Harilal et al., 2019). In this study, it is revealed that the presence of small gel pores with a nano scale indication of refined and compact structure confirmed in MIP test.

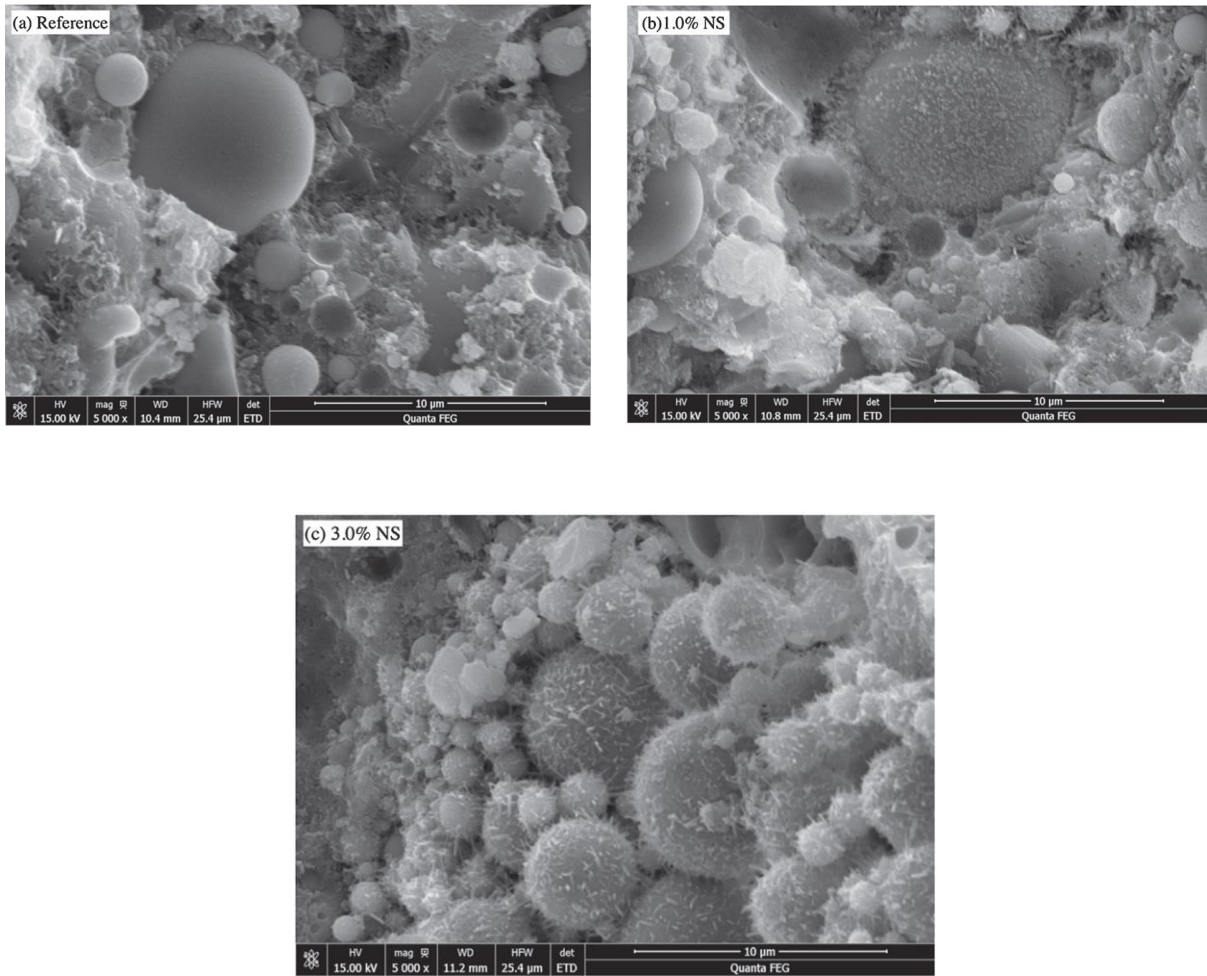


**Fig. 2.5** SEM images of 50% FA containing paste with and without NS addition adopted from (Liu et al., 2019)

## 2.4 Effect of nano materials on high volume slag (HVS) composites

### 2.4.1 Hydration properties

The hydration rate of cement and slag were accelerated and span of the dormant phase was shortened due to the addition of 2% NS in the high volume slag (50%) paste samples. Cumulative heat generation was also increased with the increasing amount of NS (Zhang et al., 2012). The degree of heat generation was increased with the addition of NS and induction period was shortened and this reduction was more with a paste samples of blast furnace slags containing 3% NS (Liu et al., 2016). A recent study investigated the heat release rate and the cumulative hydration heat of high volume fine blast furnace slag replaced paste ranging from 50% to 90% with the addition of 1% NS (Jiang et al., 2020). It is reported that the incorporation

of 1% NS promoted the hydration reaction of OPC and the pozzolanic reaction of slag. However, the hydration reactions were pronounced up to 70% replacement of OPC by fine slag. Moreover, it is showed that the super fine BFS and 1% NS addition effectively reduced the cumulative heat of hydration by 8.01%, 15.62%, 30.71% and 58.25% of paste composites containing super fine BFS of 30%, 50%, 70% and 90%, respectively. Similarly, another study (Nazari & Riahi, 2011b) showed that paste samples containing 45% slag reduced the total heat release and accelerated the peak time up to 3% NA addition.

#### **2.4.2 Fresh properties**

Initial and final setting times of high volume slag (HVS) concrete are reduced by 95 minute and 105 minute, respectively due to 2% NS inclusion compared to the reference concrete without NS (Zhang et al., 2012). On the other hand, the addition of 1% NC into a 20% BFS containing cement paste shortened the initial and final setting times by 40 and 60 minutes, respectively and surprisingly 2% NC addition shortened the initial and final setting times of the same paste by more 20 minutes compared to the BFS-OPC paste without NC addition (Bankir et al., 2020).

#### **2.4.3 Mechanical properties**

Compressive strengths of HVS mortars containing 50% slag is increased with the increasing amount of NS dosage and the addition of 2% NS increased the compressive strengths of HVS mortars by 14%, 39%, 30%, 17% and 23% at 1, 3, 7, 28, 91 days, respectively compared to the reference concrete with no NS (**Fig. 2.6**). Moreover, the early age compressive strengths of concrete specimens containing 50% slag is increased by 22% and 18% at 3 days and 7 days, respectively but no significant improvement is noticed at later ages compared to the reference concrete with no NS (Zhang et al., 2012). In another study, Liu et al. (2016) inspected the interaction between NS and blast furnace slag (BFS) where a constant 3% NS were used as supplementary cementitious material into cement along with 10%, 20%, 30% and 40% dosages of BFS. All the mortars mix maintained a constant water binder ratio of 0.50. It is summarized that the compressive strength of mortar specimens is increased by 21.71%, 17.17% and 10.67% at the age of 3, 7 and 28 days, respectively compared to the mortar without NS inclusion and the highest compressive strength (59.42MPa) is found with 30% dosage of slag and 3% NS. It is recommended that the addition up to 3% NS increased the split tensile strength of concrete specimens as a result of formation of crystalline  $\text{Ca}(\text{OH})_2$  amount in the early age of hydration while examined the splitting tensile strength of concrete using 45% of slags as replacement of

cement (Nazari & Riahi, 2011e). It is also noted that any further increase of NS causes the reduction of splitting tensile strength. Furthermore, it is reported that the increase in flexural strengths of 45% slag containing concrete by about 71%, 27% and 16% at 7, 28 and 90 days of age, respectively when 3% NT is added and any further addition of NT reduced the strengths (Nazari & Riahi, 2011d). Another study (Jiang et al., 2020) found that 1% addition of NS with up to 70% replaced OPC by super fine BFS can achieved 25% higher flexural and compressive strengths than the control OPC samples at 3 days and showed a significant improvement in flexural and compressive strengths at 7, 28 and 90 days as well. It is believed that the NS hydrated rapidly and acted as the crystallization centre for nucleation of OPC and super fine BFS and suggested that a 70% super fine BFS containing concrete of having superior strength could be achievable by only addition of 1% NS into the sample. Moreover, (Rashad et al., 2018) it is reported that 4% NS inclusion in a HVS paste containing 65% BFS increased the compressive strengths by 57% and 22% after 7 and 28 days, respectively. It is also demonstrated that 1-4% NS addition resulted a higher residual compressive strengths of those paste after exposure to 800°C for 2 hours period than the control paste without NS addition. However, 5% NS addition led to the decrease in compressive strength before and after fire exposure also noted in this study.

Additionally, in a similar investigation (Bankir et al., 2020) of 20% BFS containing mortar showed that 1% addition of NC contributed a slight increase in flexural strength than the control OPC mortar and 20% BFS containing mortar without NC addition. However, the addition of further 1% NC into the mix resulted in 20% and 29% reduction in flexural strength than the OPC and 20% BFS containing mortar, respectively. Likewise, a 10% increase in the compressive strengths is also observed due to 1% NC addition while any further in NC contents reduced the compressive strength slightly reported in that study. Nazari and Riahi (2011b) found that the addition of 1-4% NA into SCC containing 45% slag can improve the 28 days compressive strengths by 31.35%, 45.31%, 56.98% and 47.37%, respectively and concluded that 3% NA addition exhibited the better synergy between slag and NA exhibited the highest strength. Similar increment in split tensile strength and flexural strength were also reported due to the addition of 1-4% NA and the 3% NA inclusion again showed better result than any other NA addition into the samples.

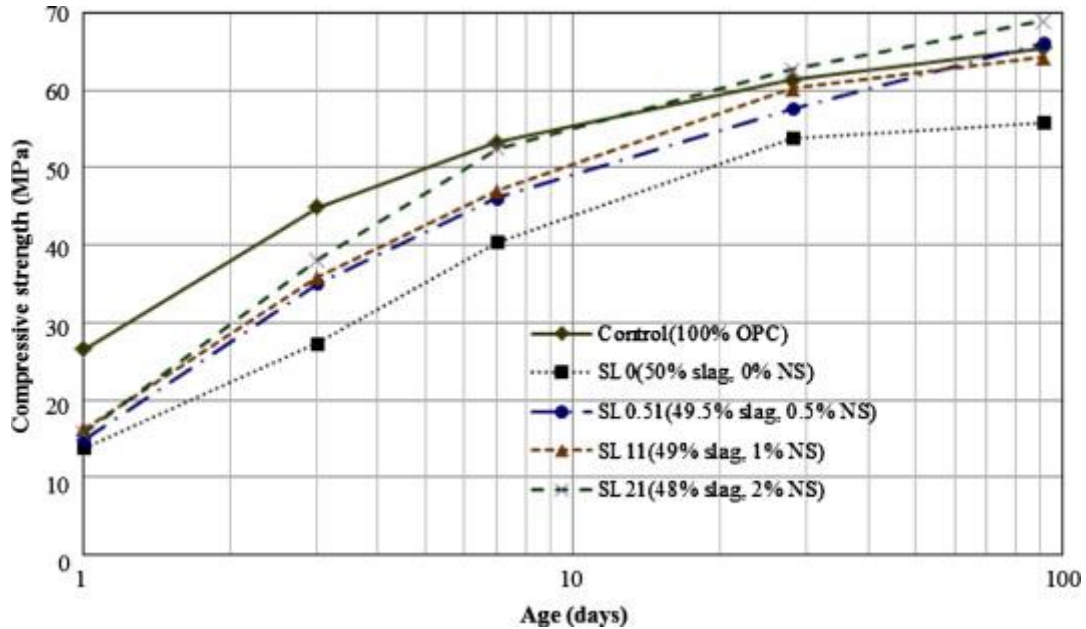


**Fig. 2.6** Effect of the nano-silica dosage on the compressive strength development of mortars adopted from (Zhang et al., 2012).

#### 2.4.4 Durability properties

Resistance of concrete to chloride-ion permeability after 28 days of curing is increased with 2% NS inclusion in a 50% OPC replaced slag concrete and the reduction was 25.71% than the reference concrete without NS. Large capillary pores of high volume slag pastes was decreased with the increasing amount of NS dosage and the critical pore diameters were decreased when 2% NS was added (Zhang et al., 2012), while another study reported that the 3% addition of NS into a 30% slag containing pastes reduced the harmful pores at 28 days and decreased the total porosity (Liu et al., 2016). Moreover, it is reported that increasing of NS dosage up to 3%, pore diameters of concrete with 45% OPC replaced by slags shifts to smaller pores which are less harmful indicated a refined pore structures and ultimately total specific pore volumes of concretes are decreased (Nazari & Riahi, 2011e) and the same pattern is also observed when NT is added into the same concrete (Nazari & Riahi, 2011d).

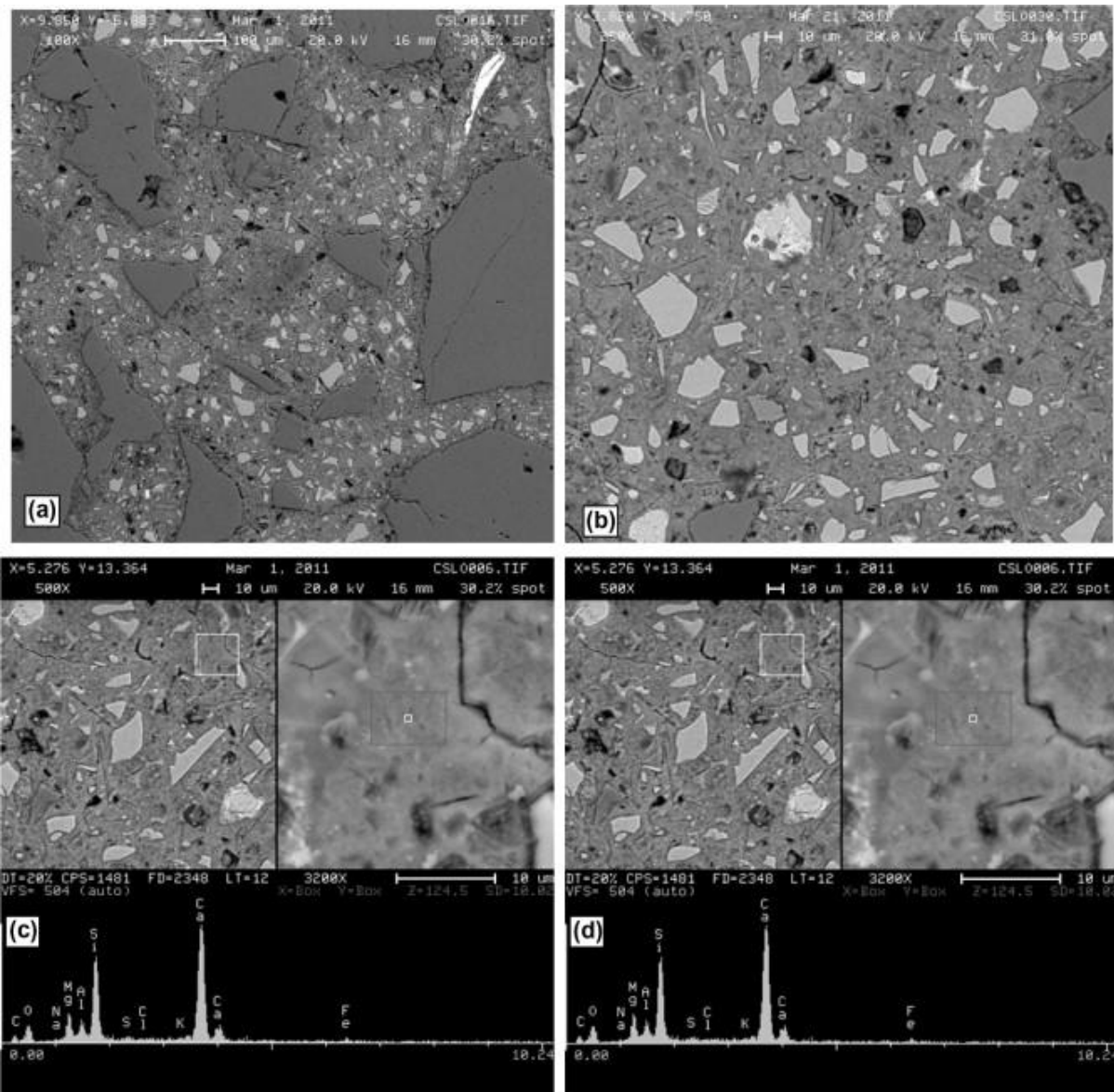


**Fig. 2.7** Typical micro-structural characteristics of reference concrete with 50% slag (CSL0) (a) paste aggregate bonds (b) hardened paste showing the residual slag particles and (c and d) Ca/Si ratio of the C-S-H gel (Zhang et al., 2012).



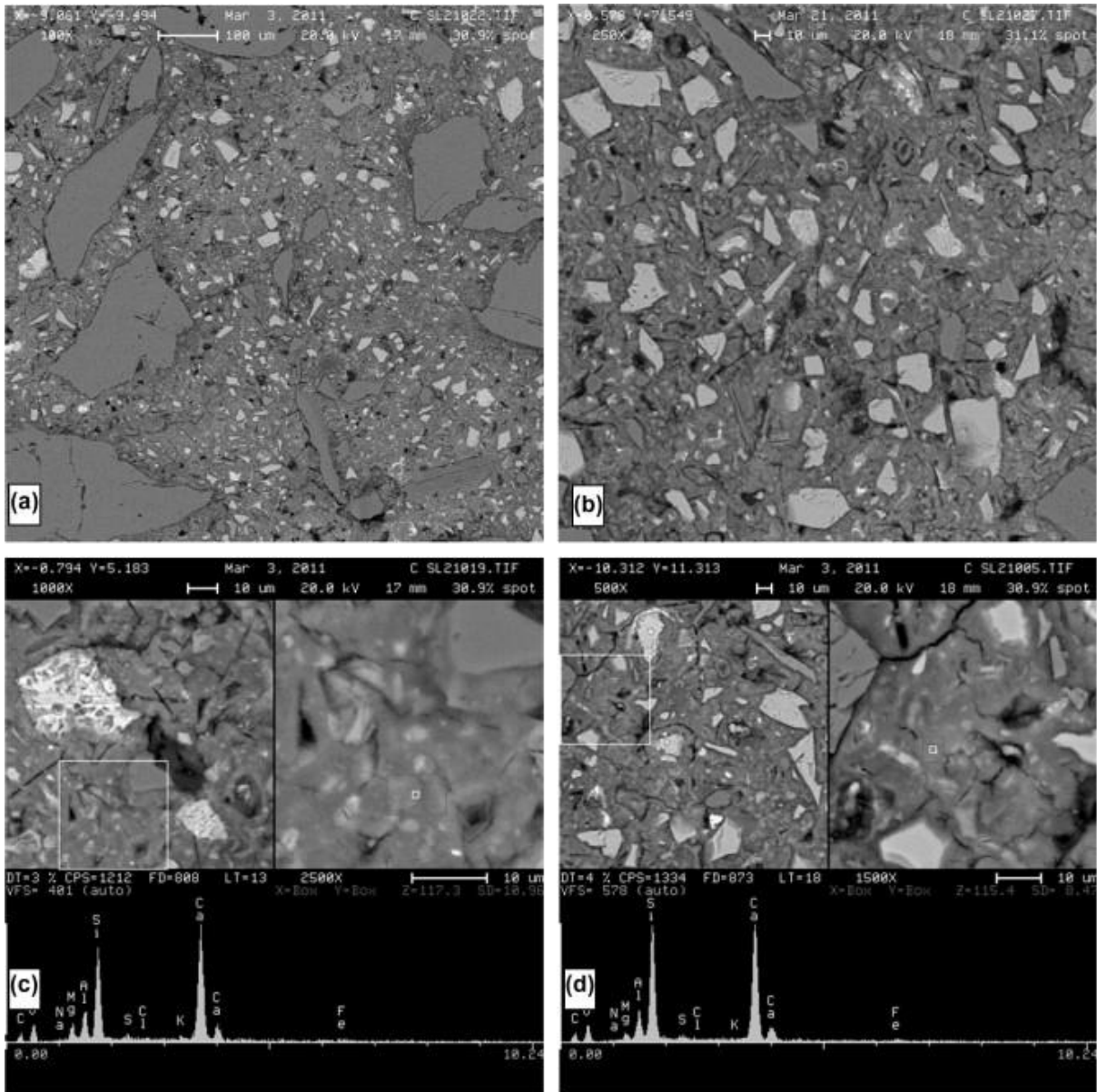


**Fig. 2.8** Typical micro-structural characteristics of 2% NS added slag concrete (CSL21) (a) paste aggregate bond (b) hardened paste showing the residual slag particles and (c and d) Ca/Si ratio of the C–S–H gel (Zhang et al., 2012).

### 2.4.5 Microstructural properties

Microstructural properties of HVS composites incorporated different types of nano materials such as NS and NT has been examined by few researchers (Nazari & Riahi, 2011d, 2011e; Zhang et al., 2012) through scanning electron microscopy (SEM) micrographs shown in **Figs.**

**2.7- 2.8** and found a more compact matrix and improved degree of hydration evaluated by thermogravimetric and XRD analysis. Another study (Jiang et al., 2020) investigated the cumulative porosity and pore size distribution of 70% super fine BFS containing hardened paste with the inclusion of 1% NS. It is concluded that the super fine BFS can play an outstanding role to reduce the large capillary pores and increasing the gel pores and the NS addition amplified that by reducing the porosity of OPC in the mix and resulted a super compacted paste matrix. Moreover, XRD data also revealed that NS addition was beneficial to improve the pozzolanic reaction of BFS and led to the consumption of CH and production of additional C-S-H gel.

### **2.5 Effect of nano materials on high volume slag-fly ash (HVS-FA) blended composites**

There is no study investigated the effect of nano materials on the high volume slag-fly ash (HVS-FA) blended concretes. However, one study found that inclusion of very fine NS into high volume fly ash-hydrated lime blended (HVFA-HL) paste can serve as nucleation sites, hence increased the early age hydration and resulted to a considerably higher peak of heat flow curve compared to HVFA-HL paste without NS (Gunasekara et al., 2020). It is also noted that the duration of dormant period was shortened of the samples containing NS. However, NS inclusion contributed to the amplification of the hydration rate of aluminate phase instead of silicate phase during the initial hydration period demonstrated in this study.

This study also investigated the effect of 3% addition of NS on the compressive strengths of 65% (49%FA + 13% HL) and 80% (59%FA+ 18%HL) fly ash-hydrated lime blended concrete mixes and it is concluded that 3% NS inclusion increased the 7days compressive strength by 50% and 98.6% and 28 days compressive strength by 10.3% and 35.9% compared to their counterpart control concrete without NS inclusion.

Similar to the HVFA and HVS composites, NS addition reduced the CH peak revealed in XRD analysis in HVFA-HL composites and produced new C-S-H gel by the pozzolanic reactions. This study also established that the addition of NS into the blended HVFA-HL mixes increased the fly ash reactivity led to the reduction of unhydrated or partially hydrated fly ash particles in early ages through the scanning electron microscopy (SEM) image analysis. HVFA-HL concrete production can reduce the carbon di-oxide emission significantly by 51-63%. However, the addition of 3% NS could add 2-15% more CO<sub>2</sub> into the atmosphere. On the other hand, NS addition leads to a slight increase in cost of concrete production than HVFA-HL

concrete without NS despite the factor of increase in strengths and reduction of CO<sub>2</sub> emission into the atmosphere can be beneficial recommended by the authors in this study.

## **2.6 Limitations and scopes**

From the above discussion, it is clear that HVS, HVFA and HVS-FA concrete can be an alternative option for low-carbon concrete. It is also apparent that the nano materials can improve the low early age strength properties and durability properties of high volume replacement of BFS and FA in concrete. Past studies have studied the properties of HVS concretes containing slag up to 50% as partial replacement of OPC containing nano materials and no study has been reported on the HVS-FA blended concrete. Though there is several research evidence suggested that a small amount of nano materials addition can make a big improvement in the early age properties and durability properties of the high volume replacement of cement by BFS, FA and BFS-FA blended mix. HVS, HVS-FA concretes can make a greener and sustainable construction materials but there very limited research have been investigated and very limited concrete properties have been studied.

## 2.7 References

- Agarkar, S. and M. Joshi, Study of effect of Al<sub>2</sub>O<sub>3</sub> nanoparticles on the compressive strength and workability of blended concrete. *Int J Curr Res*, 2012. 4: p. 382-4.
- Arefi, M., M. Javeri, and E. Mollaahmadi, To study the effect of adding Al<sub>2</sub>O<sub>3</sub> nanoparticles on the mechanical properties and microstructure of cement mortar. *Life Science Journal*, 2011. 8(4): p. 613-617.
- Balcikanli Bankir, M., et al., Effect of n-CaCO<sub>3</sub> on fresh, hardened properties and acid resistance of granulated blast furnace slag added mortar. *Journal of Building Engineering*, 2020. 29: p. 101209.
- Bentz, D.P., Activation energies of high-volume fly ash ternary blends: Hydration and setting. *Cement and Concrete Composites*, 2014. 53: p. 214-223.
- Bentz, D.P., et al., Fine limestone additions to regulate setting in high volume fly ash mixtures. *Cement and Concrete Composites*, 2012. 34(1): p. 11-17.
- De Weerd, K., et al., Synergy between fly ash and limestone powder in ternary cements. *Cement and Concrete Composites*, 2011. 41: p. 279-291.
- Drexler, K.E., C. Peterson, and G. Pergamit, Unbounding the future: the nanotechnology revolution. *Precision Engineering*, 1991. 13(4): p. 309.
- Feynman, R.P., There's plenty of room at the bottom. *Engineering and Science*, 1960: p. 22-36.
- Georgescu, M. and N. Saca, Properties of blended cement with limestone filler and fly ash content. *Scientific Bulletin*, 2009. 71: p. 1454-2331.
- Gunasekara, C., et al., Effect of nano-silica addition into high volume fly ash-hydrated lime blended concrete. *Construction and Building Materials*, 2020. 253: p. 119205.
- Güneyisi, E., et al., Fresh and rheological behavior of nano-silica and fly ash blended self-compacting concrete. *Construction and Building Materials*, 2015. 95: p. 29-44.
- Harilal, M., et al., High performance green concrete (HPGC) with improved strength and chloride ion penetration resistance by synergistic action of fly ash, nanoparticles and corrosion inhibitor. *Construction and Building Materials*, 2019. 198: p. 299-312.

Hou, P.-k., et al., Effects of colloidal nanosilica on rheological and mechanical properties of fly ash–cement mortar. *Cement and Concrete Composites*, 2013. 35(1): p. 12-22.

Huang, Q., et al., Modification of water absorption and pore structure of high-volume fly ash cement pastes by incorporating nanosilica. *Journal of Building Engineering*, 2021. 33: p. 101638.

Ibrahim, R.K., R. Hamid, and M.R. Taha, Fire resistance of high-volume fly ash mortars with nanosilica addition. *Construction and Building Materials*, 2012. 36: p. 779-786.

Jayapalan, A.R. and K.E. Kurtis, Effect of nano-sized titanium dioxide on early age hydration of Portland cement, in *Nanotechnology in construction: proceedings of the NICOM3. 3rd International symposium on nanotechnology in construction*, Z. Bittnar, et al., Editors. 2009: Prague, Czech Republic. p. 267–73.

Jiang, W., et al., Mechanical and hydration properties of low clinker cement containing high volume superfine blast furnace slag and nano silica. *Construction and Building Materials*, 2020. 238: p. 117683.

Jo, B.-W., et al., Characteristics of cement mortar with nano-SiO<sub>2</sub> particles. *Construction and Building Materials*, 2007. 21(6): p. 1351-1355.

Kawashima, S., et al., Modification of cement-based materials with nanoparticles. *Cement and Concrete Composites*, 2013. 36(Supplement C): p. 8-15.

Land, G. and D. Stephan, The influence of nano-silica on the hydration of ordinary Portland cement. *Journal of Materials Science*, 2012. 47(2): p. 1011-1017.

Li H, et al., Microstructure of cement mortar with nanoparticles. *Compos B Eng*, 2004. 35(2): p. 185-9.

Li, G., Properties of high-volume fly ash concrete incorporating nano-SiO<sub>2</sub>. *Cement and Concrete Research*, 2004. 34(6): p. 1043-1049.

Li, Z., et al., Investigations on the preparation and mechanical properties of the nano-alumina reinforced cement composite. *Materials Letters*, 2006. 60(3): p. 356-359.

Lin, D.F., et al., Improvements of nano-SiO<sub>2</sub> on sludge/fly ash mortar. *Waste Management*, 2008. 28(6): p. 1081-1087.

- Liu, M., et al., The synergistic effect of nano-silica with blast furnace slag in cement based materials. *Construction and Building Materials*, 2016. 126: p. 624-631.
- Liu, M., H. Tan, and X. He, Effects of nano-SiO<sub>2</sub> on early strength and microstructure of steam-cured high volume fly ash cement system. *Construction and Building Materials*, 2019. 194: p. 350-359.
- Liu, X., et al., Effects of colloidal nano-SiO<sub>2</sub> on the immobilization of chloride ions in cement-fly ash system. *Cement and Concrete Composites*, 2020. 110: p. 103596.
- Ma, B., et al., Influence of nano-TiO<sub>2</sub> on physical and hydration characteristics of fly ash-cement systems. *Construction and Building Materials*, 2016. 122: p. 242-253.
- Makar J.M., Margeson J., and L. J. Carbon nanotube/cement composites – early results and potential applications. . in *Proceedings of 3rd international conference on construction materials: performance, innovations and structural implications*. 2005. Vancouver, BC.
- Mei, J., et al., Influence of steam curing and nano silica on hydration and microstructure characteristics of high volume fly ash cement system. *Construction and Building Materials*, 2018. 171: p. 83-95.
- Mohseni, E., et al., Single and combined effects of nano-SiO<sub>2</sub>, nano-Al<sub>2</sub>O<sub>3</sub> and nano-TiO<sub>2</sub> on the mechanical, rheological and durability properties of self-compacting mortar containing fly ash. *Construction and Building Materials*, 2015. 84: p. 331-340.
- Murata, Y., et al., Air purifying pavement: Development of photocatalytic concrete blocks. *J Adv Oxidat Technol*, 1999. 4(2): p. 227-230.
- Nazari, A. and S. Riahi, Al<sub>2</sub>O<sub>3</sub> nanoparticles in concrete and different curing media. *Energy and Buildings*, 2011. 43(6): p. 1480-1488.
- Nazari, A. and S. Riahi, Effects of Al<sub>2</sub>O<sub>3</sub> nanoparticles on properties of self compacting concrete with ground granulated blast furnace slag (GGBFS) as binder. *Science China Technological Sciences*, 2011. 54(9): p. 2327-2338.
- Nazari, A. and S. Riahi, Splitting tensile strength of concrete using ground granulated blast furnace slag and SiO<sub>2</sub> nanoparticles as binder. *Energy and Buildings*, 2011. 43(4): p. 864-872.

Nazari, A. and S. Riahi, The effects of limewater on split tensile strength and workability of Al<sub>2</sub>O<sub>3</sub> nanoparticles binary blended concrete. *Journal of Composite Materials*, 2011. 45(9): p. 1059-1064.

Nazari, A. and S. Riahi, The effects of TiO<sub>2</sub> nanoparticles on physical, thermal and mechanical properties of concrete using ground granulated blast furnace slag as binder. *Materials Science and Engineering: A*, 2011. 528(4): p. 2085-2092.

Nazari, A. and S. Riahi, TiO<sub>2</sub> nanoparticles effects on physical, thermal and mechanical properties of self compacting concrete with ground granulated blast furnace slag as binder. *Energy and Buildings*, 2011. 43(4): p. 995-1002.

Nazari, A., et al., Influence of Al<sub>2</sub>O<sub>3</sub> nanoparticles on the compressive strength and workability of blended concrete. *J Am Sci*, 2010. 6(5): p. 6-9.

Pera, J., S. Husson, and B. Guilhot, Influence of finely ground limestone on cement hydration. *Cement and Concrete Composites*, 1999. 21: p. 99-105.

Qing, Y., et al., A comparative study on the pozzolanic activity between nano-SiO<sub>2</sub> and silica fume. *Journal of Wuhan University of Technology-Mater. Sci. Ed.*, 2006. 21(3): p. 153-157.

Qing, Y., et al., Influence of nano-SiO<sub>2</sub> addition on properties of hardened cement paste as compared with silica fume. *Construction and Building Materials* 2007. 21(3): p. 539–45.

Rao, S., P. Silva, and J. de Brito, Experimental study of the mechanical properties and durability of self-compacting mortars with nano materials (SiO<sub>2</sub> and TiO<sub>2</sub>). *Construction and Building Materials*, 2015. 96: p. 508-517.

Rashad, A.M., H.A. El-Nouhy, and S.R. Zeeidan, An Investigation on HVS Paste Modified with Nano-SiO<sub>2</sub> Impaired to Elevated Temperatures. *Arabian Journal for Science and Engineering*, 2018. 43(10): p. 5165-5177.

Said, A.M., et al., Properties of concrete incorporating nano-silica. *Construction and Building Materials*, 2012. 36: p. 838-844.

Salvetat J-P, et al., Mechanical properties of carbon nanotubes. *Appl Phys Mater Sci Process*, 1999. 69: p. 255–60.

Sato, T. and F. Diallo, Seeding effect of nano-CaCO<sub>3</sub> on the hydration of tricalcium silicate. *Journal of the Transportation Research Board*, 2010. 2141: p. 61-67.

Sato, T. and J.J. Beaudoin, Effect of nano-CaCO<sub>3</sub> on hydration of cement containing supplementary cementitious materials *Advances in Cement Research*, 2011. 23: p. 33-43.

Shaikh, F.U.A. and S.W.M. Supit, Chloride induced corrosion durability of high volume fly ash concretes containing nano particles. *Construction and Building Materials*, 2015. 99: p. 208-225.

Shaikh, F.U.A. and S.W.M. Supit, Mechanical and durability properties of high volume fly ash (HVFA) concrete containing calcium carbonate (CaCO<sub>3</sub>) nanoparticles. *Construction and Building Materials*, 2014. 70(Supplement C): p. 309-321.

Shaikh, F.U.A., S.W.M. Supit, and P.K. Sarker, A study on the effect of nano silica on compressive strength of high volume fly ash mortars and concretes. *Materials & Design*, 2014. 60: p. 433-442.

Siang Ng, D., et al., Influence of SiO<sub>2</sub>, TiO<sub>2</sub> and Fe<sub>2</sub>O<sub>3</sub> nanoparticles on the properties of fly ash blended cement mortars. *Construction and Building Materials*, 2020. 258: p. 119627.

Sobolev, K. and M. Ferrada-Gutiérrez, How nanotechnology can change the concrete world: Part 1. *American Ceramic Society Bulletin*, 2005. 84(10): p. 14–7.

Sobolev, K., et al. Engineering of SiO<sub>2</sub> nanoparticles for optimal performance in nano cement based materials. in *Nanotechnology in construction: proceedings of the NICOM3 (3rd international symposium on nanotechnology in construction)*. 2009. Prague, Czech Republic.

Srivastava, D., C. Wei, and K. Cho, Nanomechanics of carbon nanotubes and composites. *Applied Mechanics Reviews*, 2003. 56: p. 215–30.

Thomas, J.J., H.M. Jennings, and J.J. Chen, Influence of Nucleation Seeding on the Hydration Mechanisms of Tricalcium Silicate and Cement. *The Journal of Physical Chemistry C*, 2009. 113(11): p. 4327-4334.

Vallee F, et al. Cementitious materials for self-cleaning and depolluting facade surfaces. in *In: RILEM proceedings 2005. PRO 41 RILEM international symposium on environment-conscious materials and systems for sustainable development*. 2004.

Vishwakarma, V., et al., Enhancing antimicrobial properties of fly ash mortars specimens through nanophase modification. *Materials Today: Proceedings*, 2016. 3(6): p. 1389-1397.



Wang, J., et al., Synergistic effects of nano-silica and fly ash on properties of cement-based composites. *Construction and Building Materials*, 2020. 262: p. 120737.

Zaidi, A.K.A.A., B. Demirel, and C.D. Atis, Effect of different storage methods on thermal and mechanical properties of mortar containing aerogel, fly ash and nano-silica. *Construction and Building Materials*, 2019. 199: p. 501-507.

Zhang, M.-H. and J. Islam, Use of nano-silica to reduce setting time and increase early strength of concretes with high volume of fly ash or slag. *Construction and Building Materials*, 2012. 29: p. 573-580.

Zhang, M.-H., J. Islam, and S. Peethamparan, Use of nano-silica to increase early strength and reduce setting time of concretes with high volumes of slag. *Cement and Concrete Composites*, 2012. 34(5): p. 650-662.

Zhu, J., et al., Effects of colloidal nanoBoehmite and nanoSiO<sub>2</sub> on fly ash cement hydration. *Construction and Building Materials*, 2015. 101: p. 246-251.

*All reasonable efforts have been made to acknowledge the authors of the copyright material. It would be highly appreciated if I can hear from any authors has been ignored or incorrectly acknowledged.*

## Chapter 3: High volume slag and high volume slag-fly ash blended paste containing nano silica

---

This chapter presents the effect of different percentage of nano silica on the compressive strengths and microstructure of high volume slag (HVS) and high volume slag-fly ash blended pastes. In this chapter, the addition of 1-4% nano silica into the 70-90% BFS and BFS-FA replaced paste specimens and their effects on the compressive strengths after 28 days of wet curing and microstructure through mercury intrusion porosimetry, thermogravimetric analysis, x-ray diffraction analysis, scanning electron microscopy and energy dispersive x-ray spectroscopy were investigated. The reduction of carbon footprint by reducing the use of ordinary Portland cement in the concrete construction while maintaining the strength and other properties are also demonstrated in this chapter.

### 3.1 Overview

Significant research have been conducted around the world to improve the environmental friendliness of ordinary Portland cement (OPC) concrete by partially replacing OPC with various industrial by-products such fly ash, blast furnace slag (BFS), silica fume, etc. and by partially replacing virgin aggregates with recycled aggregates. However, most effective approach is the partial replacement of OPC using above by-products as carbon footprint of OPC is much higher than that of natural aggregates (Malhotra, 2002 & Mehta, 2001). The most promising way to significantly reduce the carbon footprint of OPC is the use of high volume fractions of these by-product materials in concrete.

---

The content of this chapter has been written based on the paper published in the following journal.

Shaikh, F.U.A. and A. Hosan, Effect of nano silica on compressive strength and microstructures of high volume blast furnace slag and high volume blast furnace slag-fly ash blended pastes. *Sustainable Materials and Technologies*, 2019. **20**: p. e00111.

Many research has also been conducted to study various mechanical and durability properties of concretes containing high volume fly ash and slag. Although the use of high volume fly ash and high volume slag improve workability, long term mechanical and durability properties and reduce heat of hydration, the early age mechanical and durability properties until 28 days are inferior than that of control concrete (Hooton, 2000 & Rashad, 2015).

The slow pozzolanic reaction of fly ash and slag with Portlandite ( $\text{Ca(OH)}_2$ ) from cement hydration is the reason for such inferior properties at early stage of concrete containing high volume fractions of fly ash and slag as partial replacement of OPC (Oner and Akyuz, 2007). Various micro-materials (ultrafine fly ash, silica fume, etc.) and nano-materials (nano silica, nano  $\text{CaCO}_3$ , nano  $\text{Al}_2\text{O}_3$ , etc.) are used in high volume fly ash and high volume slag concretes to address this limitation. Due to much higher specific surface area and much smaller particle sizes of these micro- and nano-materials than those of fly ash and slag, pozzolanic reaction occurs faster and higher amount of additional calcium silicate hydrate (C-S-H) gels are formed. As a result, the microstructure of the matrix of those concretes becomes denser. In addition, these micro- and nano-materials also act as fillers of the matrix to densify the microstructures.

A comprehensive review of the use of various micro- and nano-materials in high volume fly ash concrete and the effect of nano materials on the mechanical and durability properties of concrete containing slag as partial replacement of OPC are has discussed in Chapter 2. Zhang et al. (2012) studied the effect of 0.5%, 1% and 2% NS on mechanical properties and microstructures of concrete containing 50% slag as partial replacement of OPC. In their study 2% NS is found as the optimum content and increase the 3 and 7 days compressive strength by 22% and 18%, respectively. Liu et al. (2016) studied the effect of 3% NS on properties of concretes containing various quantities of slag from 10% to 40% and reported highest compressive strength of about 59 MPa in concrete containing 30% slag and 3% NS compared to 51 MPa in control concrete at 28 days. In another study, Chithra et al. (2016) studied the effect of NS on the concrete containing various copper slag contents up to 50% as partial replacement of fine aggregates. The effects of NS and nano  $\text{TiO}_2$  (NT) on the properties of concretes containing various slag contents of 15 to 60% are evaluated. Nagendra et al. (2016) reported about 37% increase in compressive strength of concrete containing 20% slag due to addition of 4% NS compared to that without NS. It can be seen in above literature review that the NS is used to improve the properties of concrete containing slag content of up to 60%. However, to improve the environmental friendliness of OPC concrete the slag content above 60% as partial replacement of OPC is required. The use of NS can improve the early stage

mechanical properties of such high volume slag concretes. This chapter presents the effects of various high volume BFS contents of 60% to 90% as partial replacement of OPC on 28 days compressive strength and microstructure changes of concrete. The effects of various hybrid combinations of BFS and class F fly ash (FA) in the above high volume fractions are also studied. The effects of nano silica contents of 1% to 4% on the 28 days compressive strength and microstructure changes of above high volume BFS and BFS-FA pastes are also evaluated in this study. Finally, carbon-di-oxide (CO<sub>2</sub>) emission analysis of all pastes are conducted to evaluate the beneficial effect of addition of high volume BFS and combined high volume BFS-FA addition on the carbon footprint.

### **3.2 Experimental program**

This study is consisted of three parts. In the first part, four high volume BFS pastes containing 60%, 70%, 80% and 90% BFS by weight as partial replacement of OPC are considered. In the second part, the effect of three hybrid combinations of BFS and FA at total contents of 60%, 70%, 80% and 90% by weight are considered, where FA is used at 30%, 40% and 50% by weight of BFS. In the third part, the effect of nano silica content of 1% to 4% by weight on the high volume BFS pastes containing 70%, 80% and 90% BFS and high volume BFS-FA pastes containing 49% BFS+21% FA and 56% BFS+24% FA are evaluated. Therefore, total thirty seven mixes are considered in this study.

### **3.3 Materials, mix proportions and casting**

The cement used in this study was ordinary Portland cement (OPC). The fly ash (FA) was class F fly ash supplied by Eraring power station of New South Wales in Australia. The ground granulated blast furnace slag (BFS) was supplied by BGC cement of Australia. The nano silica (NS) was purchased from Nanostructured & Amorphous Materials, Inc. of USA. **Table 3.1** shows the physical and chemical properties of OPC, FA, BFS and NS, while **Figs. 3.1-3.2** show the X-ray diffraction (XRD) analysis of FA, BFS and NS. It can be seen by comparing the results that NS was highly amorphous compared to FA and BFS. Among FA and BFS, BFS is more amorphous with amorphous content of 95.7% compared to 67.8% amorphous content of FA based on quantitative XRD analysis. Detail mix proportions of high volume BFS pastes, high volume BFS-FA pastes and those containing NS are shown in **Tables 3.2-3.3**. It can be seen that water/binder ratio of all mixes were kept constant at 0.4. In the case of mixes containing NS, a naphthalene sulphonate based superplasticizer was used to maintain the workability of pastes. All pastes were mixed in Hobart mixer, where cement, FA and BFS were

mixed first for approximately 3 min. Water was added and mixed for further 3 min. In the case of high volume BFS and high volume BFS-FA pastes containing NS, the NS was first ultrasonically dispersed in water containing superplasticizer using ultrasonic mixer for 30 minutes shown in **Fig. 3.3** and then added with remaining water during mixing. The paste samples of 50 mm cubes were cast and demoulded after 24 h. The specimens were cured in water at room temperature for 28 days.

**Table 3.1** Chemical analysis and physical properties of OPC, fly ash, blast furnace slag and nano silica

<b>Chemical Analysis</b>	<b>Cement (wt. %)</b>	<b>Class F Fly Ash (wt. %)</b>	<b>Blast furnace slag (wt. %)</b>	<b>Nano silica (wt. %)</b>
SiO <sub>2</sub>	21.1	51.11	32.5	99
Al <sub>2</sub> O <sub>3</sub>	5.24	25.56	13.56	-
Fe <sub>2</sub> O <sub>3</sub>	3.1	12.48	0.85	-
CaO	64.39	4.3	41.2	-
MgO	1.1	1.45	5.10	-
MnO	-	0.15	0.25	-
K <sub>2</sub> O	0.57	0.7	0.35	-
Na <sub>2</sub> O	0.23	0.77	0.27	-
P <sub>2</sub> O <sub>5</sub>	-	0.885	0.03	-
TiO <sub>2</sub>	-	1.32	0.49	-
SO <sub>3</sub>	2.52	0.24	3.2	-
LOI	1.22	0.57	1.11	-
<b>Physical Properties</b>				
Particle size	25-40% ≤7µm	50% of 10 µm	40% of 10 µm	25 nm
Specific gravity	2.7 to 3.2	2.6	-	2.2 to 2.6
Surface area (m <sup>2</sup> /g)	-	-	-	160

**Table 3.2** Mix proportions of high volume slag and high volume slag-fly ash blend cement pastes

		Mixes	OPC	BFS	Fly ash	Water/ binder
Control		OPC	1	-	-	0.4
High volume slag contents (wt.%)		60BFS	0.4	0.6	-	0.4
		70BFS	0.3	0.7	-	0.4
		80BFS	0.2	0.8	-	0.4
		90BFS	0.1	0.9	-	0.4
Effect of fly ash as partial replacement of BFS	30 wt.% of 60% BFS	42BFS18FA	0.4	0.42	0.18	0.4
	40 wt.% of 60% BFS	36BFS24FA	0.4	0.36	0.24	0.4
	50 wt.% of 60% BFS	30BFS30FA	0.4	0.30	0.30	0.4
	30 wt.% of 70% BFS	49BFS21FA	0.3	0.49	0.21	0.4
	40 wt.% of 70% BFS	42BFS28FA	0.3	0.42	0.28	0.4
	50 wt.% of 70% BFS	35BFS35FA	0.3	0.35	0.35	0.4
	30 wt.% of 80% BFS	56BFS24FA	0.2	0.56	0.24	0.4
	40 wt.% of 80% BFS	48BFS32FA	0.2	0.48	0.32	0.4
	50 wt.% of 80% BFS	40BFS40FA	0.2	0.40	0.40	0.4
	30 wt.% of 90% BFS	63BFS27FA	0.1	0.63	0.27	0.4
	40 wt.% of 90% BFS	54BFS36FA	0.1	0.54	0.36	0.4
	50 wt.% of 90% BFS	45BFS45FA	0.1	0.45	0.45	0.4

**Table 3.3** Mix proportions of high volume slag and high volume slag-fly ash blend cement pastes containing nano silica

	Nnao Silica (wt.%)	Mixes	OPC	BFS	Fly ash	Nano silica	Water/binder	Super-Plasticizer* (wt.%)
70% BFS	1%	69BFS1NS	0.3	0.69	-	0.01	0.4	-
	2%	68BFS2NS	0.3	0.68	-	0.02	0.4	-
	3%	67BFS3NS	0.3	0.67	-	0.03	0.4	0.5
	4%	66BFS4NS	0.3	0.66	-	0.04	0.4	0.5
80% BFS	1%	79BFS1NS	0.2	0.79	-	0.01	0.4	-
	2%	78BFS2NS	0.2	0.78	-	0.02	0.4	0.5
	3%	77BFS3NS	0.2	0.77	-	0.03	0.4	0.5
	4%	76BFS4NS	0.2	0.76	-	0.04	0.4	0.5
90% BFS	1%	89BFS1NS	0.1	0.89	-	0.01	0.4	0.5
	2%	88BFS2NS	0.1	0.88	-	0.02	0.4	0.5
	3%	87BFS3NS	0.1	0.87	-	0.03	0.4	1.0
	4%	86BFS4NS	0.1	0.86	-	0.04	0.4	1.0
Combined FA+BFS Total= 70%	1%	49BFS20FA1NS	0.3	0.485	0.205	0.01	0.4	0.5
	2%	49BFS19FA2NS	0.3	0.48	0.20	0.02	0.4	0.5
	3%	49BFS18FA3NS	0.3	0.475	0.195	0.03	0.4	1.0
	4%	49BFS17FA4NS	0.3	0.47	0.19	0.04	0.4	1.0
Combined FA+BFS Total= 80%	1%	56BFS23FA1NS	0.2	0.555	0.235	0.01	0.4	0.5
	2%	56BFS22FA2NS	0.2	0.55	0.23	0.02	0.4	0.5
	3%	56BFS21FA3NS	0.2	0.545	0.225	0.03	0.4	1.0
	4%	56BFS20FA4NS	0.2	0.54	0.22	0.04	0.4	1.0

Note: Superplasticizer was used as wt. % of binder (OPC+BFS+FA+NS)

### 3.4 Testing methods

Compressive strength of the specimens were tested according to ASTM: C109 using a loading rate of 0.33 MPa/s. In order to observe the changes in reaction phases in cement pastes containing high volume BFS and BFS-FA blends due to inclusion of NS thermogravimetric analysis (TGA), X-ray diffraction (XRD) analysis, Mercury intrusion porosimetry (MIP), scanning electron microscopy (SEM) and energy dispersive X-ray spectroscopy (EDS) were done on selected samples.

For the XRD analysis, the samples were measured with a D8 Advance Diffractometer (Bruker-AXS) using copper radiation and a Lynx Eye position sensitive detector. The diffractometer scanned the samples from 7° to 70° (2θ) in steps of 0.015° at a scanning rate of 0.5°/ min. XRD patterns were obtained using Cu Ka lines ( $k = 1.5406 \text{ \AA}$ ). A knife edge collimator was fitted to reduce air scatter. SEM analyses were performed using a Zeiss EVO 40XVP microscope

equipped with an energy dispersive X-ray analyser. The thermal stability of the samples was studied by thermogravimetric analysis (TGA). A Mettler Toledo TGA one star system analyser was used for all these measurements. Samples weighing 25 mg were placed in an alumina crucible and the tests were carried out in an Argon atmosphere at a heating rate of 10°C/min from 25 to 1000°C.

Mercury intrusion porosimetry (MIP) was used to measure the pore volume and pore size distribution of pastes samples. The pore diameter and intruded mercury volume were recorded at each pressure point over a pressure range of 0.0083 to 207 MPa. The pressures values were converted into equivalent pore diameters using the Washburn expression (Washburn, E.W., 1921), as expressed in Eq. (1):

$$d = -\frac{4\gamma\cos\theta}{p} \quad \text{Eq. 1}$$

where,  $d$  is the pore diameter ( $\mu\text{m}$ ),  $\gamma$  is the surface tension (mN/m),  $\theta$  is the contact angle between mercury and the pore wall ( $^\circ$ ), and  $P$  is the net pressure across the mercury meniscus at the time of the cumulative intrusion measurement (MPa).

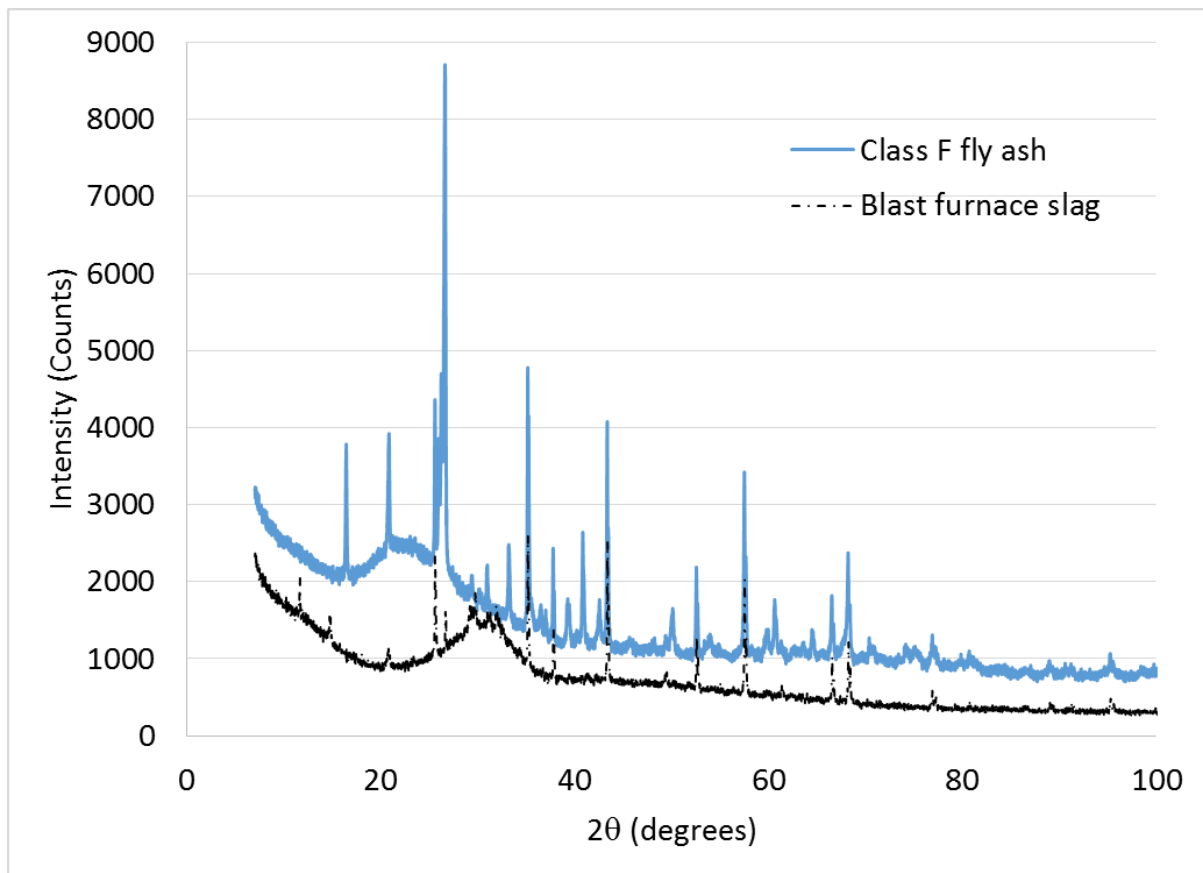


**Fig. 3.1** XRD analysis of class F fly ash and blast furnace slag



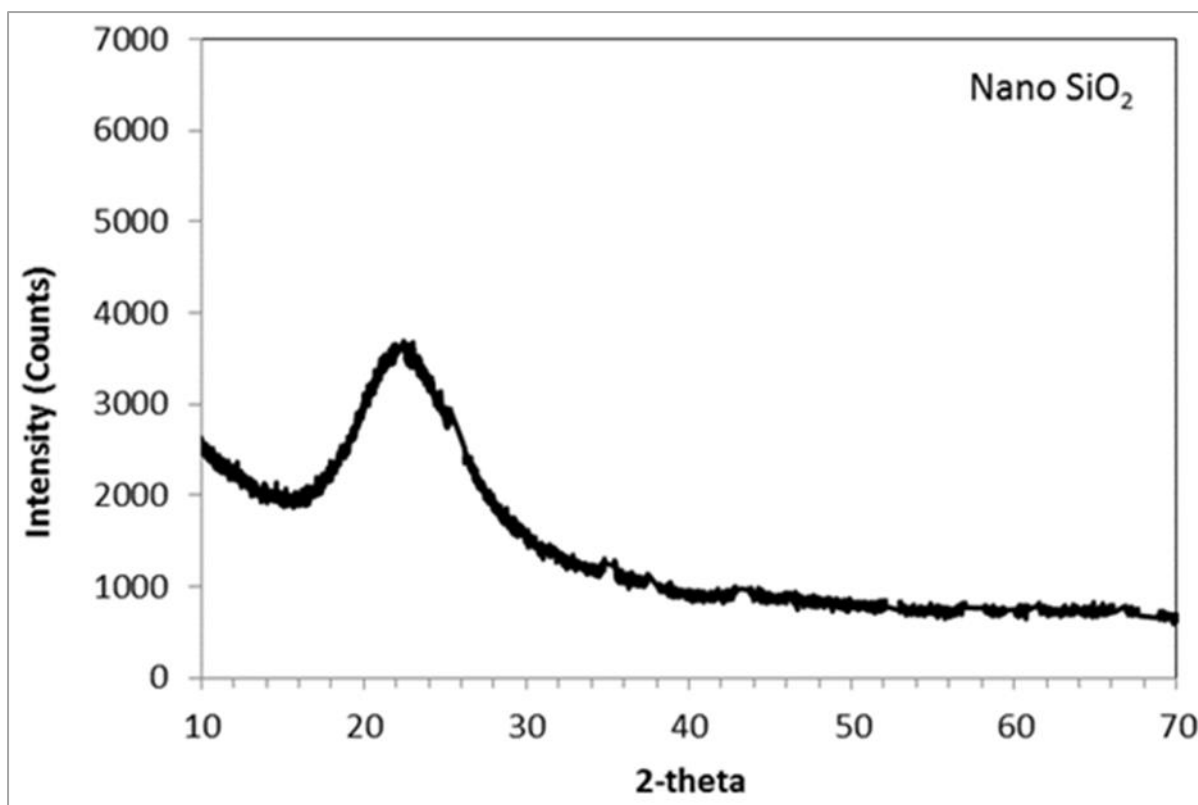


**Fig. 3.2** XRD analysis of nano silica

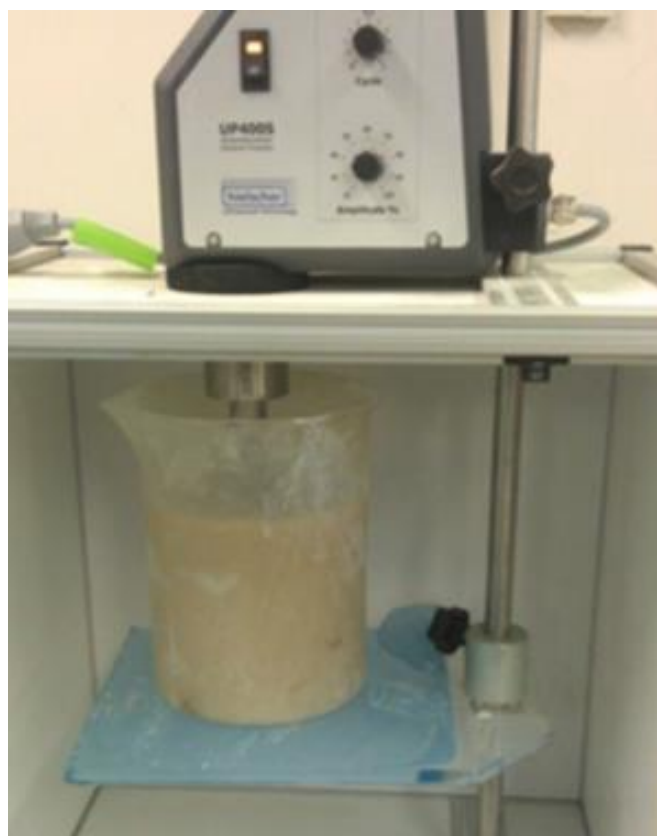


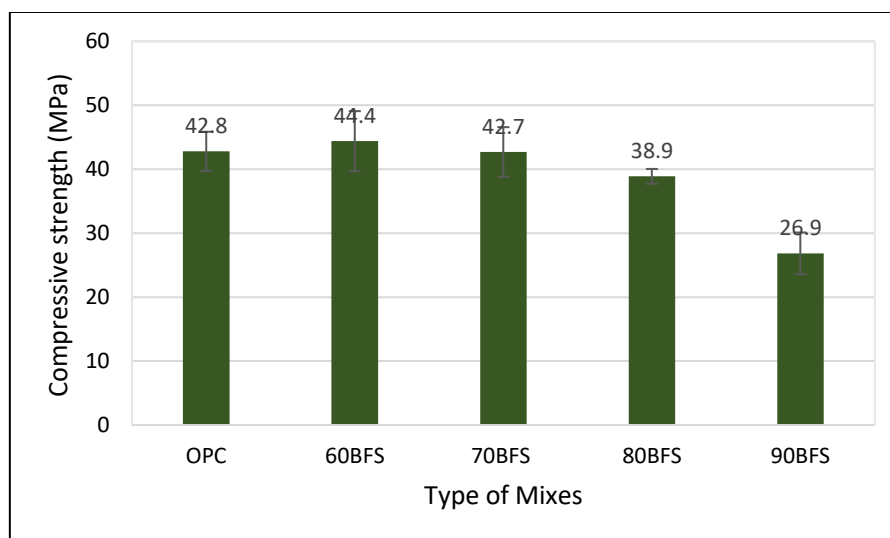
**Fig. 3.3** Ultrasonic mixing of nano silica in water containing superplasticizer

### 3.5 Results and discussion

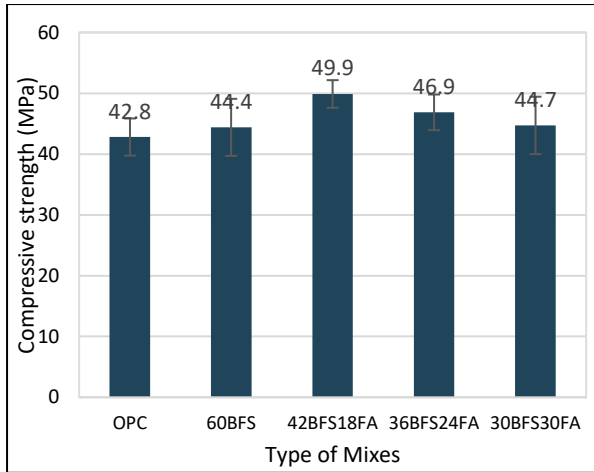
#### 3.5.1 Compressive strength

##### 3.5.1.1 Effects of high volume blast furnace slag and high volume blast furnace slag –fly ash

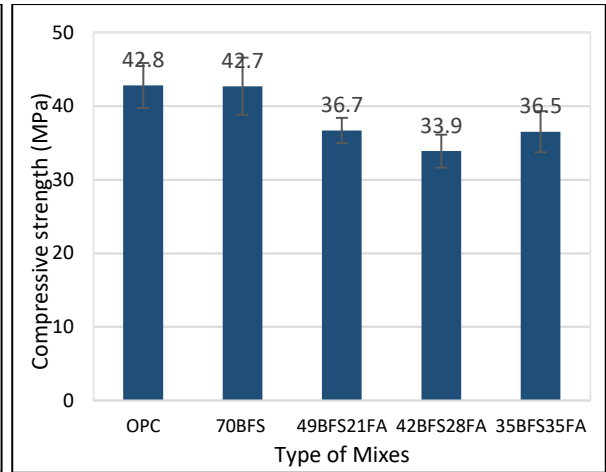
**Fig. 3.4** shows the measured 28 days compressive strength of control OPC paste and various high volume BFS and high volume BFS-FA pastes. The standard deviation (SD) in the form of error bar is also shown in each mix in the same figure. It can be seen in **Fig. 3.4a** that the compressive strength of high volume BFS pastes decrease with increase in BFS contents as partial replacement of OPC. It can also be seen that at BFS content of 60% the compressive strength is increased by 4% compared to control OPC paste and at BFS content of 70% the compressive strength is similar to OPC. However, about 9% and 37% reductions in compressive strength are observed at BFS contents of 80% and 90%, respectively. Improvement in compressive strength of cement paste containing 60% BFS is also reported in other studies (El-Chabib & Syed, 2013). The effects of various FA contents of 30%, 40% and 50% of BFS as partial replacement of BFS are shown in **Figs. 3.4b-e**. It can be seen in **Fig. 3.4b** that the compressive strength of all high volume BFS-FA pastes is higher than that of high volume BFS paste containing 60% BFS and control OPC paste. However, with increase in FA contents this improvement decreases. In the case of higher combined BFS and FA contents e.g., 70%, 80% and 90% no improvement in compressive strength is observed due to addition of FA as partial replacement of BFS and compressive strength decreases with increase in combined BFS and FA contents presumably due to reduction in total CaO content in the mixes.



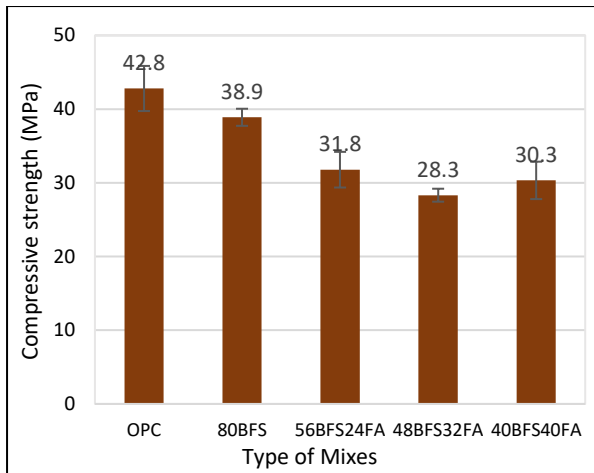
(a)



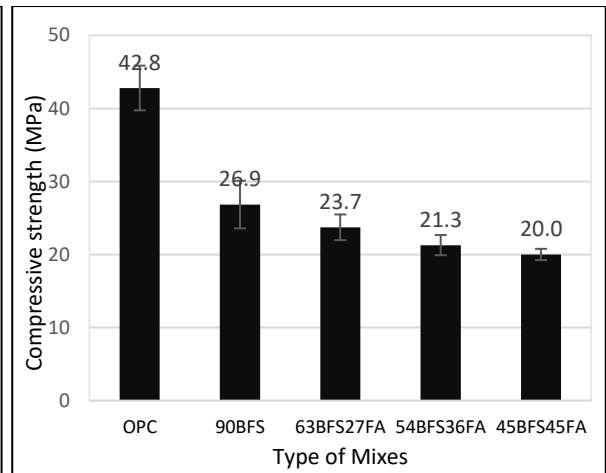
(b)



(c)



(d)



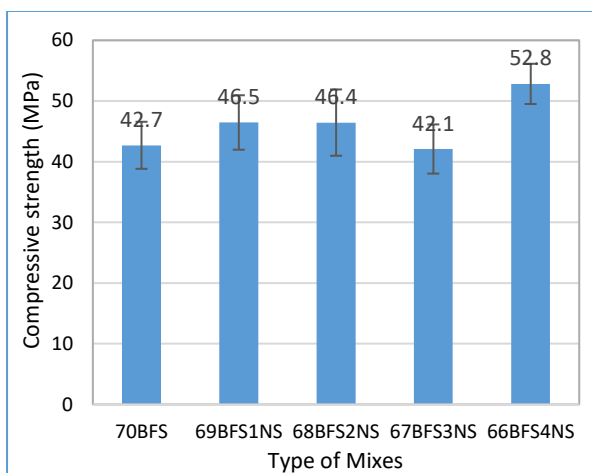
(e)

**Fig. 3.4** Compressive strength of high volume BFS pastes and combined BFS-FA pastes measured at 28 days

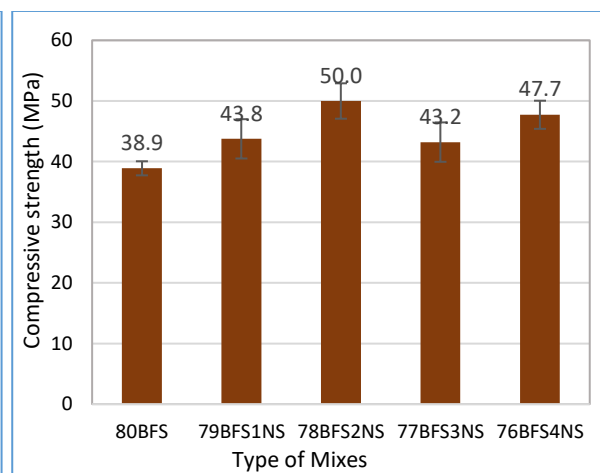
### 3.5.1.2 Effect of nano silica in high volume blast furnace slag and high volume blast furnace slag-fly ash

It can be seen in previous section that the compressive strength of high volume BFS paste containing 60% BFS is higher than the control OPC paste. Therefore, this BFS content is not considered in this part of this study. The effects of various NS contents of 1% to 4% on compressive strength of high volume BFS and high volume BFS-FA pastes are shown in **Fig. 3.5**. **Fig. 3.5a** shows that due to addition of NS the compressive strength of high volume BFS paste containing 70% BFS is higher than that without NS. The compressive strength is increased by 9% to 24% due to addition of NS. In the case of high volume BFS pastes

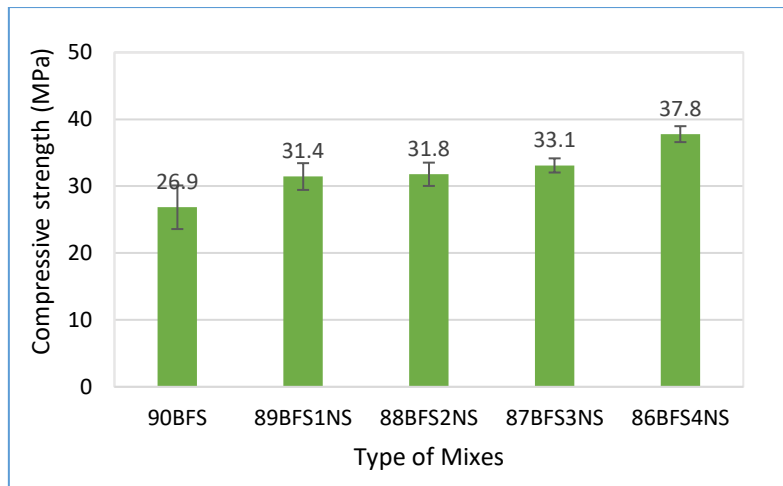
containing 80% and 90% BFS the improvement in compressive strength due to addition of NS is even better than 70% BFS content. It can be seen in **Figs. 3.5b-c** about 11-29% and 17-41% improvement in compressive strength due to addition of various amount of NS in pastes containing 80% and 90% BFS, respectively. While the compressive strength of high volume BFS pastes containing 70% and 80% BFS due to addition of NS is higher than that of control OPC paste, however, the compressive strength of paste containing 90% BFS is much lower than OPC paste despite the addition of NS. This can be due to significantly lower level of Portlandite generated in this mix due to very high volume of OPC replacement. In the case of pastes containing combined BFS and FA as shown in **Figs. 3.5d-e**, it can be seen that the addition of more than 2% NS significantly improves the compressive strength by 22-59% of paste containing total BFS and FA content of 70%, which is higher than paste containing 70% BFS. In the case of combined BFS and FA content of 80% containing NS no such significant improvement is observed but still improved the compressive strength by 5-21%, however, the compressive strength of this paste for all NS contents is still lower than that of control OPC paste. The improved compressive strength due to addition of NS in pastes containing combined BFS and FA than the pastes containing BFS can be interpreted as the better dispersion of NS in those mixes due to spherical shape of the FA particles. It can also be seen an increasing trend in compressive strength with increase in NS content up to 2% in all high volume BFS and combined BFS and FA pastes, however, beyond 2% no such increasing trend is observed and in many cases compressive strength is decreased e.g. in pastes containing 70% and 80% BFS and combined BFS and FA content of 80%.



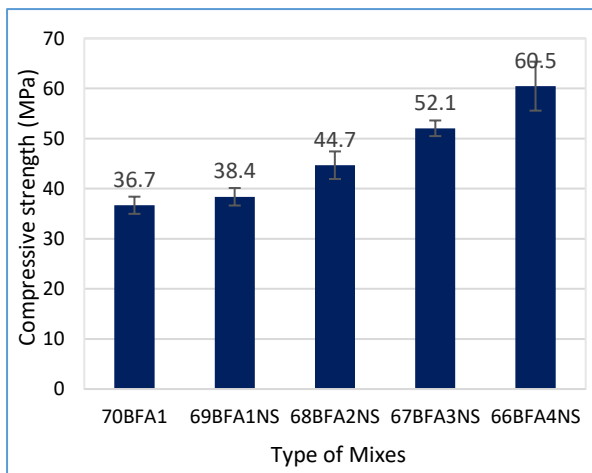
(a)



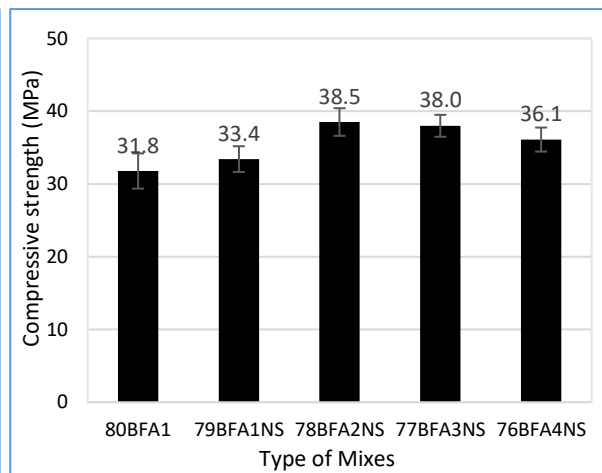
(b)



(c)



(d)



(e)

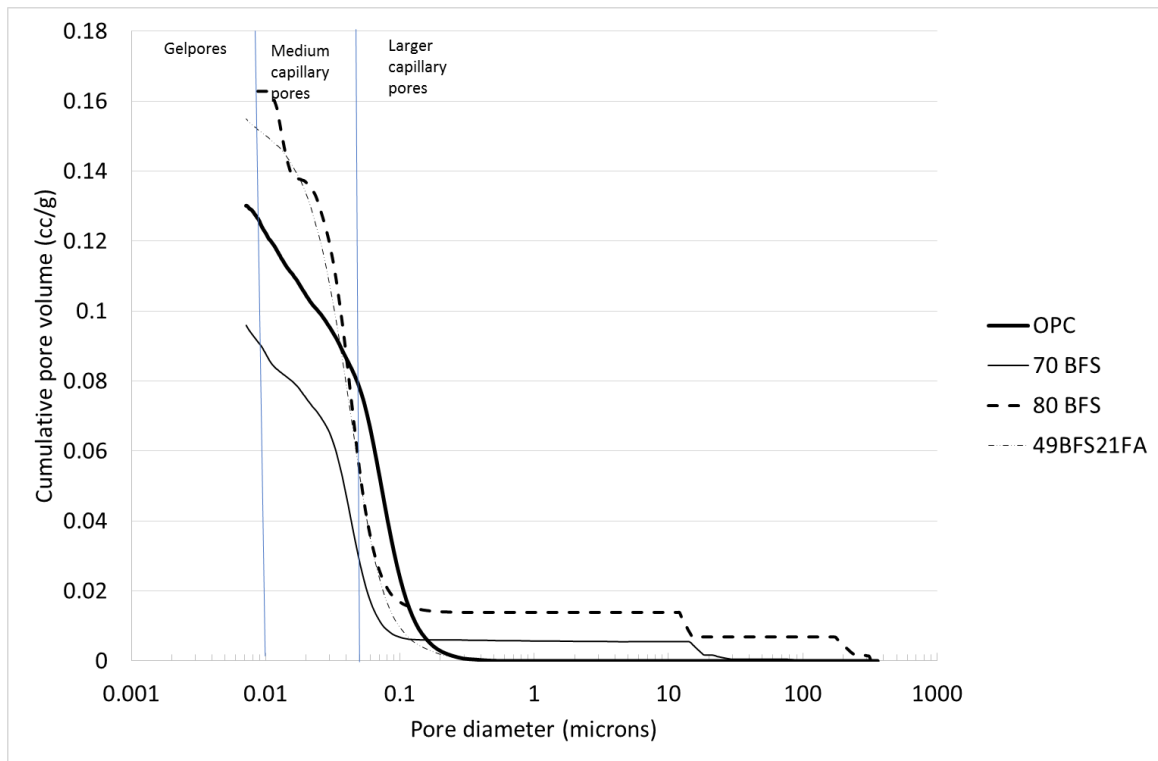
**Fig. 3.5** Effect of various nano silica contents on compressive strength of high volume BFS pastes and combined high volume BFS-FA pastes measured at 28 days

### 3.5.2 Microstructures

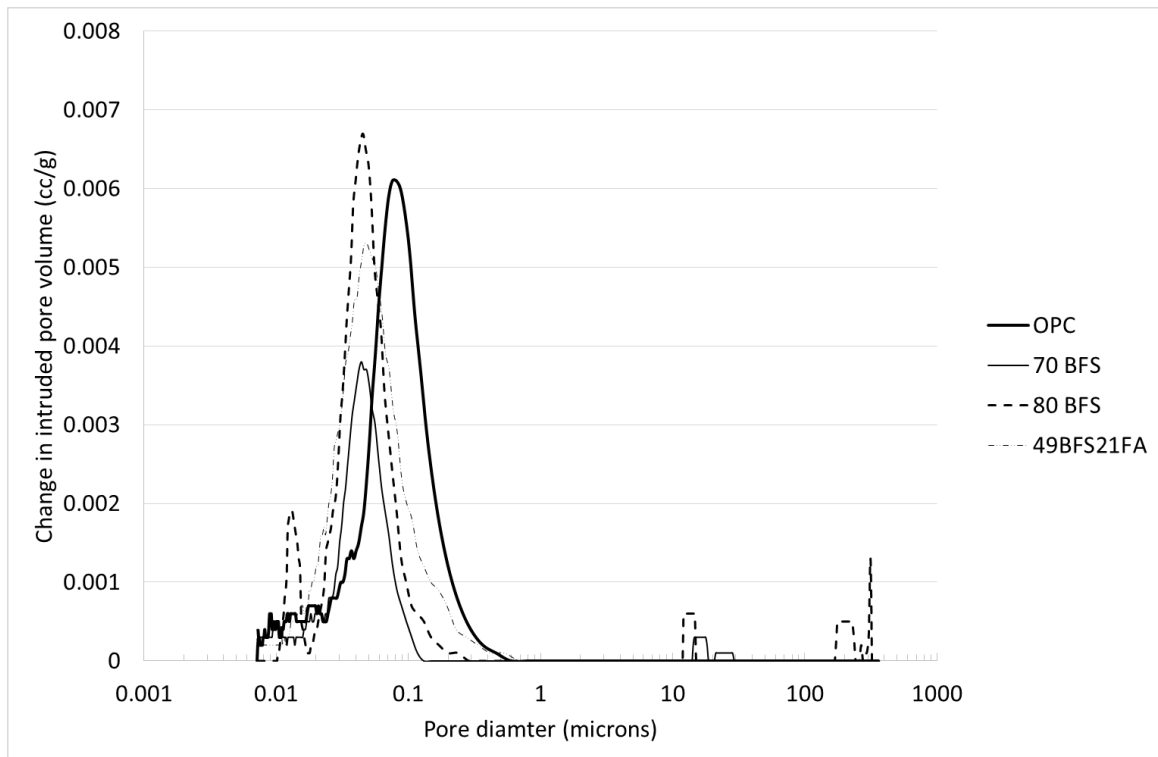
It can be seen in above compressive strength results that the high volume BFS pastes containing 70% and 80% BFS and combined BFS and FA content of 70% exhibited higher compressive strength than that of control OPC paste due to addition of NS. These mixes contain significantly less OPC hence much lower carbon footprint of concrete made using these blends. Therefore, in the microstructural analysis the changes of microstructures in terms of their pore sizes and volumes, conversion of Portlandite to secondary C-S-H through pozzolanic reaction and formation of new mineral phases are studied due to addition of NS.

### 3.5.2.1 Mercury intrusion porosimetry (MIP)

**Figs. 3.6-3.7** show the cumulative pore volume and distribution of various pore sizes of high volume BFS and combined BFS and FA pastes with and without NS. It can be seen in **Fig. 3.6a** that the pore volume of large capillary pores corresponding to pore diameter  $>0.05$  microns increases in cement paste due to addition of high volume BFS contents of 70% and 80% as partial replacement of OPC. However, the volume of medium capillary pores and gel pores corresponding to pore diameters 0.05-0.01 micron and  $<0.01$  microns, respectively are decreased due to addition of 70% BFS compared to control OPC paste. However, in the case of paste containing 80% BFS the volume of medium capillary pores and gel pores are higher than OPC paste. By comparing the pastes containing two BFS contents, it can be seen that at 70% BFS content the total pore volume of all pores is less than at 80% BFS content, which might be the reason for observed higher compressive strength in the former paste than the latter as large capillary pores might have caused stress concentration. On the other hand, in the paste containing combined BFS and FA with a total content of 70% the pore volume of larger capillary pores is reduced significantly compared to both high volume BFS pastes and control OPC paste. The distribution of pores having different diameters in all pastes is shown in **Fig. 3.6b**. The region under the curves represent the concentration of pores and the peak point of the curve represents the critical pore diameter. By comparing different curves, it can be seen that the maximum concentration of pores in OPC paste is in 0.03-0.2 microns range which is in lower side of large capillary pores. However, in the case of pastes containing 70% and 80% BFS and combined BFS and FA content of 70% the peak of their curves is shifted towards smaller pore diameter and they fall with in medium capillary pores. This indicates that due to addition of BFS and combined BFS and FA the concentration of pores is shifted from large capillary pores to medium capillary pores.



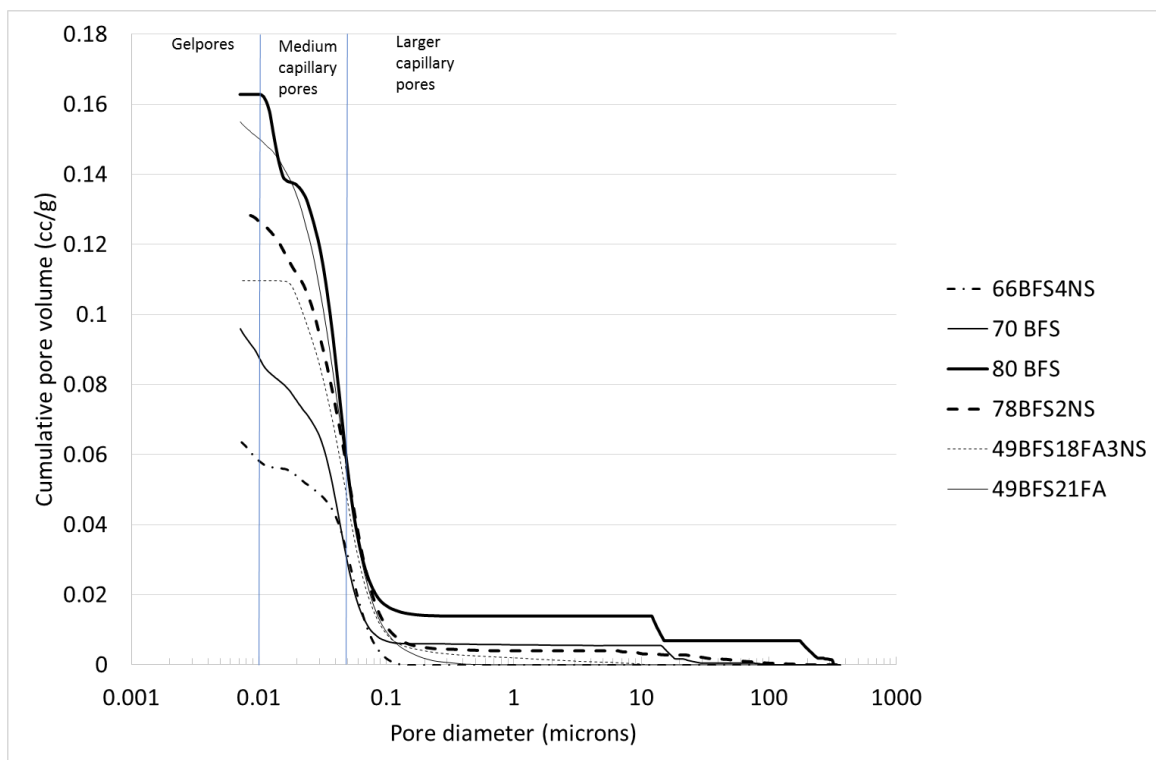
(a)



(b)

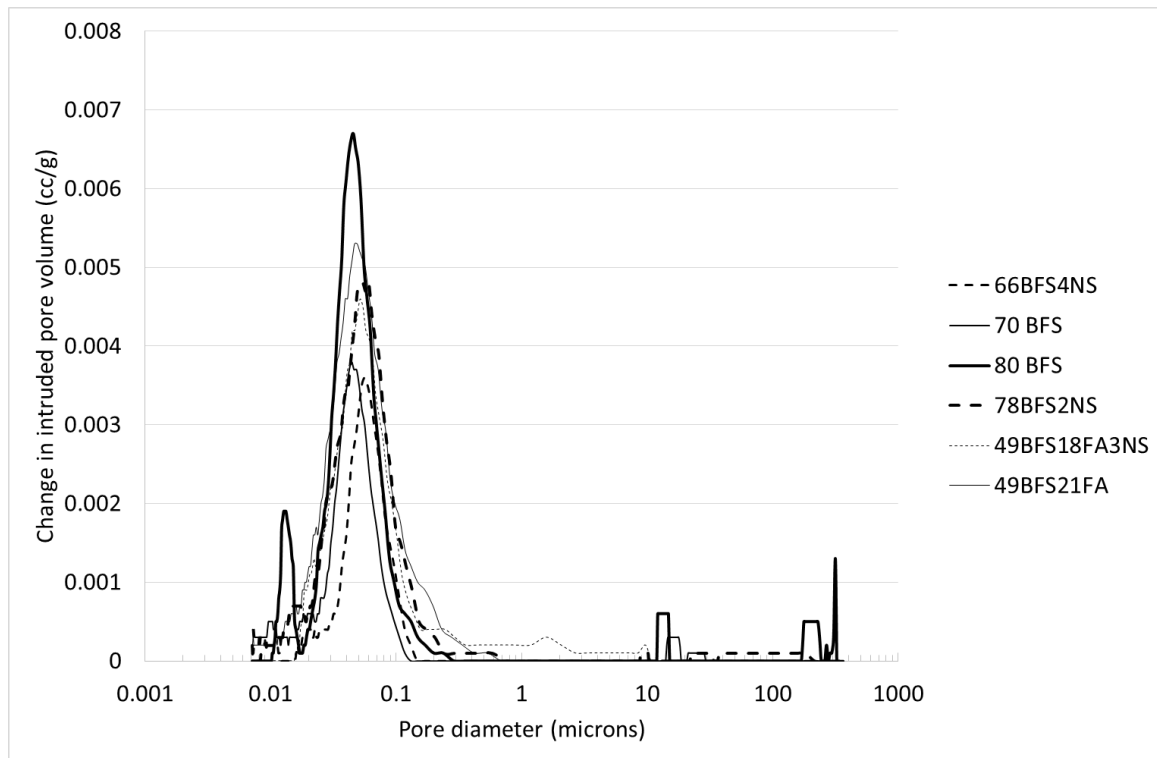
**Fig. 3.6** Cumulative pore volume and distribution of pore sizes of high volume BFS pastes and combined BFS-FA pastes measured at 28 days

The cumulative pore volume and pore size distribution of high volume BFS and combined BFS and FA pastes containing NS is shown in **Fig.3.7**. It can be seen in **Fig. 3.7a** that due to addition of NS the cumulative pore volume of all high volume BFS and combined BFS and FA pastes is significantly decreased. It can also be seen that volume of all pore sizes ranging from large and medium capillary pores as well as gel pores is reduced due to addition of NS. The cumulative pore volume of paste containing 70% BFS is reduced from 0.095 cc/g to 0.063 cc/g due to addition of 4% nano silica, whereas in paste containing 80% BFS the cumulative pore volume is reduced from 0.16 cc/g to 0.13cc/g. In the case of paste containing combined BFS and FA content of 70% the cumulative pore volume is reduced significantly from 0.15 cc/g to 0.11 cc/g due to addition of 3% NS. The formation of additional C-S-H gels due to enhanced pozzolanic reaction of NS with Portlandite in those high volume BFS and combined BFS and FA pastes could be the reasons for such significant reduction in pore volume in those pastes. However, by looking into the pore size distribution shown in **Fig. 3.7b** it can be seen that the concentration of pores is not significantly changed in high volume BFS and combined BFS and FA pastes due to addition of NS, but the volume of pores in the concentration of pore sizes in each paste containing NS is reduced.



(a)





(b)

**Fig. 3.7** Cumulative pore volume and distribution of pore sizes of high volume BFS pastes and combined BFS-FA pastes containing nano silica measured at 28 days

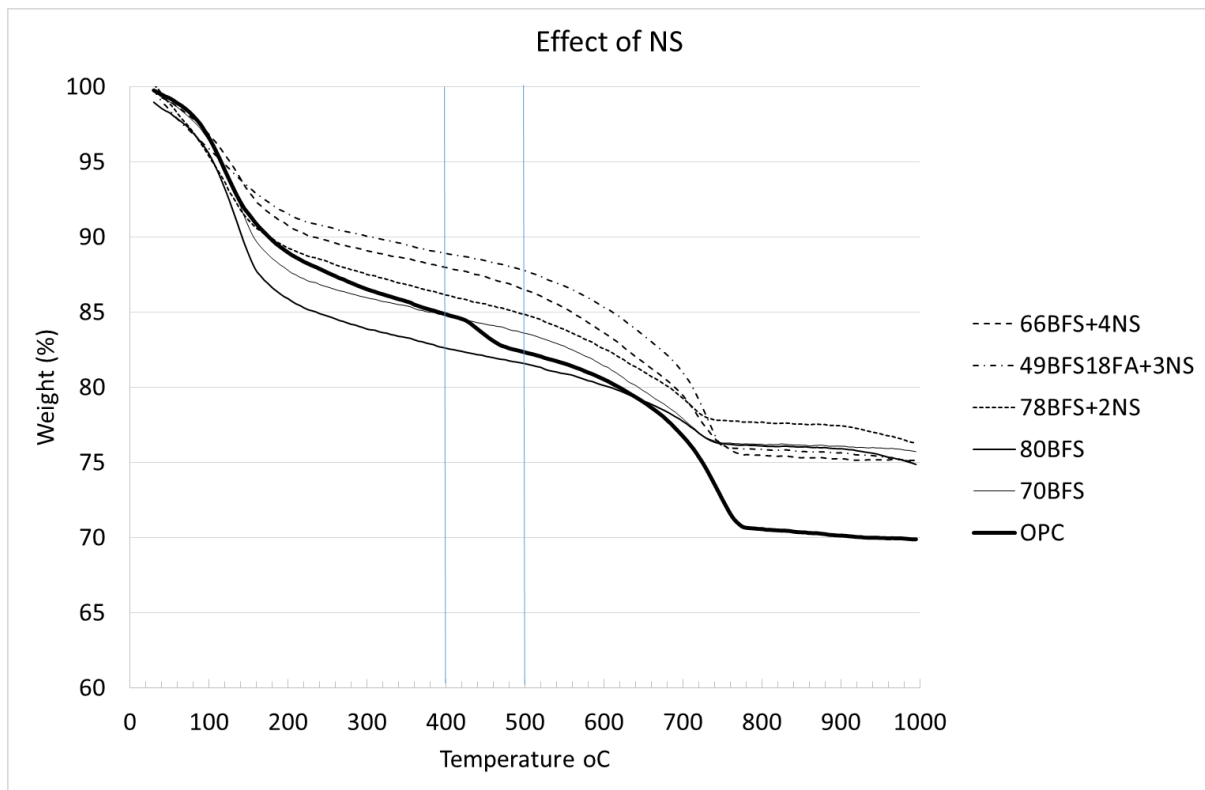
### 3.5.2.2 Thermogravimetric analysis (TGA)

Thermogravimetric analysis (TGA) curves of high volume BFS and BFS-FA pastes and those containing NS are shown in **Fig. 3.8a**. TGA curve shows the mass of a substance under control environment as a function of temperature. It has been reported that mass loss between 420°C and 540°C corresponds to the dehydration of calcium hydroxide (Keatch and Dollimore, 1975). By comparing the mass loss between those temperature range of high volume BFS and BFS-FA pastes and those containing NS, it can be seen that the mass loss of pastes containing NS is smaller than that without NS. This clearly shows lower amount of calcium hydroxide in high volume BFS and BFS-FA pastes containing NS than those without NS indicating the formation of more C-S-H in the former than the latter pastes. The amount of calcium hydroxide (CH) can also be quantified according to Taylor's formula (Taylor, 1975) shown as follows in equation (2):

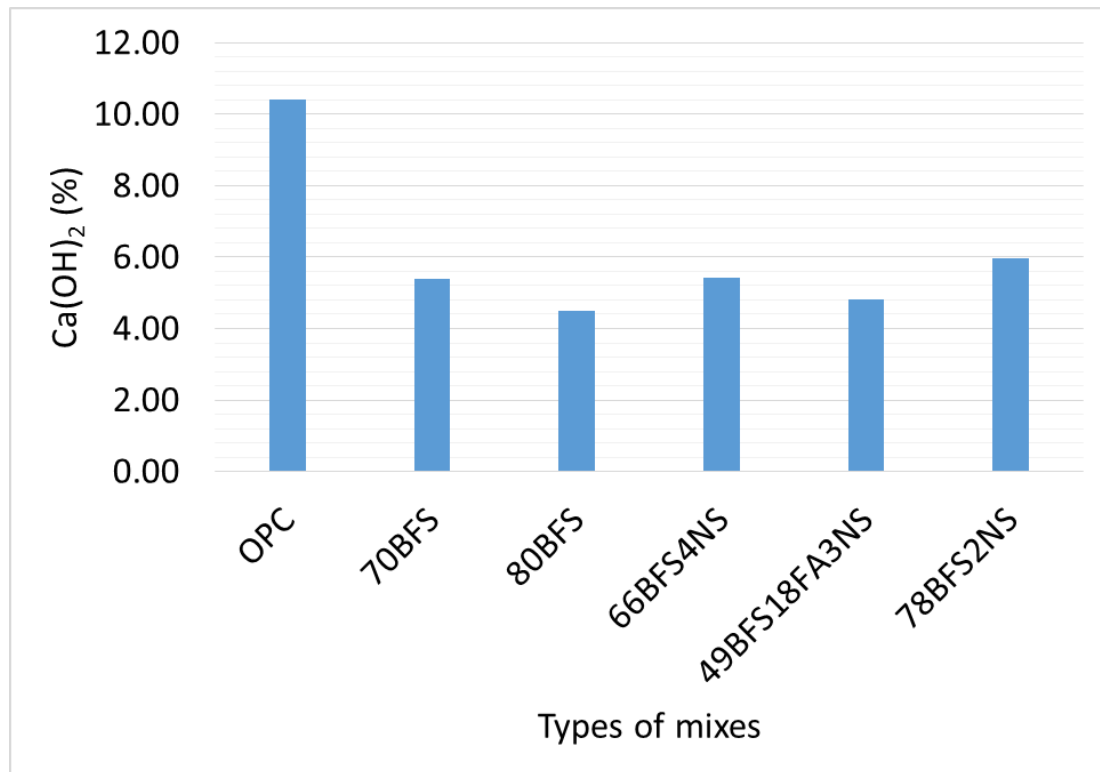
$$CH(\%) = WL_{CH}(\%) \frac{MW_{CH}}{MW_{H_2O}} \quad \text{Eq. 2}$$

Where,  $WL_{CH}$  is the weight loss during the dehydration of CH as percentage of the ignited weight (%);  $MW_{CH}$  is the molecular weight of CH;  $MW_{H_2O}$  is the molecular weight of  $H_2O$ .

The calculated CH contents are shown in **Fig. 3.8b** and it can be seen that CH contents of all high volume BFS and BFS-FA pastes and those containing NS are lower than that of OPC paste. This clearly indicate that due to pozzolanic reaction of  $SiO_2$  in BFS, FA and NS with CH in those pastes C-S-H is formed. In **Fig. 3.8b** it can also be seen lower amount of CH content in high volume BFS pastes containing 66% BFS and 4%NS and 49% BFS+18%FA+3%NS pastes than that containing 70% BFS. Surprisingly slightly higher CH content are calculated in paste 78%BFS+2%NS than the paste containing 80% BFS.



(a)



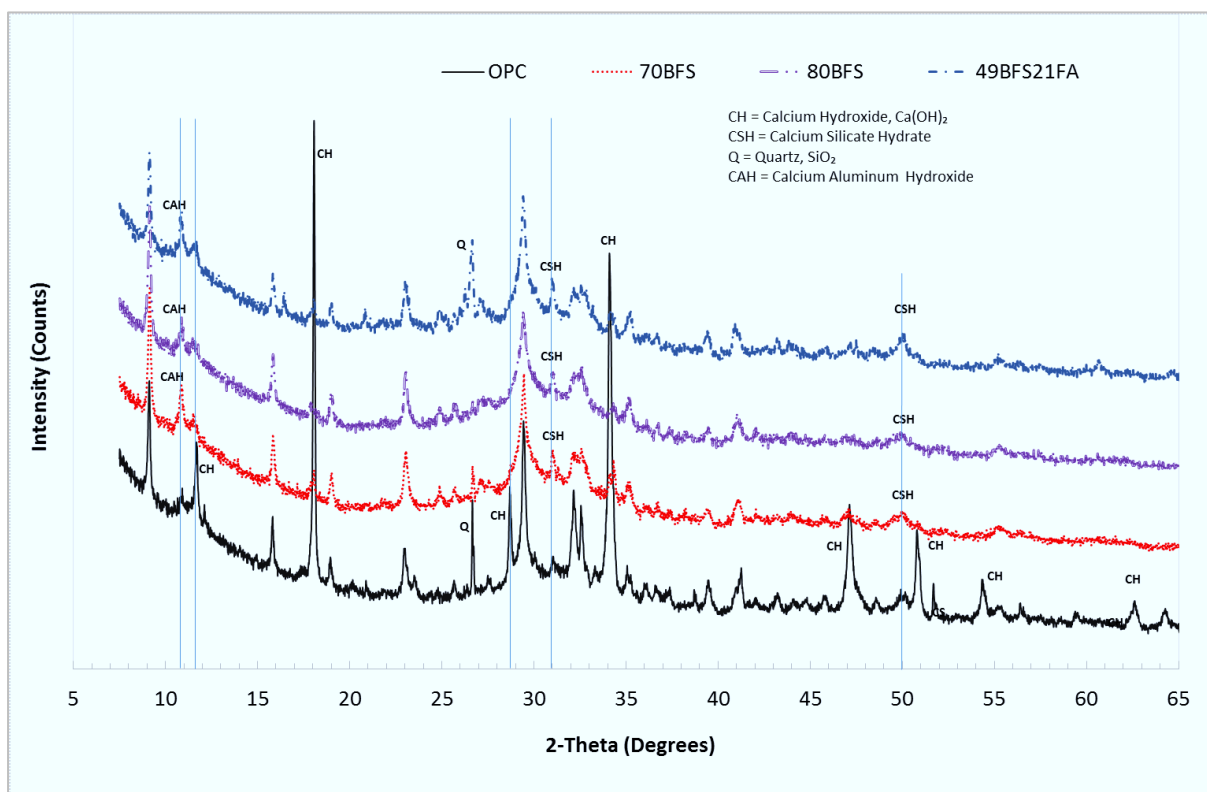
(b)

**Fig. 3.8** (a) Mass loss and (b) calculated calcium hydroxide of high volume BFS pastes and combined BFS-FA pastes with and without nano silica

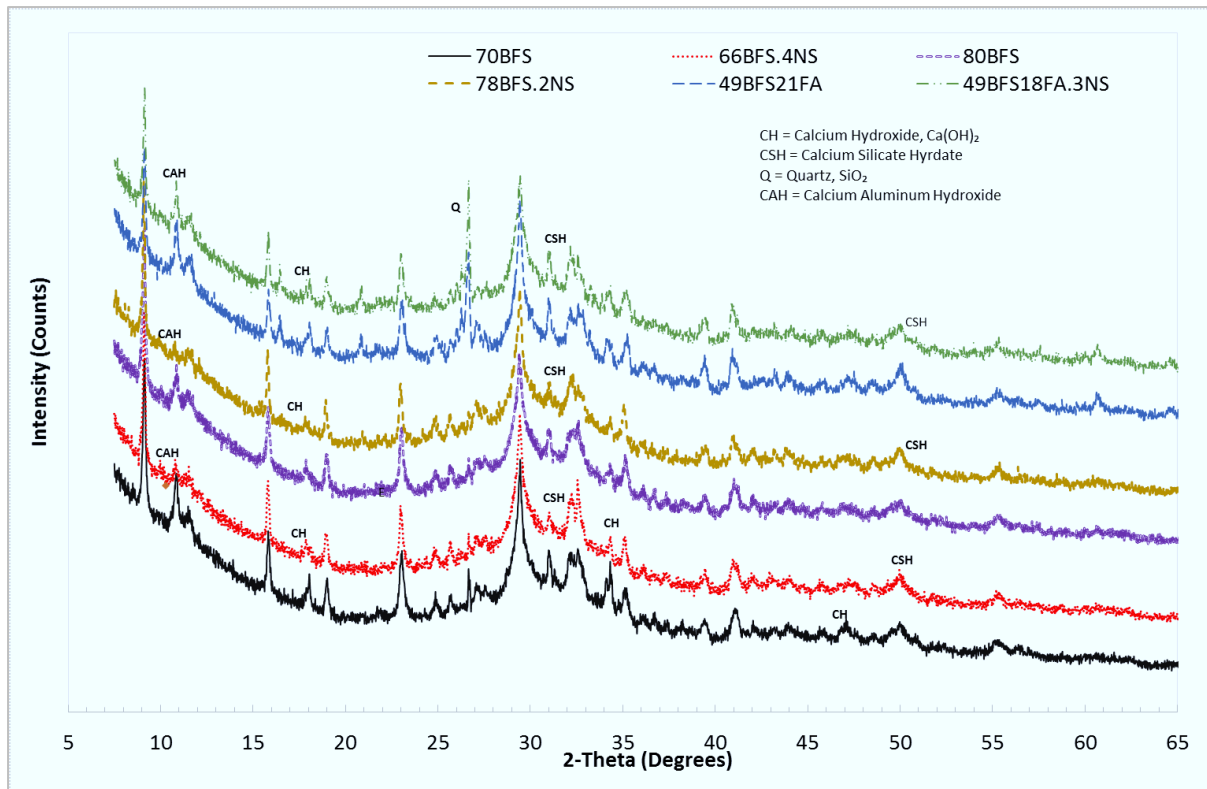
### 3.5.2.3 X-ray Diffraction (XRD) analysis

X-ray Diffraction (XRD) patterns of OPC paste and pastes containing high volume BFS and combined BFS and FA are shown in **Fig. 3.9a**. The horizontal scale is the diffraction angles measured in degrees and the vertical scale is the peaks height of the intensity of the diffraction measured in pulses/s. The diffraction spectra analysis of OPC paste and high volume BFS and combined BFA and FA pastes indicate the predominance of calcium hydroxide (CH), calcium silicate hydrate (CSH), calcium aluminate hydrate (CAH) and Quartz (Q). In the case of OPC paste, it can be seen several dominant CH peaks at  $2\theta$  angles of  $11.84^\circ$ ,  $18.04^\circ$ ,  $28.45^\circ$ ,  $34.11^\circ$ ,  $47.04^\circ$ ,  $51^\circ$ ,  $54.4^\circ$  and  $62.7^\circ$ . However, in high volume BFS pastes containing 70% and 80% BFS and combined BFS and FA content of 70% the intensity of peaks at those  $2\theta$  angles is significantly lower than the OPC paste. This clearly indicates the consumption of CH during pozzolanic reaction. On the other hand, several new peaks at  $2\theta$  angles of  $10.9^\circ$ ,  $31^\circ$  and  $50^\circ$

can be seen in high volume BFS pastes containing 70% and 80% BFS and combined BFS and FA content of 70% which are not present in OPC paste. These peaks are associated with formation of CAH and CSH. The XRD patterns of high volume BFS and combined BFS and FA pastes containing NS is shown in **Fig. 3.9b**. By comparing the XRD patterns of these pastes with their corresponding pastes without NS, it can be seen that the intensity of CH peaks at  $2\theta$  angles of  $18.04^\circ$ ,  $34.11^\circ$  and  $51^\circ$  is reduced in the pastes containing NS indicating formation of CSH as evidenced at  $2\theta$  angles of  $31^\circ$ .



(a)



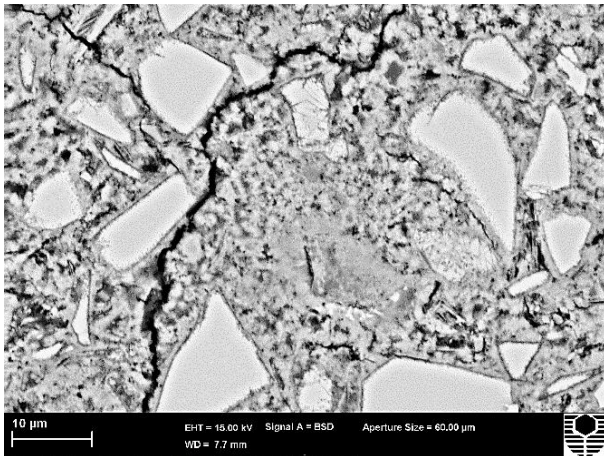
(b)

**Fig. 3.9** XRD patterns of (a) high volume BFS pastes and combined BFS-FA pastes and (b) those containing nano silica

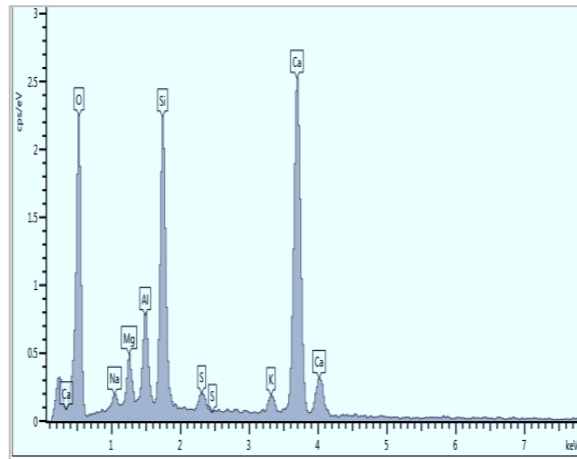
### 3.5.2.4 Scanning electron microscopy (SEM) and energy dispersive X-ray spectroscopy (EDS) analysis

Scanning electron microscopy images and EDS spectra of HVS and HVS-FA pastes with and without NS are shown in **Fig. 3.10**. It can be seen by comparing **Fig. 3.10b** with **Fig. 3.10a** that the microstructure of HVS paste containing 4% NS is much denser than HVS paste containing 70% slag. By comparing both figures it can also be revealed fewer black spots indicative of pores/voids in HVS paste containing NS than HVS paste indicating formation of additional hydration products such as CSH/CAH as shown in the figure. The positive impact of addition of NS in HVS paste is also evident in higher BFS content where HVS paste containing 78% BFS and 2% NS in **Fig. 3.10d** exhibited much denser microstructure than HVS paste containing 80% BFS in **Fig. 3.10c**. The EDS spectra in the same figure shows the formation of more CSH/CAH in the HVS paste containing NS than that of HVS paste. The similar densification of microstructure of HVS-FA paste due to addition of NS can also be seen by comparing **Fig.**

**3.10f** with **Fig. 3.10e**, where the peak of silica in EDS is much higher in paste containing NS than without NS indicating formation of more CSH/CAH in the former than the latter. The higher peak of silica in EDS is also evident in HVS pastes containing NS than without NS.

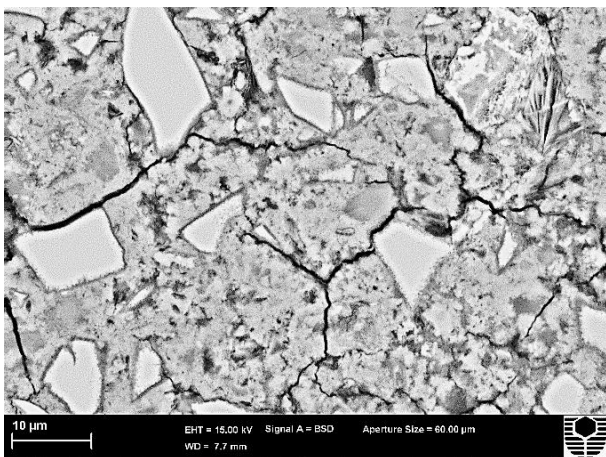


Backscattered SEM image

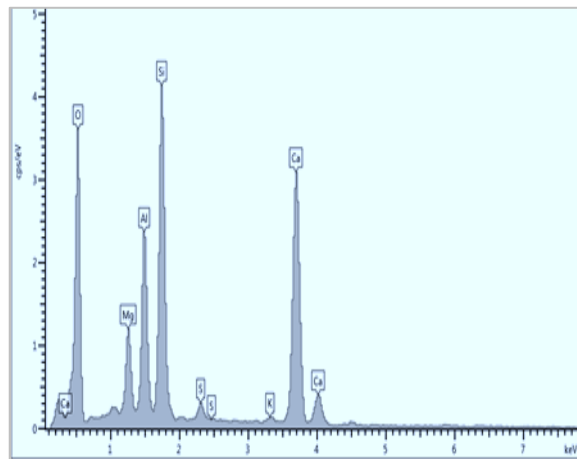


EDS spectra around slag particle

(a) 70BFS paste

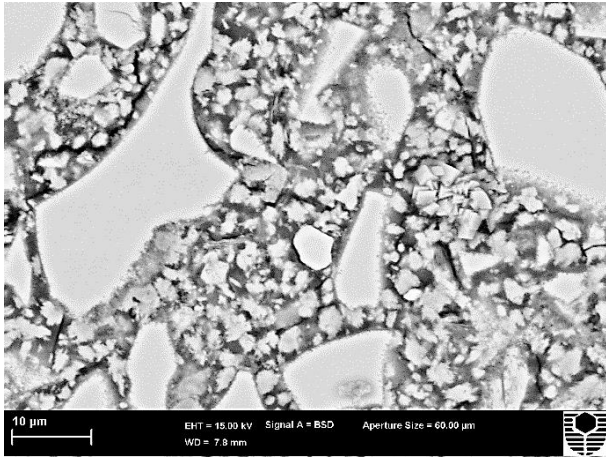


Backscattered SEM image



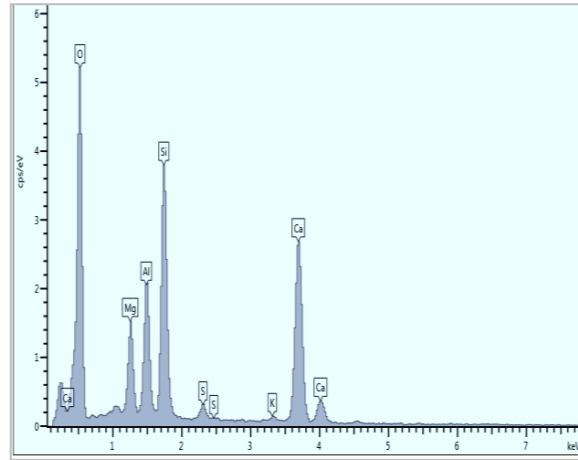
EDS spectra around slag particle

(b) 66BFS+4NS paste

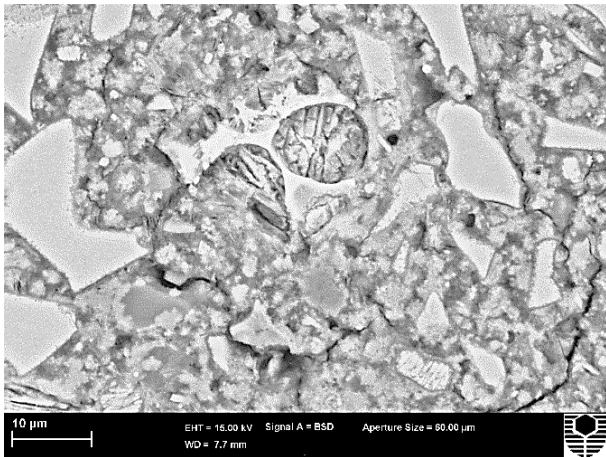


Backscattered SEM image

(c) 80BFS paste

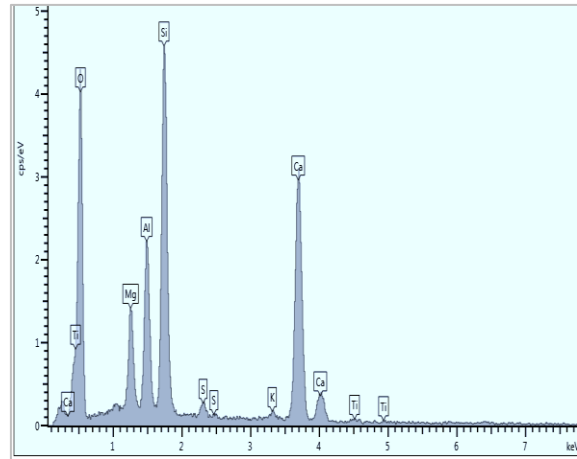


EDS spectra around slag particle

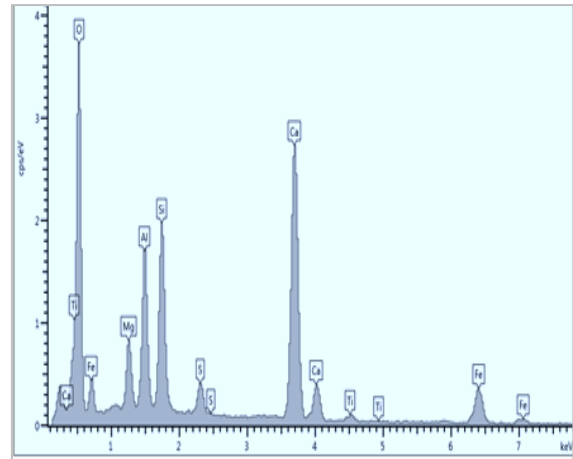
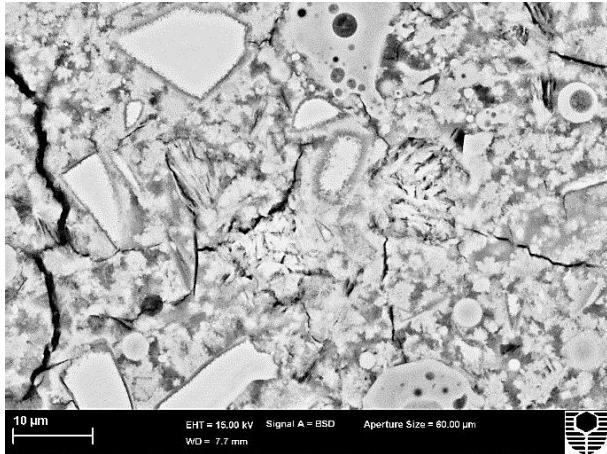


Backscattered SEM image

(d) 78BFS+2NS paste



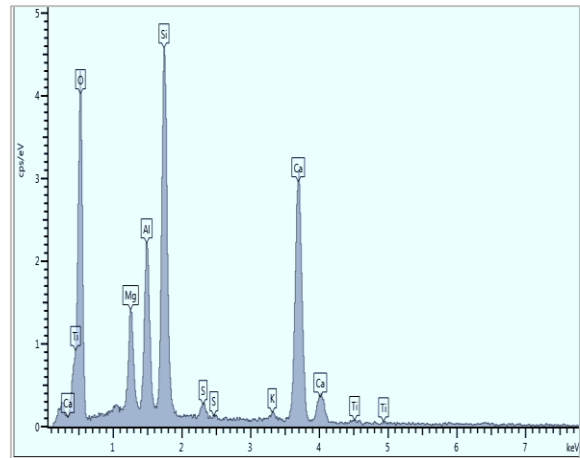
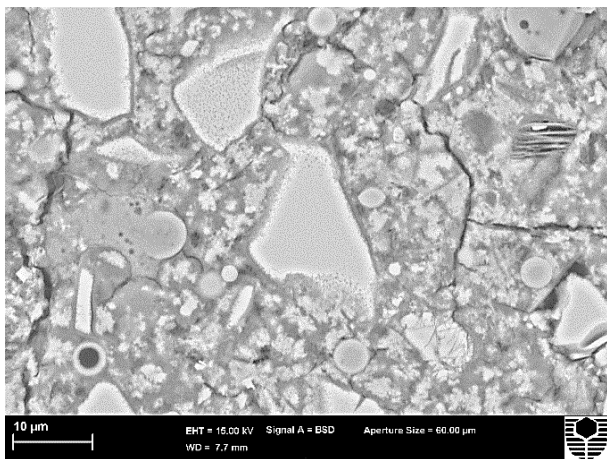
EDS spectra around slag particle



Backscattered SEM image

EDS spectra in the matrix

(e) 49BFS21FA paste



Backscattered SEM image

EDS spectra in the matrix

(f) 49BFS18FA+3NS paste

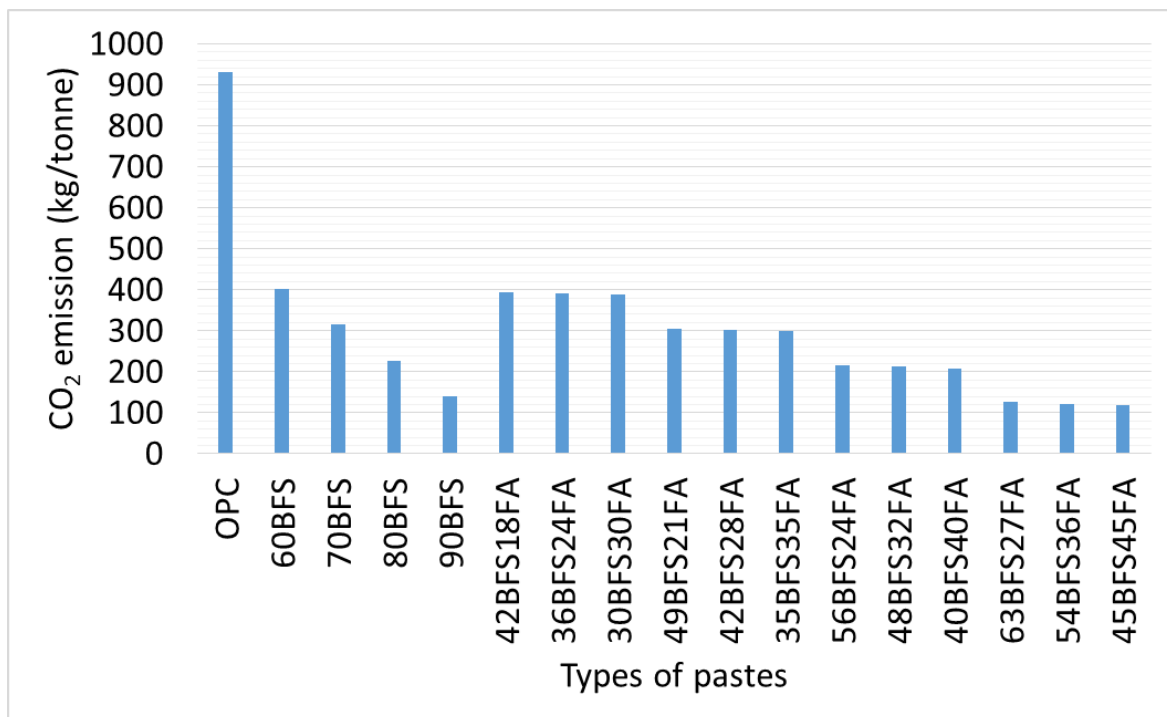
**Fig. 3.10** Backscattered scanning electron microscopic (SEM) images and EDS spectra of HVS and HVSFA pastes with and without nano silica.

### 3.5.3 CO<sub>2</sub> emission analysis

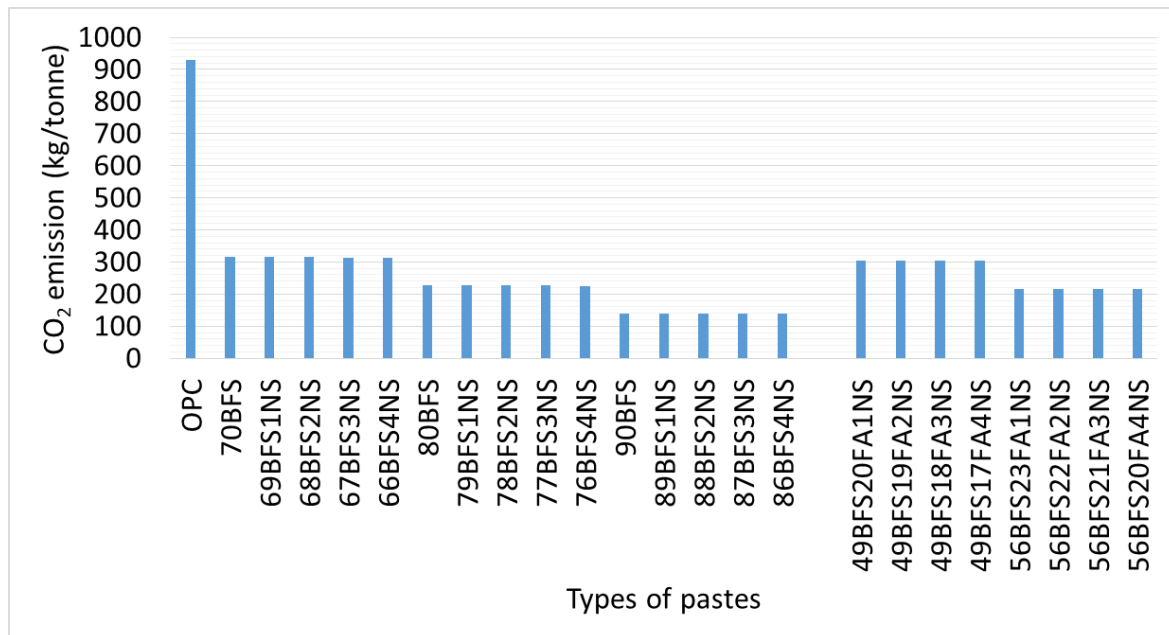
Carbon di-oxide (CO<sub>2</sub>) emission calculation of HVS and HVS-FA pastes with and without NS is very useful to bench mark their carbon footprint with conventional cement paste. Based on CO<sub>2</sub> emission value of 930 kg/tonne for OPC, 52 kg/tonne for slag and 4 kg/tonne for fly ash (King, D., 2012), the CO<sub>2</sub> emission of HVS and HVS-FA pastes is calculated and is shown in **Fig. 3.11a**. It can be seen that by using 60% BFS as partial replacement of OPC the CO<sub>2</sub>



emission is significantly dropped from 930 to 400 kg/tonne and the CO<sub>2</sub> emission values gradually decreases with increase in BFS contents. With the inclusion of various amounts of fly ash in HVS-FA pastes the CO<sub>2</sub> emission values are slightly reduced compared to that of HVS pastes of equivalent amount. The only study where Lazaro et al. (2013) used CO<sub>2</sub> emission rate as 2 kg CO<sub>2</sub>/m<sup>3</sup> of olivine nano silica compared to 170.7 kg CO<sub>2</sub>/m<sup>3</sup> for cement, which translates about 1.2% CO<sub>2</sub> emission of that of cement. The kind of NS used by Lazaro et al. (2013) is manufactured by dissolution of olivine. However, the NS used in this study was synthesized by a chemical precipitation method confirmed by the manufacturer whose CO<sub>2</sub> emission data is still not known. Therefore, by considering the CO<sub>2</sub> emission of NS in the HVS and HVS-FA pastes containing NS the total CO<sub>2</sub> emission is calculated and is shown in **Fig. 3.11b** where it can be seen that with very small quantities of NS its CO<sub>2</sub> emission value hardly effects the total CO<sub>2</sub> emission values of HVS and HVS-FA pastes. Nevertheless, it can be seen that the CO<sub>2</sub> emission of cement pastes can be significantly reduced by 66% and 76% by combined using of slag, fly ash and NS at 70% and 80% as partial replacement of cement, respectively. Moreover, comparing with the 28 days compressive strengths of those mixes with and without NS inclusion, it is clearly evident that paste mixes 78BFS2NS, 66BFS4NS and 49BFS20FA1NS exhibited significantly better performances as a green composites materials.



(a)



(b)

**Fig. 3.11** CO<sub>2</sub> emission analysis of HVS and HVSA pastes with and without nano silica.

### 3.6 Summary

This chapter presents the effect of nano silica on compressive strength and microstructures of high volume BFS and BFS-FA blended cement pastes. Within limited results the following conclusions can be made:

- ✚ High volume slag (HVS) cement paste containing 60% slag exhibited about 4% higher compressive strength than control cement paste, while the HVS cement paste containing 70% slag maintained the similar compressive strength to control cement paste.
- ✚ The high volume slag-fly ash (HVS-FA) cement pastes containing total slag and fly ash content of 60% exhibited about 5%-16% higher compressive strength than control cement paste. Significant reduction in compressive strength is observed in higher slag-fly ash blends with increasing in fly ash contents.
- ✚ The addition of 1-4% NS significantly improves the compressive strength by 9-25%, 11-29% and 17-41% of HVS cement paste containing 70%, 80% and 90% BFS, respectively. The NS addition also significantly improves the compressive strength of high volume BFS-FA cement pastes.

- ✚ The addition of BFS of 70% and 80% increase the large capillary pores of cement paste. However, the combined use of BFS and FA at 70% significantly reduced the large capillary pores. The addition of NS significantly reduces the large and medium capillary pores and gel pores of HVS and HVS-FA pastes. However, the addition of NS did not change the concentration of pore sizes.
- ✚ The thermogravimetric analysis (TGA) results confirm the reduction of calcium hydroxide (CH) in HVS/HVS-FA pastes containing nano silica indicating the formation of additional calcium silicate hydrate (CSH) gels in the system.
- ✚ The addition of NS reduced the intensity of calcium hydroxide peaks corresponding to  $2\theta$  angles of  $18.04^\circ$ ,  $34.11^\circ$  and  $51^\circ$  of HVS and HVS-FA pastes, indicating the consumption of calcium hydroxide in pozzolanic reaction.
- ✚ Scanning electron microscopic images and EDS spectra of HVS and HVS-FA pastes containing NS revealed much denser microstructure than those without NS.
- ✚ The combination of BFS, FA and NS in high volumes e.g., at 70-80%, reduces the carbon footprint of cement paste by 66-76% while maintains the similar compressive strength, densified their microstructures through forming additional hydration products compared to control cement paste.

### 3.7 References

- Chithra, S., Kumar, S.R.R.S. and Chinnaraju, K. (2016) The effect of colloidal nano silica on workability, mechanical and durability properties of high performance concrete with copper slag as partial fine aggregate. *Construction and Building Materials*. **113**: p. 794-804.
- El-Chabib, H. and A. Syed, *Properties of Self-Consolidating Concrete made with High volume of Supplementary Cementitious Materials*. *Materials in Civil Engineering*, 2013. **25(11)**: p. 1579-1586.
- Elchalakani, M., T. Aly, and E. Abu-Aisheh, *Sustainable concrete with high volume GGBFS to build Masdar City in the UAE*. *Case Studies in Construction Materials*, 2014. **1**: p. 10-24.
- H.F.W. Taylor, *Cement Chemistry*, Academic Press Limited, London, 1990.
- Hooton, R.D., *Canadian use of ground granulated blast-furnace slag as a supplementary cementing material for enhanced performance of concrete*. *Canadian Journal of Civil Engineering*, 2000. **27(4)**: p. 754-760.
- Keatch, C.J. and Dollimore, D. (1975) *Introduction to thermogravimetry*, Vol. 45, Heydon.
- King, D. (2012) The effect of silica fume on the properties of concrete as defined in concrete society report 74, cementitious materials. 37th conference on our world in concrete and structures.
- Lazaro, A., Quercia, G., Brouwers, H.J.H. and Gens, J.W. (2013) Synthesis of a green nano-silica material using beneficiated waste dunites and its application in concrete. *World journal of nano science and engineering*. 3:41-51.
- Liu, M., et al., *The synergistic effect of nano-silica with blast furnace slag in cement based materials*. *Construction and Building Materials*, 2016. **126**: p. 624-631.
- Malhotra, V.M., *Introduction: Sustainable development and concrete technology*, *ACI Board Group on Sustainable Development*. *ACI Concrete International*, 2002. **24(7)**: p. 22.
- Mehta, P.K., *Reducing the environmental impact of concrete*. *ACI Concrete International*, 2001. **23(10)**: p. 61-66.
- Nagendra, V., Sashidhar, C., Kumar, S.M.P. and Ramana, N.V. (2016) GGBS and nano silica effect on concrete. *International journal of civil engineering and technology*. 7(5):477-484.
- Nazari, A. and S. Riahi, *Splitting tensile strength of concrete using ground granulated blast furnace slag and SiO<sub>2</sub> nanoparticles as binder*. *Energy and Buildings*, 2011. **43(4)**: p. 864-872.

Nazari, A. and S. Riahi, *The effects of TiO<sub>2</sub> nanoparticles on physical, thermal and mechanical properties of concrete using ground granulated blast furnace slag as binder*. Materials Science and Engineering: A, 2011. **528**(4): p. 2085-2092.

Oner, A. and S. Akyuz, *An experimental study on optimum usage of GGBS for the compressive strength of concrete*. Cement and Concrete Composites, 2007. **29**(6): p. 505-514.

Rashad, A.M., *An investigation of high-volume fly ash concrete blended with slag subjected to elevated temperatures*. Journal of Cleaner Production, 2015. **93**(Supplement C): p. 47-55.

Washburn EW (1921) Note on a method of determining the distribution of pore sizes in a porous material. Proc Natl Acad Sci USA 7(4):115–116

*All reasonable efforts have been made to acknowledge the authors of the copyright material. It would be highly appreciated if I can hear from any authors has been ignored or incorrectly acknowledged.*

## Chapter 4: High volume slag and high volume slag-fly ash blended paste containing nano calcium carbonate

---

This chapter evaluates the compressive strengths and the microstructural changes of high volume slag and slag-fly ash blended paste due to the addition different dosages of nano calcium carbonate. The 28 days compressive strengths of the cement paste containing 70-90% blast furnace slag and slag-fly ash blend were determined. Based on the compressive strengths results, microstructural investigation through mercury intrusion properties, thermogravimetric analysis, x-ray diffraction analysis, scanning electron microscopy and energy dispersive x-ray spectroscopy were also studied and optimum content of nano calcium carbonate inclusion in both high volume slag and high volume slag-fly ash blended paste were determined. The environmental impact of high volume slag and high volume slag-fly ash blended paste based on the carbon di-oxide emission of mixes are also presents in this chapter.

### 4.1 Overview

The demand for concrete as a construction material was always in a rising trend in the past and will be very high in future due to the rapid urbanisation across the world which requires a significant amount of binding materials. Recent study expected that global demand of cement will rise by approximately 115-180% by 2020 compared to 1990s and may climbed to 400% by 2050 (Damtoft et al., 2008). Ordinary Portland Cement (OPC) is used as the binder for concrete which is extremely energy intensive and every single tonne of OPC manufacture releases roughly one tonne of carbon dioxide (CO<sub>2</sub>) during the calcination process and contributes 7% of global CO<sub>2</sub> into the atmosphere per year (Benhelal et al., 2013; Malhotra, 2002; Mehta, 2001; Tharakan et al., 2013).

---

The content of this chapter has been written based on the results published in the following journal.

Hosan, A. and F.U.A. Shaikh, Influence of nano-CaCO<sub>3</sub> addition on the compressive strength and microstructure of high volume slag and high volume slag-fly ash blended pastes. *Journal of Building Engineering*, 2020. **27**: p. 100929.

Global warming associated with CO<sub>2</sub> emission due to cement manufacturing plays a vital role to find alternative option of cement or huge reduction of cement content in concrete, which resulted in the use of several industrial by-products such as blast furnace slag (BFS), fly ash (FA), silica fume, metakaolin etc. as partial replacement of OPC in the concrete. Among various supplementary cementitious materials (SCM), slag and fly ash have been widely used as a partial replacement of cement to investigate the mechanical and durability properties of concrete as well as reducing the CO<sub>2</sub> emission into the atmosphere (Hooton, 2000; Rashad, 2015). However, the partial replacement of cement by SCM is still lies under 50% in many studies (Aghaeipour & Madhkhan, 2017; Choi et al., 2017; Herrera et al., 2011) due to the several challenges like very low early-age compressive strengths, significant autogenous and/or drying shrinkage, briskly progress of carbonation though high volume (>50%) replacement of slag and fly ash. Few researches have also been examined the use of ternary and quaternary blend of high volume slags and fly ash with cement, silica fume, and limestone filler but did not notice any significant improvement in mechanical and durability of properties of concretes due to slow pozzolanic reaction of slag and fly ash at early ages discussed in Chapter 1.

Nano-CaCO<sub>3</sub> (NC) is used as a filler materials initially as partial replacement of cement and gypsum in concrete and some studies have found it can be used as an economically beneficial materials to improve early strengths, accelerating hydration of concrete. High volume replacement of cement with fly ash increased workability and which causes the bleeding while addition of nano-CaCO<sub>3</sub> minimise those workability especially for the concrete containing 40% fly ash (Shaikh & Supit, 2015). On the other hand, 5% addition of nano-CaCO<sub>3</sub> significantly reduced the initial and final setting times of pastes samples with a 50% replacement of cement with fly ash compared to ordinary cement paste and exhibited the same setting times when sonication process applied for the mixing of nano-CaCO<sub>3</sub> (Kawashima et al., 2013). It is reported 1% replacement of fly ash by nano-CaCO<sub>3</sub> in a concrete containing 40% fly ash as partial replacement of cement improved the compressive strengths by 46% and 54% at 3 days and 28 days, respectively compared to control concrete containing 40% fly ash as partial replacement of cement. However, no such great improvement is noticed in the compressive strengths of concrete containing 59%FA and 1% nano-CaCO<sub>3</sub> (Shaikh & Supit, 2014). In this study, compressive strengths of mortars showed improvement of about 25%, 15% and 8.33% at 3, 28 and 90 days, respectively. Moreover, it is found that 1% addition of nano-CaCO<sub>3</sub> in high volume fly ash concrete containing 59% fly ash reduced the water sorptivity by 19% and

60% than ordinary concrete at 28 days and 90 days, respectively due to the formation of additional CSH gels. This study is designed to investigate the effects of various nano-CaCO<sub>3</sub> content varies from 1% to 4% on the 28 days compressive strengths of high volume slag (HVS) and high volume slag-fly ash blended (HVSFA) pastes ranges from 60% to 90% as partial replacement of cement. Effects of nano-CaCO<sub>3</sub> content in the microstructure of these pastes after 28 days of curing are also presented in this study.

#### 4.2 Experimental Details

The experimental program is divided in to two parts. In the first part, high volume slag (HVS) pastes containing 60% to 90% slag as partial replacement of cement are considered. High volume slag-fly ash blended (HVSFA) pastes containing combined fly ash and slag contents of 60% to 90% are also included in this part. In the second part, the effects of various nano-CaCO<sub>3</sub> (NC) contents of 1% to 4% on compressive strength and microstructures of HVS and HVFA pastes exhibited higher compressive strength in the first part are evaluated. Thus, thirty seven mixes were prepared to evaluate the effect of nano-CaCO<sub>3</sub> on those HVS and HVSFA pastes mixes.

**Table 4.1** Physical properties and chemical compositions of Ordinary Portland Cement (OPC), Blast Furnace Slag (BFS), Class F Fly Ash (FA) and Nano-Calcium Carbonate (NC)

		Cement	Slag	Fly-ash	Nano calcium carbonate
Chemical composition (%)	CaO	64.39	41.20	4.30	97.8*
	SiO <sub>2</sub>	21.10	32.5	51.11	-
	Al <sub>2</sub> O <sub>3</sub>	5.24	13.56	25.56	-
	Fe <sub>2</sub> O <sub>3</sub>	3.10	0.85	12.48	0.02*
	MgO	1.10	5.10	1.45	0.5*
	MnO	-	0.25	0.15	-
	K <sub>2</sub> O	0.57	0.35	0.7	-
	Na <sub>2</sub> O	0.23	0.27	0.77	-
	P <sub>2</sub> O <sub>5</sub>	-	0.03	0.88	-
	TiO <sub>2</sub>	-	0.49	1.32	-
	SO <sub>3</sub>	2.52	3.20	0.24	-
	LOI	1.22	1.11	0.57	-
Physical properties	Particle size	25-40% ≤7μm	40% of 10 μm	50% of 10 μm	15-40 nm
	Surface area ( m <sup>2</sup> /g)	-	-	-	40
	Specific gravity	2.7 to 3.2	2.6	-	-

\*Information from supplier



### 4.3 Materials

Ordinary Portland cement (OPC) was used in all pastes this study. The ground granulated blast furnace slag (BFS) was supplied by BGC cement, Australia and class F fly ash (FA) was supplied by Eraring power station of New South Wales in Australia. Dry nano- $\text{CaCO}_3$  (NC) powder used in this study was purchased from Nanostructured and Amorphous Materials, Inc. of USA with an average particle size of 15-40nm,  $40 \text{ m}^2/\text{g}$  of specific surface areas and 97.8% calcite content. Physical and chemical properties of these materials are given in the **Table 4.1** and **Figs. 4.1-4.2** shows the X-ray diffraction (XRD) analysis of cement, BFS, FA and NC. It is clear that NC was less amorphous than BFS and FA by comparing the results. However, among both SCM, the BFS is more amorphous with amorphous content of 97.5% compared to 67.8 % amorphous content of FA based on the quantitative XRD results. A naphthalene sulphonate based superplasticizer was used to maintain the workability of pastes containing NC.

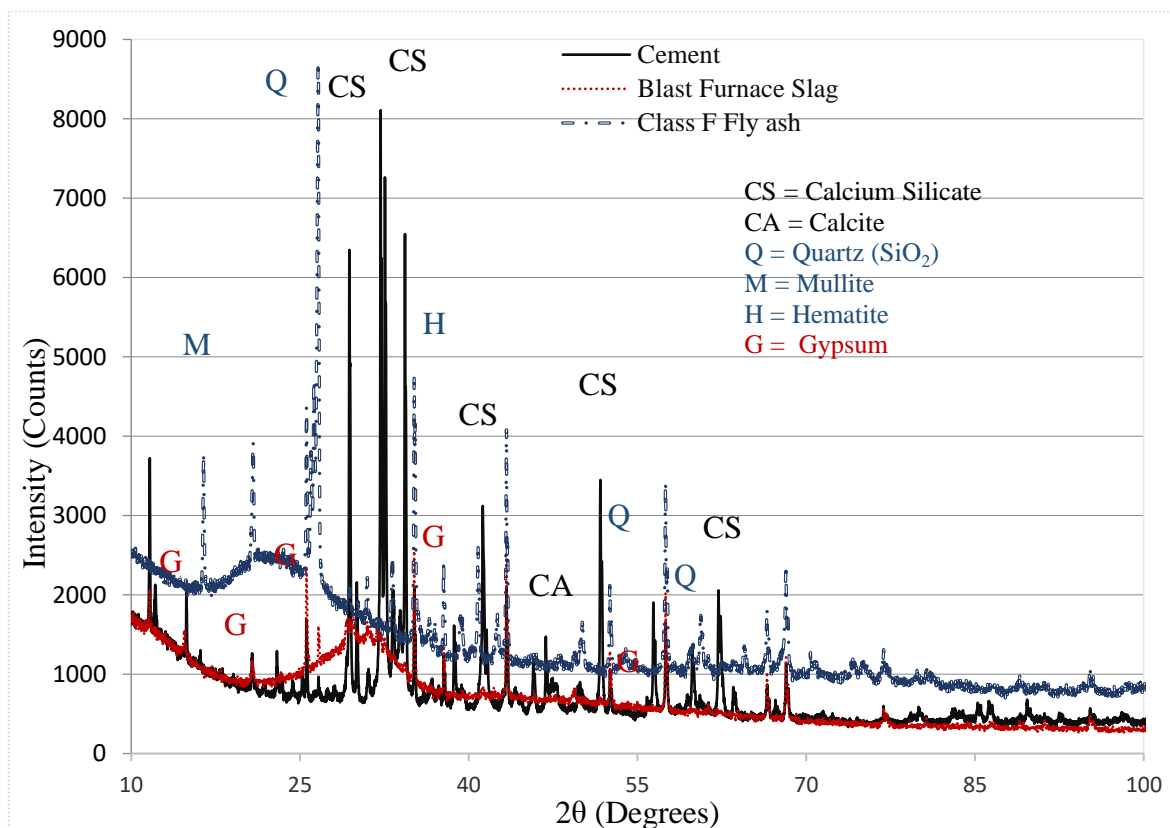


**Fig. 4.1** XRD analysis of Cement, Blast furnace slag and fly ash

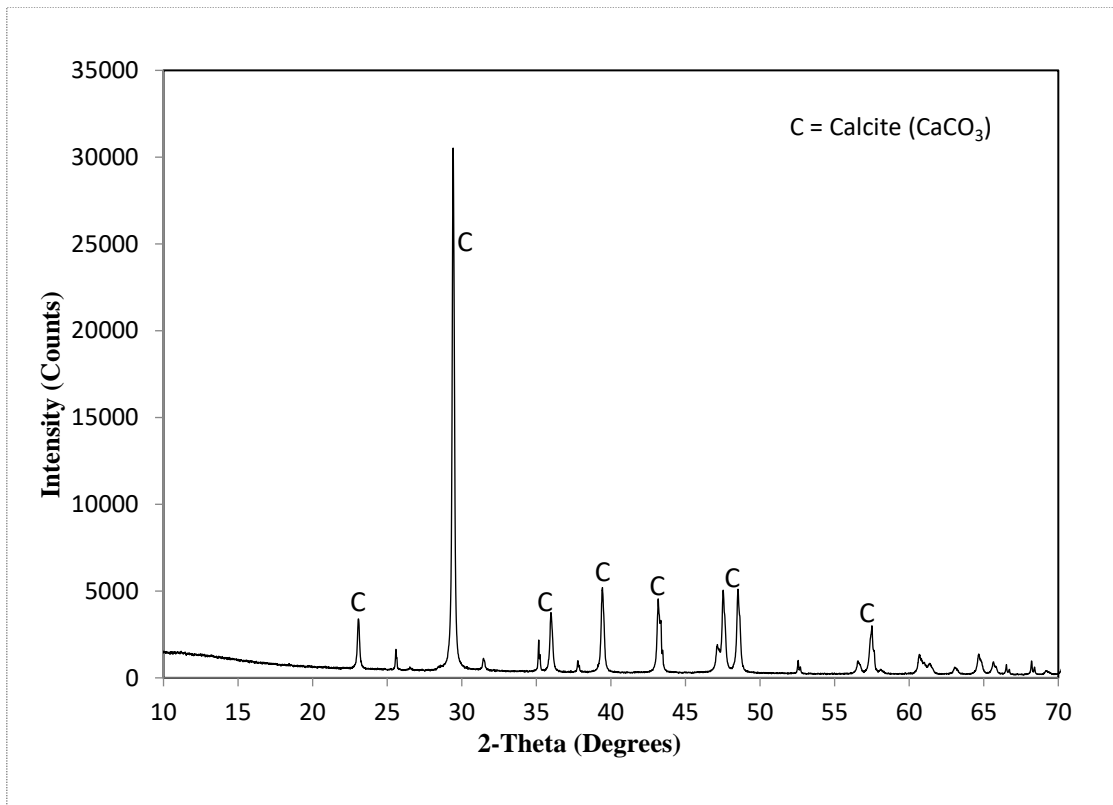


**Fig. 4.2** XRD analysis of nano calcium carbonate



**Fig. 4.3** Ultrasonic mixing of nano calcium carbonate.

#### 4.4 Mix proportions

A total sixteen mixes of high volume BFS pastes and high volume BFSFA pastes mixes were prepared by partially replacing cement at 60%, 70%, 80% and 90% in the first part of the study as shown in the **Table 4.2**. Five mixes among those were selected based on their 28 days compressive strengths for further mixes to evaluate the effect of NC on compressive strength and microstructure of those HVS and HVSFA pastes in the second part of this study as shown in **Table 4.3**. The dosages of NC were varied from 1%, 2%, 3% and 4% by total mass of cementitious materials. All the mixes had a constant water-to-cementitious materials ratio (w/b) of 0.4. Superplasticizer was used to maintain the adequate workability of pastes containing NC by ranging from 0.5% to 1 % by total mass of cementitious materials.

**Table 4.2** Mix proportions of cement paste containing high volume blast furnace slag (BFS) and slag-fly ash blend.

Mix Series	Mix ID	Mix proportion			Water/Binder	Super-Plasticizer <sup>o</sup>
		Cement	Slag	Fly ash		
OPC	Control	1.0	-	-	0.4	-
OPC+Slag	60BFS	0.4	0.6	-	0.4	-
	70BFS	0.3	0.7	-	0.4	-
	80BFS	0.2	0.8	-	0.4	0.5
	90BFS	0.1	0.9	-	0.4	0.5
OPC+Slag+Fly ash	42BFS18FA	0.4	0.42	0.18	0.4	-
	36BFS24FA	0.4	0.36	0.24	0.4	-
	30BFS30FA	0.4	0.30	0.30	0.4	-
	49BFS21FA	0.3	0.49	0.21	0.4	-
	42BFS28FA	0.3	0.42	0.28	0.4	-
	35BFS35FA	0.3	0.35	0.35	0.4	-
	56BFS24FA	0.2	0.56	0.24	0.4	-
	48BFS32FA	0.2	0.48	0.32	0.4	-
	40BFS40FA	0.2	0.40	0.40	0.4	-
	63BFS27FA	0.1	0.63	0.27	0.4	-
	54BFS36FA	0.1	0.54	0.36	0.4	-
	45BFS45FA	0.1	0.45	0.45	0.4	-

<sup>o</sup>% of total mass of cementitious materials

**Table 4.3** Mix proportions of high volume slag and slag-fly ash blended cement pastes incorporation of nano-calcium carbonate (NC).

Mix Series	% Nano Calcium Carbonate by mass	Mix ID	Mix Proportion					Super-plasticizers <sup>o</sup>
			Cement	Slag	Fly-ash	Nano Calcium carbonate	Water/Binder	
70% BFS	1%	69BFS1NC	0.3	0.69	-	0.01	0.4	-
	2%	68BFS2NC	0.3	0.68	-	0.02	0.4	-
	3%	67BFS3NC	0.3	0.67	-	0.03	0.4	0.5
	4%	66BFS4NC	0.3	0.66	-	0.04	0.4	0.5
80% BFS	1%	79BFS1NC	0.2	0.79	-	0.01	0.4	-
	2%	78BFS2NC	0.2	0.78	-	0.02	0.4	-
	3%	77BFS3NC	0.2	0.77	-	0.03	0.4	0.5
	4%	76BFS4NC	0.2	0.76	-	0.04	0.4	1.0
90% BFS	1%	89BFS1NC	0.1	0.89	-	0.01	0.4	-
	2%	88BFS2NC	0.1	0.88	-	0.02	0.4	0.5
	3%	87BFS3NC	0.1	0.87	-	0.03	0.4	1.0
	4%	86BFS4NC	0.1	0.86	-	0.04	0.4	1.0
70% (BFS+ FA)	1%	49BFS20FA1NC	0.3	0.485	0.205	0.01	0.4	-
	2%	49BFS19FA2NC	0.3	0.48	0.20	0.02	0.4	-
	3%	49BFS18FA3NC	0.3	0.475	0.195	0.03	0.4	-
	4%	49BFS17FA4NC	0.3	0.47	0.19	0.04	0.4	0.5
80% (BFS+ FA)	1%	56BFS23FA1NC	0.2	0.555	0.235	0.01	0.4	-
	2%	56BFS22FA2NC	0.2	0.55	0.23	0.02	0.4	-
	3%	56BFS21FA3NC	0.2	0.545	0.225	0.03	0.4	-
	4%	56BFS20FA4NC	0.2	0.54	0.22	0.04	0.4	0.5

<sup>o</sup>% of total mass of cementitious materials

#### 4.5 Specimen preparation and curing

All mixes were prepared using a Hobart mixer at room temperature where dry cement, BFS and FA were mixed first for approximately for 3 minutes. In the first phase, water was added and mixed for further 1 minute at low speed followed by adding superplasticizers when required and then again mixed for 1 minute at high speed. In the second phase, NC and water were mixed together with superplasticizers and then dispersed by using ultrasonic mixer with 100% amplitude for 45 minutes as shown in **Fig. 3**. That sonicated mixture of NC and water were then added with dry mix of cement, BFS and FA and mixed for 1 minute at high speed. For each mix, six 50 mm cube specimens were cast and demoulded after 24 hours. After demoulding, specimens were cured in water for 28 days at room temperature. Five specimens were tested for compressive strengths of each mixes after 28 days of curing and small portions were cut from the sixth cube sample to perform X-ray diffractions (XRD), scanning electron microscope (SEM), energy dispersive x-ray spectroscopy (EDS), mercury intrusion porosimetry (MIP) and thermal analysis (TGA) of control paste, HVS and HVSFA pastes and pastes containing NC.

## 4.6 Testing Methods

The compressive strength of all pastes were measured at 28 days according to ASTM: C109 using a loading rate of 0.33 MPa/s. For each mix, at least five specimens were tested and the average value of all are reported. In order to observe the changes in reaction phases in cement pastes containing high volume BFS and BFS-FA blends due to inclusion of NC thermogravimetric analysis (TGA), X-ray diffraction (XRD) analysis, Mercury intrusion porosimetry (MIP), scanning electron microscopy (SEM) and energy dispersive X-ray spectroscopy (EDS) were done on selected samples based on their average compressive strengths at 28 days.

For the XRD analysis, the samples were measured with a D8 Advance Diffractometer (Bruker-AXS) using copper radiation and a Lynx Eye position sensitive detector. The diffractometer scanned the samples from 5° to 65° (2θ) in steps of 0.015° at a scanning rate of 0.5°/min. XRD patterns were obtained using Cu Kα lines (k = 1.5406 Å). A knife edge collimator was fitted to reduce air scatter.

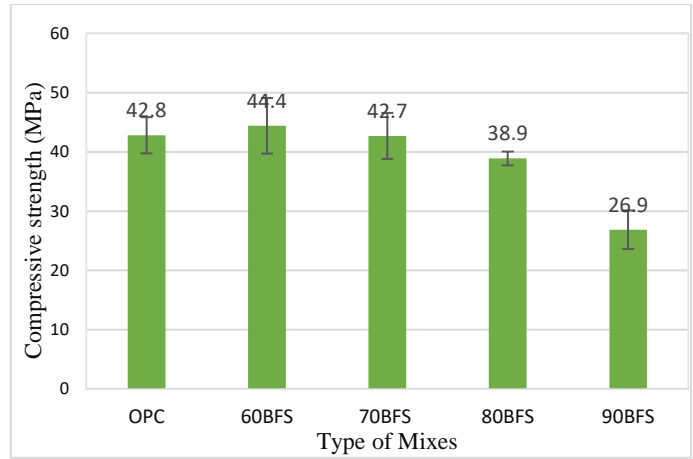
SEM analysis were carried out using a NEON microscope in the backscattered electron mode equipped with an energy dispersive X-ray analyser to identify the phases. All the samples were cut by using a diamond precision cutter and then placed in a vacuum desiccator for at least three days. After removed from the desiccator the samples were impregnated with epoxy resin mounted, polished and carbon coated and then kept in a vacuum desiccator before performed the SEM test.

The thermal stability of the samples was studied by thermogravimetric analysis (TGA). A Mettler Toledo TGA one star system analyser was used for all these measurements. Samples weighing 25 mg were placed in an alumina crucible and the tests were carried out in an Argon atmosphere at a heating rate of 10°C/min from 25 to 1000°C.

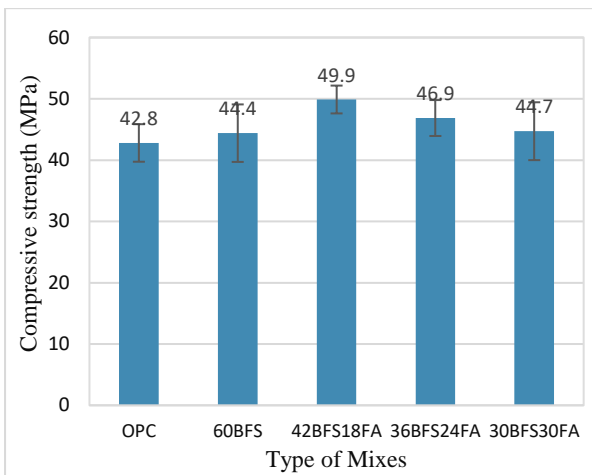
Mercury intrusion porosimetry (MIP) was used to measure the pore volume and pore size distribution of pastes samples. The pore diameter and intruded mercury volume were recorded at each pressure point over a pressure range of 0.0083 to 207 MPa. The pressures values were converted into equivalent pore diameters using the Washburn expression (Washburn, 1921) as expressed in Eq. (1):

$$d = - \frac{4\gamma \cos\theta}{p} \quad \text{Eq. 1}$$

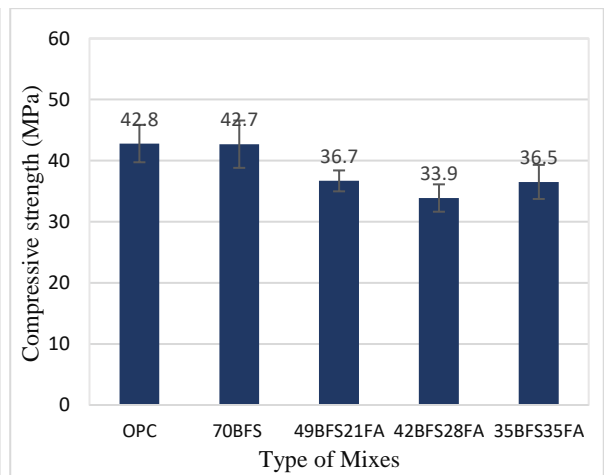
where, d is the pore diameter (µm), γ is the surface tension (mN/m), θ is the contact angle between mercury and the pore wall (°), and P is the net pressure across the mercury meniscus at the time of the cumulative intrusion measurement (MPa).



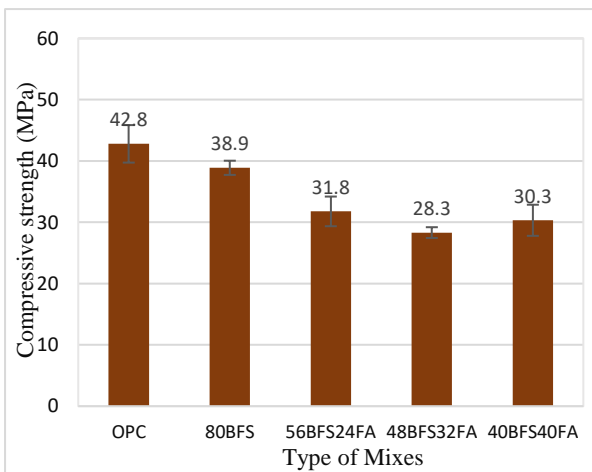
a)



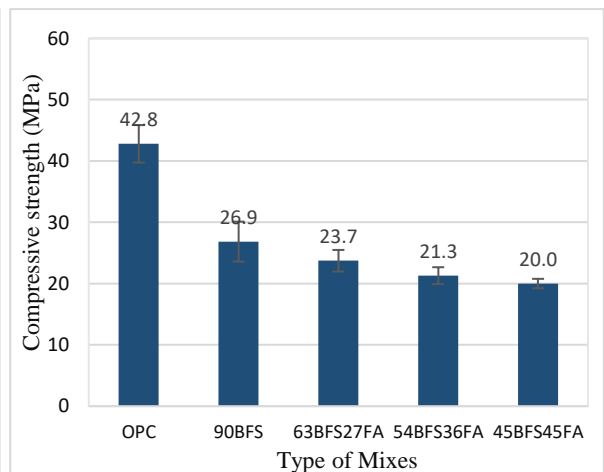
b)



c)



d)



e)

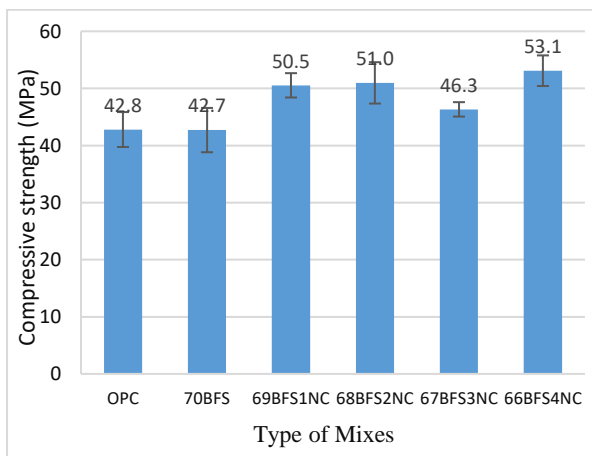
**Fig. 4.4** Effect of high volume slag and slag-fly ash blend mixes on the compressive strengths of cement paste at 28 days of age.

## 4.7 Results and Discussion

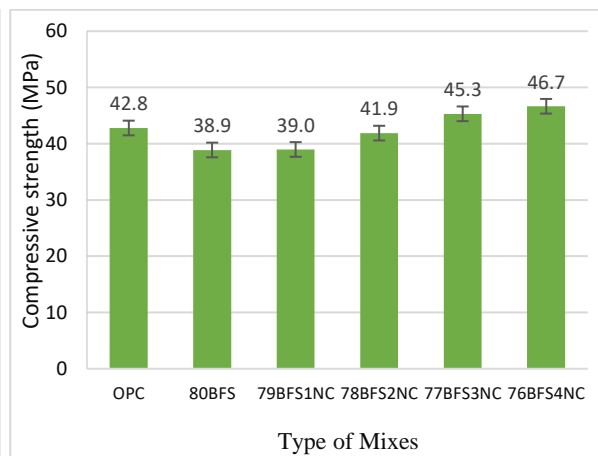
### 4.7.1 Compressive strength development

#### 4.7.1.1 Effect of high volume slag and high volume slag-fly ash blend

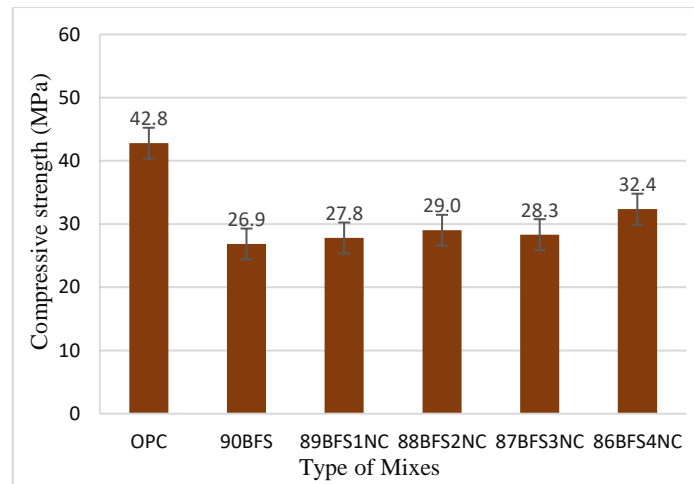
Compressive strengths of different high volume slag and high volume slag-fly ash blend pastes at 28 days with their standard deviation (SD) in form of error bar are shown in **Fig. 4.4** in comparison of control OPC paste. It is clearly evident from **Fig. 4.4a** that the compressive strength of HVS pastes decrease when partial replacement of cement by blast furnace slag increased more than 60%. The compressive strength of HVS paste containing 60% slag paste is 4% higher than the control OPC cement paste and very similar to the HVS cement paste containing 70% slag. However, about 9% reduction in compressive strength is observed in HVS paste containing 80% slag compared to control while huge reduction is noticed when the replacement increased to 90% as expected which is due to the extremely lower OPC content and slow hydration reaction of slag particles. Similar trends of compressive strengths of high volume slag composites at 28 days also reported in other studies (Choi et al., 2017; Oner & Akyuz, 2007). The effects of different fly ash contents of 30%, 40% and 50% as partial replacement of slag on 28 days compressive strengths of HVSFA pastes are shown in Figs. 4.4b-e. It can be seen in **Fig. 4.4b** that the compressive strengths of HVSFA pastes containing combined slag and fly ash content of 60% are higher than the control OPC and the HVS paste containing 60% slag in which the highest compressive strength is showed by 30% replacement of slag by fly ash. On the other hand, the compressive strengths of HVSFA pastes containing combined slag and fly ash contents of 70%, 80% and 90% are lower than the control OPC paste and HVS pastes. Due to lower CaO content of HVSFA pastes than the HVS pastes, the higher reduction of compressive strength is observed in the HVSFA pastes.



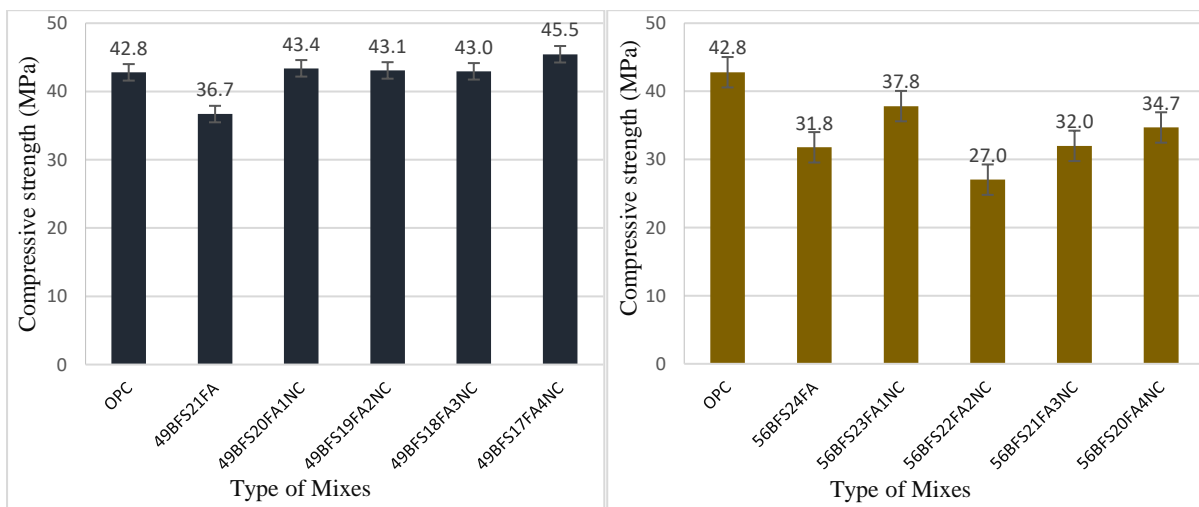
a)



b)



c)



d)

e)

**Fig. 4.5** Effect of Nano calcium carbonate on the compressive strengths of high volume slag and slag-fly ash blended paste at 28 days of age.

#### 4.7.1.2 Effect of nano- $\text{CaCO}_3$

The results in the first part show that the HVS paste containing 60% slag shows higher compressive strengths than control OPC paste and HVSFA paste containing combined slag and fly ash content of 90% shows significantly lower compressive strengths than control OPC as well as HVS paste 90% slag. Therefore, those two mixes were not considered in the second part of this study. Average compressive strengths at 28 days of different high volume slag and high volume slag-fly ash blend pastes incorporating various NC contents of 1% to 4% are shown in **Fig. 4.5** in comparison to that of control OPC and their respective reference paste. It can be seen from **Fig. 4.5a** that the NC inclusion increased the 28 days compressive strengths of HVS paste containing 70% slag by 8% to 24% for different NC contents compared to OPC paste and reference HVS paste, where the highest improvement was with 4% NC. In addition,



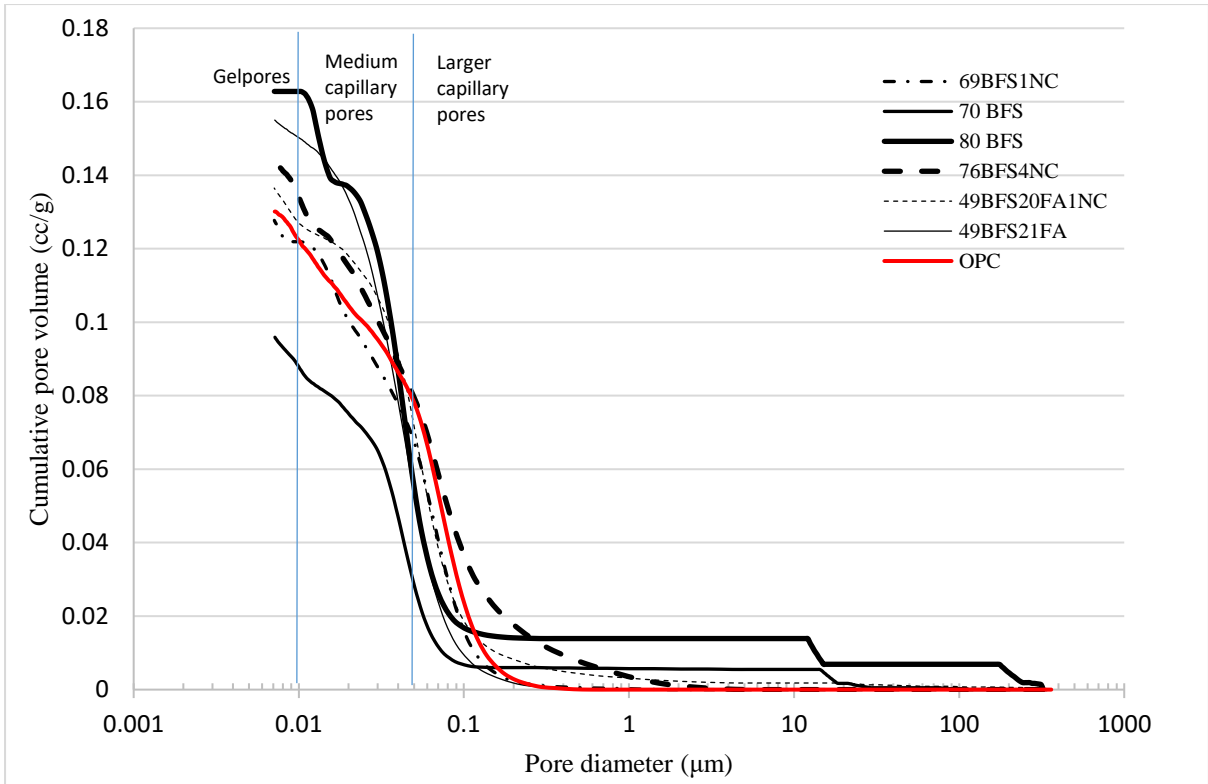
the compressive strength of HVS paste containing 80% slag is increased by 16% and 12% due to the addition of 3% and 4% NC, respectively compared to control reference paste without NC and is also higher than the control OPC paste. On the other hand, the addition of NC improved the compressive strengths of HVS paste containing 90% slag by about 3-20% compared to the reference HVS paste, however, the compressive strengths are much lower than the control OPC paste despite the addition of NC. This can be the reason of significantly lower level of Portlandite (CH) generation due to lower amount of OPC in the mixes and the higher level of NC required to activate those high volume of slag which would be costlier than the commercially available cementitious materials in the market.

The effects of NC on 28 days compressive strengths of paste containing combined slag and fly ash contents of 70% and 80% are shown in **Figs. 4.5d-e**. It can be seen that the NC inclusion improved the compressive strengths by 16-24% of paste containing combined slag and fly ash content of 70% compared to their reference paste and these improvements were higher than the compressive strength of OPC paste. On the other hand, the NC addition also improved the compressive strength of paste contains combined slag and fly ash content of 80% at all NC contents except the NC content of 2%. However, these improvements are not enough to exceed the compressive strength of control OPC paste.

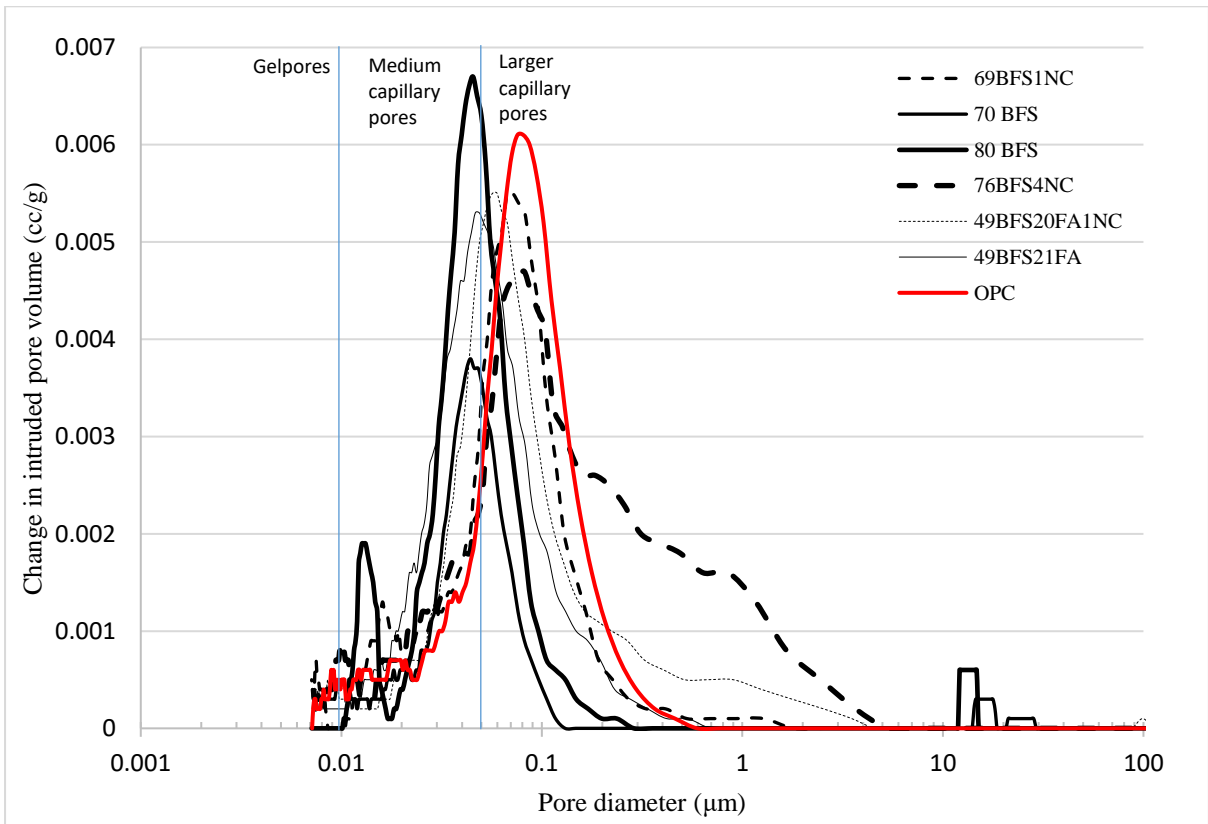
It can be easily seen from the above 28 days compressive strengths analysis that addition of NC improved the compressive strengths of HVS paste containing 70% slag and HVSFAs paste containing combined slag and fly ash contents of 70% significantly and showed higher compressive strength than that of control OPC paste almost every mixes. These mixes can reduce the carbon footprint of concrete significantly as they contain significantly lower volume of OPC.

#### **4.7.2 Microstructure**

It is clear from the compressive strength results that the addition of NC enhanced the compressive strengths of HVS and HVSFAs pastes significantly which is an evidence of early pozzolanic reaction of slag and fly ash and formation of dense microstructure than their reference control pastes as well as control OPC paste. Therefore, microstructural analysis in terms of their pore sizes and pore volume, pozzolanic reaction of slag and fly ash, formation of calcium silicate hydrate (CSH)/ calcium aluminate hydrate (CAH) gels and thus new mineral due to the addition of NC into those HVS and HVSFAs pastes were conducted.



a)



b)

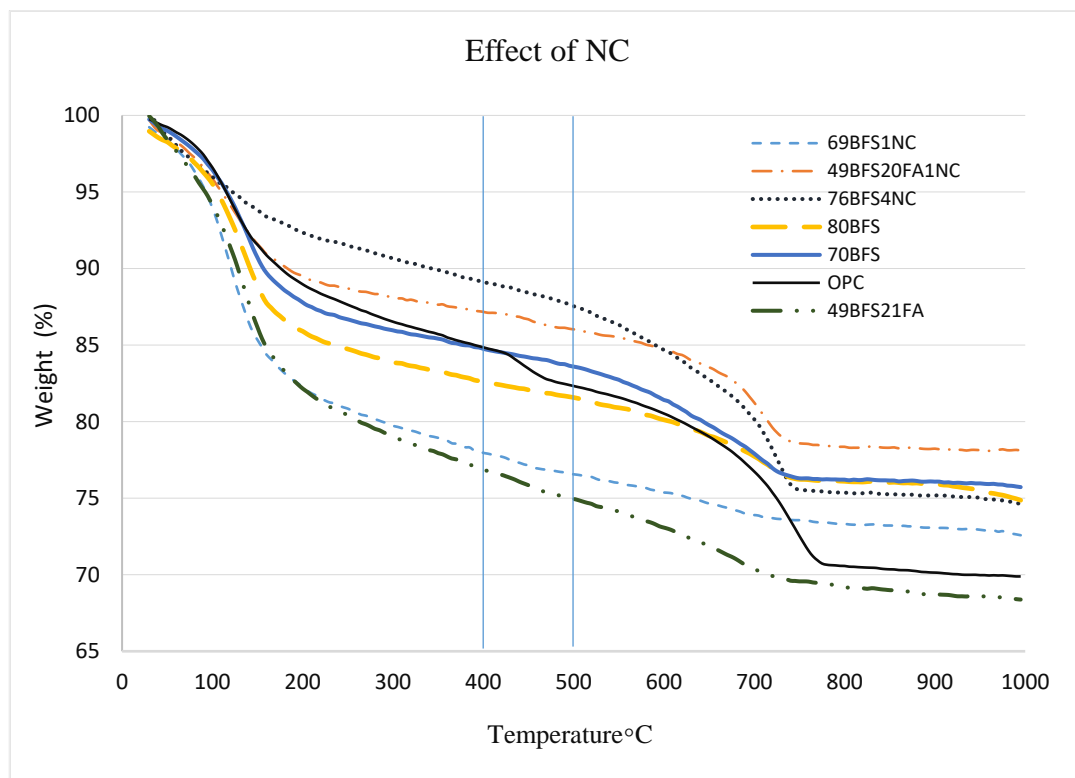
**Fig. 4.6** Effect of nano- $\text{CaCO}_3$  on the a) cumulative pore volume and b) pore size distribution of HVS and HVSFA pastes.

#### 4.7.2.1 Mercury intrusion porosimetry (MIP)

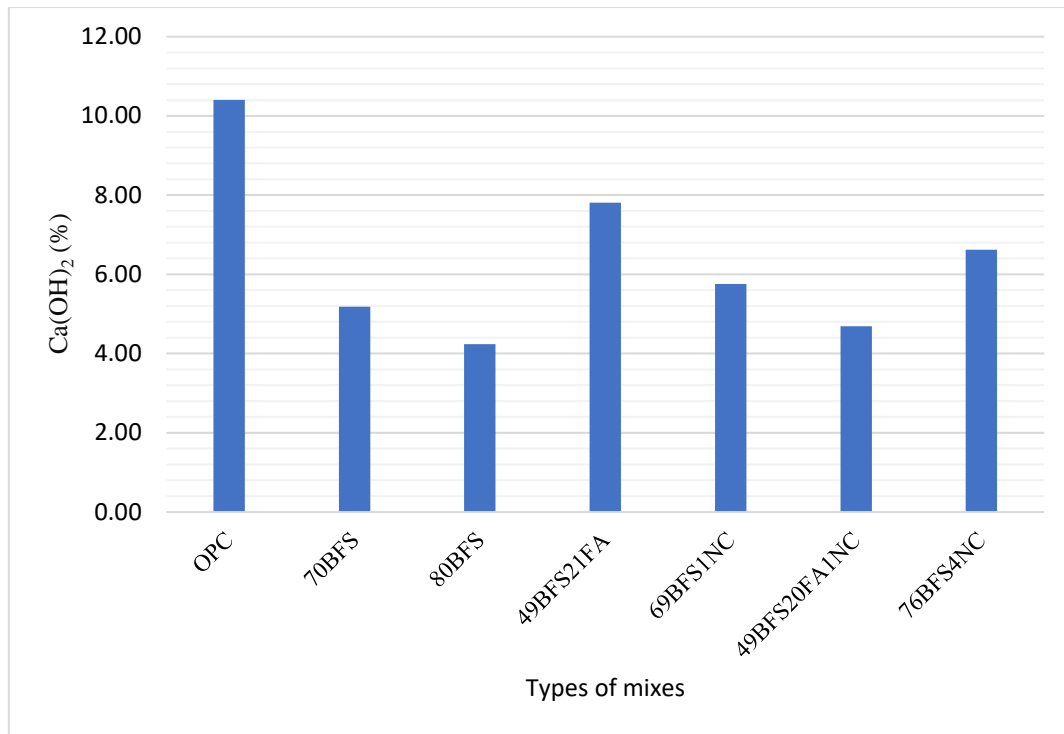
Effects of NC on cumulative pore volume and pore size distribution of various HVS and HVSFAs pastes at 28 days is shown in **Fig. 4.6**. The pores in cement paste are divided into large capillary pores from (10–0.05  $\mu\text{m}$ ), medium capillary pores (0.05–0.01  $\mu\text{m}$ ) and gel pores (<0.01  $\mu\text{m}$ ) (Mindess S et al., 2003) and the pores with diameter down to 0.006  $\mu\text{m}$  detected by using mercury intrusion porosimeter. It can be seen from **Fig. 4.6a** that the volume of larger capillary pores of HVS pastes containing 70% and 80% slag is higher than the OPC paste. However, the HVSFAs paste contains combined fly ash and slag of 70% showed lower volume of large capillary pores than the OPC paste. This is due to the combination of spherical shape fly ash particles and slag particles of angular shape. However, the volume of medium capillary and gel pores of HVS paste containing 70% slag are lower than the OPC paste while HVS paste containing 80% slag and HVSFAs paste containing combined slag and fly ash content of 70% exhibited the higher volume of medium capillary and gel pores than OPC paste. The distribution of pores having different diameters of all pastes is shown in **Fig. 4.6b**. The diameter at which the slope of the volume-diameter curve is the steepest and corresponds to the mean size of the pore entryways that allows maximum percolation throughout the pore system is the critical diameter which is the region under the curves represents the concentration of the pores and peak point of the curves (Mindess et al., 2003). The results show that the concentration of pores of HVS paste containing 70% slag and that containing 80% slag is very similar but the volume of pores is much higher in the case of paste containing 80% slag than that containing 70% slag. This could be the reason for higher compressive strength in latter paste than the former paste. On the other hand, if we compare between paste containing 80% slag and combined slag and fly ash of 70%, it is clear that total capillary pore considering their respective gel, medium and large capillary pores are similar which is also resemble in their corresponding compressive strengths. It can also be seen that critical pore diameter of all HVS and HVSFAs pastes are in between medium and larger capillary pores region while critical pore diameter of control OPC is in the region of larger capillary pores.

The cumulative pore volume and pore size distribution of HVS and HVSFAs pastes containing NC are also shown in the **Fig. 4.6a-b**. The results show that addition of 1% NC in HVS paste containing 70% slag reduced the larger capillary pores and increased gel pores significantly which might be the evidence of densified micro-structure through formation of C-S-H gel. However, the volume of medium capillary pores is increased in the paste containing 70% slag despite addition of NC although it is lower than the control OPC paste. On the other hand,

volume of gel pores of paste containing 80% slag and paste containing combined slag and fly ash of 70% are decreased surprisingly due to the addition of NC but higher than the control OPC paste. Significant reduction in medium capillary pores is observed of both mixes and large capillary pores volume was not affected due to the addition of NC. It can be seen slight changes of the critical pore diameter region of the HVS and HVSFA pastes due to the addition of NC in **Fig. 4.6b** compared to their reference pastes. In addition, the cumulative pore volume of the pastes containing 80% slag and combined slag and fly ash content of 70% reduced significantly due to the addition of 1% and 4% NC, respectively. This could be the reason of enhanced pozzolanic reaction of high volume slag and fly ash due to the addition of NC and formed additional C-S-H and C-A-H gels in mixes. Reduced larger and medium capillary pores of HVS and HVSFA pastes with NC compared to control OPC paste will contribute to the resistance of penetration of detrimental ingredients into the composites.



a)



b)

**Fig. 4.7** TGA analysis a) High volume slag and High volume slag-fly ash blended pastes with and without nano-CaCO<sub>3</sub> and b) Ca(OH)<sub>2</sub> contents.

#### 4.7.2.2 Thermogravimetric analysis (TGA)

The results of thermogravimetric analysis (TGA) of HVS and HVSFA pastes with and without NC compared to control OPC paste are shown in **Fig. 4.7a**. The curves show the normalized mass loss of a substance in percent (current mass divided by initial mass) under control environment as a function of temperature. It has been reported that mass loss between 420°C and 540°C corresponds to the dehydration of calcium hydroxide (Keatch & Dollimore, 1975). It can be seen from the TGA curves that mass loss between those temperature ranges of HVS paste containing 70% slag due to the addition of NC is lower than their reference paste as well as control OPC paste. This is clearly the evidence of lower amount calcium hydroxide in paste containing NC than the control paste indicating formation of more C-S-H gel which was also shown in the MIP analysis. However, in case of HVS paste containing 80% slag and HVSFA paste containing combined slag and fly ash content of 70% the weight loss is higher due to addition of NC than their respective reference pastes and control OPC paste and it is more pronounced in the case of HVSFA paste. The amount of calcium hydroxide (CH) can also be quantified according to Taylor's formula (Taylor, 1990) shown as follows in equation (2):

$$CH(\%) = WL_{CH}(\%) \frac{MW_{CH}}{MW_{H_2O}} \quad \text{Eq. 2}$$

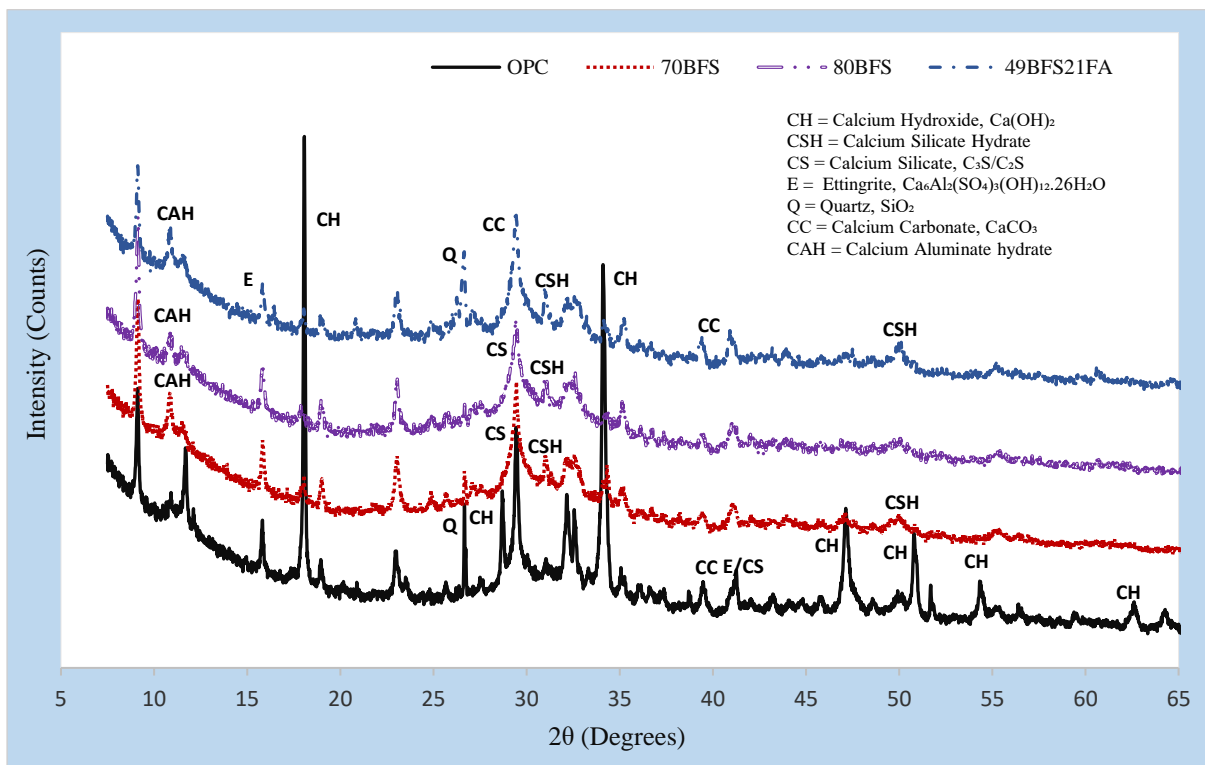
Where,  $WL_{CH}$  is the weight loss during the dehydration of CH as percentage of the ignited weight (%);  $MW_{CH}$  is the molecular weight of CH;  $MW_{H_2O}$  is the molecular weight of  $H_2O$ .

**Fig. 4.7b** shows the calculated CH contents of pastes with and without NC. It is clear that the CH content in all HVS and HVSFA pastes with and without NC are lower than the control OPC paste which indicate that through pozzolanic reaction of  $SiO_2$  in slag and fly ash with CH the C-S-H is formed in those pastes. It can be also be seen that addition of NC reduced the CH content significantly by 37% in HVSFA paste which can be interpreted due to the reaction of  $SiO_2$  of fly ash with CH in that paste sample. However, slightly higher amount of CH is found in HVS paste containing 70% slag due to the addition of 1% NC and these increment is greater in HVS paste containing 80% slag after inclusion of NC. This shows that NC did not produce much C-S-H in those paste rather formed calcium aluminium hydroxide (CAH) hydrate and calcium carbonate hydrate due to the reaction with calcium oxide of slag which is also found in X-ray diffraction analysis of this study.

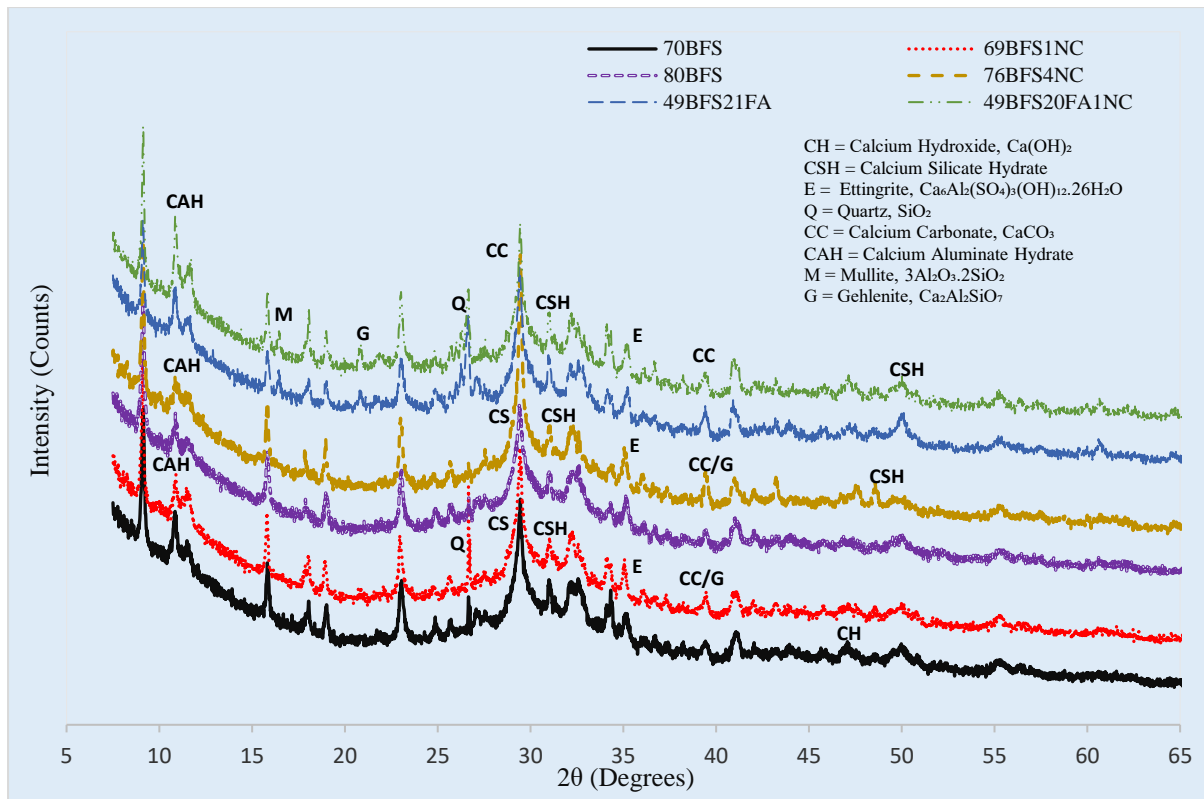
#### 4.7.2.3 X-ray Diffraction (XRD) analysis

The reactions during cement hydration of HVS and HVSFA pastes with and without NC at 28 days are studied through XRD analysis. The horizontal scale is the diffraction angels measured in degrees and the vertical scale is the peaks height of the intensity of the diffraction measured in pulses/s. XRD patterns of control OPC paste and different HVS and HVSFA pastes are shown in **Fig. 4.8a**. The Diffraction spectra analysis showed that enormous amount of calcium hydroxide was formed in OPC paste as expected. By comparing diffraction spectrum of HVS containing 70% and 80% slag and HVSFA containing combined slag and fly ash content of 70%, it is clear that the intensity of CH peaks in those high volume mixes are significantly lower than the OPC paste and higher peak of calcium silicate hydrate (C-S-H) at  $2\theta$  angle of  $31.4^\circ$  and calcium aluminate hydrate (C-A-H) at  $2\theta$  angle of  $10.8^\circ$  is also found. This could be the reason of high volume of slag and fly ash and less OPC which reduced the CH peaks and formed higher C-A-H and C-S-H due to pozzolanic reaction. Increased of gehlenite ( $Ca_2Al_2SiO_7$ ) at  $2\theta$  angle of  $20.8^\circ$  and  $39.5^\circ$  and quartz at  $2\theta$  angle of  $27^\circ$  of paste mix

containing combined BFS+FA than HVS paste containing BFS only could be the presence of FA in that mix. **Fig. 4.8b** shows comparison of XRD pattern of HVS and HVSFA pastes with and without inclusion of NC. It can be seen that the intensity of CH peak did not show any noticeable changes due to the addition of NC except a slight reduction of intensity at  $2\theta$  angle of  $47^\circ$ . In addition, slight increase of C-A-H peak at  $2\theta$  angle of  $10.8^\circ$  is observed in paste samples with NC. Moreover, the intensity of C-S-H peaks at  $2\theta$  angle of  $31.4^\circ$  is also increased due to the addition of NC and increase in intensity of Ettringite is also noticeable at  $2\theta$  angle of  $36^\circ$  in the paste mixes with NC. Moreover, addition of NC increased calcium carbonate (CC) significantly at  $2\theta$  angle of  $39.5^\circ$  in all HVS and HVSFA pastes expectedly. In the case of HVSFA paste new mineral peaks of Mullite (M) and Gehlenite (G) can be seen at  $2\theta$  angles of  $16.5^\circ$  and  $20.8^\circ$ , respectively with increase of Gehlenite peak due to addition of NC.



a)



b)

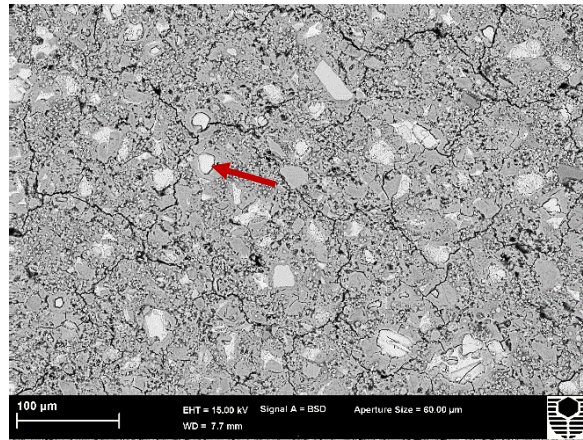
**Fig. 4.8** XRD patterns of a) HVS and HVSFA paste b) HVS and HVSFA paste containing nano- $\text{CaCO}_3$

#### 4.7.2.4 Scanning electron microscopy (SEM) and energy dispersive X-ray spectroscopy (EDS) analysis

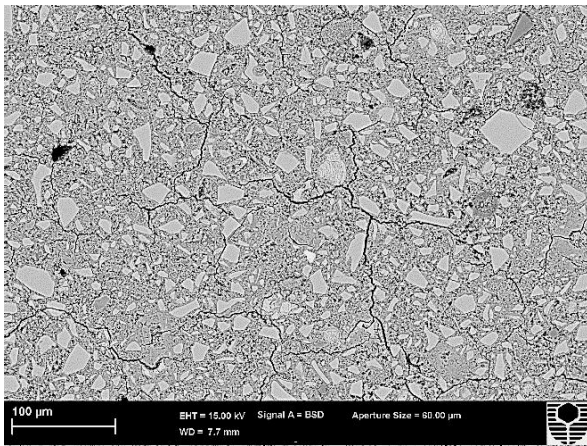
Backscattered electron images of control OPC, high volume slag and high volume slag-fly ash blended pastes at lower magnification are shown in **Fig. 4.9** after 28 days of curing. It can be seen from the images that OPC paste indicates a comparatively dense microstructure with less internal cracks and lower black spots than the other HVS and HVSFA pastes without NC. Fewer number of represent more hydrated products and black spots are indication of pores/voids in the microstructure. However, there are few unhydrated cement in OPC paste (shown by arrow) which are obviously lower than the unhydrated/ partially hydrated slag particle in HVS paste and unhydrated or partially hydrated fly ash particle in HVSFA paste. On the other hand, by comparing SEM images of HVS and HVSFA pastes, it is clear that HVS paste containing 70% slag has denser microstructure than the other HVS and HVSFA pastes. Addition of NC improves the microstructure by reducing width of internal cracks of all HVS and HVSFA pastes can also be seen from the images of lower magnification in **Fig. 4.10**. In



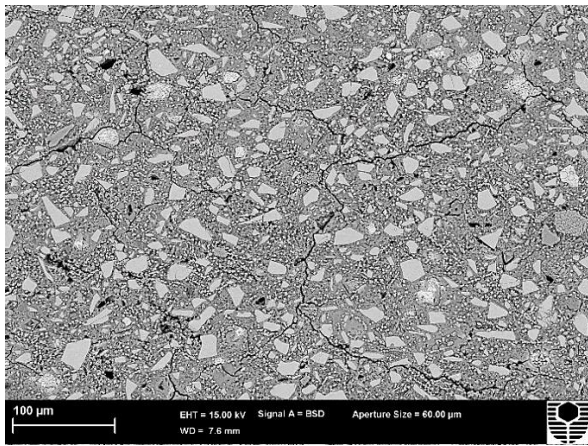
addition, among all HVS and HVSFA pastes, high volume slag paste containing 69%BFS and 1% NC showed much denser microstructure than others, which is also clearly revealed in the compressive strength discussion.



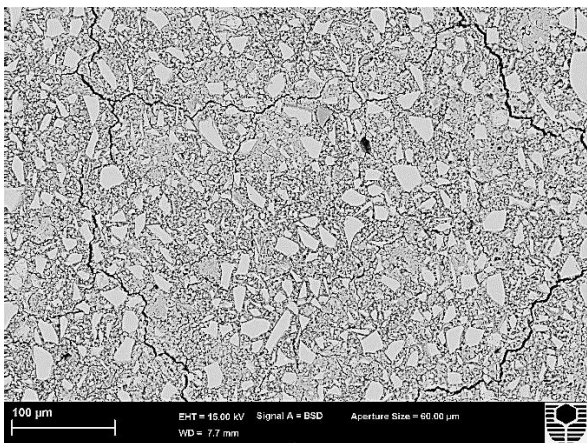
a) OPC paste



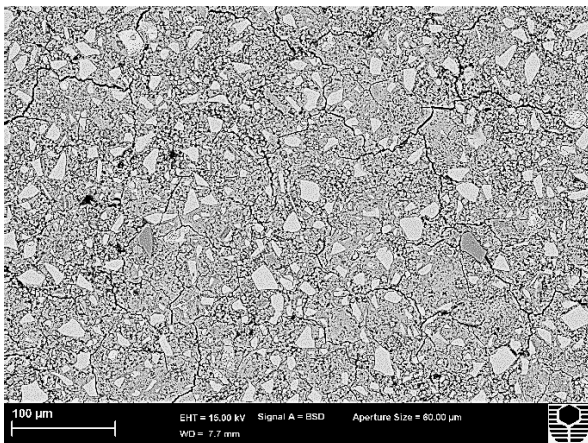
b) 70BFS



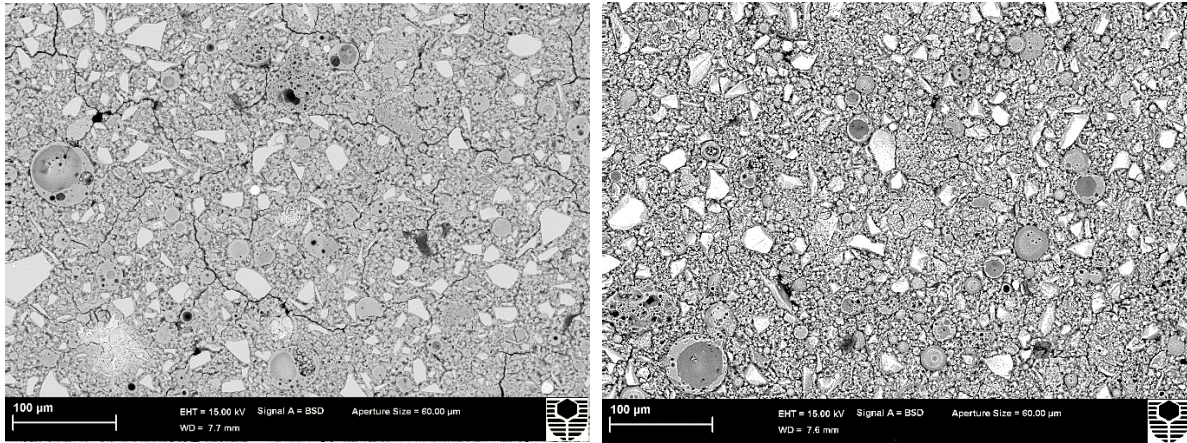
c) 69BFS1NC



d) 80BFS



e) 76BFS4NC

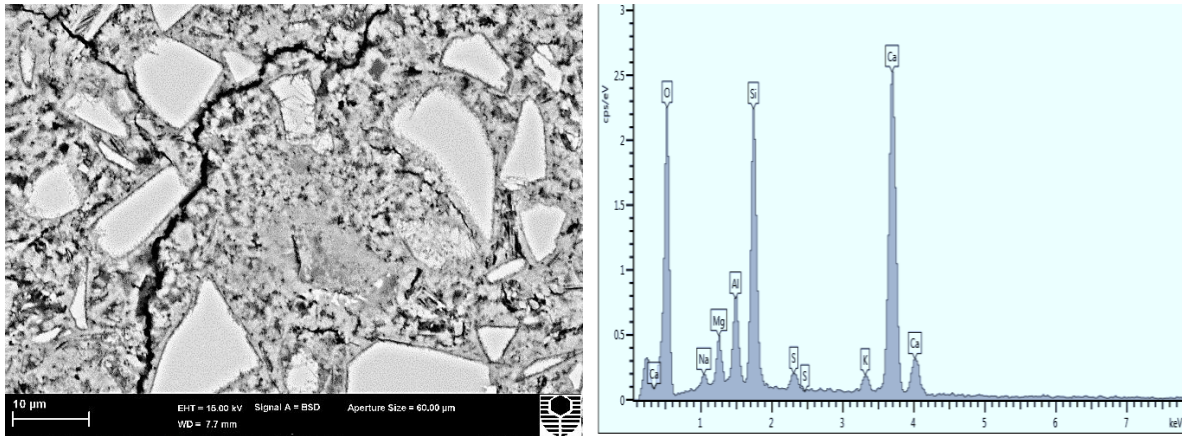


f) 49BFS21FA

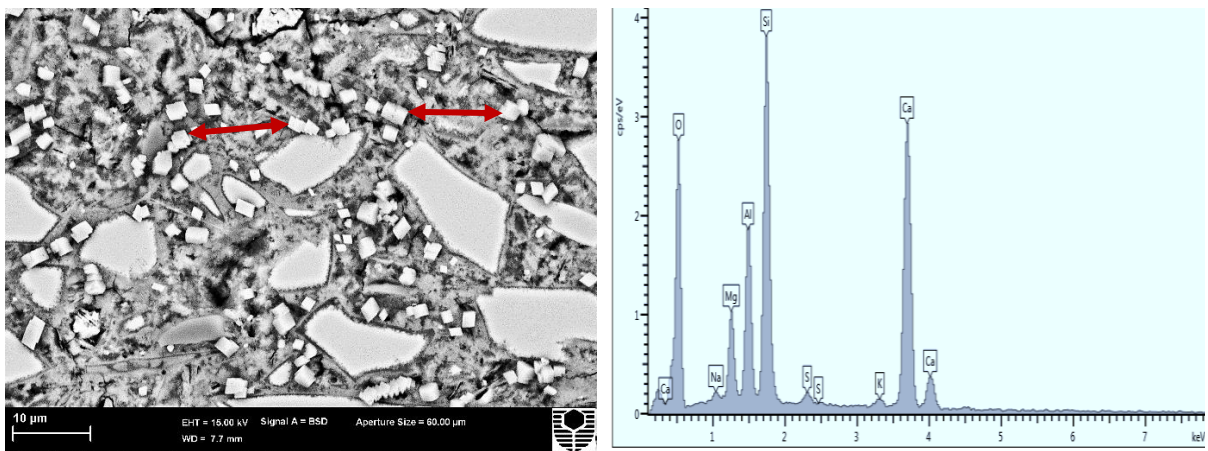
g) 49BFS20FA1NC

**Fig. 4.9** Backscattered electron images of a) OPC b) 70BFS c) 69BFS1NC d) 80BFS e) 76BFS4NC f) 49BFS21FA g) 49BFS20FA1NC pastes at lower magnification

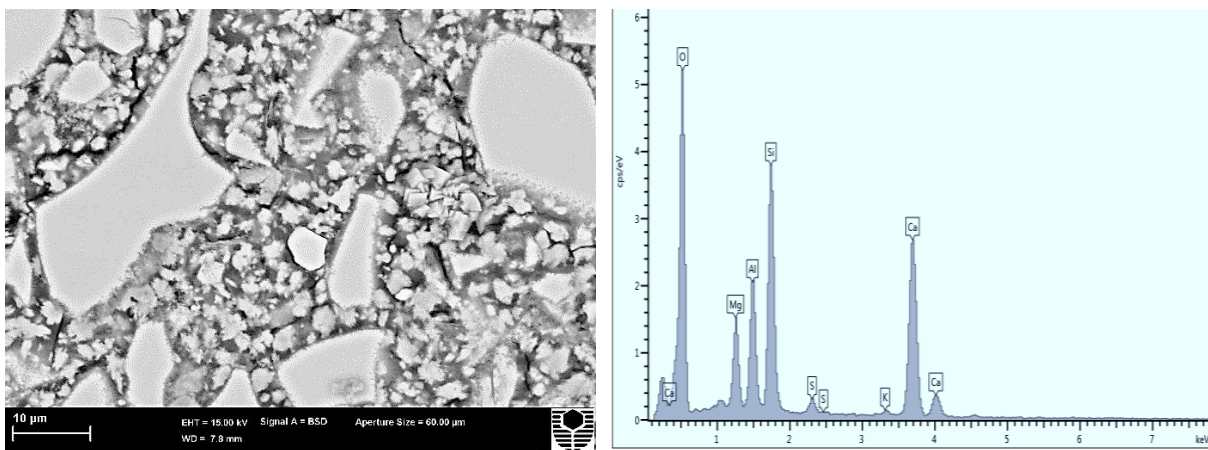
Scanning electron microscopy images with higher magnification and EDS spectra of HVS and HVSFA pastes with and without NC are shown in **Fig. 4.10**. It can be seen by comparing **Fig. 4.10a** and **Fig 4.10b** that a thin rim had formed around the slag particle of HVS paste containing 1% NC and evidence of more hydration products (indicated by arrow in SEM images) than the HVS paste containing 70% slag. In addition, Ca/Si ratio of the C-S-H gel from EDS spectra around a slag particle of paste containing NC is lower than the paste without NC which indicates that the presence of NC in the paste accelerated the pozzolanic action of slag and increased the Si content of C-S-H gel. Similar denser microstructural formation such as thin rim around slag and fly ash particles also can be seen in the HVS paste containing 80% slag and HVSFA paste containing combined slag and fly ash of 70% due to addition of NC by comparing the higher magnification images and EDS spectra of those mixes. On the other hand, by comparing all the HVS and HVSFA paste with NC, it is easily come to the conclusion that the paste containing 70% slag had much denser microstructure with much higher hydrated particles and lower pores than the other mixes. In addition, higher peak of silica in EDS spectra is also evident in HVS and HVSFA pastes containing NC than their reference pastes, which also indicates formation of more CSH/CAH in the matrix.



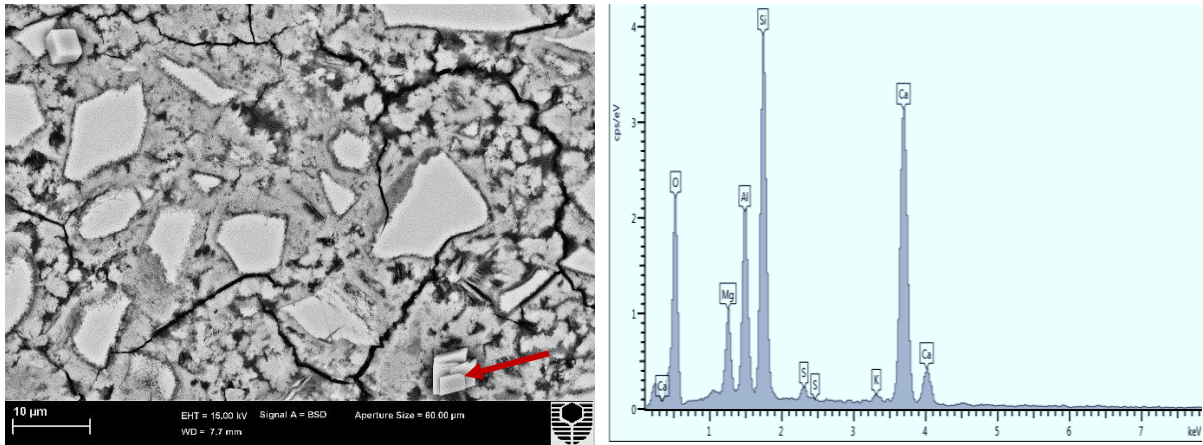
a) Backscattered electron image and EDS trace around a slag particle of 70BFS paste



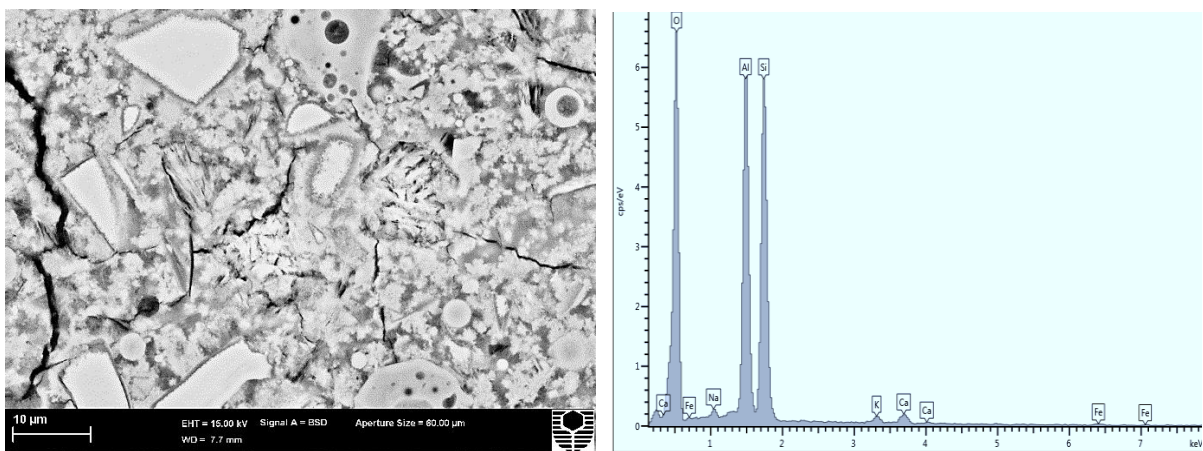
b) Backscattered electron image and EDS spectra around a slag particle of 69BFS1NC paste



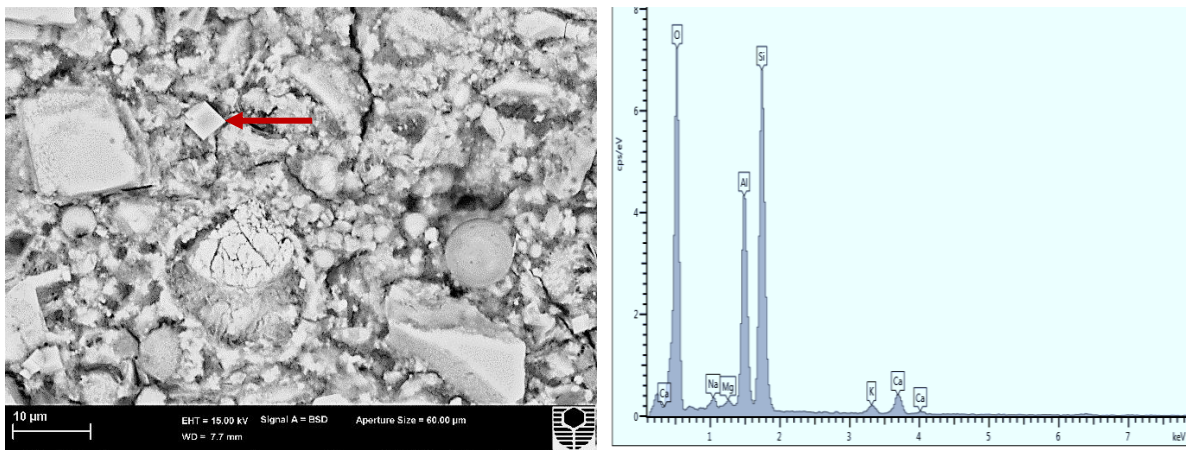
c) Backscattered electron image and EDS trace around a slag particle of 80BFS paste



d) Backscattered electron image and EDS trace around a slag particle of 76BFS4NC paste



e) Backscattered electron image and EDS trace around a fly ash particle of 49BFS21FA paste

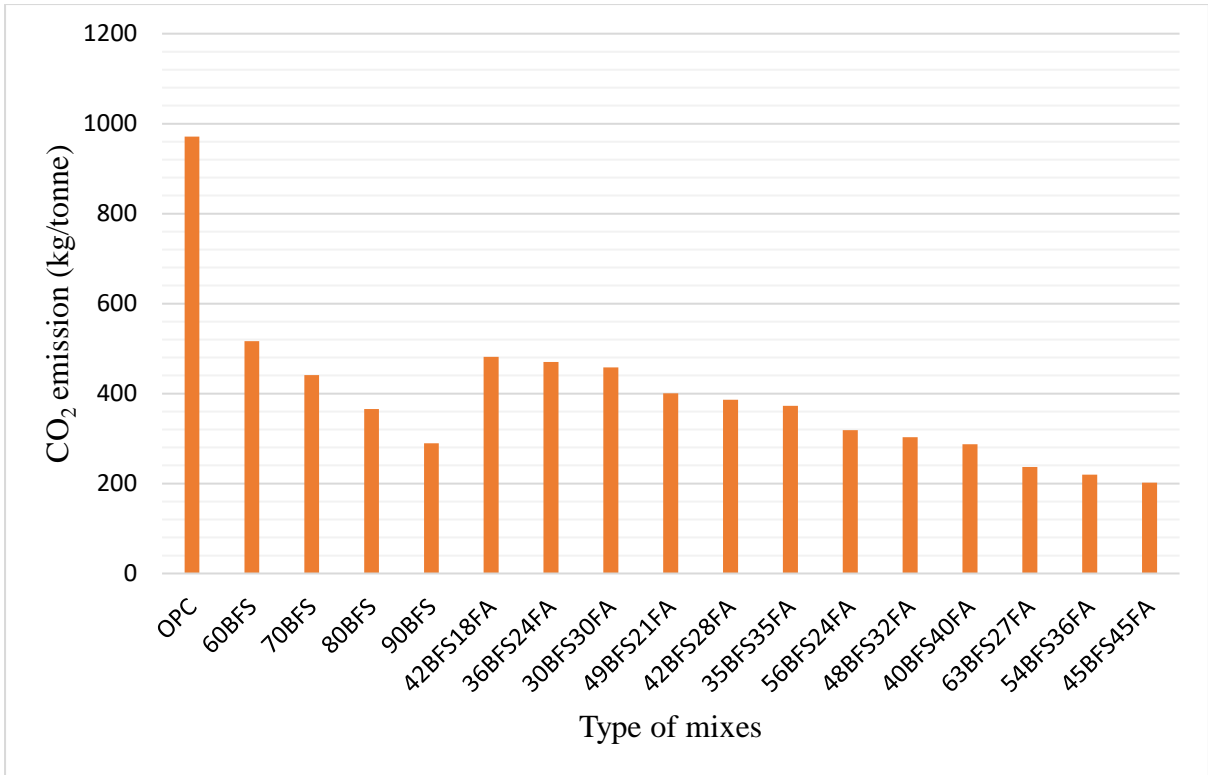


f) Backscattered electron image and EDS trace around a fly ash particle of 49BFS20FA1NC paste

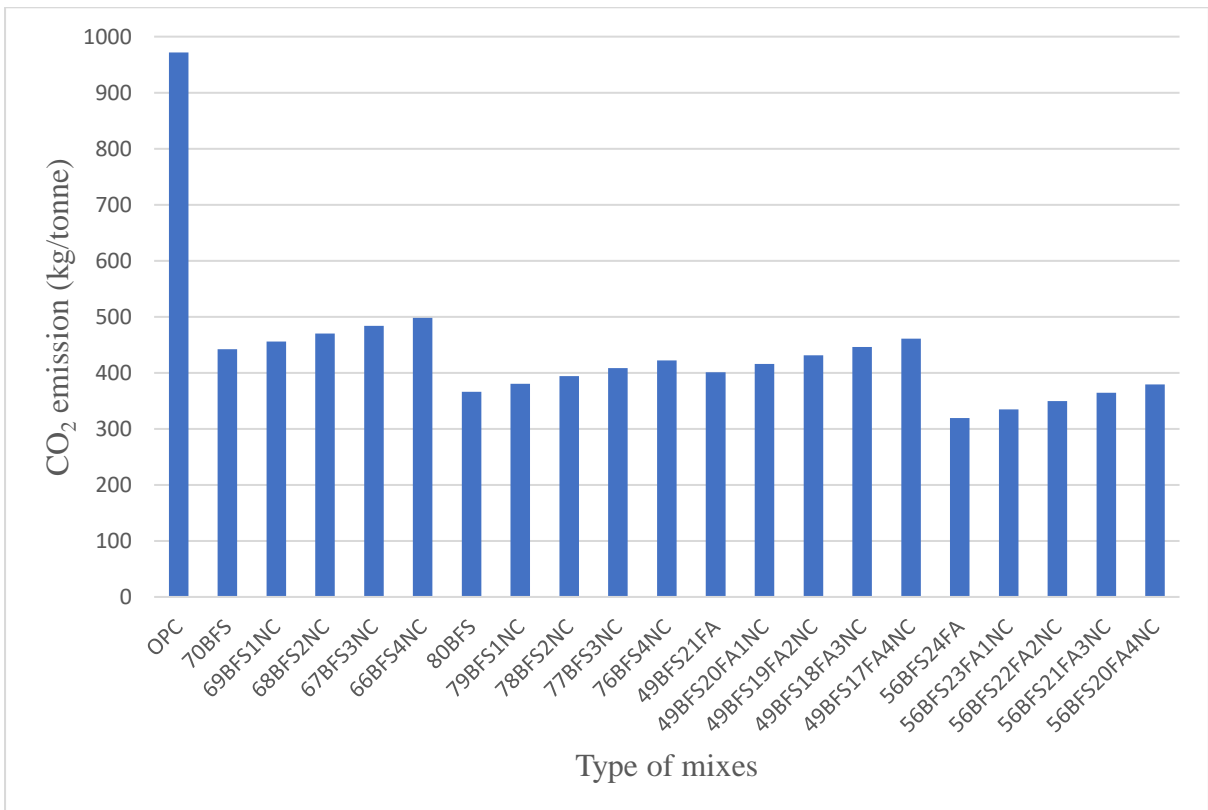
**Fig. 4.10** Backscattered electron images and EDS spectra of different HVS and HVSFA pastes with and without NC

### 4.7.3 CO<sub>2</sub> emission analysis

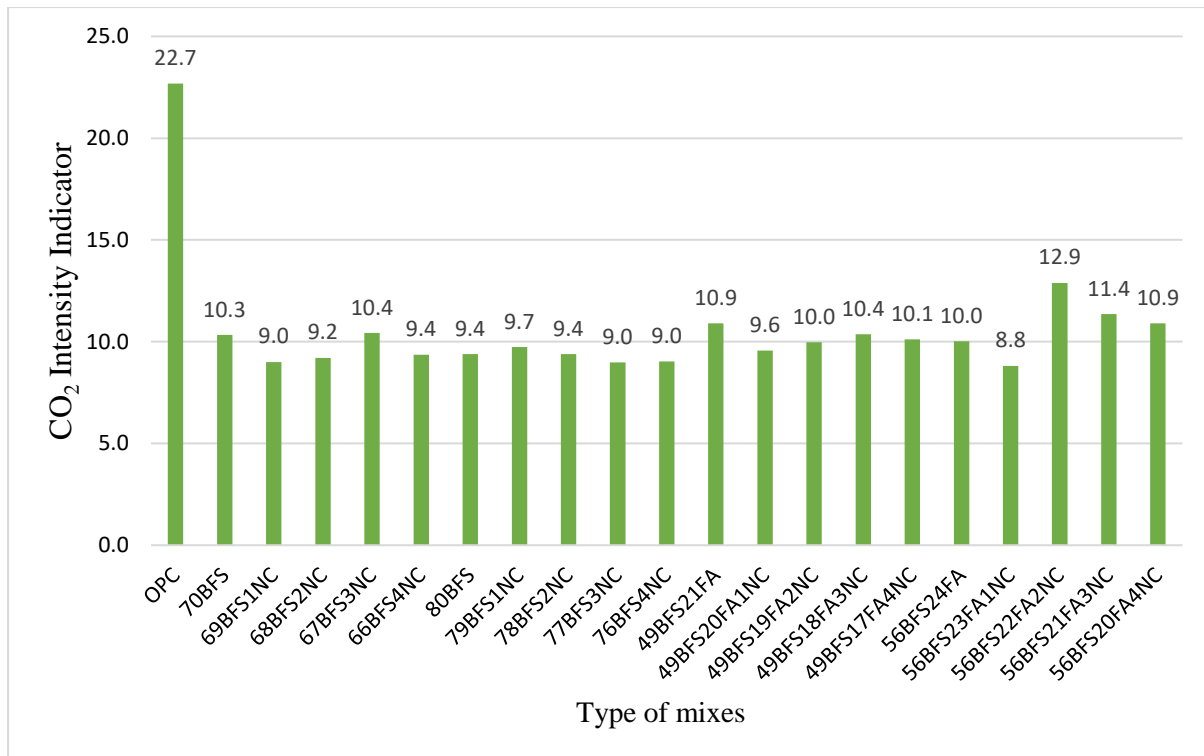
Carbon di-oxide (CO<sub>2</sub>) emission analysis of different HVS and HVSFA paste with and without NC are shown in **Figs. 4.11a-b**. All the CO<sub>2</sub> emission value of 971 kg/tonne for OPC, 214 kg/tonne for slag, 18.9 kg/tonne for fly ash and 1610 kg/tonne for nano-CaCO<sub>3</sub> are collected from SimaPro software database. It can be seen from the **Fig. 4.11a** that significant reduction of CO<sub>2</sub> emission with the increasing content of OPC replacement in all HVS pastes. Moreover, a further reduction observed due to the inclusion of fly ash in all HVSFA paste compared to that of HVS paste of same OPC replacement. However, a slight gradual increase in CO<sub>2</sub> emission found in all HVS and HVSFA paste with the increase content of additional NC compared to their control paste without NC shown in **Fig. 4.11b**, though the amount of CO<sub>2</sub> emissions are way lower than the control OPC paste. On the other hand, **Fig. 4.11c** shows the CO<sub>2</sub> intensity indicator ( $c_i = c/p$ ) (Damineli et al., 2010) for all the paste mixes with NC which are considered according to their 28 days compressive strengths along with their control mixes without NC, where  $c$  is the total CO<sub>2</sub> emission and  $p$  is the average compressive strength in MPa. It can be seen that three mixes of HVS pastes having similar value of  $c_i = 9.0$ . However, considering the 28 days compressive strength values of those three paste mixes of HVS paste, it is clear that 1% NC inclusion in HVS paste containing 70% slag and 4% NC inclusion in HVS paste containing 80% slag could produce a sustainable mix with considerably low CO<sub>2</sub> emission. It can also be seen that 1% NC inclusion in both HVSFA paste containing combined 70% and 80% (BFS+FA) exhibited lower  $c_i$  values among all the HVSFA pastes. Nevertheless, compressive strength of both mixes at 28 days age clearly favours the HVSFA paste containing combined 70% (BFS+FA) with significantly lesser CO<sub>2</sub> emission.



a)



b)



c)

**Fig. 4.11** CO<sub>2</sub> emission and CO<sub>2</sub> intensity indicator analysis of HVS and HVSFA pastes with and without nano-CaCO<sub>3</sub>.

#### 4.8 Summary

Based on the above discussion of various contents of nano calcium carbonate on the 28 days compressive strengths and changes in microstructure of high volume blast furnace slag and high volume blast furnace slag-fly ash blended pastes the following conclusions can be drawn:

- Compressive strength of high volume slag (HVS) paste containing 60% slag is increased by 4% than control OPC paste and HVS paste containing 70% slag had similar compressive strengths to control OPC paste after 28 days of curing. However, any further replacement of OPC by slag caused a significant reduction in compressive strengths.
- Compressive strength of high volume slag-fly ash (HVSFA) paste containing combined slag and fly ash of 60% is about 5%-16% higher than control OPC paste and are much lower with the increased contents of combined slag and fly ash after 28 days of curing.
- Inclusion of 1%-4% nano-CaCO<sub>3</sub> (NC) in the HVS paste containing 70%, 80% and 90% slag increased the compressive strengths at 28 days by approximately 8-24%, 1-16% and 2-20%, respectively compared to the reference HVS paste without NC.

However, compressive strengths were lower than the control OPC paste in almost every mix except the HVS paste containing 70% slag.

- The addition of NC significantly improved the compressive strengths of HVSFA paste containing combined slag and fly ash of 70% by 16-24% than the reference control paste without NC and maintained higher compressive strengths than control OPC paste at 28 days. However, in case of HVSFA paste with combined slag and fly ash of 80% had lower compressive strengths than control OPC paste in all mixes.
- The addition of NC in the HVS paste containing 70% slag reduced larger capillary pores and increased gel pores and medium capillary pores. In case of HVS paste with 80% slag and HVSFA paste containing combined slag and fly ash of 70%, gel pores and medium capillary pores are decreased but did not show any notable change in larger capillary pores. However, cumulative pore volume is reduced in both mixes.
- Significant reduction in  $\text{Ca(OH)}_2$  is noticed in all HVS and HVSFA pastes than control OPC paste and paste containing combined slag and fly ash of 70% due to the addition of 1% NC than the reference control paste without NC. However, the addition of NC increased the  $\text{Ca(OH)}_2$  contents in both HVS pastes confirmed in thermogravimetric analysis.
- No significant changes are observed in calcium hydroxide peaks due to the addition of NC in HVS and HVSFA pastes in XRD analysis. However, increased intensity of Ettringite (E), calcium silicate hydrate (CSH), calcium aluminate hydrate (CAH) and calcium carbonate are found due to the addition of NC in all HVS and HVSFA pastes.
- Incorporation of NC densified the internal microstructure compared to the reference HVS and HVSFA pastes without NC addition revealed in scanning electron microscopic images and EDS trace analysis.
- HVS and HVSFA paste containing 70% slag and slag-fly ash blend significantly reduced  $\text{CO}_2$  emission and maintain better compressive strength than control OPC paste with the inclusion of 1% NC.



## 4.9 References

- Aghaeipour, A. and M. Madhkhan, Effect of ground granulated blast furnace slag (GGBFS) on RCCP durability. *Construction and Building Materials*, 2017. 141: p. 533-541.
- Benhelal, E., et al., Global strategies and potentials to curb CO<sub>2</sub> emissions in cement industry. *Journal of Cleaner Production*, 2013. 51(Supplement C): p. 142-161.
- Choi, Y.C., J. Kim, and S. Choi, Mercury intrusion porosimetry characterization of micropore structures of high-strength cement pastes incorporating high volume ground granulated blast-furnace slag. *Construction and Building Materials*, 2017. 137: p. 96-103.
- Damineli, B.L., et al., Measuring the eco-efficiency of cement use. *Cement and Concrete Composites*, 2010. 32(8): p. 555-562.
- Damtoft, J.S., et al., Sustainable development and climate change initiatives. *Cement and Concrete Research*, 2008. 38(2): p. 115-127.
- Duran Atiş, C. and C. Bilim, Wet and dry cured compressive strength of concrete containing ground granulated blast-furnace slag. *Building and Environment*, 2007. 42(8): p. 3060-3065.
- Durán-Herrera, A., et al., Evaluation of sustainable high-volume fly ash concretes. *Cement and Concrete Composites*, 2011. 33(1): p. 39-45.
- Güneyisi, E. and M. Gesoğlu, A study on durability properties of high-performance concretes incorporating high replacement levels of slag. *Materials and Structures*, 2008. 41(3): p. 479-493.
- Hooton, R.D., Canadian use of ground granulated blast-furnace slag as a supplementary cementing material for enhanced performance of concrete. *Canadian Journal of Civil Engineering*, 2000. 27(4): p. 754-760.
- Kawashima, S., et al., Modification of cement-based materials with nanoparticles. *Cement and Concrete Composites*, 2013. 36(Supplement C): p. 8-15.
- Keatch, C.J. and D. Dollimore, *Introduction to thermogravimetry*. Vol. 45. 1975, Heydon.
- Malhotra, V.M., *Introduction: Sustainable development and concrete technology*, ACI Board Group on Sustainable Development. *ACI Concrete International*, 2002. 24(7): p. 22.
- Mehta, P.K., *Reducing the environmental impact of concrete*. *ACI Concrete International*, 2001. 23(10): p. 61-66.

Mindess S, Young JF, and D. D., Concrete. 2nd ed. Upper Saddle River. 2003, NJ: Prentice Hall.

Oner, A. and S. Akyuz, An experimental study on optimum usage of GGBS for the compressive strength of concrete. Cement and Concrete Composites, 2007. 29(6): p. 505-514.

Rashad, A.M., An investigation of high-volume fly ash concrete blended with slag subjected to elevated temperatures. Journal of Cleaner Production, 2015. 93(Supplement C): p. 47-55.

Şahmaran, M., et al., Self-healing of mechanically-loaded self consolidating concretes with high volumes of fly ash. Cement and Concrete Composites, 2008. 30(10): p. 872-879.

Shaikh, F.U.A. and S.W.M. Supit, Chloride induced corrosion durability of high volume fly ash concretes containing nano particles. Construction and Building Materials, 2015. 99: p. 208-225.

Shaikh, F.U.A. and S.W.M. Supit, Mechanical and durability properties of high volume fly ash (HVFA) concrete containing calcium carbonate (CaCO<sub>3</sub>) nanoparticles. Construction and Building Materials, 2014. 70(Supplement C): p. 309-321.

Taylor, H.F.W., Cement Chemistry. 1990, London: Academic Press Ltd.

Tharakan, J.L.P., D. Macdonald, and X. Liang, Technological, economic and financial prospects of carbon dioxide capture in the cement industry. . Energy Policy 2013. 61: p. 1377-1387.

Wainwright, P.J. and N. Rey, The influence of ground granulated blastfurnace slag (GGBS) additions and time delay on the bleeding of concrete. Cement and Concrete Composites, 2000. 22(4): p. 253-257.

Washburn, E.W., Note on a Method of Determining the Distribution of Pore Sizes in a Porous Material. Proceedings of the National Academy of Sciences of the United States of America, 1921. 7(4): p. 115-116.

Younsi, A., et al., Performance-based design and carbonation of concrete with high fly ash content. Cement and Concrete Composites, 2011. 33(10): p. 993-1000.

*All reasonable efforts have been made to acknowledge the authors of the copyright material. It would be highly appreciated if I can hear from any author has been ignored or incorrectly acknowledged.*

## **Chapter 5: Nano characterisation of ITZ of HVS and HVS-FA concretes containing nano silica and nano calcium carbonate**

---

This chapter discusses the effect of addition of nano silica and nano calcium carbonate on the interfacial transition zone of high volume slag (HVS) and high volume slag-fly ash (HVS-FA) blended concretes. Elastic modulus and hardness of ITZ and their surrounding areas through nano indentation techniques, highly magnified microscopic images of those ITZ through scanning electron microscopy (SEM) and energy-dispersive X-ray spectroscopy (EDS) techniques were used to characterise the nano- and microstructure of the ITZ area between aggregates and matrix. In addition, 28 days compressive strengths of those HVS and HVS-FA concrete were also used to make a comparison of the changes of the ITZ in this chapter.

### **5.1 Overview**

Significant research and development works are occurring in concrete industry to reduce the carbon footprint of concrete and cementitious composites through developing various low carbon binders. The use of various industrial by-products, such as fly ash (FA), silica fume and ground granulated blast furnace slag (BFS) as partial replacement of ordinary Portland cement (OPC) in concrete is the most widely adopted practice to produce low carbon binders. The use of lower amount of these by-products, such as 5-15% silica fume, 10-30% fly ash and 10-50% BFS as partial replacement of OPC in concrete is also adopted by many researchers and significant volume of research results exist on their effect on various properties of concrete (Mehta, 1982; Carette & Malhotra, 1983; Thomas et al., 1999, Barbhuiya et al., 2009).

---

The content of this chapter has been written based on the results published in the following journal.

Hosan, A., et al., Nano- and micro-scale characterisation of interfacial transition zone (ITZ) of high volume slag and slag-fly ash blended concretes containing nano SiO<sub>2</sub> and nano CaCO<sub>3</sub>. *Construction and Building Materials*, 2020: p. 121311.

The use of high volume fraction of the above by-products especially FA and BFS is also adopted by many researchers to develop green concretes (Malhotra & Mehta, 2002; Siddique, 2004; Naik et al., 1994). However, due to the use of significantly low volume of OPC and high volume of FA or BFS in those green concretes the development of strength and other properties are slow due to their slow pozzolanic reactions and the formation of small amount of hydration products e.g., calcium silicate hydrate (CSH) and calcium hydroxide (CH). Although additional CSH is formed in those concretes through pozzolanic reaction, its amount is rather limited. As a result, low early age strength development, presence of higher amount of pores and slow improvement of mechanical and durability properties are reported for those green concretes containing high volume FA and BFS (Siddique, 2004; Naik et al., 1994).

Recently, various nano materials are used to improve the properties of concrete as well as green concretes containing high volume FA and BFS (Kawashima et al., 2013; Li et al., 2004; Zhang & Islam, 2012). Significant improvement in mechanical and durability properties of high volume FA and high volume BFS concretes due to addition of nano silica (NS), nano calcium carbonate (NC), nano alumina (NA), nano clay, etc. are reported in the literature review chapter 2. Significant improvement in early age strength and durability properties including corrosion resistance were reported in the high volume FA and high volume BFS concretes due to addition of small amount of NS, NC, NA, etc. (Shaikh & Supit, 2014; Shaikh & Supit, 2015). The carbon footprint of those green concretes are also significantly low even with the use of small amount of nano materials compared to the OPC concrete (Hosan & Shaikh, 2020; Shaikh & Hosan, 2019; Shaikh & Hosan, 2019). Densification of the matrix of above green concretes through formation of additional CSH gels and pore filling effect of nano materials are reported as the reasons for such improvement. Interfacial transition zone (ITZ) is a thin layer around the aggregates and is the zone between aggregates and paste or mortar matrix in concrete. The ITZ plays an important role on the mechanical and durability properties of concrete. It is reported that the microstructure of ITZ is relatively less compact and porous than the matrix of concrete (Li et al., 2012; Akcaoglu et al., 2005) and the thickness of ITZ ranges between 9-51 $\mu$ m (Nezerka et al., 2019; Zheng et al., 2005; Yue et al., 2020). These deficiencies of ITZ influence the properties of concrete, especially in high volume FA and high volume BFS concretes. This is because less amount of primary hydration products (e.g., CSH and CH) are produced due to the presence of higher amount of FA or BFS than the OPC.

Recently, the authors developed high volume BFS and high volume FA-BFS binders for green concrete containing small amounts of NS, NC and NA (Hosan & Shaikh, 2020; Shaikh &

Hosan, 2019; Shaikh & Hosan, 2019). Different high volume BFS contents and combined FA and BFS contents of 70% to 90% as partial replacement of OPC and 1-4% nano materials (NS, NC and NA) are considered. Results show that the addition of 1% NC improved the 28 days compressive strength of pastes containing 69% BFS and combined FA and BFS content of 69%. The NS content of 2% and 3% showed similar improvement in compressive strength of the paste containing 78% BFS and combined BFS and FA content of 67%, respectively. In fact, the compressive strength of above four HVS and HVS-FA concretes due to addition of NS and NC is exceeded their counterpart OPC paste's value (Hosan & Shaikh, 2020; Shaikh & Hosan, 2019; Shaikh & Hosan, 2019). Preliminary microstructure analysis of those matrix shows improved and denser microstructure of the above green binders due to addition of NS and NC than their respective control HVS and HVS-FA binders. While ITZ plays an important role on the properties of concrete, a thorough understanding of the improvement of ITZ of HVS and HVS-FA concretes containing 70-80% FA and BFS due to the addition of nano materials will be very helpful to predict its role on the properties of these green concretes. This paper uses cutting edge nanoindentation technique to quantify the formation of additional hydration products in ITZ area of the above HVS and HVS-FA concretes due to the addition of NS and NC. Scanning electron microscopy (SEM) and energy dispersive X-ray spectroscopy (EDS) analysis techniques were also used to identify the elements and composition of the hydration products in the ITZ area. Compressive strength of the HVS and HVS-FA concretes containing NS and NC are also evaluated to confirm the improvement of ITZ due to addition of the nano materials.

## **5.2 Experimental Program**

### **5.2.1 Materials**

The ordinary Portland cement (OPC) used in this study was purchased from a local cement company and it fully complies with the requirements of Australian Standard AS 3972 (AS 3972-1997). The blast furnace slag (BFS) was supplied by a local cement company in Western Australia and class F fly ash (FA) was provided by a coal-fired power plant in Australia which also conform to Australian standards (AS 3582.1, 1998; AS 3582.2, 2001). All coarse and fine aggregates used in this study were bought from local suppliers ensuring the quality met the required standards (AS 2758.1:2014). Aggregates were soaked in water for at least 24 hours and exposed to open air to achieve saturated and surface dry (SSD) condition. Dry nano- $\text{CaCO}_3$  (NC) with an average particle size of 15-40nm, 40  $\text{m}^2/\text{g}$  of specific surface area, and 97.8% calcite content was purchased from Nanostructured and Amorphous Materials, Inc. of USA.

Dry nano-SiO<sub>2</sub> (NS) with an average particle diameter of 25nm, specific surface area of 160 m<sup>2</sup>/g, and with 99% purity was purchased from a commercial nano materials manufacturer. Tap water from the concrete laboratory was used in all mixes and a naphthalene sulphonate based superplasticizer (SP) was used to maintain the workability by measuring slump for all mixes as high volume replacement of slag and slag-fly ash blend used in this study. The Physical and chemical properties of all cementitious materials are given in **Table 5.1** and the X-ray diffraction (XRD) analysis of OPC, BFS, FA, NC and NS are shown in **Figs. 3.2, 4.1-4.2**. It can be seen by comparing the results that NS is highly amorphous compared to NC. Among OPC, BFS and FA, BFS is more amorphous with its amorphous content of 95.7% compared to 67.8% amorphous content of FA and 24 % amorphous content of OPC based on quantitative XRD analysis performed by Centre for Materials Research, MMF, Curtin University, Perth, Australia.

**Table 5.1** Physical properties and chemical compositions of Ordinary Portland Cement (OPC), Blast Furnace Slag (BFS), Class F Fly Ash (FA), Nano Calcium Carbonate (NC) and Nano Silica (NS)

		Cement	Slag	Fly-ash	Nano calcium carbonate	Nano silica
Chemical composition (%)	CaO	64.39	41.20	4.30	97.8*	-
	SiO <sub>2</sub>	21.10	32.5	51.11	-	99*
	Al <sub>2</sub> O <sub>3</sub>	5.24	13.56	25.56	-	-
	Fe <sub>2</sub> O <sub>3</sub>	3.10	0.85	12.48	0.02*	-
	MgO	1.10	5.10	1.45	0.5*	-
	MnO	-	0.25	0.15	-	-
	K <sub>2</sub> O	0.57	0.35	0.7	-	-
	Na <sub>2</sub> O	0.23	0.27	0.77	-	-
	P <sub>2</sub> O <sub>5</sub>	-	0.03	0.88	-	-
	TiO <sub>2</sub>	-	0.49	1.32	-	-
SO <sub>3</sub>	2.52	3.20	0.24	-	-	
LOI	1.22	1.11	0.57	-	-	
Physical properties	Particle size	25-40% ≤7µm	40% of 10 µm	50% of 10 µm	15-40 nm	25 nm
	Surface area ( m <sup>2</sup> /g)	-	-	-	40	160
	Specific gravity	2.7 to 3.2	2.6	-	-	2.2 to 2.6

\*Information provided by supplier

### 5.2.2 Mix design and sample preparation

All the concrete mixes were designed with a total binder quantity of 400 kg/m<sup>3</sup> and a constant water/binder ratio of 0.4. However, superplasticizer was used when needed to maintain the concrete mixes workable with a target slump of 100-125 mm. Coarse and fine aggregates mass and ratios were kept constant for all mixes. **Table 5.2** shows the mix proportions and measured

slump of all control and mixes with supplementary cementitious materials with and without NC and NS. It can be seen from the dosage of superplasticizers in **Table 5.2** that the required dosage of superplasticizers increased with the increasing percentage of BFS and nano materials to maintain the target slump for a workable concrete mix. A designated ID was given for each mix considering binder name and amount present on the mixes. For example, 69BFS.1NC means a mix containing 69% BFS and 30% OPC with the inclusion of 1% NC of the total binder. The amount of BFS, BFS-FA, and nano materials dosage were selected from the results of the authors' other investigations on paste samples (Hosan & Shaikh, 2020; Shaikh & Hosan, 2019; Shaikh & Hosan, 2019).

Concrete was mixed in a pan mixer at ambient temperature. Firstly, all the dry ingredients such as cement, coarse aggregates, fine aggregates, and SCM's (in case of HVS and HVS-FA mixes) were mixed for 4-5 minutes considering the high amount of aggregates and volume of concrete. Next, water was added and again mixed for around 2-3 minutes until a homogenous mixture was reached. Besides, mixes containing NC and NS were prepared by mixing the nano materials powder with partial (depending on the percentage of nano materials inclusion) water and superplasticizers required for the concrete mixes. That mix was then dispersed ultrasonically by an ultrasonic mixer shown in **Fig. 4.4** with 100% amplitude and maximum cycle for 45 minutes for 1% NC, 60 minutes and 75 minutes for 2% and 3% of NS, respectively used in both mixes (Hosan & Shaikh, 2020; Shaikh & Hosan, 2019). The remaining water was added with that mixed and stirred again manually before added slowly into the concrete mixes while the pan mixer was running to ensure proper dispersion of both NC and NS particles into the concrete mixes. Additional superplasticizer was added to attain the target slump for all mixes shown in **Table 5.2**.

Standard cylindrical samples with a diameter of 100 mm and a height of 200 mm were cast for compressive strength and microstructural analysis. To explore the microstructural changes of different concrete mixes, a small portion of concrete with an interfacial transition zone (ITZ) were cut from each mix after 28 days of curing by using a diamond precision saw and dried naturally to make sure it is free from moisture.

**Table 5.2** Mixing proportions of concretes (Kg/m<sup>3</sup>) and measured slump

Mix ID	Binding Materials			Nano Materials		Aggregates			Water	Super plasticisers	w/b	Slump (mm)
	Cement	Slag	Fly ash	Nano-SiO <sub>2</sub>	Nano-CaCO <sub>3</sub>	20 mm Granite	10 mm Granite	Sand				
OPC	400	-	-	-	-	789	395	684	163	-	0.4	120
70BFS	120	280	-	-	-	789	395	684	163	2.2	0.4	110
69BFS.1NC	120	276	-	-	4	789	395	684	163	2.4	0.4	113
80BFS	80	320	-	-	-	789	395	684	163	2.85	0.4	112
78BFS.2NS	80	312	-	8	-	789	395	684	163	4.34	0.4	116
70BFS-FA	120	196	84	-	-	789	395	684	163	1.15	0.4	125
69BFS-FA.1NC	120	194	82	-	4	789	395	684	163	1.95	0.4	120
67BFS-FA.3NS	120	190	78	12	-	789	395	684	163	4.11	0.4	110

### 5.2.3 Experimental methods

#### 5.2.3.1 Nano indentation test

In this study, nano indentation was used to determine the elastic modulus and hardness at the ITZ of the specimens of OPC, HVS and HVS-FA concrete mixtures with and without nano materials addition. The test data were then analysed to determine the effect of nano materials on the thickness of the ITZ. A small portion of concrete samples containing the interface of aggregates and mortar were cut from the concrete cylinders of each mix after 28 days of curing by ensuring the surface as smooth as possible. The samples were then dried, cast in a cylindrical resin mould and placed in a vacuum desiccator for 3 days to ensure the samples were free from any entrapped air. All the samples were grinded by using sandpapers of 52.2  $\mu\text{m}$ , 35  $\mu\text{m}$ , 21.8  $\mu\text{m}$ , 15.3  $\mu\text{m}$  and then polished by using diamond suspension solutions of 9  $\mu\text{m}$ , 6  $\mu\text{m}$ , 3  $\mu\text{m}$ , 1  $\mu\text{m}$ , 0.25  $\mu\text{m}$  and 0.1  $\mu\text{m}$  sizes. A methanol based liquid was used during the polishing process to avoid further binder hydration and then the samples were cleaned with running water to free from the diamond particles and dust.





**Fig. 5.1** Nanoindentation test setup in Agilent Nano Indenter G200

After the specimens were prepared, nano indentation test was conducted on the aggregate-paste interface by using Agilent Nano Indenter G200 shown in **Fig. 5.1** with a constant indentation load rate for each sample. Before applying the load, samples were scanned by an optical microscope to choose a suitable ITZ location of the samples to indent as shown in **Fig. 5.2a**. **Figs. 5.3a and 5.3b** show a typical load-depth curve and a Berkovich indenter with a three-sided pyramid diamond tip, respectively. A total of 108 indents were performed in an array of  $90 \mu\text{m} \times 110 \mu\text{m}$  shown in **Fig. 5.2b** with a grid spacing of  $10 \mu\text{m}$  to avoid the damage caused by the adjacent indent during indentation. A loading-unloading cycle was performed at each indent point and held for 2 secs when it reached the maximum load before unloading to avoid the creep effects. From the data of load-depth curve, the indentation modulus ( $E$ ) and hardness ( $H$ ) were calculated by using Oliver and Pharr method (Oliver & Pharr, 1992) using Eqns. 1-4.

$$H = \frac{P_{max}}{A_c} \quad (1)$$

where,  $P_{max}$  = maximum load during indentation and  $A_c$  = contact area of indenter at maximum load.

$$E_r = \frac{S\sqrt{\pi}}{2\sqrt{A_c}} \quad (2)$$

where,  $E_r$  = reduced modulus and  $S$  = stiffness of the unloading curve which is defined by Eq. 3.

$$S = \frac{dP}{dh} = \frac{2 E_r \sqrt{A_c}}{\sqrt{\pi}} \quad (3)$$

where,  $h$  = indentation depth

The reduced modulus ( $E_r$ ) is related to the elastic modulus ( $E$ ) and Poisson's ratio of specimen and indenter, respectively, which can be determined by Eq. 4.

$$\frac{1}{E_r} = \frac{1-\nu^2}{E} + \frac{1-\nu_i^2}{E_i} \quad (4)$$

where,  $E$  = elastic modulus and  $\nu$  = Poisson's ratio of specimen,  $E_i$  and  $\nu_i$  are those of indenter, respectively. For the indenter used in the present study, the  $E_i$  and  $\nu_i$  are 1140 GPa and 0.07, respectively.

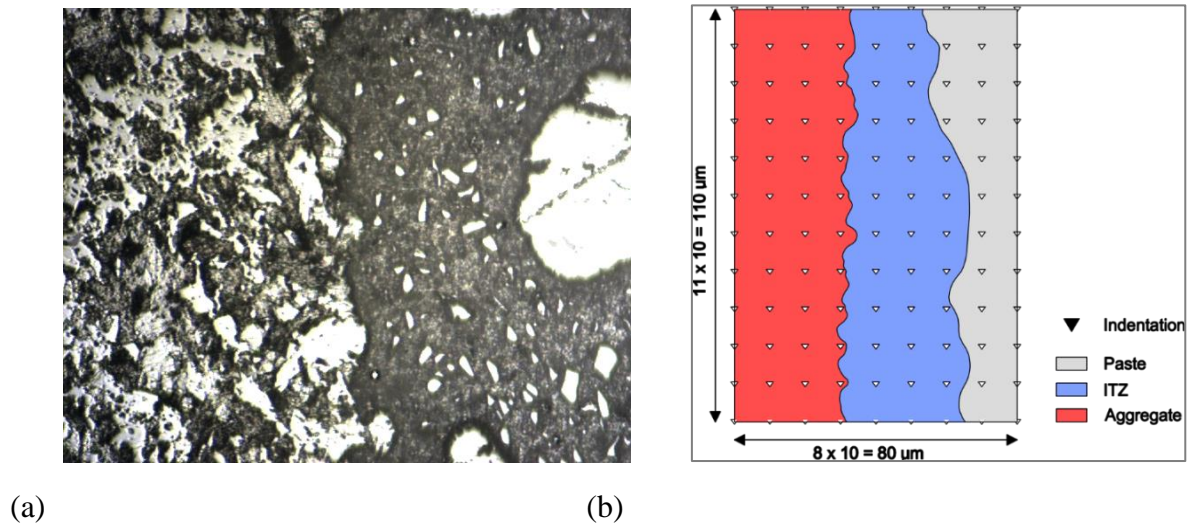


**Fig. 5.2** (a) Typical indent area and (b) Indent plan (total 9x12=108 indents)

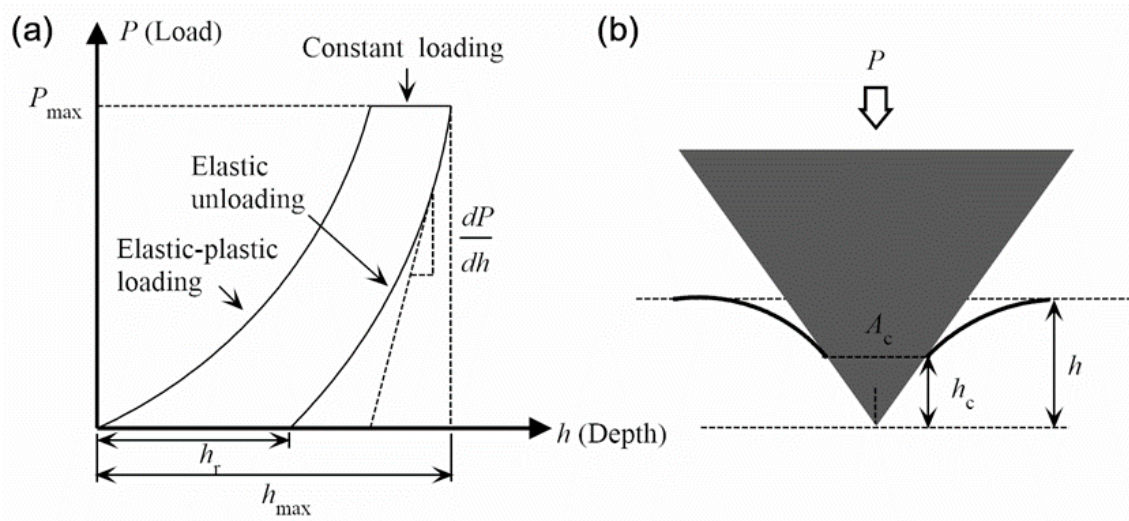


**Fig. 5.3** Nano indentation principle (a) a typical load-displacement curve (b) a typical indenter with three-sided pyramidal diamond

### 5.2.3.2 Scanning electron microscopy (SEM) and energy dispersive X-ray spectroscopy (EDS)

Microstructural investigation of high volume slag and high volume slag-fly ash blended concretes with and without nano materials addition was performed by using a MIRA3 TESCAN SEM machine. It is a variable pressure field emission scanning electron microscope (VP-FESEM) equipped with backscattered electron (BSE) detector and energy-dispersive X-ray spectroscopy (EDS) analyser to collect SEM images along with EDS spectrum to analyse the phases. The samples were prepared by taking a small portion of dried concrete samples after 28 days of wet curing and placed them in a vacuum desiccator for minimum three days to remove all the moisture from the samples. Samples were then drenched in an epoxy resin mount, polished and then 20 mm thick carbon coating was applied to reduce the chance of getting charged during imaging and spectrum collection. The SEM and EDS were carried out at a constant accelerating voltage of 15kV and around 15 mm of working distance by using BSE detectors for all concrete samples. SEM images and EDS spectra were collected in and around ITZ area for each concrete mix.

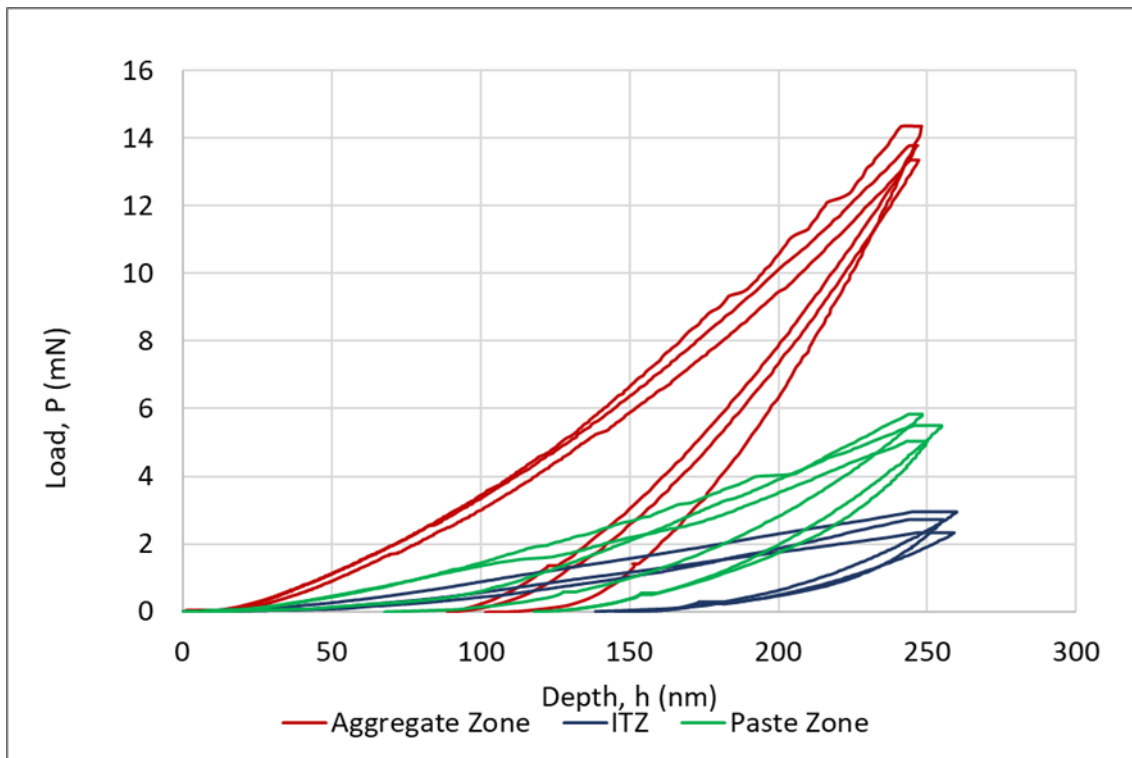


**Fig. 5.4** Typical load-depth diagram of different zones in concrete

### 5.2.3.3 Compressive strength

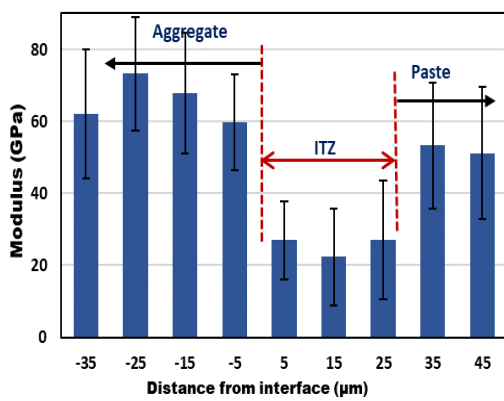
Compressive strength was measured using a MATEST testing apparatus according to ASTM C873 standard with a loading rate of 0.33 MPa/s until failure of concrete specimens after 28 days of curing. Diameters of the cylinders were measured and the cylinders were sulphur capped at least 4 hours prior to the test. Compressive strengths were calculated as the maximum crushing load divided by the average cross-sectional area of the specimens. At least three specimens were tested and the average value of three results are reported in this study.

## 5.3 Results and discussions

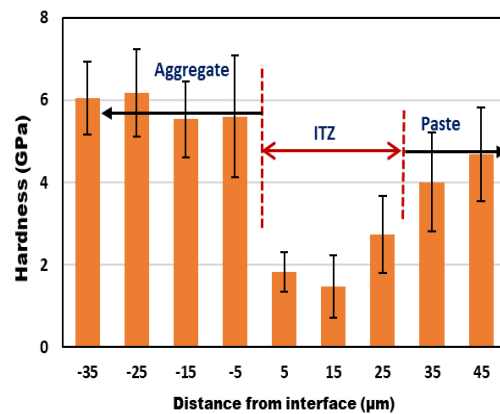
### 5.3.1 Interfacial transition zone (ITZ) based on nanoindentation

The area close to the aggregate of all samples is selected using inbuilt microscope of nano indenter to perform the nano indentation test. The typical load-depth curves obtained from nanoindentation test at any indent point is shown in **Fig. 5.4**. Contour map of modulus and hardness distribution of each concrete is developed using modulus and hardness values of 108 indentation points and can be clearly distinguished by the colour of each contour line (see **Fig. 5.5c-d**). In addition, distribution of modulus and hardness of three zones are also shown for each concrete (see **Fig. 5.5a-b**). Each bar in modulus and hardness distribution represents

average value of 12 indent points. It can be seen from **Figs. 5.5a- b** that modulus of OPC sample from distance -35 to -5  $\mu\text{m}$  varies from 42 to 89 GPa with their average values vary from 61 to 72 GPa with average hardness ranging from 5.6 to 6 GPa. Reported results show that modulus and hardness of typical quartz aggregate are  $76.3 \pm 15.1$  GPa and  $5.14 \pm 3.08$  GPa, respectively (Sorelli et al., 2008). Therefore, this zone can be reasonably considered in aggregate. A sharp fall of modulus and hardness values are observed from distance 5 to 25  $\mu\text{m}$ , where modulus values vary from 9 to 42 GPa followed by increase in modulus values from 32 to 71 GPa in 25 to 45  $\mu\text{m}$  range (see **Figs. 5.5c-d**). It has been reported that the modulus of loose-packed CSH is  $\leq 10 \pm 2$  GPa, low density CSH is from  $11 \pm 2$ - $24 \pm 2$  GPa, high density CSH is from  $29 \pm 2$ - $33 \pm 2$  GPa and CH is from  $35 \pm 2$ - $50 \pm 2$  GPa (Sorelli et al., 2008; Shaikh et al., 2016; Constantinides & Ulm, 2004). Therefore, the hydration products from aggregate to 45  $\mu\text{m}$  distance can be assumed to be consisted of all above hydration products. However, the lower modulus values in 5 to 25  $\mu\text{m}$  range than those in 25 to 45  $\mu\text{m}$  range can reasonably be considered as ITZ zone presumably due to the presence of higher micro pores next to aggregate than the zone away from the aggregate. Similarly, based on this assumption of values of modulus and hardness of each samples, the width of ITZ of each mix was measured and compared to evaluate the effect of nano materials addition on the ITZ of HVS and HVS-FA concretes. A summary of modulus, hardness and thickness of ITZ of all concretes are shown in **Table 5.3**.



(a)



(b)

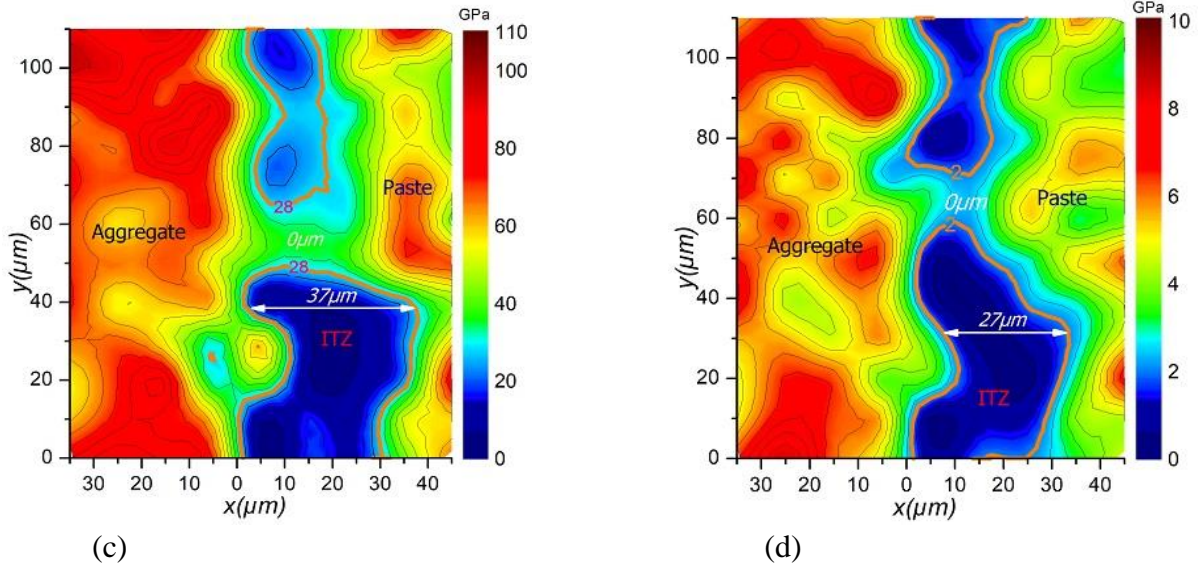


**Fig. 5.5** (a) Modulus distribution (b) hardness distribution and contour map of (c) indentation modulus (d) hardness distribution in ITZ of OPC concrete mix.

### 5.3.1.1 Effect of nano calcium carbonate on ITZ

The effect of 1% NC addition in HVS and HVS-FA mixes can be seen in **Figs. 5.6- 5.9**. The modulus in ITZ of 70BFS sample ranged from 12 GPa to 19 GPa and average hardness varied from 0.98 to 2.41 GPa and exhibited the width of ITZ from 19 to 40 μm can be seen in **Fig. 5.6**. On the other hand, the lowest value of average modulus in ITZ zone of concrete mix 69BFS.1NC is 26 GPa (around 37% higher) and a similar trend is witnessed in the hardness distribution values in the mix due to the addition of 1% NC as shown in **Fig. 5.7a-b**. Moreover, the longest width of the ITZ was also reduced to 26 μm from 40 μm (35% reduction) due to the inclusion of 1% NC (see **Fig. 5.7c-d**). Similarly, an outstanding improvement in average modulus and hardness of the ITZ of 69BFS-FA.1NC mix is also observed as a result of the addition of 1% NC in 70BFS-FA sample shown in **Figs. 5.8-5.9**. The lowest average modulus in ITZ zone in 70BFS-FA sample is increased from 2.40 GPa to 24 MPa due to 1% NC inclusion and similar improvement of hardness in the ITZ is also found in concrete mix 69BFS-FA.1NC. Furthermore, a significant reduction of the thickness of the ITZ can also be perceived from the contour maps of those two mixes. The thickness of ITZ zone of the 70BFS-FA concrete ranged from 35 to 50 μm, while an extremely narrower ITZ ranging from 0 μm to 26 μm is observed in 69BFS.1NC concrete sample as a result of 1% replacement of NC. Both samples with NC exhibited higher average modulus and hardness in ITZ than the ITZ zone in control OPC concrete mix and also showed slimmer width of ITZ zone attributable to the 1%

NC. It can be seen that the NC addition improved the microstructure of ITZ zone of concrete mixes by filling the large pores of HVS and HVS-FA concrete mixes due to its finer properties and correspondingly by accelerating the hydration process and forming new C-S-H gels in the matrix.

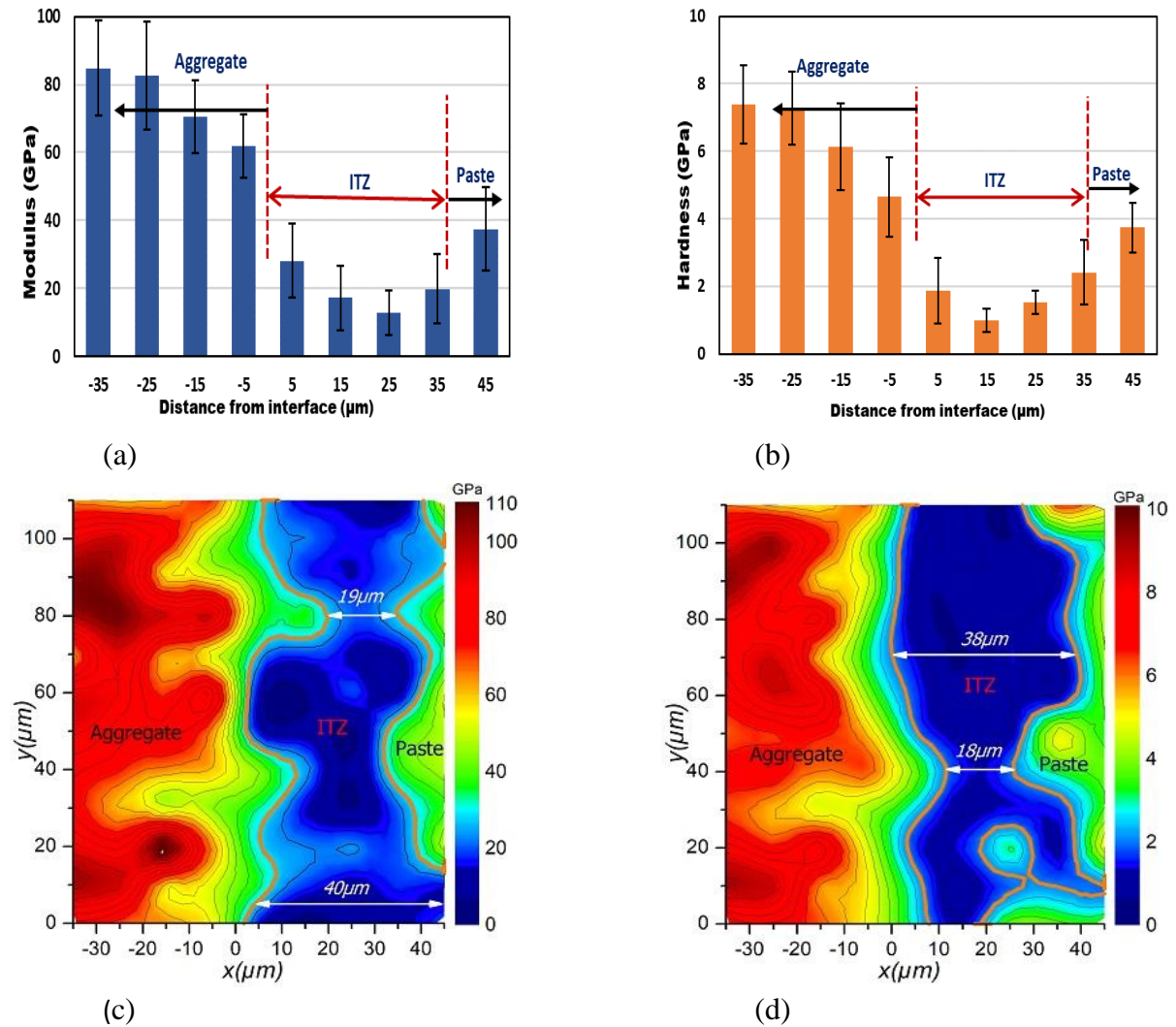


**Fig. 5.6** (a) Modulus distribution (b) hardness distribution and contour map of (c) indentation modulus (d) hardness distribution in ITZ of 70BFS concrete mix.

### 5.3.1.2 Effect of nano silica on ITZ

An extremely weaker ITZ with average modulus ranging from 1.5 to 12 GPa and average hardness ranging from 0.5 to 2 GPa was measured in the concrete mix containing 80% BFS can be seen in **Fig. 5.10**. A wider ITZ thickness varies between 40  $\mu\text{m}$  and 50  $\mu\text{m}$  is also observed in that concrete mix (**Fig. 5.10c-d**). However, with the addition of 2% NS into the HVS concrete, a generous increase in average modulus (13 to 21 GPa) and average hardness

(1.20 to 3 GPa) are observed as shown in **Fig. 5.11**. Similarly, a marginal reduction of width of the ITZ is also observed due to the 2% addition of NS with ITZ width ranging from 10  $\mu\text{m}$  to 45  $\mu\text{m}$ .

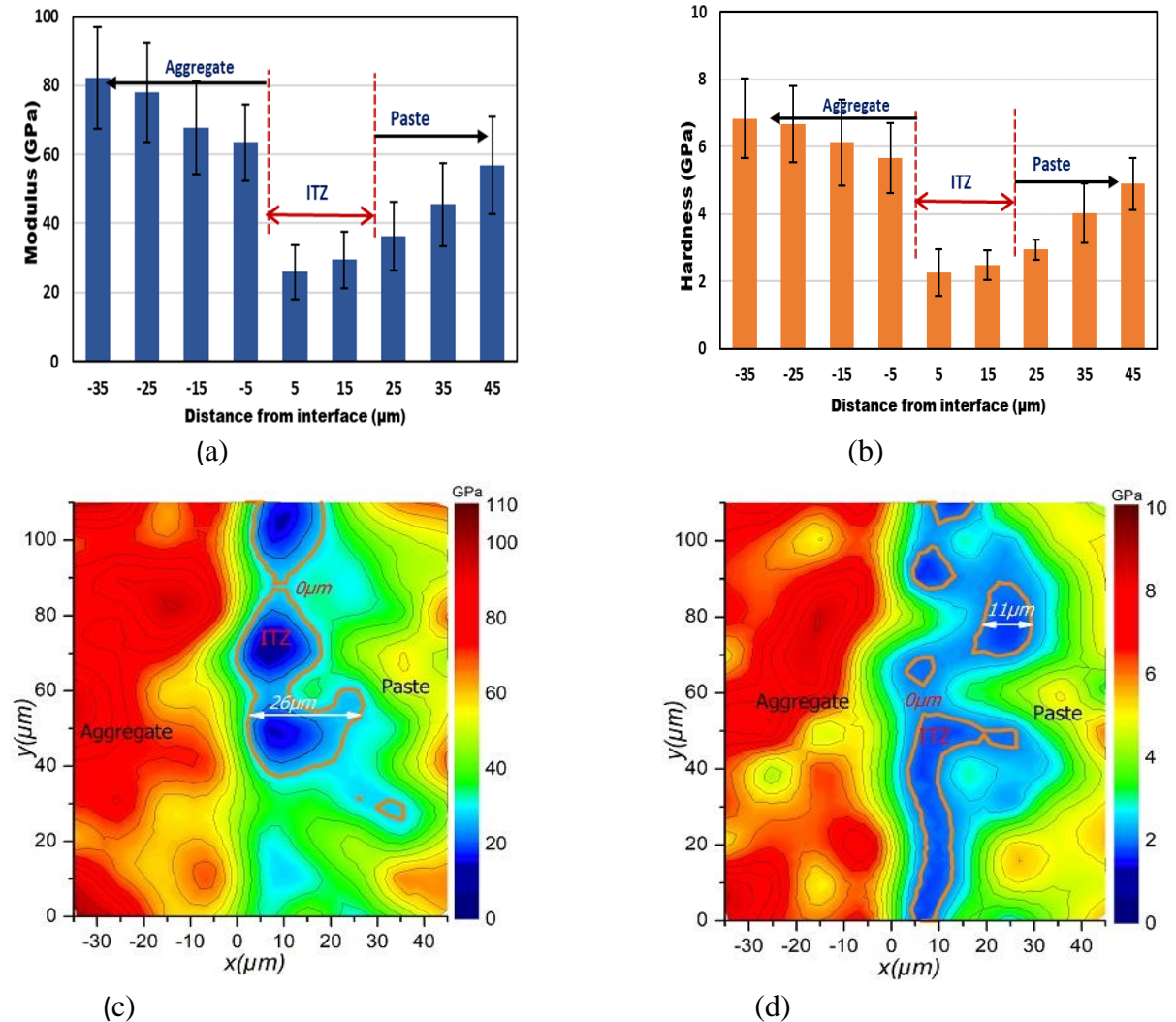


**Fig. 5.7** (a) Modulus distribution (b) hardness distribution and contour map of (c) indentation modulus (d) hardness distribution in ITZ of 69BFS.1NC concrete mix.

On the other hand, a substantial increase in average modulus of ITZ ranging from 23 to 26 GPa is observed in the concrete mix 67BFS.3NS than their corresponding BFS-FA mix which showed of average modulus fluctuating from 2.40 to 16 GPa as shown in **Fig. 5.12**. Equal improvement can be witnessed in **Fig. 5.12b** in the average hardness values of ITZ of 67BFS.3NS concrete mix due to addition of 3% NS. The values of average elastic modulus and hardness of 67BFS.3NS mix are much higher than even control OPC concrete. Additionally, a substantial reduction of thickness of the ITZ of 67BFS.3NS concrete is also observed with an



irregular shape varying from 1 to 37  $\mu\text{m}$  compared to the thickness ranging from 35 to 50  $\mu\text{m}$  of counterpart control concrete with no NS addition (**Fig. 5.12 c-d**). It can be clearly seen that the NS addition enhanced the formation of additional hydration products in ITZ zone of HVS-FA sample in higher degree than the HVS concrete mix and showed consistent results with compressive strength. This probably can be explained by the higher level replacement of BFS in the mix. However, it is evident that addition of NS formed a compact ITZ by filling the pores and promoting the formation of new C-S-H gels and therefore a thinner ITZ with enhanced properties are observed.

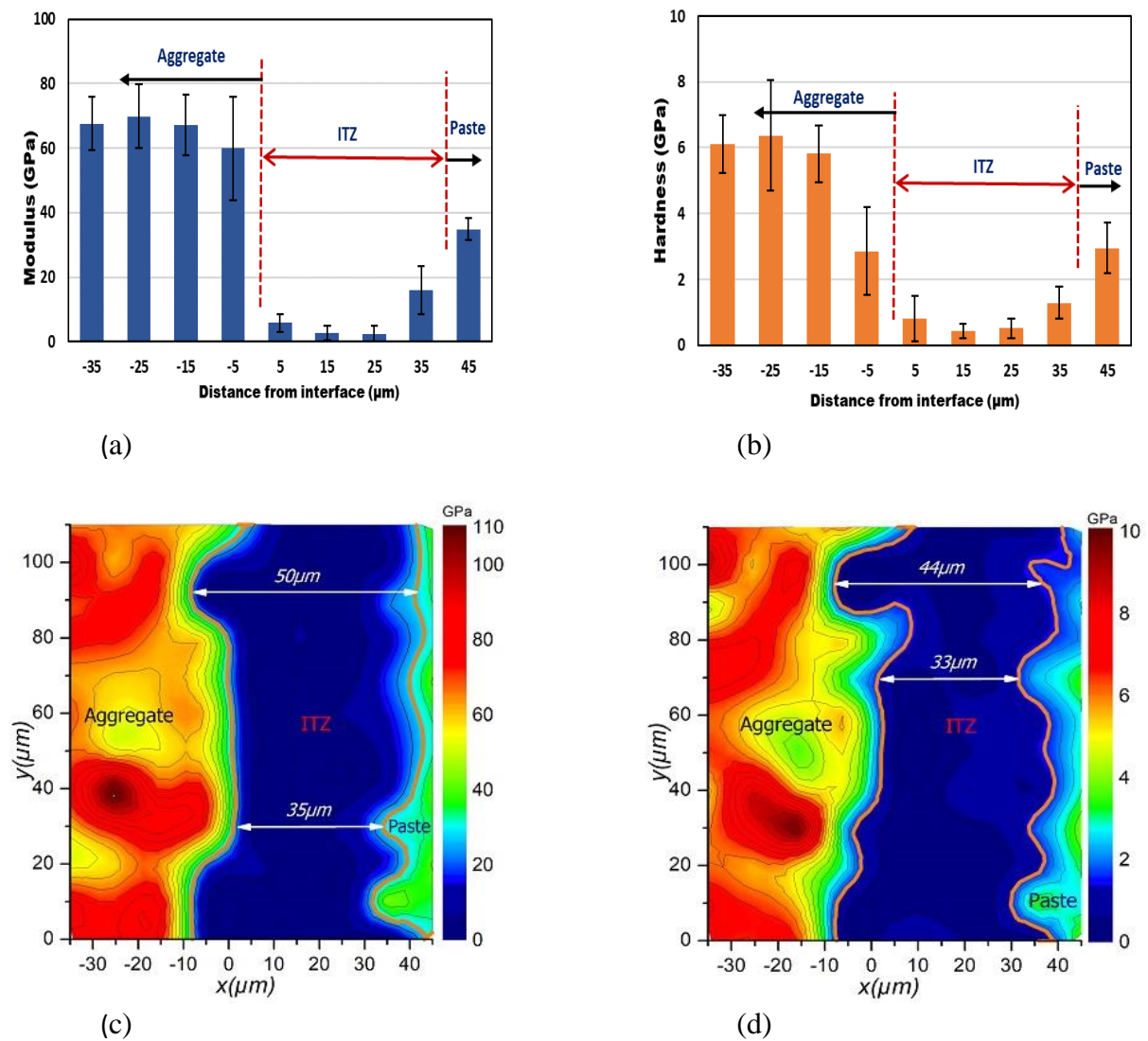
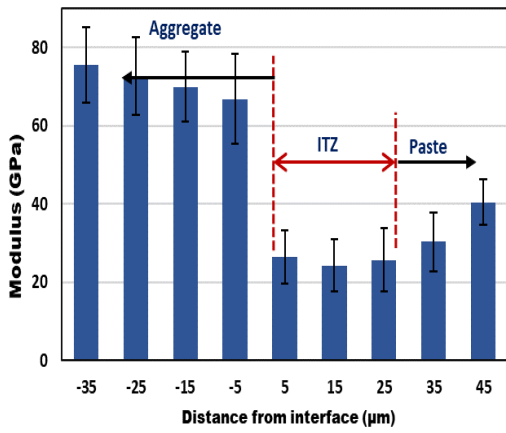
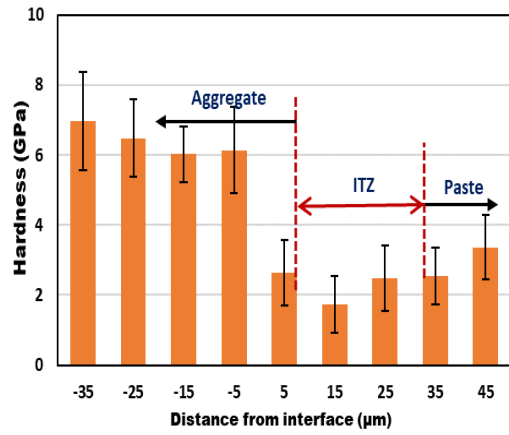


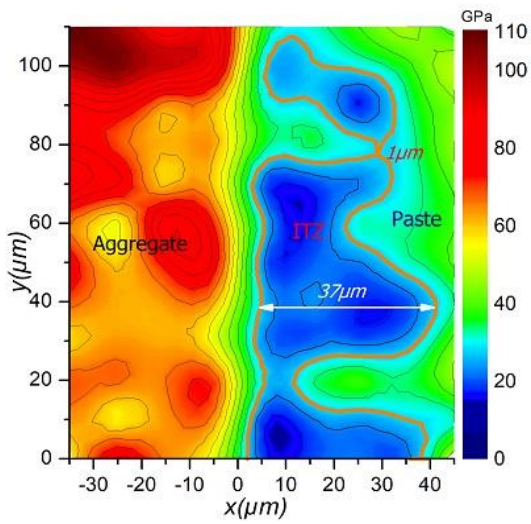
**Fig. 5.8** (a) Modulus distribution (b) hardness distribution and contour map of (c) indentation modulus (d) hardness distribution in ITZ of 70BFS-FA concrete mix.



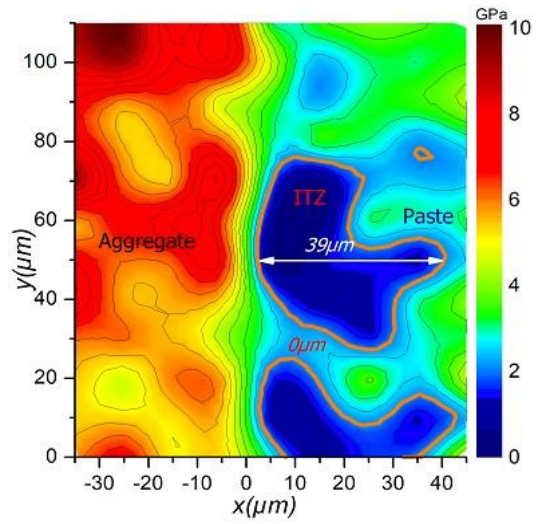
(a)



(b)

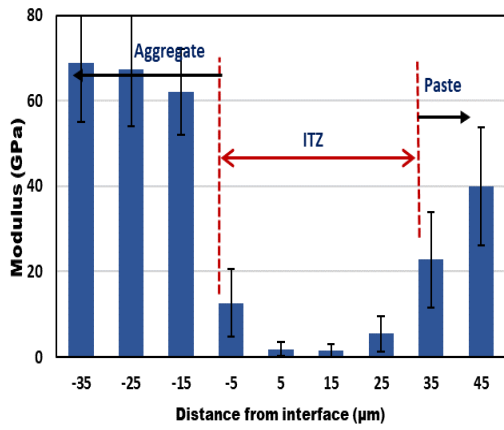


(c)

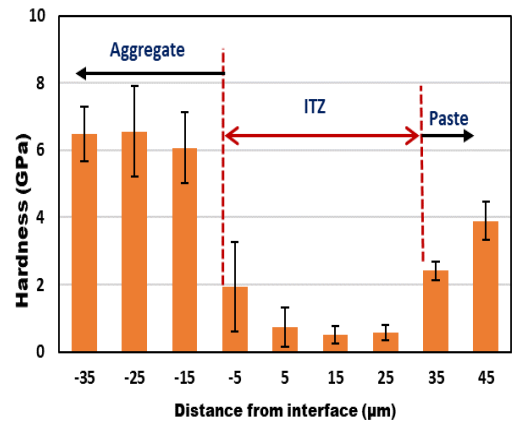


(d)

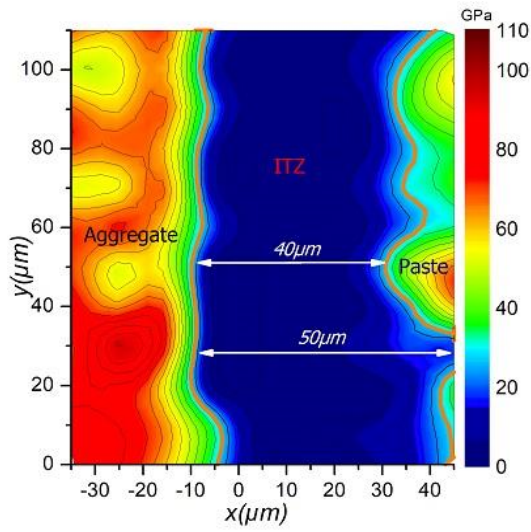
**Fig. 5.9** (a) Modulus distribution (b) hardness distribution and contour map of (c) indentation modulus (d) hardness distribution in ITZ of 69BFS-FA.1NC concrete mix.



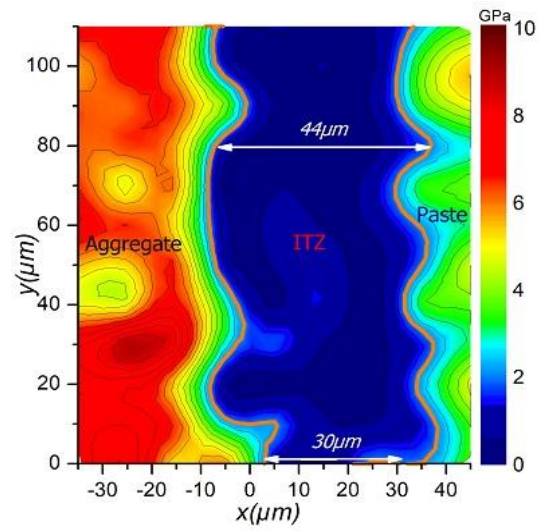
(a)



(b)

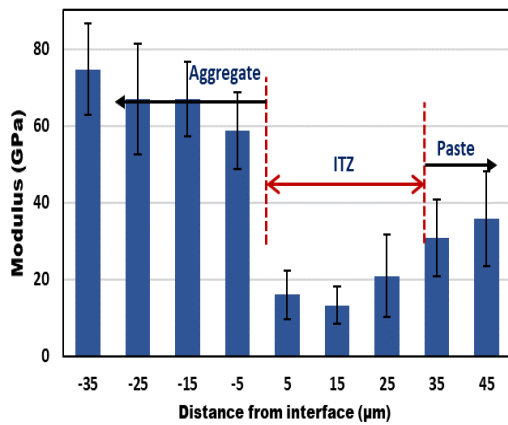


(c)

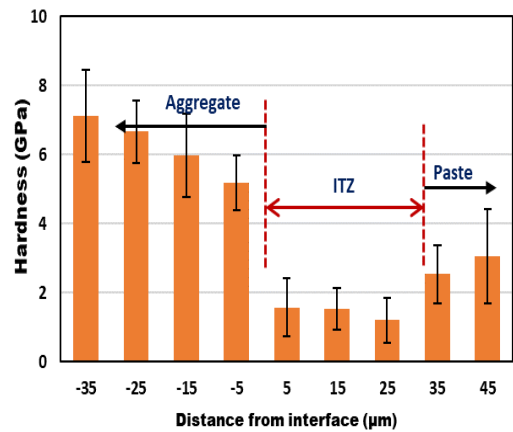


(d)

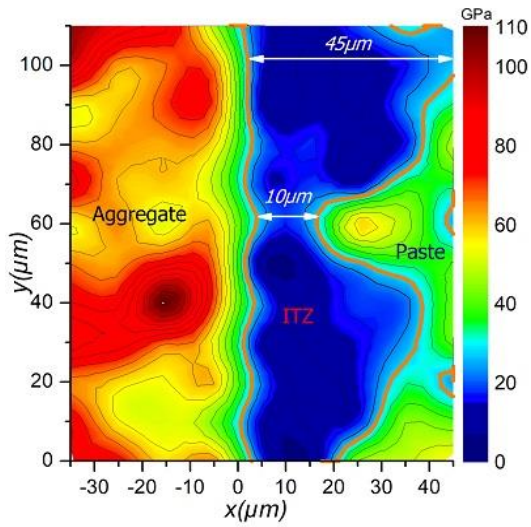
**Fig. 5.10** (a) Modulus distribution (b) hardness distribution and contour map of (c) indentation modulus (d) hardness distribution in ITZ of 80BFS concrete mix.



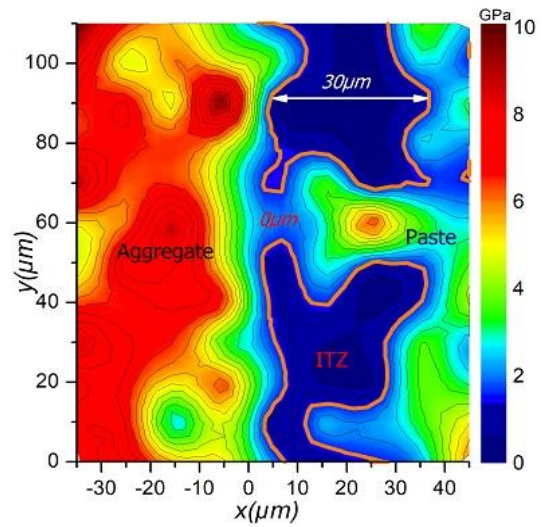
(a)



(b)

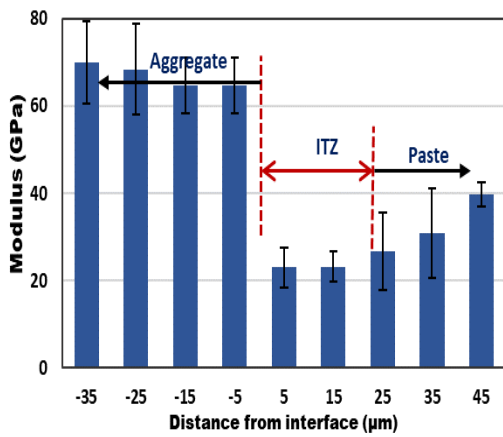


(c)

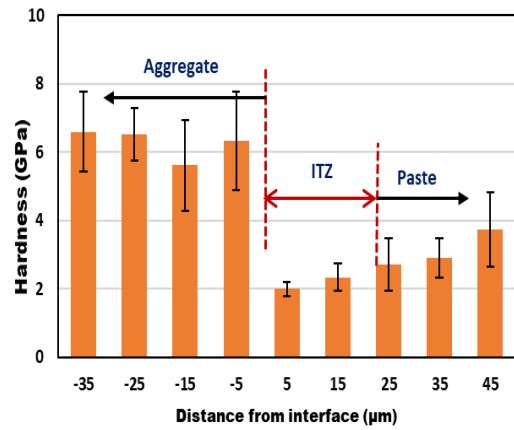


(d)

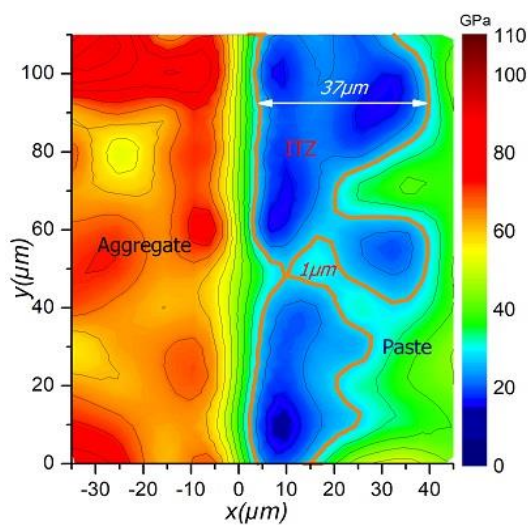
**Fig. 5.11** (a) Modulus distribution (b) hardness distribution and contour map of (c) indentation modulus (d) hardness distribution in ITZ of 78BFS.2NS concrete mix.



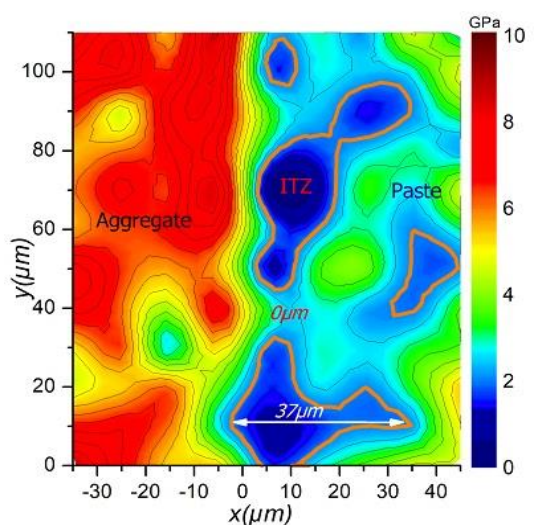
(a)



(b)



(c)



(d)

**Fig. 5.12** (a) Modulus distribution (b) hardness distribution and contour map of (c) indentation modulus (d) hardness distribution in ITZ of 67BFS-FA.3NS concrete mix.

### 5.3.2 ITZ based on SEM and EDS analysis

**Fig. 5.13** shows the SEM images of ITZ of all concrete mixes with and without nano materials (NC and NS) addition. It can be understood from **Fig. 5.13a** that a compact microstructure between aggregate and mortar in the ITZ of control OPC concrete with existence of few pores and un-hydrated cement grains (white lumps) in the paste zone reflected a solid microstructural matrix. On the other hand, it can also be perceived from **Fig. 5.13b** that the ITZ of HVS concrete mix containing 70% BFS having wider micro cracks including a tiny gap between aggregate and paste zone. A higher amount of unhydrated cement (white lumps) and slag particles presence can also be observed in that image. Furthermore, the ITZ of concrete mixes 70BFS-FA (**Fig. 5.13d**) and 80BFS (**Fig. 5.13f**) exhibited a huge gap between aggregate and paste with higher amount of unhydrated slag and fly ash particles, larger pores and micro cracks created a weaker ITZ which is also reflected in the results of nano indentation tests as well as compressive strength values. The effect of NC addition on the ITZ of concrete mixes 69BFS.1NC and 69BFS-FA.1NC can be seen in **Figs. 5.13c** and **e**. It is clearly evident that NC addition reduced the micro cracks of the ITZ zone and reduced the pores in the area between aggregate and paste of the mix 69BFS.1NC though a few larger pores presence observed in the mix. A higher degree of hydration led to stronger bond between aggregate and paste and shaped a compacted microstructure due to addition of NC. In case of HVS-FA concrete mix, the NC inclusion narrowed the gap in the ITZ to an unnoticeable micro cracks created a compact matrix between aggregate and paste than their corresponding control concrete.

The influence of NS addition in the HVS and HVS-FA can be comprehended in **Figs. 5.13g** and **h**. A remarkable improvement in ITZ zone having narrower gap between aggregate and paste of concrete mix 78BFS.2NS can be seen. It is also noticeable that the hydration degree of slags increased in the ITZ zone though a small percentage of unhydrated cement presence can be seen in **Fig. 5.13g**. This marginal improvement in ITZ of concrete mix 78BFS.2NS as a results of NS addition also consistent with the results of nano indentation test. On the other hand, the NS addition in the HVS-FA mix reduced the pores substantially to form compact matrix between aggregate and paste created a stronger ITZ also reflected in the modulus and hardness values found in the nano indentation test. It is evident that NS addition increased the hydration of slag and fly ash particles and reduced the pores which increased the density of ITZ of superior performance than the control concrete.

The analysis of elements of hydration products in the ITZ area of HVS and HVS-FA concretes with and without NS and NC obtained from EDS analysis is shown in **Fig. 5.14**. It can also be

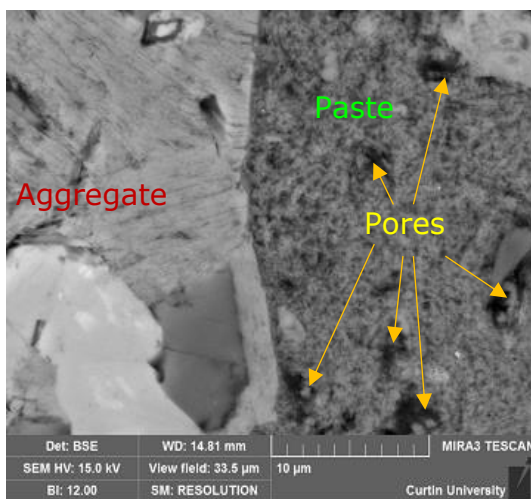
seen from the comparison of EDS traces taken in the ITZ area of all concrete mixes that both HVS and HVS-FA concretes having higher level of oxygen than the OPC concrete, particularly in the HVS-FA concrete which is a confirmation of more permeable voids between the aggregates and binder paste interface of that individual concrete mix. Nevertheless, an addition of 1% NC and 2-3% NS in both HVS and HVS-FA mixes reduce the oxygen level indication of higher degree of dense microstructure. Besides, increase peaks of Ca, Si and Al in those matrix in the ITZ area is also indication of formation of additional hydration products due to the addition of NS and NC in the system that point out the development of new C-S-H and C-S-A-H gels. Overall, it is clear from the microstructural investigation that the addition of NS and NC densified the matrix and formed a denser and compacted aggregate and binder paste interface subsequently formed a concrete with higher strengths and durability.

**Table 5.3** Modulus, hardness and length of ITZ of different concrete mixes with and without nano materials

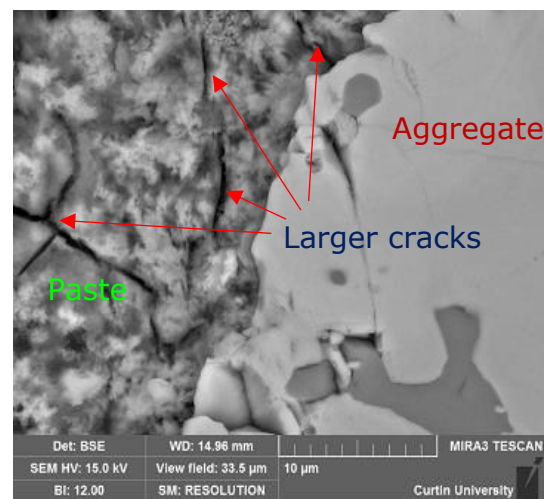
Mix ID	Modulus, GPa	Hardness, GPa	Thickness, $\mu\text{m}$
OPC	22-27	1.5-2.7	0-37
70BFS	12-28	1.0-2.4	19-40
69BFS.1NC	25-30	2.2-3.0	0-26
80BFS	1-12	0.5-2.0	40-50
78BFS.2NS	13-21	1.2-1.6	10-45
70BFS-FA	2-16	0.4-1.3	35-50
69BFS-FA.1NC	24-27	1.7-2.5	1-37
67BFS-FA.3NS	23-27	2.0-2.7	1-37

Average values of modulus, hardness and thickness of ITZ zone of all concretes are summarised in **Table 5.3**. It can be seen that the modulus of three HVS and HVS-FA concretes are lower than that of those containing NS and NC. The average modulus of ITZ in 80BFS and 70BFS-FA concrete are 1-12 GPa and 2-16 GPa, respectively. In contrast, the modulus of ITZ in 70BFS concrete is 12-28 GPa. Reported results show that the modulus of loose-packed CSH is  $\leq 10 \pm 2$  GPa, low density CSH is from  $11 \pm 2$ - $24 \pm 2$  GPa, high density CSH is from  $29 \pm 2$ - $33 \pm 2$  GPa and CH is from  $35 \pm 2$ - $50 \pm 2$  GPa (Sorelli et al., 2008; Shaikh et al., 2016; Constantinides & Ulm, 2004). Therefore, the observed modulus values in ITZ in 80BFS and 70BFS-FA concretes represents the presence of many micro pores in loose pack CSH and low density CSH which is also consistent with SEM images of the corresponding concretes. The observed modulus of ITZ in 70BFS concrete is higher than the two HVS and HVS-FA concretes.

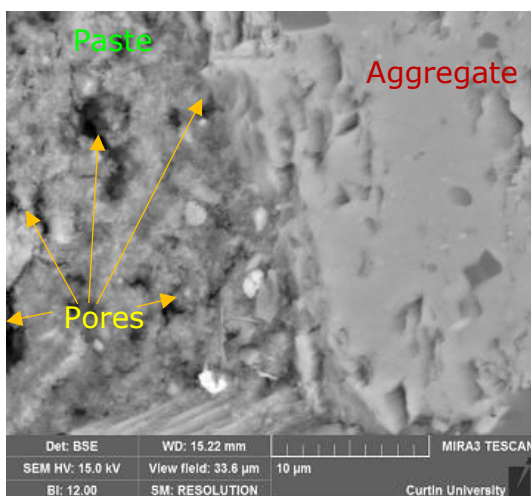
However, micro pores still exist in the ITZ area which can also be confirmed from the SEM image where pores and micro cracks can be seen in the matrix near the aggregate. On the other hand, the modulus of ITZ in 69BFS1NC concrete is 25-30GPa, in 69BFS-FA1NC concrete is 24-27GPa, in 67BFS-FA3NS concrete is 23-27GPa and in 78BFS2NS concrete is 13-21GPa. These modulus values are within the range of low and high density CSH and SEM images of ITZ area in those concretes also confirm these observations of dense microstructure and fewer micro pores or micro-cracks and higher peaks of Ca and Si and lower peak of O<sub>2</sub> in the EDS spectra. The thickness of ITZ in HVS and HVS-FA concretes containing NS and NC is smaller than their control HVS and HVS-FA concretes. This reduction in thickness is due to the formation of additional CSH gels and filling of micro pores by NS and NC particles in those concretes, which is also reflected in the SEM images of the corresponding concretes.



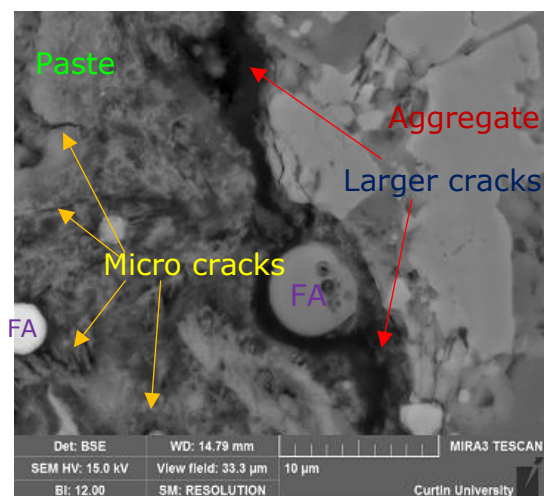
(a) OPC



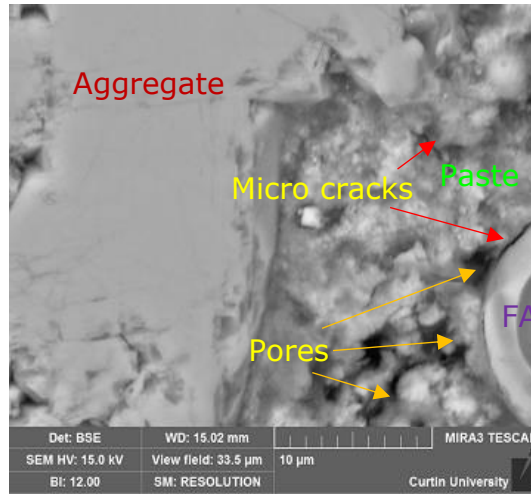
(b) 70BFS



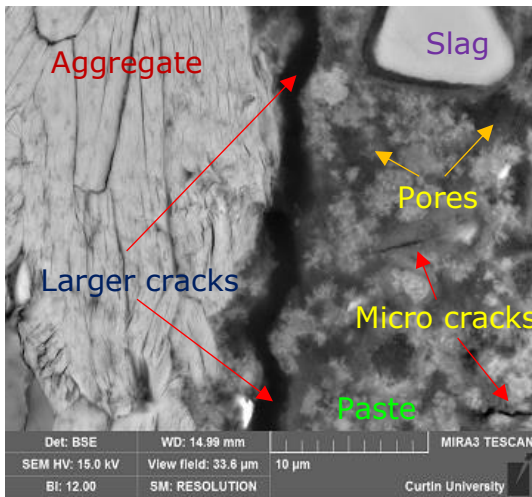
(c) 69BFS.1NC



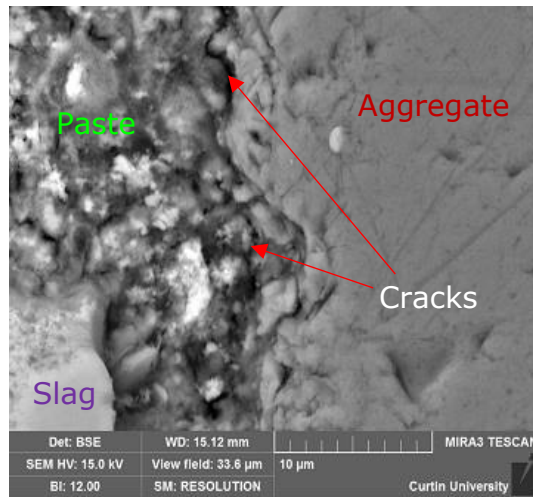
(d) 70BFS-FA



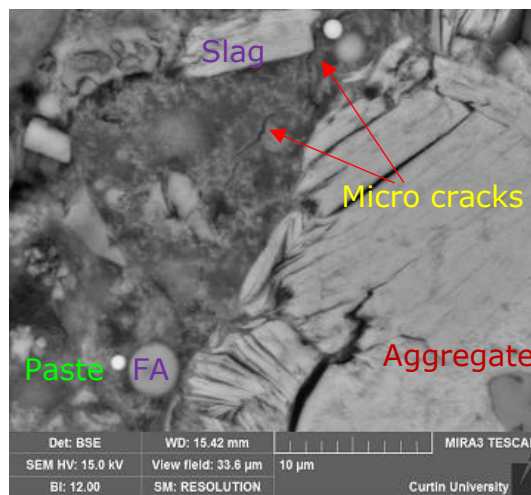
(e) 69BFS-FA.1NC



(f) 80BFS



(g) 78BFS.2NS

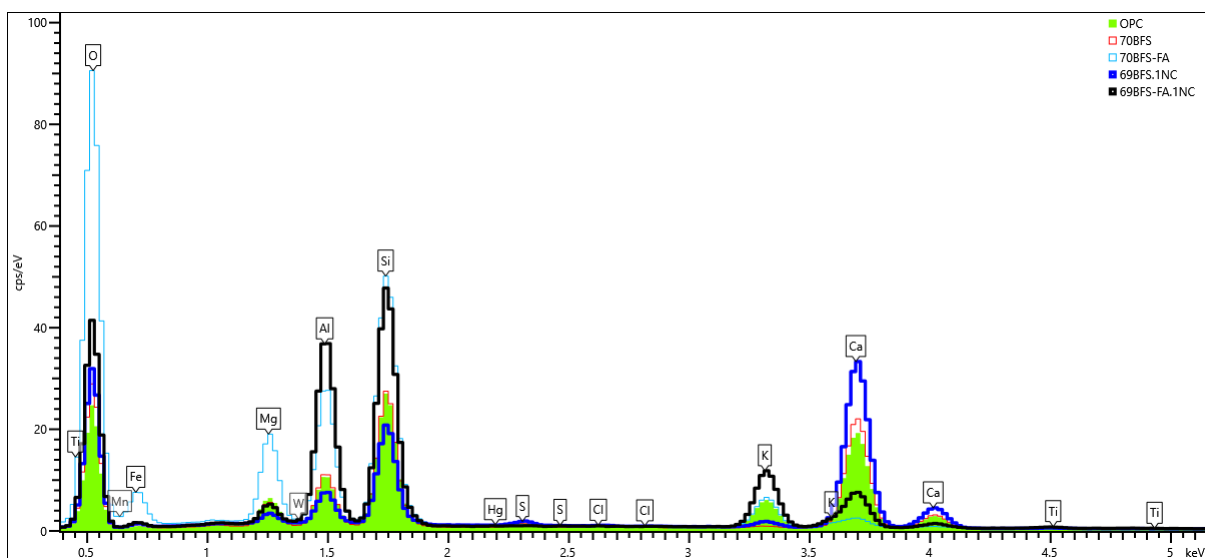


(h) 67BFS-FA.3NS

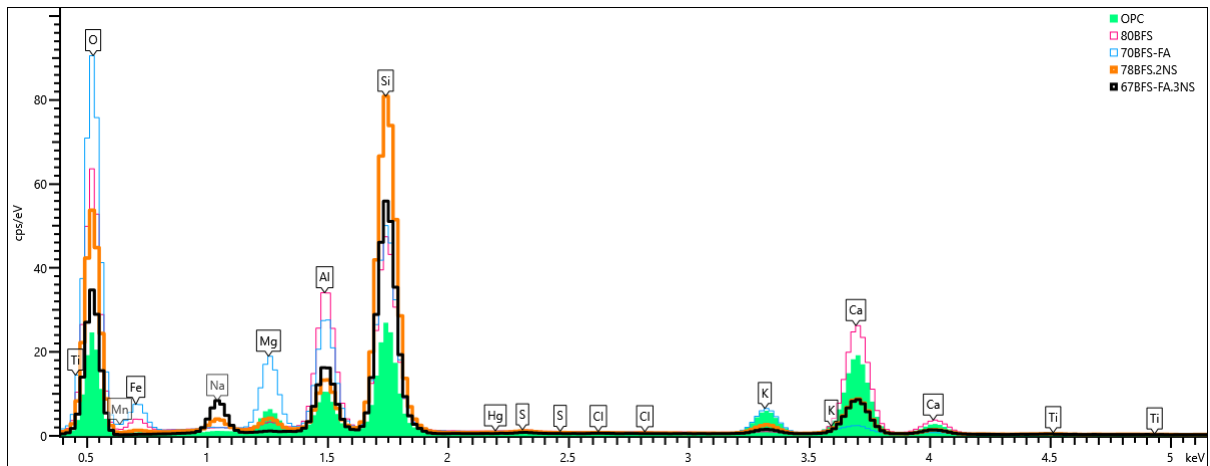
**Fig. 5.13** SEM images of different concrete mixes after 28 days of curing with and without nano materials addition



The improved microstructure of ITZ area of HVS and HVS-FA concretes due to addition of NC and NS observed above is also evident in the improvement of 28 days compressive strength values of those concretes shown in **Fig. 5.15**. It can be seen in **Fig. 5.15** that the compressive strength of concretes containing 70% BFS is increased by about 20% and 10%, respectively due to addition of 1% NS and 3% NS, while for concrete containing 80% BFS the improvement is about 35% due to addition of 2% NS and for concrete containing combined FA and BFS content of 70% the improvement is about 19% due to addition of 1% NC and 2% NS. These significant improvement in compressive strength in these HVS and HVS-FA concretes is due to the improvement in the microstructure of ITZ area around the aggregates as confirmed in previous results as well as densification of microstructure of matrix due to formation of additional CSH gels and reduction of capillary pores observed in earlier studies by the authors (Hosan & Shaikh, 2020; Shaikh & Hosan, 2019).



(a)



(b)

Fig. 5.14 EDS spectra of different concrete mixes containing (a) NC and (b) NS.

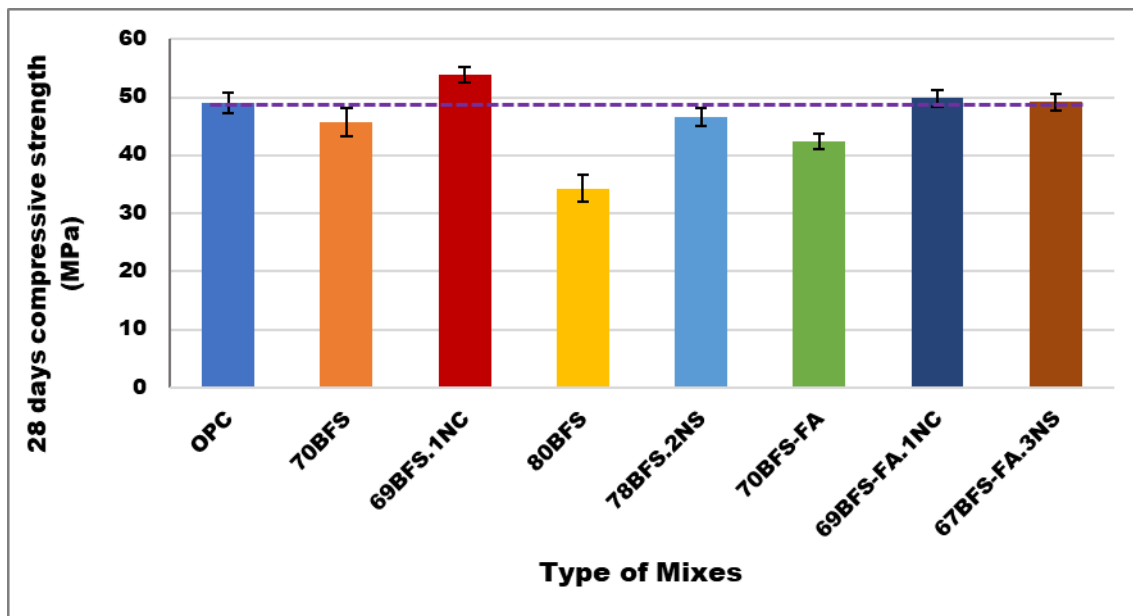


Fig. 5.15 Compressive strength of HVS and HVS-FA concretes containing NS and NC

## 5.4 Summary

This chapter investigated the effect of addition of nano calcium carbonate (NC) and nano silica (NS) on the compressive strength and the changes in microstructural of the interfacial transition zone (ITZ) between aggregate and matrix of HVS and HVS-FA concretes. Based on the experimental results found in this investigation, the following calculations can be made.

- ✚ Addition of 1% NC and 2-3% NS in both HVS, and HVS-FA concretes increased the compressive strengths significantly. All HVS and HVS-FA concretes containing NC and NS exceeded the compressive strength of OPC concrete with only exception of concrete containing 80% BFS containing 2% NS whose strength was just 5% lower than the OPC concrete.
- ✚ The nanoindentation test results show higher modulus of ITZ area around coarse aggregates of HVS and HVS-FA concretes due to addition of NS and NC compared to their control concretes indicating formation of additional CSH due to pozzolanic reactions and pore filling of nano materials. The ITZ width around coarse aggregates in those HVS and HVS-FA concretes is also decreased due to addition of NS and NC.
- ✚ A significant higher compact microstructure with much lower porosities and fewer cracks of ITZ area in HVS and HVS-FA concretes is observed due to addition of NS and NC in the SEM analysis. The EDS analysis also reveal higher peaks of Ca and Si and lower peak of O in those concretes due to addition of NS and NC confirming formation of higher CSH in the ITZ.

## 5.5 References

- Akcaoglu, T., Tokyay, M. and Celik, T. (2005) Assessing the ITZ micro-cracking via scanning electron microscope and its effect on the failure behaviour of concrete. *Cement and concrete research*. 35(2):358-363.
- Australia, S., *Aggregates and rock for engineering purposes Concrete aggregates*, in AS 2758.1:2014 2014, Standards Australia.
- Australia, S., *Portland and blended cements*, in AS 3972-1997. 1997, Standard Australia.
- Australia, S., *Supplementary cementitious materials for use with portland and blended cement Fly ash*, in AS 3582.1-1998 1998, Standards Australia.
- Australia, S., *Supplementary cementitious materials for use with portland and blended cement Slag - Ground granulated iron blast-furnace*, in AS 3582.2-2001 2001, Standard Australia.
- Barbhuiya SA, Gbagbo JK, Russell MI, Basheer PAM. Properties of fly ash concrete modified with hydrated lime and silica fume. *Construct Build Mater* 2009;23:3233–9.
- Carette G, Malhotra VM. Early age strength development of concrete incorporating fly ash and condensed silica fume. *ACI SP79-41*, Vol. 79; 1983. p. 765–84.
- Constantinides, G., and Ulm, F.-J. (2004). “The effect of two types of C–S–H on the elasticity of cement-based materials: Results from nanoindentation and micromechanical modelling.” *Cem Concr Res.*, 34(1), 67–80.
- Hosan, A. and Shaikh, F.U.A. (2020) Influence of nano-CaCO<sub>3</sub> addition on the compressive strength and microstructure of high volume slag and high volume slag-fly ash blended pastes. *Journal of building engineering*. Vol. 27, 100929.
- Kawashima S, Hou P, Corr DJ, Shah SP. Modification of cement based materials with nanoparticles. *Cem Concr Compos* 2013;36:8–15.
- Li H, Xiao H, Yuan J, Ou J. Microstructure of cement mortar with nano-particles. *Compos: Part B* 2004;35:185–9.
- Li, W., Xiao, J., Sun, Z., Kawashima, S. and Shah, S.P. (2012) Interfacial transition zones in recycled aggregate concrete with different mixing approaches. *Construction and building materials*. 35:1045-1055.

M.H. Zhang, J. Islam, Use of nano-silica to reduce setting time and increase early strength of concretes with high volume fly ash or slag, *Constr. Build. Mater.* 29 (2012) 573–580.

Malhotra VM, Mehta PK. High-performance, high-volume fly ash concrete: materials, mixture proportioning, properties, construction practice, and case histories; 2002.

Mehta PK, Gjørv OE. Properties of Portland cement concrete containing fly ash and condensed silica fume. *Cem Concr Res* 1982;12:587–95.

Naik TR, Singh SS, Hossain MM. Permeability of concrete containing large amounts of fly ash. *Cem Concr Res* 1994;24(5):913–22.

Nezerka, V., Bily, P., Hrbek, V. and Fladr, J. (2019) Impact of silica fume, fly ash and metakaolin on the thickness and strength of the ITZ in concrete. *Cement and concrete composites.* 103:252-262.

Oliver, W.C. and G.M. Pharr, *An improved technique for determining hardness and elastic modulus using load and displacement sensing indentation experiments.* *Journal of Materials Research*, 1992. 7(6): p. 1564-1583.

Shaikh, F. U. A., and Supit, S. W. M. (2014). “Mechanical and durability properties of high volume fly ash (HVFA) concrete containing calcium carbonate (CaCO<sub>3</sub>) nanoparticles.” *Constr. Build. Mater.*, 70, 309–321.

Shaikh, F. U. A., and Supit, S. W. M. (2015). “Compressive strength and durability properties of high volume fly ash concretes containing ultrafine fly ash.” *Constr. Build. Mater.*, 82, 192–205.

Shaikh, F.U.A. and Hosan, A. (2019) Effect of nano alumina on compressive strength and microstructure of high volume slag and slag-fly ash blended pastes. *Frontiers in Materials.* (doi:10.3389/fmats.2019.00090)

Shaikh, F.U.A. and Hosan, A. (2019) Effect of nano silica on compressive strength and microstructures of high volume blast furnace slag and high volume blast furnace slag-fly ash blended pastes. *Sustainable Materials and Technologies.* Vol. 17, e00111.

Shaikh, F.U.A., Supit, S.W.M. and Barbhuiya, S. (2016) Microstructure and nanoscale characterisation of HVFA cement paste containing nano-SiO<sub>2</sub> and nano-CaCO<sub>3</sub>. *Journal of materials in civil engineering.* 04017063-1.

Siddique R. Performance characteristics of high-volume class F fly ash concrete. *Cem Concr Res* 2004;34(3):487–93.

Sorelli, L., Constantinides, G., Ulm, F. J., and Toutlemonde, F. (2008). “The nano-mechanical signature of ultra high performance concrete by statistical nanoindentation techniques.” *Cem Concr Res.*, 38(12), 1447–1456.

Thomas MDA, Shehata MH, Shashiprakash SG, Hopkins DS, Cail K. Use of ternary cementitious systems containing silica fume and fly ash in concrete. *Cem Concr Res* 1999;29:1207–14.

Yue, Y., Zhou, Y., Xing, F., Gong, G., Hu, B. and Guo, M. (2020) An industrial applicable method to improve the properties of recycled aggregate concrete by incorporating nano silica and micro CaCO<sub>3</sub>. *Journal of cleaner production.* 259:120920.

Zheng, J.J., Li, C.Q. and Zhou, X.Z. (2005) Thickness of interfacial transition zone and cement content profiles around aggregates. *Magazine of concrete research.*57(7):397-406.

*All reasonable efforts have been made to acknowledge the authors of the copyright material. It would be highly appreciated if I can hear from any author has been ignored or incorrectly acknowledged.*

## **Chapter 6: Mechanical and durability properties of HVS and HVS-FA concretes containing nano silica**

---

This chapter presents the effect of optimum content of nano silica on the early and long term compressive strengths of high volume slag (HVS) and high volume slag-fly ash (HVS-FA) blended concrete up to 180 days. Durability properties such as sorptivity, drying shrinkage, volume of permeable properties, rapid chloride permeability test of those HVS and HVS-FA concrete containing nano silica are also discussed in this chapter. Microstructural changes due to the addition of nano silica through scanning electron microscope (SEM) and energy-dispersive X-ray spectroscopy (EDS) have investigated and compared with the ordinary concrete.

### **6.1 Overview**

Ordinary Portland Cement (OPC) is considered to be an inevitable ingredient of concrete production. However, environmental and economic concerns directed researchers to focus on the high volume cement replacement with industrial by product such as blast furnace slag (BFS), fly ash (FA), silica fume (SF) etc. due to its huge impact on global climate change by releasing carbon di-oxide into the atmosphere and massive consumption of virgin materials during production (Elchalakani et al., 2014; Tharakan et al., 2013). A number of studies have been conducted to substitute cement with BFS in high volume, however, observed challenges of very low early strengths, notable autogenous and/or drying shrinkage, large scale of bleeding, high level of porosity, higher water absorption and tendency for rapidly progress carbonation when the replacement was more than 55-60% (Aghaeipour & Madhkhan, 2017; Choi et al., 2017; Duran & Bilim, 2007; Güneysi & Gesoğlu, 2008; Hill & Sharp, 2002; Oner & Akyuz, 2007; Wainwright & Rey, 2000).

---

The content of this chapter has been written based on the results published in the following journal.

Hosan, A. and F.U.A. Shaikh, Influence of nano silica on compressive strength, durability, and microstructure of high-volume slag and high-volume slag-fly ash blended concretes. *Structural Concrete*. <https://doi.org/10.1002/suco.202000251>

On the other hand, several researches have been investigated the high volume replacement of cement with a blend of slag and fly ash and reported lower early age compressive strengths, longer initial and final setting time (Demirboğa et al., 2004; Jeong et al., 2015; Kuder et al., 2012) due to the relaxed pozzolanic reaction of slag and fly ash.

Nowadays, the influence of nano silica (NS) on the mechanical properties, durability properties and microstructure of concrete with binary mix of slag and fly ash. For instance, Zhang et al. (Zhang & Islam, 2012; Zhang et al., 2012) found that addition of 2% NS increased the compressive strength of 50% slag replaced concrete by 22% and 18% at 3 and 7 days, respectively and reduced initial and final setting time by 95 and 105 minutes, respectively compared to the reference concrete containing 50% slag as partial replacement of cement. Moreover, 2% incorporation of NS reduced the initial and final setting times by 28.1% and 22.1%, respectively with compared to that of the reference concrete without NS and it acted as a reactive filler which reduced the bleeding and increased the density of the concrete. The hydration rate of cement and fly ash were accelerated and span of dormant phase was shortened due to the addition of 1% NS in the cement paste containing 49% fly ash in that study. It was also demonstrated that the addition of 2% NS by mass of cementitious materials densified the paste-aggregate interface compared to the control without nano silica. The chloride-ion permeability resistance of concretes increased with 2% addition of nano-SiO<sub>2</sub> in comparison to that of reference concrete with no silica inclusion, of which charge passed reduced by 25.64% at age of 28 days. Recently, Liu et al. (2016) summarized that compressive strength of the mortar specimens increased by 21.71%, 17.17% and 10.67% at 3, 7 and 28 days, respectively compared to the mortar without NS inclusion and highest compressive strength (59.42MPa) was found with 30%wt. dosage of slag and 3%wt. NS. The degree of heat generation was increased with the addition of nano silica and induction period was shortened and this reduction was more with paste samples of BFS with 3%wt NS.

On the other hand, high volume fly ash (HVFA) concrete delays the maximum heating and it happens at around 30-40h while inclusion of nano-SiO<sub>2</sub> accelerates the maximum heating and is similar to that of ordinary concrete which occurs at around 15-25h. It has also reported that a little inclusion of nano-SiO<sub>2</sub> accelerates the pozzolanic activity of fly ash rapidly and about 19% increase in temperature with 4% addition of nano-SiO<sub>2</sub> in concrete with 50% FA as partial replacement of cement with compare to the concrete with no inclusion of nano-SiO<sub>2</sub>. Addition of 4% nano-SiO<sub>2</sub> increased early age compressive strengths of HVFA concrete significantly as well as the long term compressive strengths. It is reported 4% nano-SiO<sub>2</sub> inclusion with



50% FA replaced concrete enhanced the compressive strengths by 80.35% at 3 days and 68.57% at 7 days with respect to HVFA concrete without nano-SiO<sub>2</sub> (Li, 2004). Shaikh et al. (2014) observed slightly (5%~9%) improvement of compressive strengths of mortars containing 40% and 50% fly ash at 7 and 28 days. On the other hand, 33% and 48% improvement reported in the mortars containing 60% and 70% fly ash respectively at age of 28 days. They also conducted the compressive strengths test of concretes specimens containing 2% nano-SiO<sub>2</sub> replaced concrete containing 40% and 60% FA. They have found that 2% nano-SiO<sub>2</sub> significantly improved the 3 days compressive strengths of both HVFA concretes and is more pronounced (95% improvement) with concrete containing 60% fly ash but no such improvements observed at ages of 7, 28, 56 and 90 days. They also reported 38% reduction of chloride ion permeability at 28 days of concrete with 38% FA and 2% nano-SiO<sub>2</sub> and 9% and 20% reduction found at 28 days and 90 days respectively, in the HVFA concrete containing 58% FA and 2% nano-SiO<sub>2</sub>. The water sorptivity values of HVFA concretes containing 38% FA and 2% nano-SiO<sub>2</sub> reduced and were 27-32% lower than that of concretes with no nano-SiO<sub>2</sub>. In addition, it was also found more active in reducing water absorption of concrete containing 58%FA and 2% nano-SiO<sub>2</sub>. Replacing of 2% FA with nano-SiO<sub>2</sub> lowered the chloride diffusion coefficient about 21% and 14% of the concrete containing 40% FA and 60% FA respectively compared to that of no nano-SiO<sub>2</sub> and resistance of concrete against corrosion improved by the incorporation of nano-SiO<sub>2</sub> reported in that study (Shaikh & Supit, 2015).

From the above literature review it is clear that nano-SiO<sub>2</sub> addition improves the mechanical and durability properties of binary composites of slag and fly ash replaced cement pastes, mortars and concretes. However, most of the study reported a replacement of binary mixes of slag and fly ash up to 60% and no high volume slag-fly ash blended concrete has been studied yet. Based on the findings of (Shaikh & Hosan, 2019), this study aims to evaluate the effect of nano-SiO<sub>2</sub> addition on the early and later ages compressive strengths, durability properties such as sorptivity, drying shrinkage, volume of permeable voids (VPV), rapid chloride permeable test (RCPT) and microstructural changes in interfacial transition zones (ITZ) of high volume slag (HVS) and high volume slag-fly ash (HVS-FA) blended concrete.

## **6.2. Experimental procedure**

### **6.2.1 Materials**

The ordinary Portland cement (OPC) used in this study was purchased from a local cement company. The blast furnace slag (BFS) was supplied by a local cement company in Western

Australia and class F fly ash (FA) was provided by a coal fired power plant in Australia. All coarse and fine aggregates used in this study bought from local supplier ensuring the ASTM C127 standard. Aggregates were soaked in water for at least 24 hours and exposed to open air to achieve saturated surface dry (SSD) condition. Dry nano-SiO<sub>2</sub> (NS) with an average particle diameter of 25nm, specific surface areas of 160 m<sup>2</sup>/g and with 99% purity was purchased from commercial nano materials manufacturer. Tap water from concrete laboratory was used in all mixes and a naphthalene sulphonate based superplasticizer (SP) used to maintain the workability by measuring slump for all mixes as high volume replacement of slag and slag-fly ash blend used in this study. Physical and chemical properties of all cementitious materials are given in the **Table 3.1** and **Figs. 3.2 & 4.1** shows the X-ray diffraction (XRD) analysis of OPC, BFS, FA and NS. It can be seen by comparing the results that NS is highly amorphous compared to FA and BFS. Among BFS and FA, BFS is more amorphous with amorphous content of 95.7% compared to 67.8% amorphous content of FA based on quantitative XRD analysis performed by Centre for Materials Research, MMF, Curtin University, Perth, Australia.

### 6.2.2 Concrete mix design

All the concrete mixes were designed with a total binder quantity of 400 kg/m<sup>3</sup> and a constant water/binder ratio of 0.4. However, superplasticizer was used when needed to maintain the concrete mixes workability with a target slump of 100-130 mm. Coarse and fine aggregates mass and ratios were kept constant for all mixes. **Table 6.1** shows the mix proportions of all control and mixes with supplementary cementitious materials (SCMs) with and without NS. A designated ID was given for each mix considering binder name and amount present on the mixes. For example, 80BFS means a mix containing 80% BFS and 20% OPC of total binder.

**Table 6.1** Mixing proportions of different concrete mixes (Kg/m<sup>3</sup>) and measured slump

Mix ID	Binding Materials			Nano Silica	Aggregates			Water	Super plasticizers	Slump (mm)
	Cement	Slag	Fly ash		Sand	20 mm	10 mm			
OPC	400	-	-	-	684	789	395	163	-	120
80BFS	80	320	-	-	684	789	395	163	2.85	112
78BFS.2NS	80	312	-	8	684	789	395	163	4.34	116
70BFS-FA	120	196	84	-	684	789	395	163	1.15	125
67BFS-FA.3NS	120	190	78	12	684	789	395	163	4.11	110

### 6.2.3 Casting concrete specimens

Concrete mixes were prepared in a pan mixer at ambient temperature. Firstly, all the dry ingredients such as cement, coarse aggregates, fine aggregates and SCMs (in case of HVS and HVS-FA mixes) were mixed for 4-5 minutes considering high amount of aggregates and volume of concrete. Next, water was added and again mixed for around 2-3 minutes until a homogenous mix was reached. In addition, mixes containing NS were prepared by mixing the NS powder with partial water such as half and two-third of total amount water required for the mixes containing 2% and 3% NS, respectively and superplasticizers required for the concrete mixes. That mix was then dispersed ultrasonically by an ultrasonic mixer with 100% amplitude and maximum cycle for 60 minutes and 75 minutes for 2 % and 3 % of NS, respectively used in both mixes (Arefi et al., 2011; Elkady et al., 2013). The remaining water was added with that mixed and stirred again manually before added slowly into the concrete mixes while pan mixer was running to ensure proper dispersion of NS particles into the concrete mixes. Additional superplasticizer was added to attain the target slump for all mixes can be seen in **Table 6.1**. The dosage of superplasticizers are varies for different mixes with the amount of slag, slag-fly ash blend and the percentage of added NS in the mixes also shown in Table 2.

Standard cylindrical samples with diameter of 100 mm and height of 200 mm were cast for compressive strengths and durability properties such as sorptivity, volume of permeable voids (VPV) and rapid chloride permeability test (RCPT) based on ASTM standards. A prismatic 75 mm square cross-sectional and 285 mm long concrete samples with gauge studs at both ends ensuring gauge lengths of 250 mm were also cast for drying shrinkage test according to ASTM standard. All the specimens were mixed in a vibrating table with three layers for cylindrical samples and two layers for shrinkage samples according to standards. All the specimens were demoulded after 24 hours and cylindrical samples were then cured in lime saturated water at room temperature. For durability test such as sorptivity, VPV and RCPT, a 50 mm discs were cut from the cylindrical samples at 28 and 90 days of concrete age and the tests were performed according to their standards. Shrinkage specimens were cured in lime saturated water first part of curing according to ASTM C157 standard and then placed in a room with controlled relative humidity of 50% and at a temperature of 23°C and then readings were taken at 7, 14, 28, 35, 56, 91, 120, 150, 180, 270, 330 and 365 days of concrete age (ASTM, 2017). To explore the microstructural changes of different concrete mixes, a small portion of concrete with an interfacial transition zone (ITZ) were cut from each mix by using a diamond precision saw and dried by naturally to make sure it is free from moisture.

## **6.2.4 Testing procedure**

### **6.2.4.1 Compressive strengths**

Compressive strengths were measured in MATEST testing apparatus according to ASTM C873 (2015) standard with a loading rate of 0.33 MPa/s until failure at 3, 7, 28, 56, 90 and 180 days of concrete age of all mixes. Diameters of the cylinders were measured and sulphur capped at least 4 hours prior to the test. Compressive strengths were calculated as the maximum crushing load divided by the average cross-sectional area of the specimens. For each test age, at least three samples were tested and average value of three were reported in this study.

### **6.2.4.2 Sorptivity Test**

The rate of water absorption (sorptivity) of all concrete mixes were investigated after 28 and 90 days of water curing. At least two samples of each concrete mixes were prepared and tested according to the ASTM C1585 to determine the rate of water absorption by measuring the mass of concrete specimens regularly from 1 min to 6 hours and absorption (I) was calculated by change in mass divided by cross sectional area of the specimens and the density of water.

### **6.2.4.3. Drying shrinkage**

Drying shrinkage test was performed according to ASTM C157 (2017) standard. Lengths of the samples were measured at 7, 14, 28, 35, 56, 91, 120, 150, 180, 270, 330 and 365 days of concrete age in the curing room with controlled humidity and temperature. At least three samples were cast and all the specimens were measured at the same time for each concrete mix. Shrinkage strain was calculated as the difference between initial and measured length (length change) divided by the gauge length (250 mm) according to standard and average of three samples obtained.

### **6.2.4.4 Volume of permeable voids (VPV)**

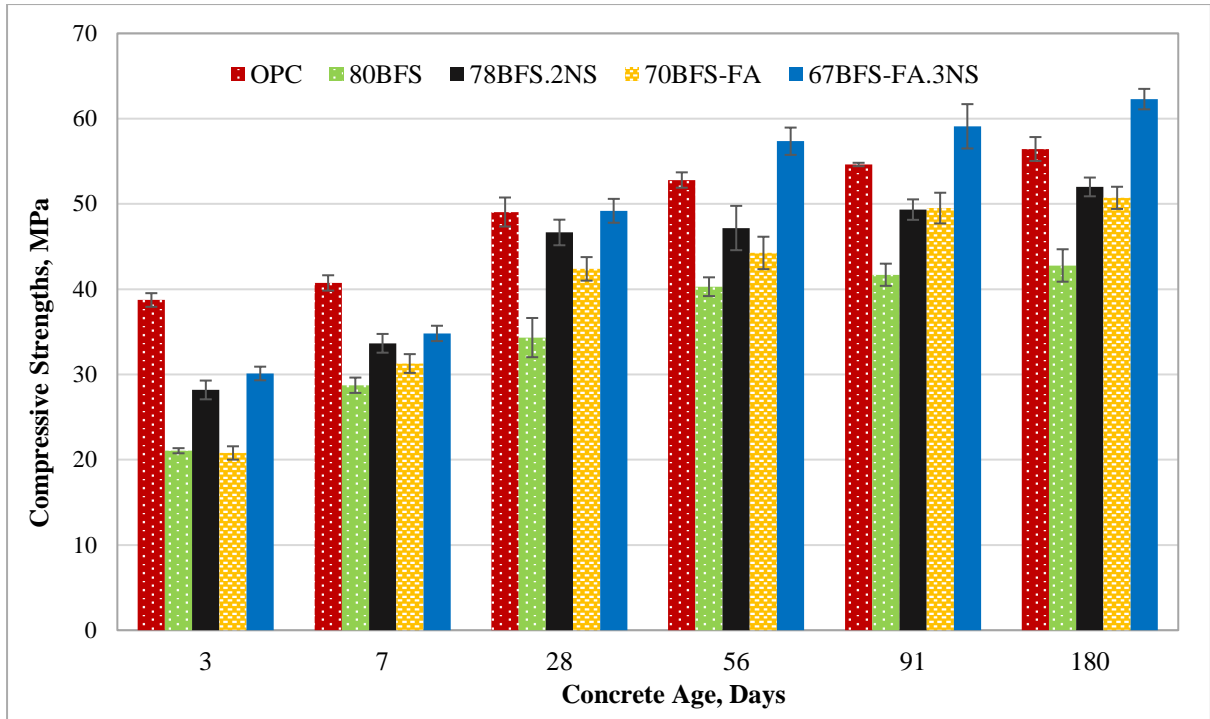
Volume of permeable voids of 100 mm diameter and 50 mm thick samples of all concrete mixes were measured at 28 and 90 days of concrete age according to ASTM C642 (2013a) standards. These tests were conducted to determine the voids present in the concrete specimens and is measured by boiling the 50 mm cut concrete discs from different part of concrete cylinders at 105°C in a water bath for at least 5 hours and then weighing the samples in water. Initial weight of oven dried samples and after at least 24 hours of immersion in water were measured and at least three samples were used for each concrete mix for this test.

#### ***6.2.4.5 Rapid chloride permeability test (RCPT)***

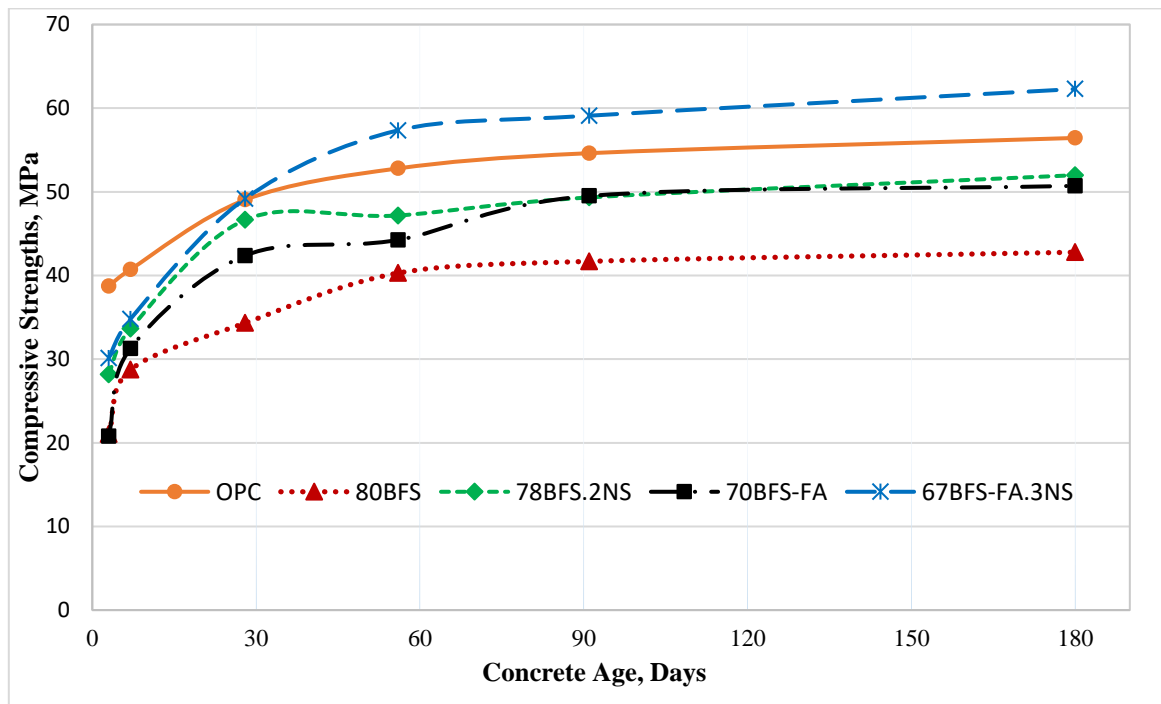
To determine the concrete performance against the entrance of chloride ion is known as the rapid chloride permeability test (RCPT). At least three 50 mm discs from each concrete mixes after 28 and 90 days of curing period were prepared by coating them with a sealer materials and then vacuum conditioning with a desiccator for at least 5 hours according to the ASTM C1202 (2019) standard. Samples were then placed under water and afterwards exposed to a constant 60 voltage for 6 hours on the cells in which one cell was filled with 3% NaCl solution and another cell was filled with 0.3N NaOH solution. The total charge passed through the concrete samples were collected by using a Perma2 testing apparatus and average values are presented in this study.

#### ***6.2.4.6 Scanning electron microscope (SEM) and energy-dispersive X-ray spectroscopy (EDS)***

Microstructural investigation of different HVS and HVS-FA concrete with and without NS addition were performed by using MIRA3 TESCAN, a variable pressure field emission scanning electron microscope (VP-FESEM) equipped with backscattered electron (BSE) detector and energy-dispersive X-ray spectroscopy (EDS) analyser to collect SEM images along with EDS spectrum to analyse the phases. The samples were prepared by taking a small portion of dried concrete samples after 28 days of wet curing and placed them in a vacuum desiccator for minimum three days to remove all the moisture from the samples. Samples were then drenched in an epoxy resin mount, polished and then 20 mm thick carbon coat has been applied to reduce the chances of getting charged during image and spectrum collection. The SEM and EDS were carried out at a constant accelerating voltage of 15kV and around 15 mm of working distance by using BSE detectors for all concrete samples. SEM images and EDS spectrums were collected in ITZ to investigate the porosity and bonding between the binder and aggregate.



a)



b)

**Fig. 6.1** Compressive strengths of different HVS and HVS-FA mixes with and without NS

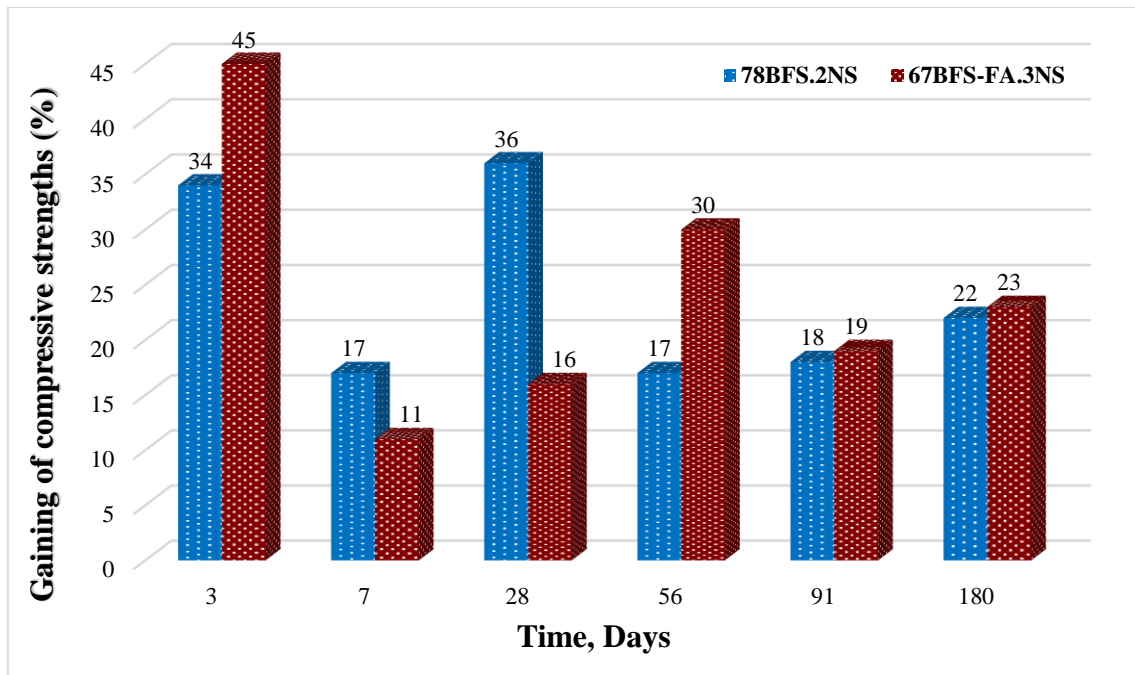


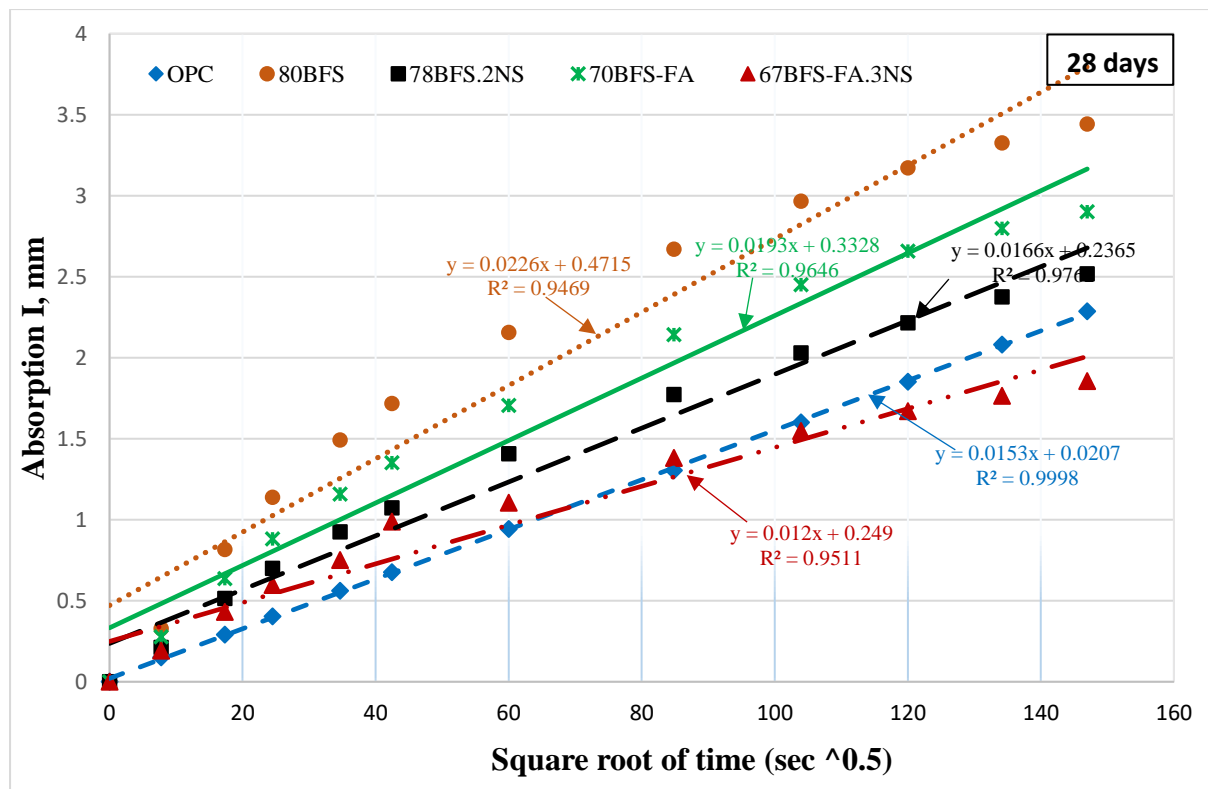
**Fig. 6.2** Gaining of compressive strengths of HVS and HVS-FA concrete due to the addition of NS

### 6.3. Results and discussions

#### 6.3.1 Compressive strengths

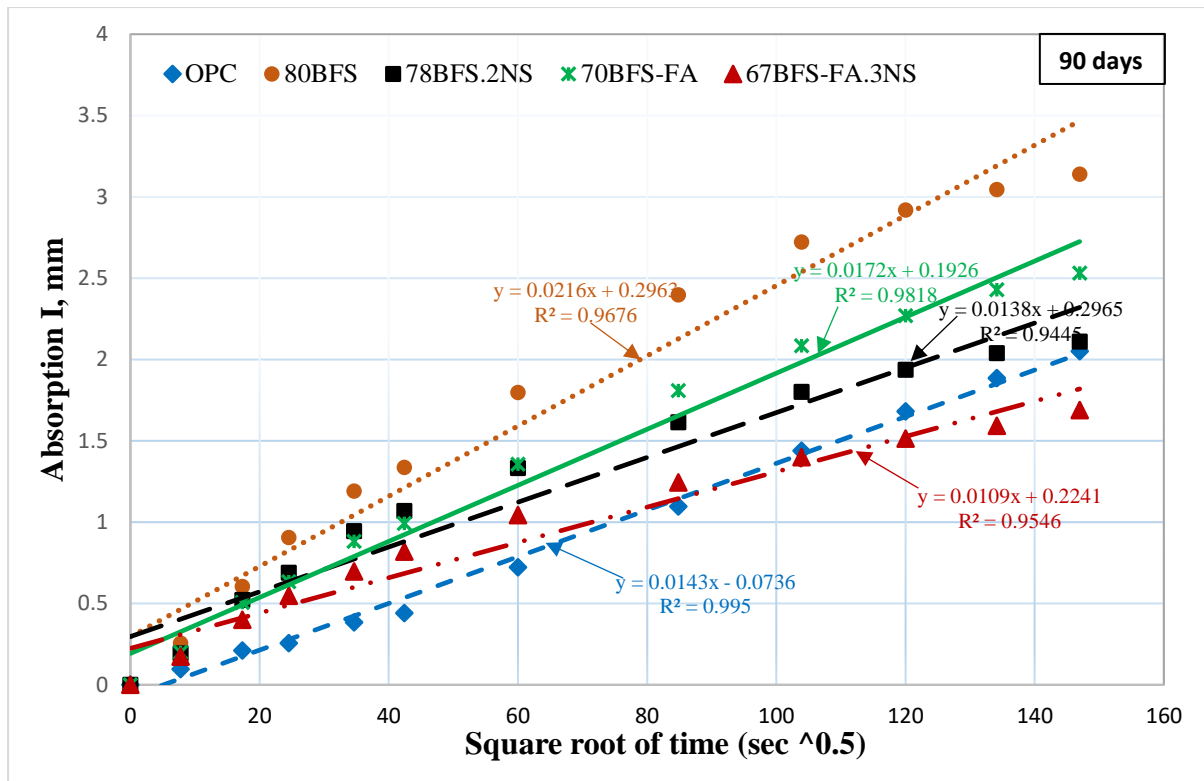
Comparison of average compressive strengths of different concrete mixes with and without NS including control OPC concrete at various ages are shown in **Fig. 6.1**. It can be seen that the compressive strengths of HVS and HVS-FA concretes decreased around 50% at the age of 3 days than the control OPC concrete. However, the compressive strengths of HVS-FA concrete picked up at later ages though it was always considerably lower than the control OPC concrete. On the other hand, HVS concrete with 80% BFS showed significant reduction even in the later ages than both control OPC concrete and HVS-FA concrete containing 49% BFS and 21% FA which is bit contrasting to the results of Elachalakani et. al. (2014). The addition of NS enhanced the compressive strengths of both concrete mixes at early ages as well as later ages as can also be seen from the **Fig 6.1** and at 28 days exhibited similar compressive strengths to control OPC concrete. It is clear that HVS-FA concrete containing combined BFS and FA of 67% showed significant improvement and superior performance in compressive strengths than the control OPC concrete at later ages due to the addition of 3% NS into the mixes. This could be the indolent activation of FA presence in that mix and 3% NS addition triggered the activation expressively after 28 days of curing. Moreover, the addition of 2% NS into the HVS concrete containing 78% BFS did not show such increased in the compressive strengths in the

later ages though it exhibited noteworthy improvement than its control concrete without NS addition can be witnessed from the **Fig. 6.2** which presented the compressive strengths gain of both HVS and HVS-FA concrete than their respective control concrete due to the addition of NS addition at 3, 7, 28, 56, 91 and 180 days of age. It is clear that HVS concrete containing 78% BFS and 2% NS exhibited better performances at early ages till 28 days and HVS-FA concrete containing 67% BFS-FA and 3% NS showed significantly better in later ages. Furthermore, both concrete mixes performed exceedingly well at 3 days which was a main concern in high volume cement replaced concretes. The compressive strength is increased dramatically by 34% and 45% in HVS and HVS-FA concretes, respectively after 3 days due to the NS inclusion than their respective control concrete. It is also found that both HVS and HVS-FA concretes performed similar in gaining compressive strengths at later ages due to the NS inclusion compare to their control concrete without NS. It has revealed in microstructure analysis of HVS and HVS-FA pastes that the formation of more C-S-H/C-A-H gels due to the addition of NS and dense microstructure with lower porosity in the first part of the study discussed in the literature review. However, the lack of publications of NS effect on the compressive strengths of HVS and HVS-FA concrete, this outcome cannot be compared at the moment.



a)





b)

**Fig. 6.3** Water absorption of different concrete mixes with and without NS at a) 28 days b) 90 days

### 6.3.2 Water sorptivity

The rate of water absorption of control OPC concrete, HVS and HVS-FA concretes with and without NS addition after 28 days and 90 days of curing is shown in **Figs. 6.3a and b**. It is evident that HVS and HVS-FA concrete exhibited substantially higher water absorption than the control OPC concrete due to higher pores in both ages of concrete as expected. However, the HVS-FA concrete containing combined BFS and FA of 70% showed relatively lower water absorption than the HVS concrete containing 80% BFS and could be the reason of lower volume replacement of cement and presence of angular shape BFS and spherical shape fly ash particles lowered the pores in the mix. It can be noticed that the addition of 2% NS in HVS concrete containing 78% BFS and 3% NS addition in HVS-FA concrete containing combined BFS and FA of 67% reduced the absorption expressively by approximately 27% and 38%, respectively after 28 days and by 36% and 37%, respectively after 90 days of curing than their control concretes without NS which is evidence of combined effect of NS addition and curing age of concrete on the water absorption. However, similar to the compressive strengths results, the HVS-FA concrete containing combined BFS and FA of 67% performed excessively better

than the HVS concrete containing 78% BFS and exhibited superior performance in both ages than control OPC concrete. **Fig. 6.4** illustrates the comparison of sorptivity values ( $10^{-4}$  mm/sec<sup>1/2</sup>) of control, HVS and HVS-FA concretes mixes at 28 days and 90 days of age and can be clearly seen that HVS concrete showed equivalent at 28 days and relatively better performance at 90 days of curing than control OPC concrete due to addition of 2% nano-SiO<sub>2</sub>. On the other hand, HVS-FA concrete exposed overwhelmingly better properties against water absorption reduced by approximately 21% and 24% after 28 days and 90 days of curing respectively than control OPC concrete displayed consistent outcome of compressive strengths is an evidence of NS influence on the prompt hydration of cementitious materials and forming new C-S-H gels lead to lower porosity and higher density of the mixes.

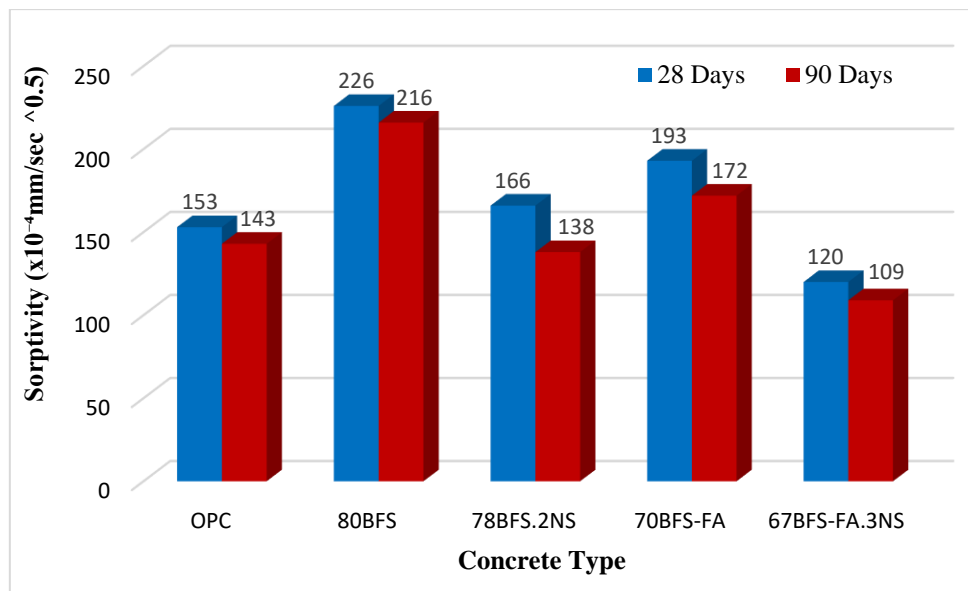


**Fig. 6.4** Sorptivity of different concrete mixes with and without NS after 28 days and 90 days

### 6.3.3 Drying shrinkage

**Fig. 6.5** compares the shrinkage strain ( $10^{-6}$ ) of control, HVS and HVS-FA concretes with and without nano-SiO<sub>2</sub> addition at 14, 21, 28, 35, 56, 91, 120, 150, 180, 270, 330 and 365 days of concrete age. Similar to the other study discussed in literature review, HVS and HVS-FA concretes exhibited massively higher shrinkage strain than control OPC concrete at any stage of concrete age and as expected HVS concrete containing 80%BFS showed more pronounced

shrinkage at later ages than the HVS-FA concrete containing combined BFS and FA content of 70%, which could be the reason of higher volume of replacement. It can be seen that NS addition reduced the early shrinkage of both HVS and HVS-FA concretes significantly than their respective control concretes and till 90 days of age both concretes exhibited superior performance in shrinkage control compare to the OPC concrete. However, the drying shrinkage of HVS concrete containing 78% BFS and 2% NS peaked at 120 days and showed equivalent shrinkage to the OPC concrete until 180 days and comparable shrinkage at later ages which indicates that NS addition improved properties of HVS concrete in early ages by rapid acceleration of hydration process. On the other hand, HVS-FA concrete containing combined BFS and FA of 67% exhibited exceedingly superior shrinkage controlling than OPC concrete at later ages as well and presented consistent result to the compressive strengths exposed the clear indication of early hydration of BFS and FA due to nano-SiO<sub>2</sub> inclusion and triggering of FA particles at later ages.

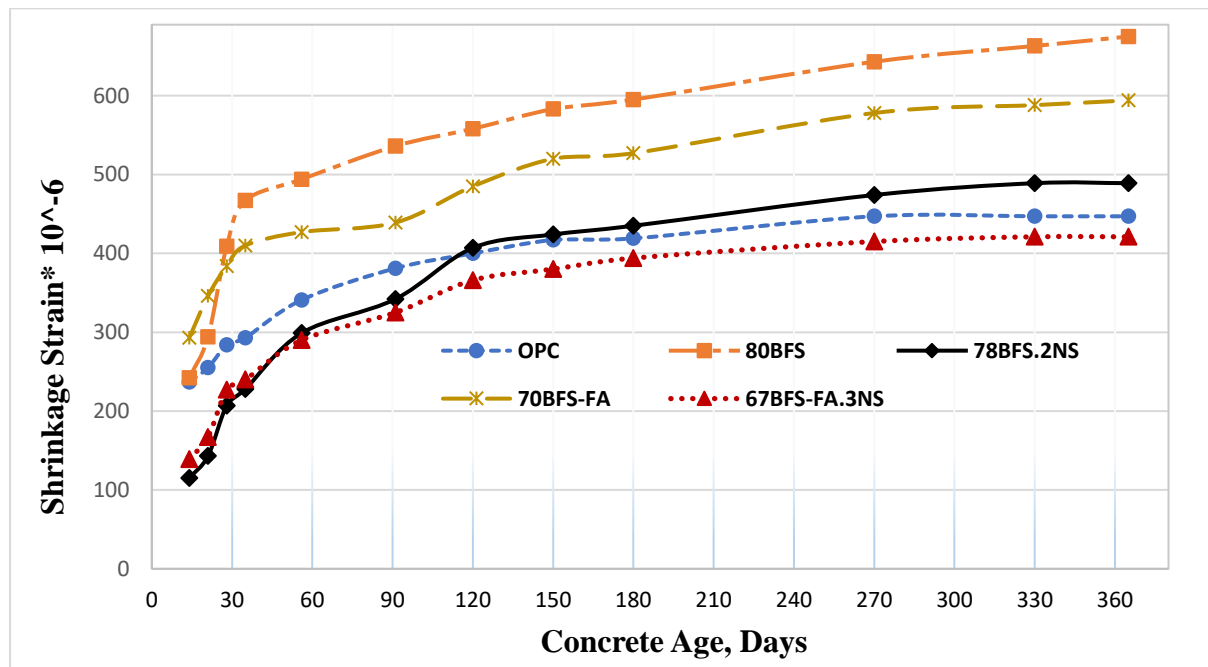


**Fig. 6.5** Shrinkage strain of different concrete mixes with and without NS at different age of concrete

### 6.3.4 Volume of permeable voids (VPV)

Average volume of permeable voids of different HVS and HVS-FA concrete mixes with and without nano-SiO<sub>2</sub> addition including control OPC concrete after 28 and 90 days of curing is shown in **Fig. 6.6**. As anticipated, the percentage of permeable voids increased greatly in HVS containing 80% BFS and HVS-FA concrete containing combined BFS and FA of 70% after 28 days of curing than control OPC concrete due to the high volume of cement replacement. However, a considerable reduction of VPV observed with the increasing curing period in HVS concrete containing 80% BFS displayed comparable VPV to control OPC concrete after 90 days of curing. On the other hand, a significant amount of reduction observed in HVS-FA concrete after 90 days of curing and showed lower voids than OPC concrete. It can be seen that 2 % NS addition in HVS concrete with 78% BFS reduced the permeable voids reasonably by around 14% and 10% after 28 days and 90 days of curing respectively than the HVS concrete containing 80% BFS and showed lower amount of permeable voids than OPC concrete after 90 days of curing. Alternatively, about 23% reduction of VPV is found in HVS-FA concrete after 28 days of concrete due to 3% NS addition compare to HVS-FA concrete without NS, however, no further reduction observed with the curing period which is contrary to the other test parameters.

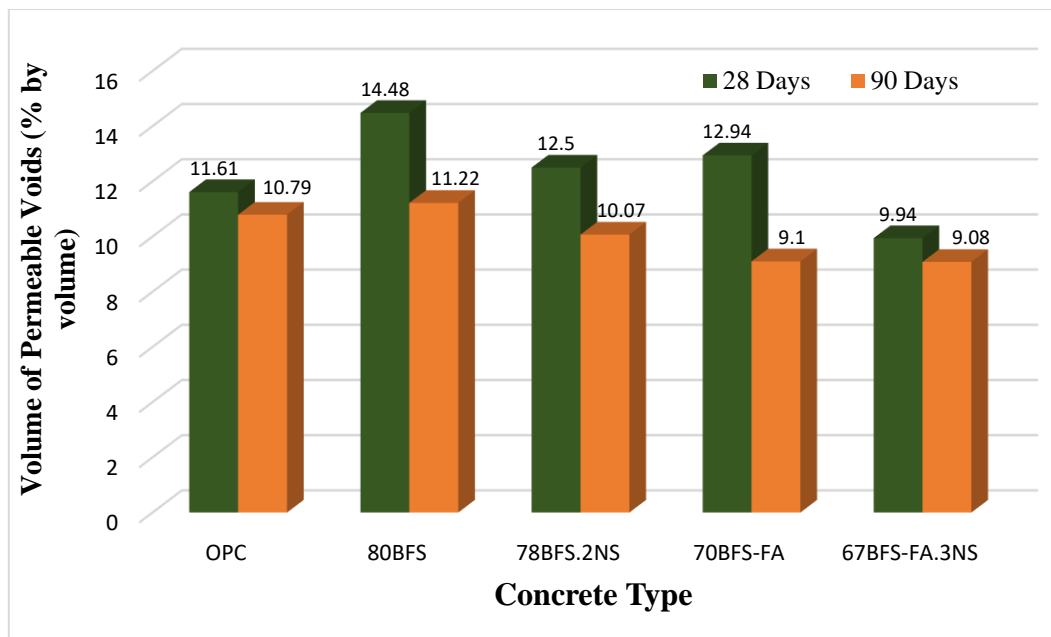


**Fig. 6.6** Average volume of permeable voids of concrete mixes with and without NS

### **6.3.5 Rapid chloride permeability**

Comparison of average charge passed through concrete samples of different HVS and HVS-FA mixes with and without NS addition is presented in Fig. 6.7 and compared with that of control OPC concrete. It can be noticed that both HVS and HVS-FA concretes showed a substantial reduction of chloride ion penetration compared to the OPC concrete and based on ASTM C1202 standard which were a very low stage of chloride ion permeability. However, surprisingly HVS concrete containing 80% BFS showed slightly better resistant against penetration of chloride ion than the 70% BFS-FA containing HVS-FA concrete which is conflicting to other test results, however, Elchalakani et. al. (2014) also found similar results of increased resistance against chloride ion permeability with the increasing BFS contents. It can also be seen that the addition of NS further reduced the chloride ion penetration in both HVS and HVS-FA concretes and is more pronounced at both ages in HVS concrete and at 90 days in HVS-FA. It can be seen that the inclusion of 2% NS in HVS concrete containing 78% BFS reduced the chloride ion penetration significantly by 47% at both 28 days and 90 days of curing and reduced to very close to negligible stage of chloride ion permeability according to ASTM C1202 standard after 90 days of curing. In case of HVS-FA concrete, a slight reduction by 7% witnessed after 28 days, however, a considerably significant reduction of chloride ion penetration by 35.5% is observed after 90 days of curing due to the 3% addition of NS. As expected, resistance against chloride ion permeability increased with the curing age of both concretes with and without NS addition. However, the improvement is more prominent with the NS addition can be seen from the results. A higher resistance against chloride ion permeability is a clear evidence of denser structure with lower porosity.

A comparison on improvement of different properties of HVS and HVS-FA concretes containing NS after 28 days and 90 days of curing can be seen in Fig. 6.8 and it is clearly perceived that a consistent relationship of those improvement is noticeable. However, improvement in volume of permeable voids were lower among them in both mixes which already been explained in the section 6.3.4. It is also visible that properties improvement was higher after 90 days of curing as obvious except volume of permeable voids in both mixes of HVS and HVS-FA concrete. Nevertheless, a significant improvement of VPV and RCPT observed in HVS-FA concrete even without NS inclusion could be the reason of blended mix of slag and fly ash.

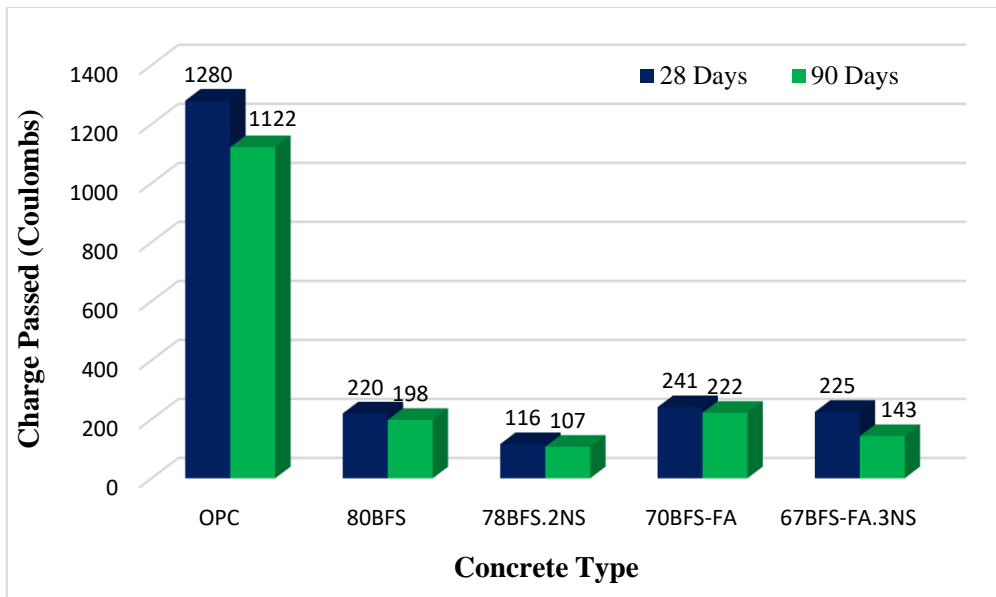


**Fig. 6.7** Average charge passed through concrete mixes with and without NS after 28 and 90 days of curing

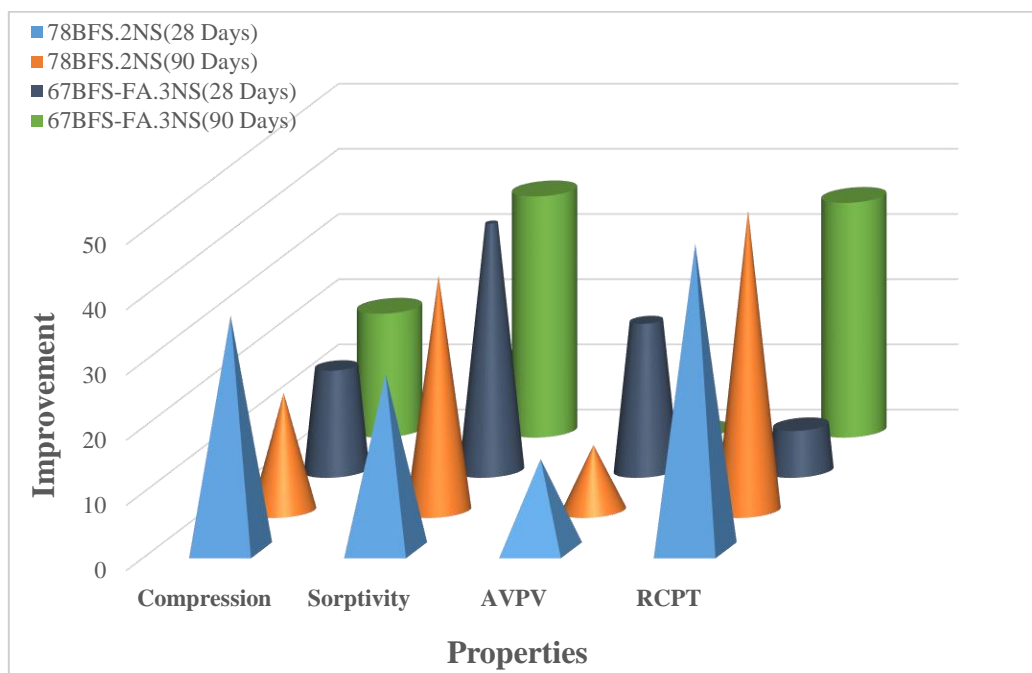
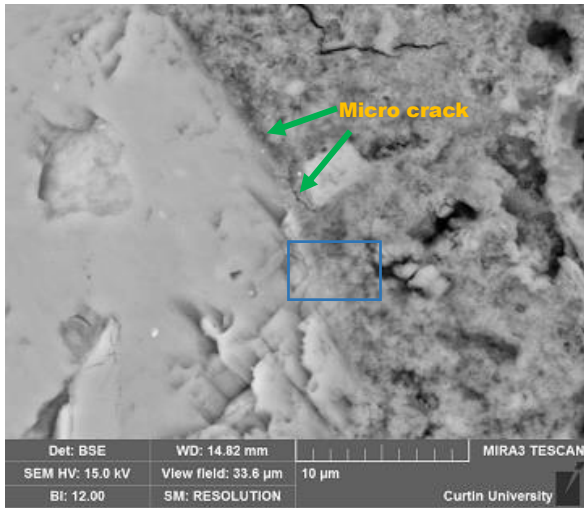
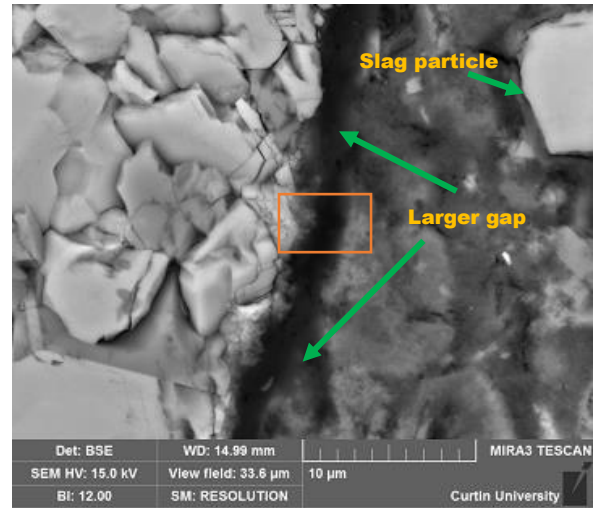


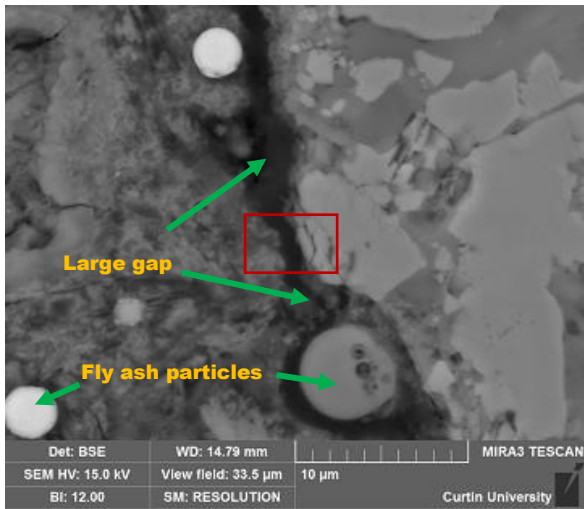
**Fig. 6.8** Improvement of different properties of concrete samples containing NS



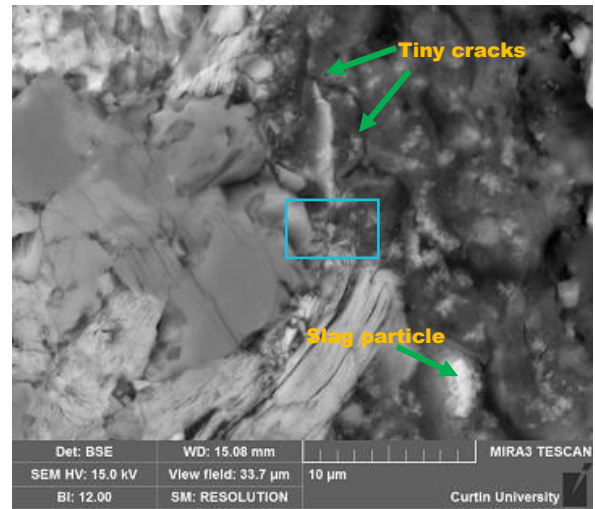
a) OPC



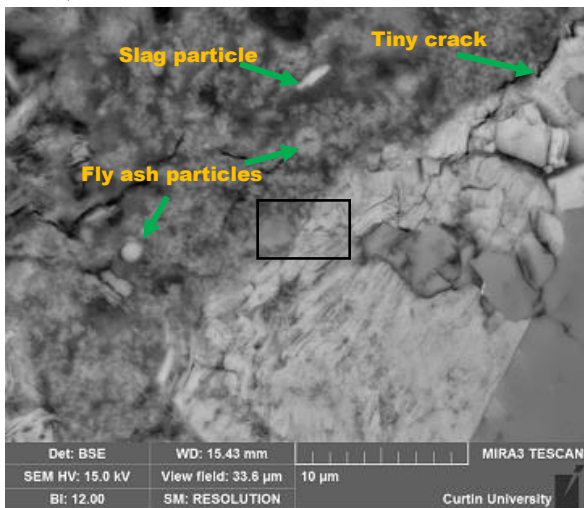
b) 80BFS



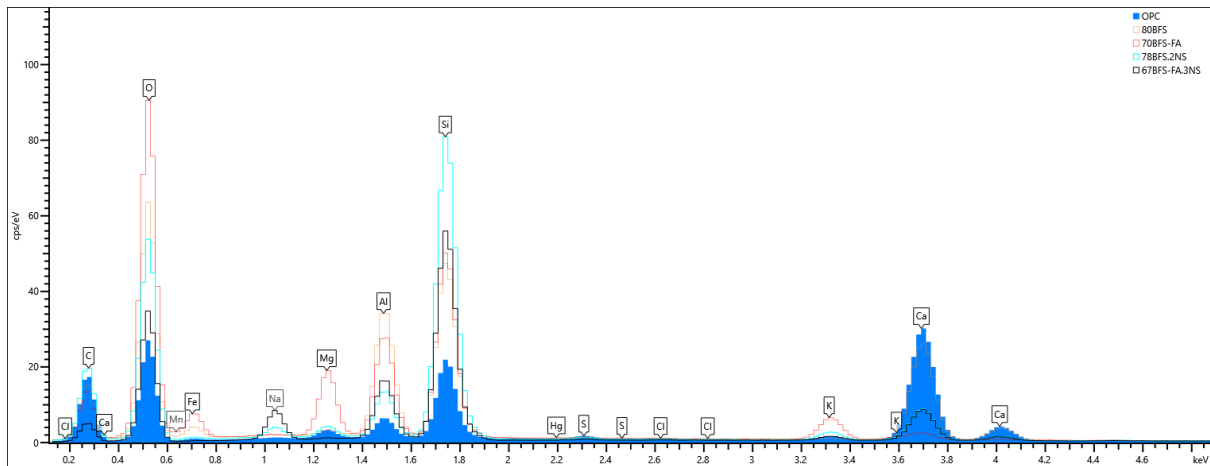
c) 70BFS-FA



d) 78BFS.2NS



e) 67BFS-FA.3NS



f) Comparison of EDS spectrum of different mixes

**Fig. 6.9a-f** BSE images and comparison of EDS traces at ITZ of different concrete mixes with and without nano-SiO<sub>2</sub> after 28 days of curing.

### 6.3.6 Microstructural modification through SEM images and EDS spectrum

Concrete considered to be composite of phases consist of binder-sand mortar, aggregates and interfacial transition zone (ITZ) and the degree of dense ITZ is closely related to the strength and other durability properties of the concrete mixes. BSE images and comparison of EDS spectrum taken in ITZ of all HVS and HVS-FA concrete mixes with or without addition of NS including control OPC after 28 days of wet curing are shown in **Figs. 6.9a-f**. From the micrographs shown in **Figs. 6.9a-c**, it is easily noticeable that both HVS and HVS-FA concrete having a huge gap in ITZ between aggregates and binder paste, while unnoticeable micro cracks are observed in control OPC concrete is an indication of early hydration of cement grains in early age of concrete. On the other hand, the presence of un-hydrated slag and fly ash grains in HVS and HVS-FA concretes can be observed in the micrographs which led to a porous and weaker microstructure caused lower compressive strengths and durability performance. In addition, presence of a huge traces of oxygen in EDS spectrums of HVS and HVS-FA concretes than OPC concrete is also an evidence of existence of more permeable gap in ITZ of both concrete. Effect of a small percentage of NS addition on those two HVS and HVS-FA concretes can be seen in the SEM images of **Figs. 6.9d-e**, exhibited a very dense microstructure consisting of tiny gap between aggregates and binder pastes interface. Moreover, slag and fly ash grains are mostly hydrated or partially hydrated also visible along with fully hydrated cement particles in the higher magnified images due to the addition of NS which enhanced the early hydration of large volume of replaced slag and fly ash particles resulted a higher degree of denser bond



between the particles in the ITZ. Furthermore, it is clearly evident in EDS traces of presence of additional Si and Ca than the spectrum of their respective reference concretes, might be the additional amorphous silica in the matrixes and formation of new C-S-H gel due to the inclusion of NS. It would be worth noting that, reduction of large volume oxygen in EDS traces of concrete mixes with NS than the HVS and HVS-FA concrete without NS demonstrated a compacted higher degree of dense microstructure resulted in higher compressive strengths and improved durability performance than the control OPC concrete described in sections before.

#### **6.4. Summary**

Based on the above results of early and long-term compressive strengths and various durability properties of high volume slag and high volume slag-fly ash blended concretes with and without nano silica, the following conclusions can be made:

- ❖ Compressive strength of HVS concrete containing 78% BFS is increased by around 34% and 36% at 3 days and 28 days, respectively due to the addition of 2% nano silica than their control HVS concrete containing 80% BFS and showed comparable compressive strengths to the OPC concrete at later ages.
- ❖ Addition of 3% nano silica in HVS-FA concrete containing combined fly ash and slag content of 67% improved the compressive strengths dramatically by 45% at 3 days compared to the control concrete with no nano silica and also exceeded the compressive strengths of OPC concrete at 28 days and exhibited significantly higher compressive strengths than control OPC concrete at later ages.
- ❖ The rate of water absorption of HVS concrete is reduced by around 27% and 36 % and of HVS-FA concrete by 38% and 37% after 28 and 90 days, respectively due to the addition of small amount of nano silica compared to their control concretes without nano silica. Sorptivity vales of HVS concrete containing 78% BFS were equivalent and HVS-FA concrete containing combined fly ash and slag content of 67% were superior to OPC concrete in both ages due to the addition of 2% and 3% nano silica, respectively.
- ❖ Extensive resistance against early shrinkage is showed by both HVS and HVS-FA concretes due to the addition of nano silica and the shrinkage in HVS-FA concrete was noticeably lower than the OPC concrete in the later ages as well. However, HVS

concrete containing 78% BFS did not performed well in later ages and showed similar shrinkage to OPC concrete.

- ❖ Volume of permeable voids of HVS concrete containing 78% BFS and 2% nano silica is reduced by 14% and 10% after 28 days and 90 days of curing, respectively than the control concrete without nano silica and exhibited lower VPV than OPC concrete after 90 days of curing. On the other hand, significant reduction of VPV by 23% after 28 days of curing is observed in HVS-FA concrete containing combined fly ash and slag content of 67% due to the inclusion of 3% NS than the control concrete containing 70% BFS-FA blend and displayed considerably lower than control OPC concrete in all ages.
- ❖ Tremendous resistance against chloride ion penetration is shown by both HVS and HVS-FA concretes with and without NS than the OPC concrete after 28 and 90 days of curing by lowering the passing charge to very low category of ASTM C1202 standard. Addition of 2% NS in HVS concrete containing 78% BFS accelerated the resistance by reducing passing charge through concrete samples by 47% after both 28 days and 90 days respectively than the control concrete. On the other hand, reduction was not much greater at 28 days for HVS-FA concrete containing 67% BFS-FA blend, however, a huge reduction of 35.5% observed at 90 days of age due to the inclusion of 3% nano-SiO<sub>2</sub>.
- ❖ Higher degree of dense ITZ observed in higher magnified micrographs of HVS and HVS-FA concrete due to the effects of NS on the interface and confirmation of new and additional C-S-H gel also witnessed from EDS spectrum collected in the ITZ of concrete mixes.

## 6.5 References

- Aghaeipour, A., & Madhkhan, M. (2017). Effect of ground granulated blast furnace slag (GGBFS) on RCCP durability. *Construction and Building Materials*, *141*, 533-541.
- Arefi, M. R., Javaheri, M. R., Mollaahmadi, E., Zare, H., Abdollahi, B., & Eskandari, M. (2011). Silica nanoparticle size effect on mechanical properties and microstructure of cement mortar. *Journal of American Science*, *7*, 231-238.
- ASTM. (2013a). Standard Test Method for Density, Absorption, and Voids in Hardened Concrete. In.
- ASTM. (2013b). Standard Test Method for Measurement of Rate of Absorption of Water by Hydraulic Cement Concretes. In.
- ASTM. (2015). Standard Test Method for Compressive Strength of Concrete Cylinders Cast in Place in Cylindrical Molds. In.
- ASTM. (2017). Standard Test Method for Length Change of Hardened Hydraulic-Cement Mortar and Concrete. In.
- ASTM. (2019). Standard Test Method for Electrical Indication of Concrete, 2019;s Ability to Resist Chloride Ion Penetration. In.
- Choi, Y. C., Kim, J., & Choi, S. (2017). Mercury intrusion porosimetry characterization of micropore structures of high-strength cement pastes incorporating high volume ground granulated blast-furnace slag. *Construction and Building Materials*, *137*, 96-103.
- Demirboğa, R., Türkmen, İ., & Karakoç, M. B. (2004). Relationship between ultrasonic velocity and compressive strength for high-volume mineral-admixed concrete. *Cement and Concrete Research*, *34*(12), 2329-2336.
- Duran Atış, C., & Bilim, C. (2007). Wet and dry cured compressive strength of concrete containing ground granulated blast-furnace slag. *Building and Environment*, *42*(8), 3060-3065.
- Elchalakani, M., Aly, T., & Abu-Aisheh, E. (2014). Sustainable concrete with high volume GGBFS to build Masdar City in the UAE. *Case Studies in Construction Materials*, *1*, 10-24.
- Elkady, H., Serag, M., & Elfeky, M. (2013). Effect of Nano Silica De-agglomeration, and Methods of Adding Super-plasticizer on the Compressive Strength, and Workability of Nano Silica Concrete. *Civil and Environmental Research*, *3*, 2222-2863.

- Güneyisi, E., & Gesoğlu, M. (2008). A study on durability properties of high-performance concretes incorporating high replacement levels of slag. *Materials and Structures*, 41(3), 479-493.
- Hill, J., & Sharp, J. H. (2002). The mineralogy and microstructure of three composite cements with high replacement levels. *Cement and Concrete Composites*, 24(2), 191-199.
- Jeong, Y., Park, H., Jun, Y., Jeong, J.-H., & Oh, J. E. (2015). Microstructural verification of the strength performance of ternary blended cement systems with high volumes of fly ash and GGBFS. *Construction and Building Materials*, 95, 96-107.
- Kuder, K., Lehman, D., Berman, J., Hannesson, G., & Shogren, R. (2012). Mechanical properties of self consolidating concrete blended with high volumes of fly ash and slag. *Construction and Building Materials*, 34, 285-295.
- Oner, A., & Akyuz, S. (2007). An experimental study on optimum usage of GGBS for the compressive strength of concrete. *Cement and Concrete Composites*, 29(6), 505-514.
- Tharakan, J. L. P., Macdonald, D., & Liang, X. (2013). Technological, economic and financial prospects of carbon dioxide capture in the cement industry. . *Energy Policy*, 61, 1377-1387.
- Wainwright, P. J., & Rey, N. (2000). The influence of ground granulated blastfurnace slag (GGBS) additions and time delay on the bleeding of concrete. *Cement and Concrete Composites*, 22(4), 253-257.

*All reasonable efforts have been made to acknowledge the authors of the copyright material. It would be highly appreciated if I can hear from any authors has been ignored or incorrectly acknowledged.*

## **Chapter 7: Mechanical and durability properties of HVS and HVS-FA concretes containing nano calcium carbonate**

---

This chapter evaluates the compressive strengths of high volume slag (HVS) and high volume slag-fly ash (HVS-FA) blended concretes containing optimum content of nano calcium carbonate (NC) at early age and later ages. This chapter also presents the effect of small amount of NC addition on the durability properties such as sorptivity, volume of permeable voids, drying shrinkage, rapid chloride permeability of HVS and HVS-FA concrete. In addition, microstructural analysis of interfacial transition zone of HVS and HVS-FA concrete through scanning electron microscopy (SEM) images and energy-dispersive X-ray spectroscopy (EDS) are demonstrated in this chapter.

### **7.1 Overview**

Concrete is the key part of rapid progress of the modern world and Ordinary Portland cement (OPC) is the unavoidable binding materials using in the concrete production. Study projected an approximate 115-180% increase of cement demand in 2020 compared to 1990s and may climbed to 400% by 2050 (Damtoft et al., 2008). However, every tonne of cement manufacture consumes around 1.5 tonne of raw materials and releases roughly 0.9 tonne of carbon di-oxide (CO<sub>2</sub>) which is almost 7% of the total emission of CO<sub>2</sub> into the atmosphere (Benhelal et al., 2013; Malhotra, 2002; Mehta, 2001;). A number of researches have been conducted to reduce the use of cement in large volume (>50%) in concrete and replace it with other cementitious materials such as blast furnace slag (BFS), fly ash (FA), rice husk ash (RHA), silica fume (SF), metakaolin etc. to produce sustainable concrete with low carbon emission and cost.

---

The content of this chapter has been written based on the results under review in the following journal.

Hosan, A. and F.U.A. Shaikh, Compressive strength development and durability properties of high volume slag and slag-fly ash blended concretes containing nano-CaCO<sub>3</sub>. *Journal of Materials Research and Technology*. <https://doi.org/10.1016/j.jmrt.2021.01.001>

Duran and Bilim (2007) found that wet cured compressive strengths of 60 % BFS replaced concretes equivalent to that of control OPC concrete at 28 days. However, Güneyisi and Gesoğlu (2008) reported a systematic decrease in compressive and splitting tensile strengths with the increase in slag content for the early age. However, the strengths increased with slag replacement up to 60% for 90 days wet cured specimens. Similarly, Oner and Akyuz (2007) observed lower early ages strengths of high volume BFS concrete than the control mixtures. However, the strengths increased with the curing period and exceeds the control after one year of curing. Moreover, it has noted that compressive strengths were maximum when slag addition was around 55% of that total binder content. Moreover, Wainwright and Rey (2000) demonstrated that the 55% slag addition amplified the bleed capacity by 30% with compared to plain OPC concrete. Aghaeipour and Madhkhan (2017) found that concrete mix designs containing 60% slag led to enhanced penetration depth thus moisture content increased. On the other hand, few researched examined properties of slag-fly ash blended concrete and reported very low early strengths, increased initial and final setting time and notable drying shrinkage due to sluggish pozzolanic reaction of slag and fly ash (Demirboğa et al., 2004; Gesoğlu & Özbay, 2007; Kuder et al., 2012).

It is reported that addition of 10% nano-CaCO<sub>3</sub> as partial cement replacement along with 50% fly ash enhanced the hydration of cement and hydration was superior with the higher amount of addition of nano-CaCO<sub>3</sub> (Sato & Beaudoin, 2011). Moreover, significant improvement of early age micro-hardness and modulus of elasticity found in that study due to the addition of nano-CaCO<sub>3</sub>. In another study, (Kawashima et al., 2013) it was summarised that 5% nano-CaCO<sub>3</sub> addition accelerate the rate of hydration of the 50% fly ash replaced cement pastes and helped to accelerate the initial and final setting times and showed similar settings time of OPC pastes when nano-CaCO<sub>3</sub> mixed by sonication process. In a recent investigation, (Meng et al., 2017) it is demonstrated that the addition of nano-CaCO<sub>3</sub> slurry improved the early age compressive strength of concrete with and without fly ash significantly due to the enhanced hydration of cement from seeding effect and hence compact microstructure formed. In addition, it has reported 1% replacement of FA by nano-CaCO<sub>3</sub> in a 60% FA containing mortars improved compressive strengths by 100% and 111% at ages 7 days and 28 days compared with 60%FA mortars without nano addition (Supit & Shaikh, 2014) and revealed more pronounced effect of nano-CaCO<sub>3</sub> on the early age compressive strengths than 28 days compressive strengths. Compressive strengths of concrete containing 39% fly ash improved by about 44-46% due to the addition of 1% nano-CaCO<sub>3</sub> at their early ages compared to the control concrete

without nano-CaCO<sub>3</sub>. However, no significant improvement observed in case of concrete containing 59% FA with the inclusion of 1% nano-CaCO<sub>3</sub>. Moreover, it is also found that 1% addition of nano-CaCO<sub>3</sub> in high volume fly ash (HVFA) concrete containing 59% FA reduced the water sorptivity by 19% and 60% than ordinary concrete at 28 days and 90 days respectively due to the formation of CSH gel (Shaikh & Supit, 2014a). This study also reported 7% and 21% reduction of the volume of permeable voids at 28 and 90 days curing respectively, and the chloride ion permeability resistance of concretes increased with inclusion of 1% nano-CaCO<sub>3</sub> which was about 11% and 8% reduction of charge passed at ages of 28 days and 90 days. The chloride diffusion of HVFA concrete containing 59% FA and 1% nano-CaCO<sub>3</sub> were 32% lower than that of HVFA concrete without nano-CaCO<sub>3</sub> (Shaikh & Supit, 2015). While the above scientific research showed that addition of nano-CaCO<sub>3</sub> can improve the early age strengths, reduce setting time and drying shrinkage and improve durability properties of cementitious composites, there is no such study found of the effect of nano-CaCO<sub>3</sub> on the high volume slag (HVS) and high volume slag-fly ash (HVS-FA) composites. Therefore, this study aims to investigate the effect of nano-CaCO<sub>3</sub> on the compressive strengths at early age and later ages and durability properties such as sorptivity, volume of permeable voids (VPV), rapid chloride permeability test (RCPT) and drying shrinkage of the HVS and HVS-FA concretes.

## **7.2 Outline of the Experiments**

### **7.2.1 Materials**

Ordinary Portland Cement Type I (OPC) used in this study was purchased from a local cement company. The blast furnace slag (BFS) was supplied by BGC cement, Western Australia and class F fly ash (FA) was provided by Eraring power station, NSW, Australia. All coarse and fine aggregate used in this study bought from local supplier ensuring the ASTM C127 standard quality. Aggregates were soaked for at least 24 hours to achieve saturated and surface dry (SSD) condition. Dry nano-CaCO<sub>3</sub> (NC) with an average particle size of 15-40nm, 40 m<sup>2</sup>/g of specific surface areas and 97.8% calcite content was purchased from Nanostructured and Amorphous Materials, Inc. of USA. Tap water from concrete laboratory used in all mixes and a naphthalene sulphonate based superplasticizer used to maintain the workability by measuring slump for all mixes as high volume replacement of slag and slag-fly ash blend used in this experiment. Physical and chemical properties of all cementitious materials are given in the **Table 4.1** and **Figs. 4.1-4.2** shows the X-ray diffraction (XRD) analysis of cement, BFS, FA and NC. It is clear that NC was less amorphous than BFS and FA by comparing the results.

However, among both supplementary cementitious materials (SCM), the BFS is more amorphous with amorphous content of 97.5% compared to 67.8 % amorphous content of FA based on the quantitative XRD results.

### 7.2.2 Mix proportions

All the concrete mixes were designed with a total binder quantity of 400 kg/m<sup>3</sup> and a constant water/binder ratio of 0.4. However, superplasticizer used when needed to maintain the concrete mixes workable with a target slump of 100-120 mm. Coarse and fine aggregates mass and ratios were kept constant for all mixes. **Table 7.1** shows the mix proportions of all control and mixes with supplementary cementitious materials with and without nano-CaCO<sub>3</sub>. A designated ID was given for each mix considering binder name and amount present on the mixes. For example, 70BFS means a mix containing 70% BFS and 30% OPC of total binder.

**Table 7.1** Mixing proportions of different concrete mixes (Kg/m<sup>3</sup>)

Mix ID	Binding Materials			Nano CaCO <sub>3</sub>	Aggregates			Water	Super plasticizers	Slump (mm)
	Cement	Slag	Fly ash		Sand	20 mm	10 mm			
OPC	400	-	-	-	684	789	395	163	-	120
70BFS	120	280	-	-	684	789	395	163	2.20	110
69BFS.1NC	120	276	-	4	684	789	395	163	2.40	113
70BFS-FA	120	196	84	-	684	789	395	163	1.15	125
69BFS-FA.1NC	120	194	82	4	684	789	395	163	1.95	120

### 7.2.3 Sample preparation

Concrete mixes were prepared in a pan mixer at ambient temperature. Firstly, all the dry ingredients such as cement, coarse aggregates, fine aggregates and SCM's (in case of HVS and HVS-FA mixes) were mixed for 4-5 minutes considering high amount of aggregates and volume of concrete. Next, water was added and again mixed for around 2-3 minutes until a homogenous mix was reached. In addition, mix containing NC were prepared by dry NC powder were mixed with partial water and superplasticizers required for the concrete mixes. That mix was then dispersed ultrasonically by an ultrasonic mixer shown in **Fig. 4.3** with 100% amplitude and maximum cycle for 45 minutes (Hosan & Shaikh, 2020). For mixes containing NC, the prepared NC solution was added into the dry mix followed by addition of the remaining water and mixed for about 2-3 minutes. Slump test was performed for each mix to ensure slump values of 100-120mm. For concrete with slump values lower than this range additional superplasticizer was added to achieve the above slump range.



Standard cylindrical samples with diameter of 100 mm and height of 200 mm were cast for compressive strengths and durability such as sorptivity, volume of permeable voids and rapid chloride permeability test based on ASTM standards. A prismatic 75 mm square cross-sectional and 285 mm long concrete samples with gauge studs at both ends ensuring gauge lengths of 250 mm were also cast for drying shrinkage test according to ASTM standards. All the specimens were mixed in a vibrating table with three layers for cylindrical samples and two layers for shrinkage samples according to standards. All the test samples were demoulded after 24 hours and cylindrical samples were then cured in lime saturated water at room temperature. For durability test such as sorptivity, VPV and RCPT, a 50 mm discs were cut from the cylindrical samples at 28 and 90 days of concrete age and then test were performed according to their standards. Shrinkage moulds were cured in lime saturated water first part of curing and then placed in a room with controlled relative humidity of 50% and at a temperature of 23°C and then readings were taken at 7, 14, 28, 35, 56, 91, 120, 150, 180, 270, 330 and 365 days of concrete age. To investigate the microstructural modifications of different concrete mixes due to the addition of NC, a small portion of concrete with an interfacial transition zone (ITZ) were cut from each mixes by using a diamond precision saw and dried by naturally to make sure it is free from moisture.

#### ***7.2.4 Testing methods***

Compressive strengths were measured in MATEST testing apparatus according to ASTM C873 (2015) standard with a loading rate of 0.33 MPa/s until failure at 3, 7, 28, 56, 90 and 180 days of concrete age of all mixes. Diameters of the cylinders were measured and sulphur capped at least 4 hours prior to the test. Compressive strengths were calculated as the maximum crushing load divided by the average cross-sectional area of the specimens. For each test age, at least three samples were tested and average value of three were reported in this study.

The rate of water absorption (sorptivity) of all concrete mixes were investigated after 28 and 90 days of water curing. At least two samples of each concrete mixes were prepared and tested according to the ASTM C1585 to determine the rate of water absorption by measuring the mass of concrete specimens regularly from 1 min to 6 hours and absorption (I) was calculated by change in mass divided by cross sectional area of the specimens and the density of water.

Volume of permeable voids of 100 mm diameter and 50 mm thick samples of all concrete mixes were measured at 28 and 90 days of concrete age according to ASTM C642(2013a) standards. These tests were conducted to determine the voids present in the concrete specimens and is measured by boiling the 50 mm cut concrete discs from different part of concrete cylinders at 105°C in a water bath for at least 5 hours and then weighing the samples in water. Initial weight of oven dried samples and after at least 24 hours of immersion in water were measured and at least three samples were used for each concrete mix for this test.

To determine the concrete performance against the entrance of chloride ion is known as the rapid chloride permeability test (RCPT). At least three 50 mm discs from each concrete mixes after 28 and 90 days of curing period were prepared by coating them with a sealer materials and then vacuum conditioning with a desiccator for at least 5 hours according to the ASTM C1202(2019) standard. Samples were then placed under water and afterwards exposed to a constant 60 voltage for 6 hours on the cells in which one cell was filled with 3% NaCl solution and another cell was filled with 0.3N NaOH solution. The total charge passed through the concrete samples were collected by using a Perma2 testing apparatus and average values are stated in this study.

Drying shrinkage test was performed according to ASTM C157(2017) standard. Lengths of the samples were measured at 7, 14, 28, 35, 56, 91, 120, 150, 180, 270, 330 and 365 days of concrete age in the curing room with controlled humidity and temperature. At least three samples were cast and all the specimens were measured at the same time for each concrete. Shrinkage strain was calculated as the difference between initial and measured length (length change) divided by the gauge length (250 mm) according to standard and average of three samples obtained.

Microstructural investigation of different HVS and HVS-FA concrete with and without NS addition were performed by using MIRA3 TESCAN, a variable pressure field emission scanning electron microscope (VP-FESEM) equipped with backscattered electron (BSE) detector and energy-dispersive X-ray spectroscopy (EDS) analyser to collect SEM images along with EDS spectrum to analyse the phases. The samples were prepared by taking a small portion of dried concrete samples after 28 days of wet curing and placed them in a vacuum desiccator for minimum three days to remove all the moisture from the samples. Samples were then drenched in an epoxy resin mount, polished and then 20 mm thick carbon coat has been applied to reduce the chances of getting charged during image and spectrum collection. The

SEM and EDS were carried out at a constant accelerating voltage of 15kV and around 15 mm of working distance by using BSE detectors for all concrete samples. SEM images and EDS spectrums were collected in ITZ to investigate the porosity and bonding between the binder and aggregate.

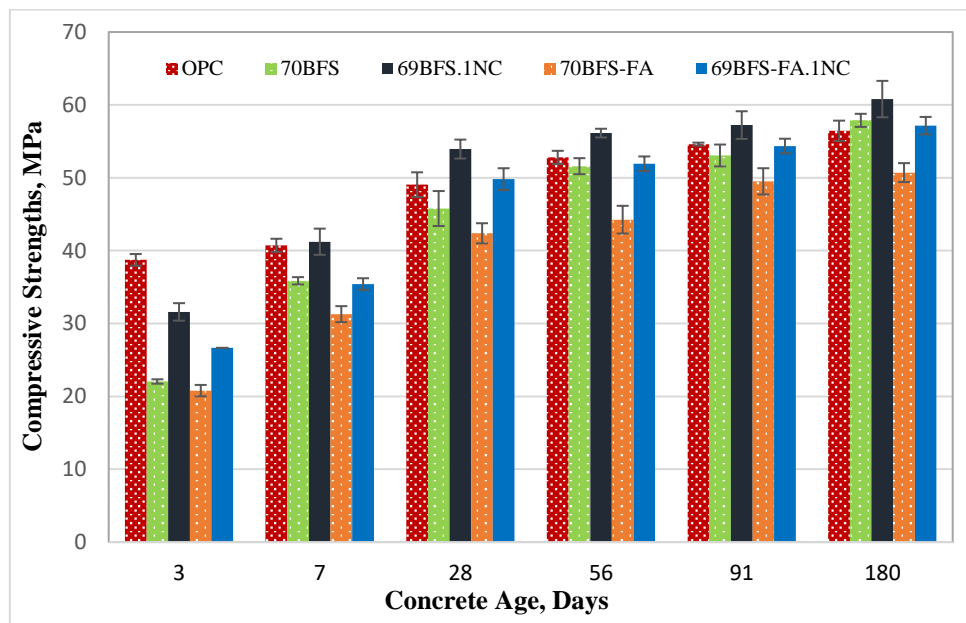


**Fig. 7.1** Average compressive strengths of different types concretes with and without NC at various ages of concrete

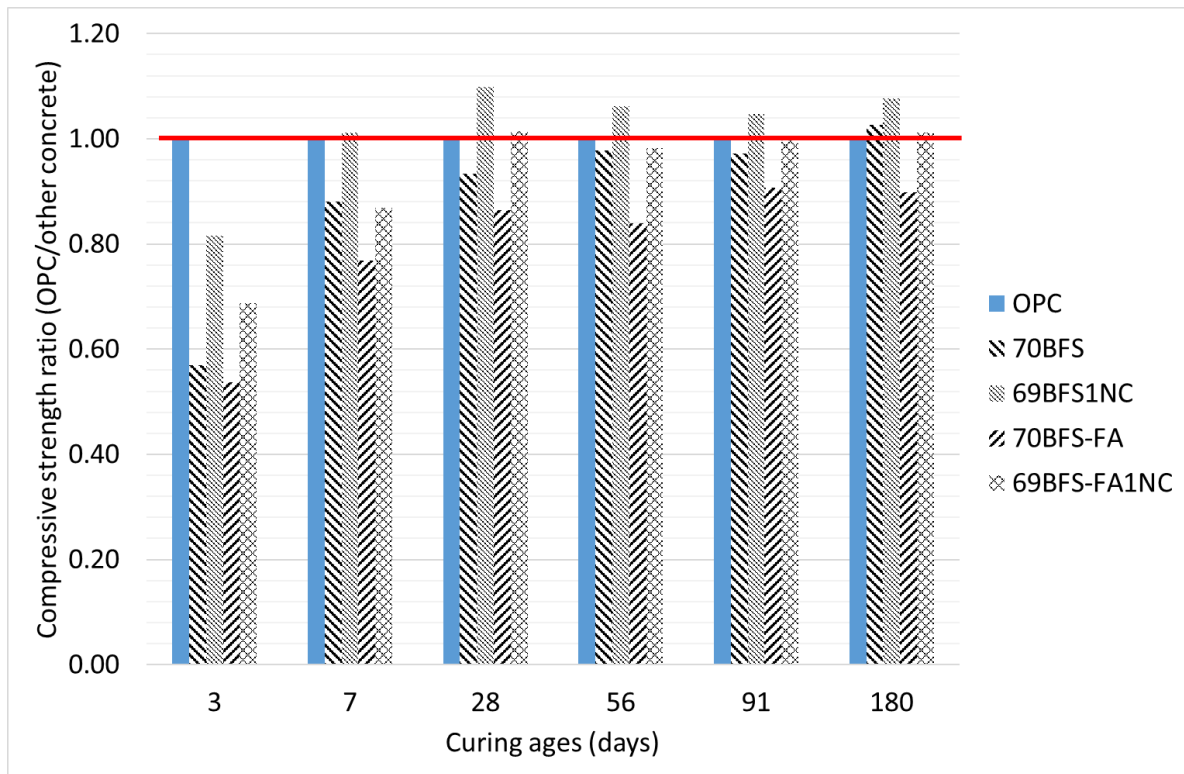


**Fig. 7.2** Benchmarking of compressive strength of HVS and HVS-FA concretes with control OPC concrete

## 7.3 Results and discussions

### 7.3.1 Compressive strengths

Average compressive strengths of control OPC concrete and concretes containing 70% BFS and combined BFS-FA blend of 70% with and without NC at the age of 3, 7, 28, 56, 90 and 180 days are shown in **Fig. 7.1**. It can be seen in the figure that the early age (3 and 7 days) compressive strength of HVS and HVS-FA concretes is very low compared to control OPC concrete and presented an increasing trend at later ages due to the slow pozzolanic reaction at early ages and then prompted at later ages of high volume BFS and FA present in those mixes also noted in previous studies (Elachalakani et al., 2014; Duran & Bilim, 2007; Güneysi & Gesoğlu, 2008). It is also interesting to see in the figure that the rate of increase in compressive strength of HVS concrete containing 70% BFS is much higher than that containing combined BFS-FA content 70%. The higher amount of CaO presents in BFS and its higher amorphous content than that of FA could be the reason for such improvement rate. It can also be noticed that the addition of 1% NC improved the early age compressive strengths significantly

compared to their control concretes without NC an indication of enhanced hydration of cementitious materials facilitated by the faster pozzolanic reaction by NC. However, these values are still lower than the 3 days compressive strength of control OPC concrete. Interestingly, the HVS concrete containing 69% BFS and 1% NC exhibits comparable compressive strength to the OPC concrete at 7 days (see **Fig. 7.1**). This trend continues with higher compressive strength than control OPC concrete up to 6 months. It is also interesting to see that the improvement in the compressive strength of HVS-FA concrete containing 69% of BFS-FA due to addition of NC is slightly lower than the HVS concrete containing 69% BFS in early ages and exhibited higher improvement in later ages due to the presence of FA in that mix and it reached the compressive strength of control OPC concrete at all ages. Nevertheless, both HVS and HVS-FA concretes showed higher compressive strength at later ages (28 days onwards) when benchmarked with the control OPC concrete. A very useful utilization of industrial by-products in a very high volume replacement of OPC in concrete with 54% reduced carbon footprint than the control (Shaikh & Supit, 2015).

**Fig. 7.3** presents the percentage improvement in compressive strengths of HVS and HVS-FA concretes due to the addition of 1% NC compared to their control concretes without NC at all ages. It can be seen that the compressive strengths of HVS concrete containing 69% BFS is increased significantly by 43% at 3 days and 15% at 7 days due to the addition of 1% NC. However, the improvement in HVS-FA concrete containing combined BFS-FA content of 69% at early ages is not as great as HVS concrete containing 69% BFS but showed about 10-18% improvement in compressive strength from 28 days onwards. The significant increase in compressive strength of HVS and HVS-FA concretes at 3 days can be attributed to the faster pozzolanic reaction of  $\text{CaCO}_3$  nano particles with  $\text{SiO}_2$  and  $\text{Al}_2\text{O}_3$  of BFS and FA which produced additional C-S-H and C-A-H (calcium aluminate hydrate) in the matrix also showed in similar studies of high volume slag and slag-fly ash blended composites (Hosan & Shaikh, 2020; Balcikanli et al., 2020). This has helped in reducing the porosity and densifying the matrix together with the pore filling effect of NC. The overall higher improvement in compressive strength of HVS concrete compared to HVS-FA concrete due to addition 1% NC at early ages (e.g. 3 and 7 days) can be attributed to the higher amount of CaO in BFS (about 41.2% see Table 1), which has resulted in higher amount of C-S-H in the matrix and in the presence of  $\text{CaCO}_3$  nano particles the total ratio of Ca/Si is increased which is reflected in the EDS analysis of the matrix in the ITZ to be discussed in the microstructural analysis section. It is also interesting to see that the concrete containing same amount of combined BFS-FA

showed better improvement in compressive strength development at later ages (e.g. >56 days) than that containing the same amount of BFS and equal amount of CaCO<sub>3</sub> nano particles. This can be attributed to the slow pozzolanic reaction of FA particles than that of BFS. Slow development of compressive strength and other properties of concrete containing FA is reported by numerous researchers (Güneyisi & Gesoğlu, 2008; Gesoğlu & Özbay, 2007; Kuder et al., 2012).

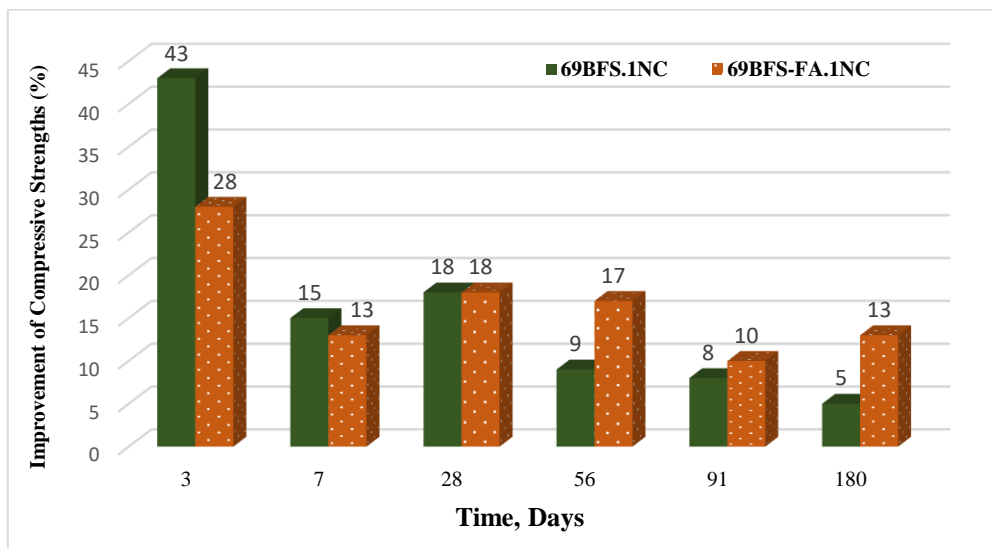
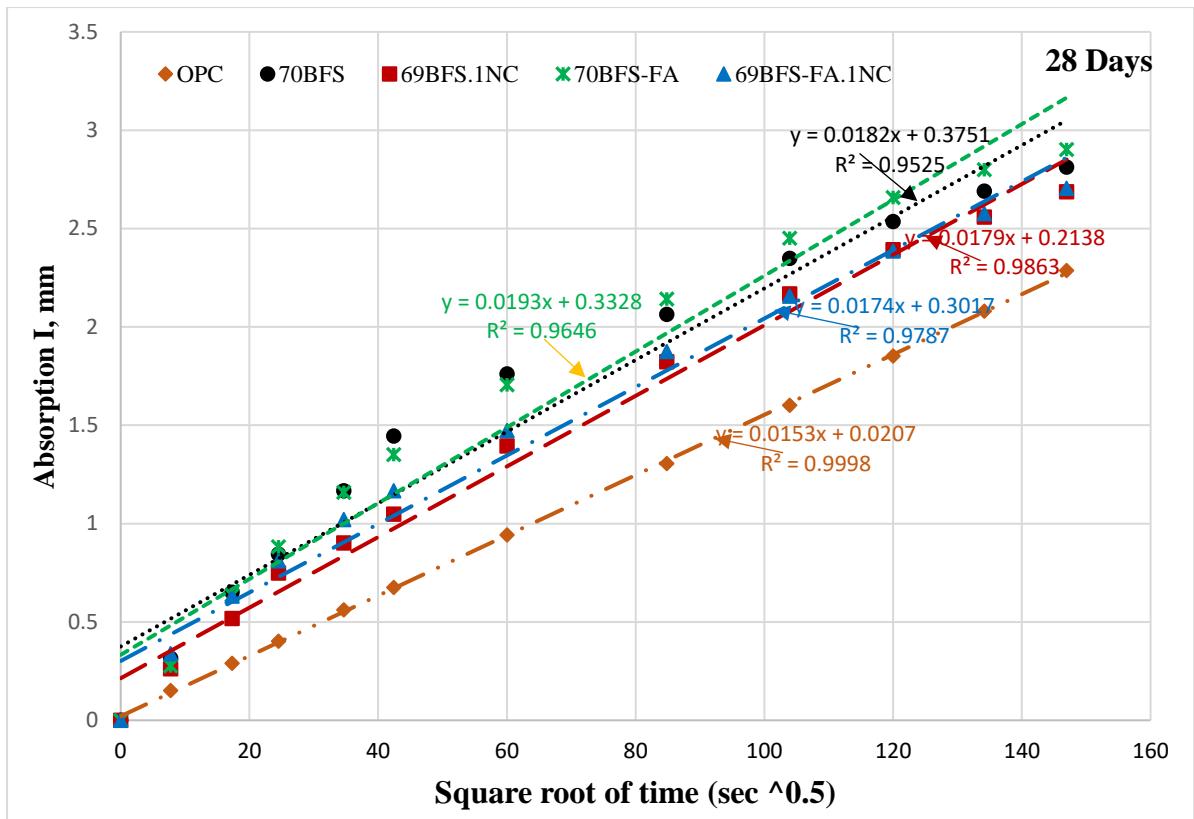
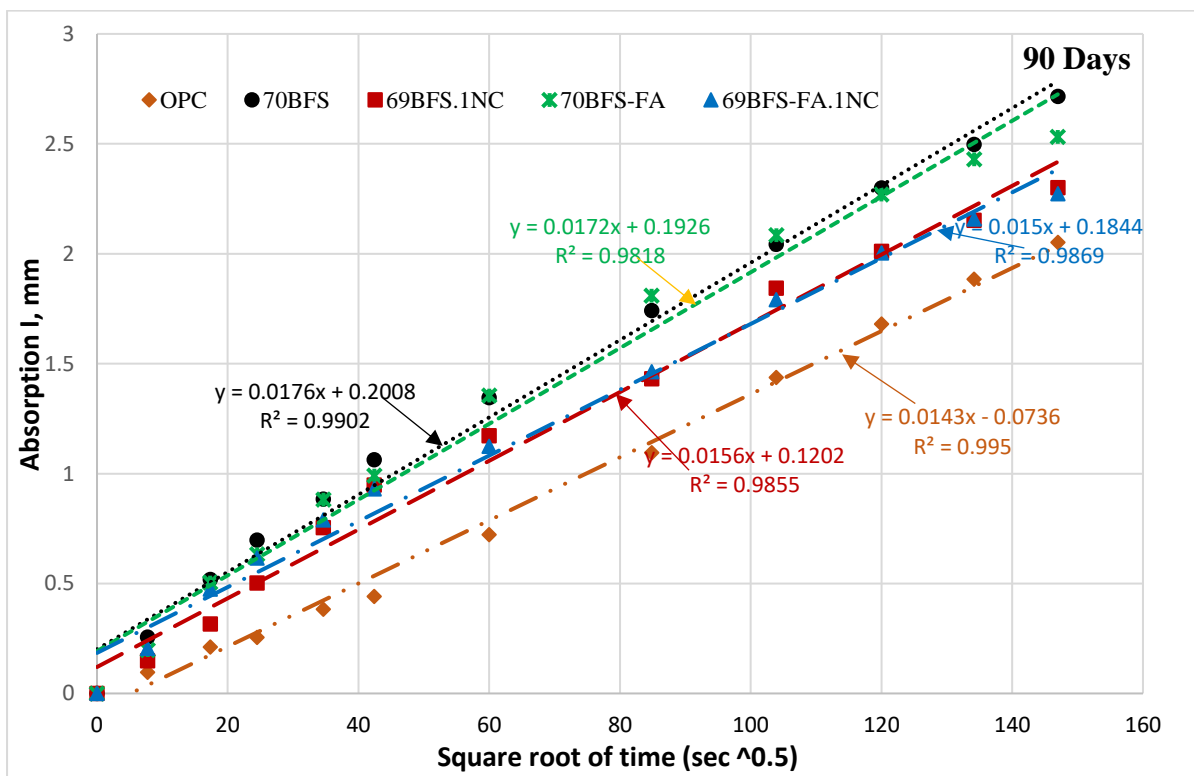


**Fig. 7.3** Improvement of compressive strengths of HVS and HVS-FA concretes containing 1% NC.



a)



b)

**Fig. 7.4** Water absorption of different type concrete with and without NC at a) 28 and b) 90 days of age.

### 7.3.2 Durability properties

**Fig. 7.4** shows the rate of water absorption of control OPC concrete, HVS and HVS-FA concretes with and without NC after 28 and 90 days of curing. The best-fit straight lines of all concrete mixes are also shown in the same figures where it can be seen that the  $R^2$  values of most of the best fit lines are greater than 0.98. The results show that the inclusion of 1% NC reduced the rate of water absorption of both HVS and HVS-FA concretes at both ages. The reduction between the HVS and HVS-FA concretes containing NC with their respective control concretes is much greater after 90 days of curing. However, the reduction is slightly higher in HVS-FA concrete than HVS concrete due to the addition of NC. The slope of the best fit lines represent the sorptivity of the concrete and is shown in **Fig. 7.5** for all concrete mixes. It can also be seen in Fig. 7 that the sorptivity values ( $10^{-4}$  mm/sec<sup>1/2</sup>) of HVS concrete containing 1% NC are 179 at 28 days and reduced to 156 at 90 days of age which is very close to the control OPC concrete. In case of HVS-FA concrete containing 1% NC, the sorptivity values ( $10^{-4}$  mm/sec<sup>1/2</sup>) are 174 and 150 at 28 days and 90 days, respectively and also very close to the sorptivity values of control OPC concrete. It can also be seen that curing period also effected the rate of water absorption of the HVS and HVS-FA concretes containing NC than the control OPC, HVS and HVS-FA concretes without NC. The formation of additional hydration products due to pozzolanic reaction of NC, BFS and FA with cement hydration products e.g. CH and pore filling by CaCO<sub>3</sub> nano particles might have resulted in reduced porosity of the matrix.

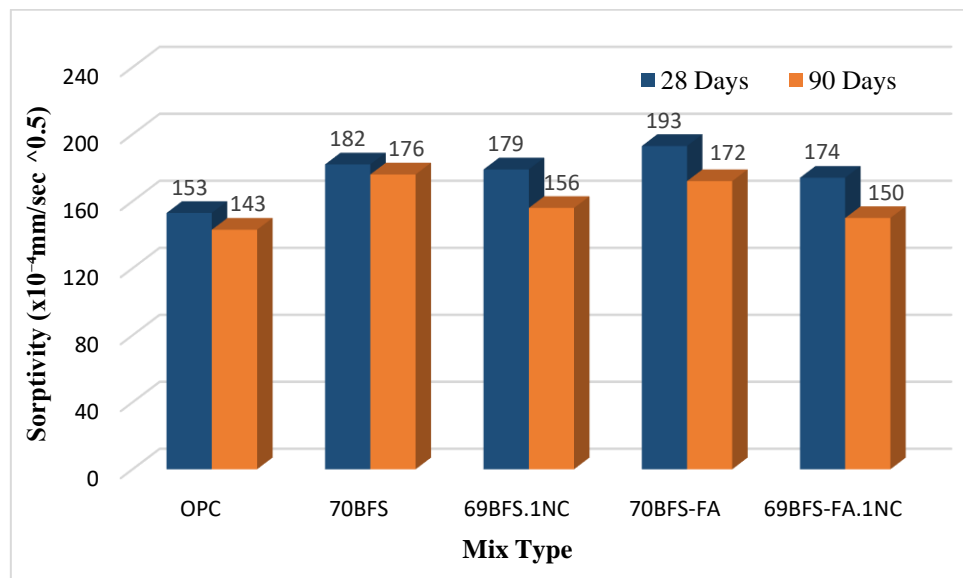


**Fig. 7.5** Sorptivity of different concrete mixes at 28 and 90 days.



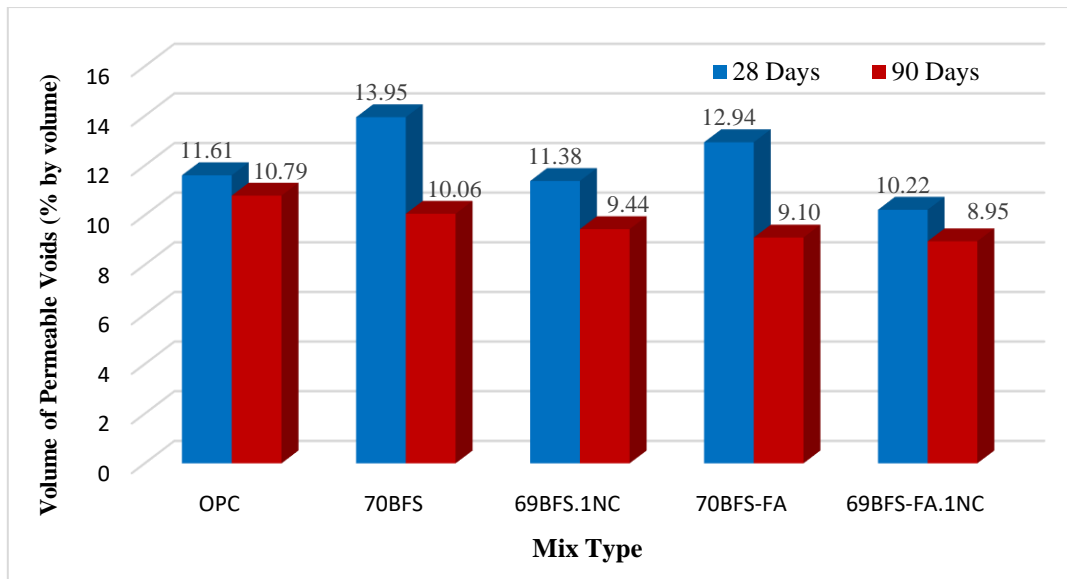


**Fig. 7.6** Average volume of permeable voids of concrete mixes with and without NC at 28 and 90 days.

Volume of permeable voids of different concrete mixes with and without NC after 28 and 90 days of wet curing are shown in **Fig. 7.6**. It can be seen that the HVS and HVS-FA concretes exhibited higher volume of permeable voids than the control OPC concrete at 28 days of curing as found in other previous research studies discussed earlier. However, after 90 days of curing the permeable voids in both mixes is decreased even below the control OPC concrete and the reduction is high in HVS-FA mix. This can be attributed to the formation of more additional hydration products due to pozzolanic reaction of BFS and FA with the cement hydration products. The beneficial effect of nano- $\text{CaCO}_3$  on the reduction of VPV of HVS and HVS-FA concretes is also evident in the same figure. It can be seen that the addition of 1% nano- $\text{CaCO}_3$  in both mixes reduced the VPV significantly by 18% and 21% than their control concretes without nano- $\text{CaCO}_3$  at 28 days of concrete age and shows slightly lower VPV than the control OPC concrete which is consistent with the strengths results of those concrete mixes. However, VPV reduction for both mixes is not great at 90 days, as just about 6% and 1% VPV is reduced at 90 days than the control HVS and HVS-FA concretes without nano- $\text{CaCO}_3$ . It can be seen that there is an inconsistency of the sorptivity and VPV values of HVS and HVS-FA concrete after 90 days curing with and without NC inclusion. It could be the reason of using two 50 mm concrete discs from the top part of the concrete cylinder for sorptivity test while four different 50 mm discs from top and bottom part of the concrete cylinder used for AVPV

test which resulted the average VPV values slightly lower due to the higher compactness of concrete on the bottom part of the concrete cylinders.

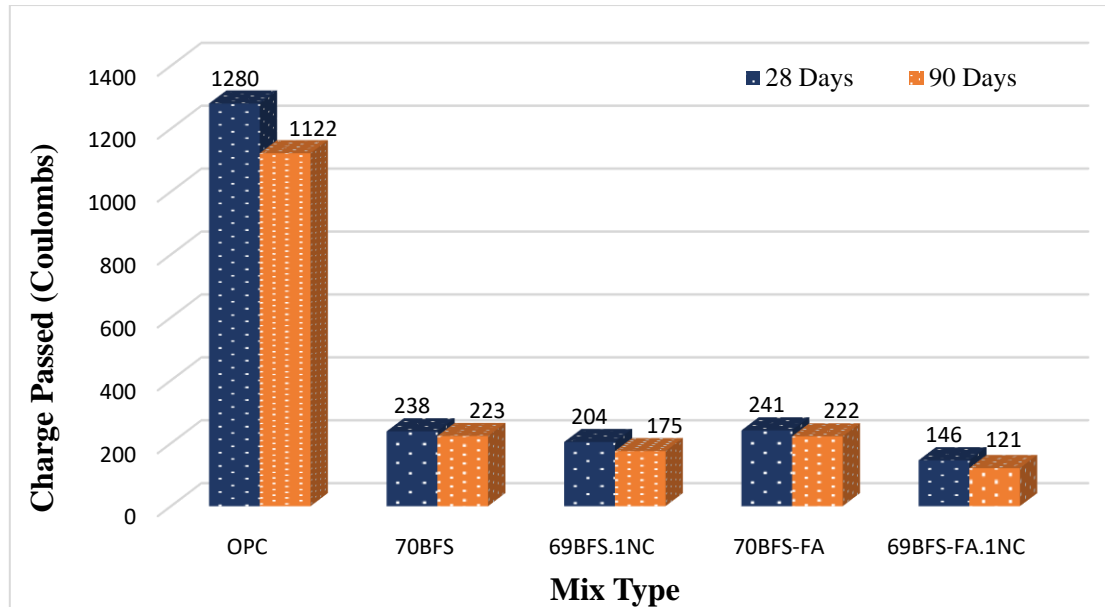


**Fig. 7.7** Chloride ion penetration of different concretes with and without NC at 28 and 90 days.

**Fig. 7.7** shows the chloride ion penetration of different concrete mixes with and without nano- $\text{CaCO}_3$  at 28 days and 90 days. It can be seen that the HVS and HVS-FA concretes with or without nano- $\text{CaCO}_3$  showed outstanding resistance against penetration of chloride ion at both ages which is classified as very low level of chloride ion permeability according to ASTM C1202 standard and similar trend also found in another study (Elachalalani et al., 2014). It can also be seen that the addition of 1% nano- $\text{CaCO}_3$  also reduced the penetration of chloride ion and is more prominent in HVS-FA concrete in both ages, where about 39% and 45% reduction of chloride ion penetration at 28 and 90 days is observed. However, no such significant reduction observed in HVS concrete containing 70% BFS, where about 14% and 22% reduction at 28 days and 90 days, respectively is observed due to the addition of nano- $\text{CaCO}_3$ . Nevertheless, both HVS and HVS-FA concretes exhibited reduction in chloride ion penetration due to addition of 1% nano- $\text{CaCO}_3$  and exhibit very low level of chloride ion permeability. The lower charge passed through the concrete specimens is an indirect indication of denser microstructure of the matrix and the ITZ in those HVS and HVS-FA concretes.

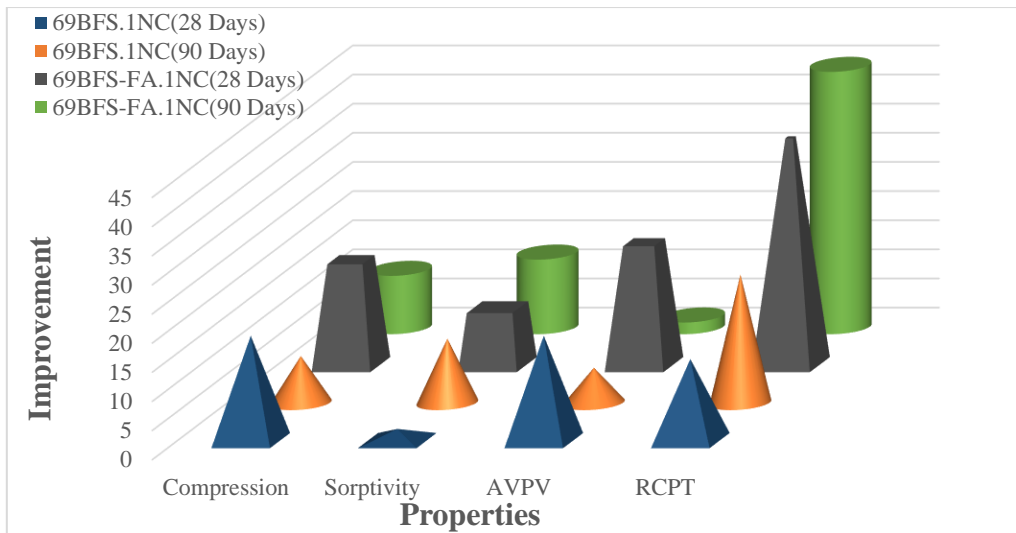


**Fig. 7.8** Improvement comparison of different properties due to NC addition

**Fig. 7.8** presents a comparison of improvement of different properties due to the addition of 1%NC into HVS and HVS-FA concretes after 28 days and 90 days of curing. It is clear that improvement rates were higher in HVS-FA concrete than HVS concrete due to the inclusion of 1% NC despite the fact that HVS concrete showed almost similar or even better performance than control OPC concrete without the addition of NC except very age (3 days and 7 days). However, addition of NC minimised those shortcomings of HVS concrete and also accelerated the hydration process throughout the whole period of curing.

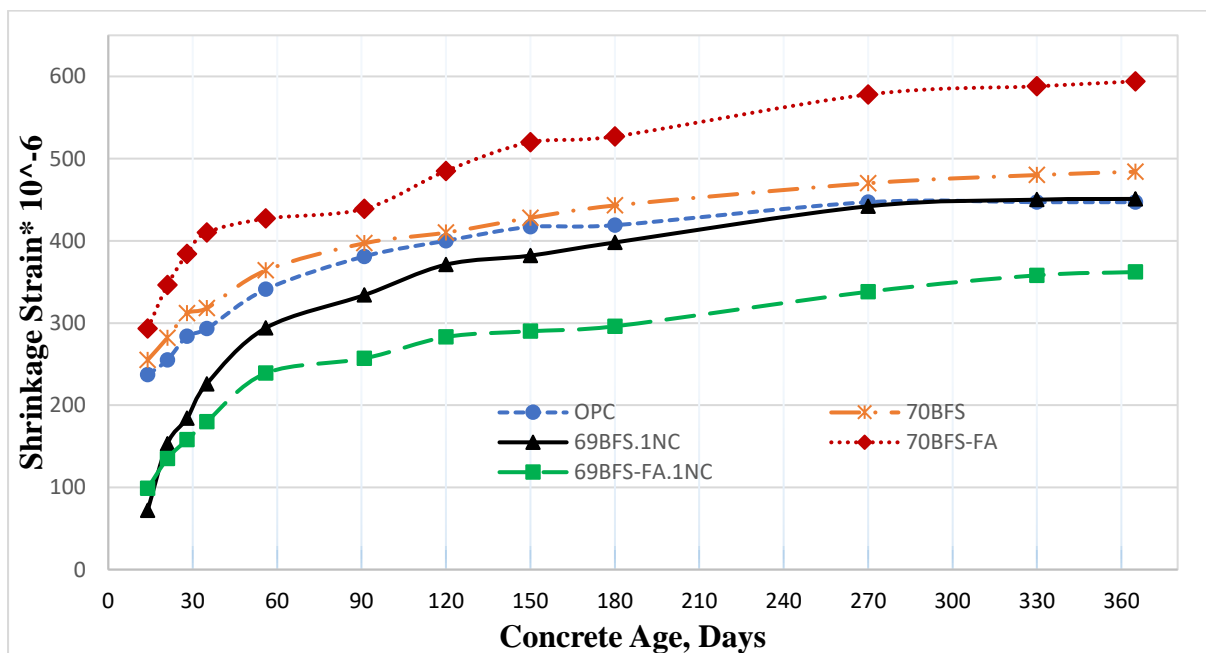


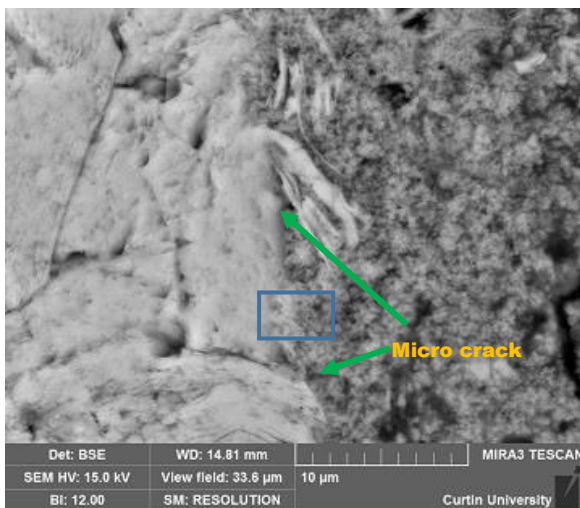
**Fig. 7.9** Drying shrinkage strain of control OPC, HVS and HVS-FA with and without NC at various ages of concrete mixes.

Drying shrinkage of concrete and cement based materials is an important durability property as excessive shrinkage cause cracking of cement matrix and ITZ around aggregates. Measured shrinkage strains ( $10^{-6}$ ) of control OPC concrete, HVS and HVS-FA concrete mixes with and without nano- $\text{CaCO}_3$  addition over one year are presented in **Fig. 7.9**. It can be seen that contrary to the previous study (Zhao et al., 2017) HVS-FA concrete without nano- $\text{CaCO}_3$  exhibited higher shrinkage strain than the control OPC concrete at any age could be the reason of higher volume of slag (49% by wt.) presence in the mix than the volume of FA (21% by wt.) where higher slag volume governed the initial hydration. However, HVS concrete containing 70% BFS showed almost similar shrinkage to the control concrete until 180 days and slightly higher shrinkage in later ages than the control OPC concrete showed consistency to the past studies (Aly & Sanjayan, 2008 & Won, 2013) due to the higher volume of slag. The beneficial effect of nano- $\text{CaCO}_3$  inclusion in HVS and HVS-FA concretes can also be seen in the same figure. It can be seen that 1% nano- $\text{CaCO}_3$  addition reduced the early drying shrinkage of both mixes than the control OPC concrete as well as the HVS and HVS-FA concretes without nano- $\text{CaCO}_3$ . The most significant reduction is in HVS-FA concrete containing 69% BFS-FA and 1% nano- $\text{CaCO}_3$ . However, the reduction between control OPC concrete and HVS concrete containing 69% BFS and 1% nano- $\text{CaCO}_3$  decreased with the ages. The lower drying shrinkage of HVS and HVS-FA concretes containing 1% NC can be attributed to the formation of additional hydration products through pozzolanic reaction and the nano filling and seeding effect of the NC (Meng & Wang, 2017) and similar reduction of drying shrinkage also found when nano- $\text{SiO}_2$  added with HVS and HVS-FA blended concretes (Hosan & Shaikh, 2020). The compact microstructure in those concretes containing NC yields less cracks and reduces the water loss through pore refining effect and hydrophilicity increasing effect (Du et al., 2019). The reduction of capillary pores in pastes of those HVS and HVS-FA concretes due to addition of NC observed in another study by the authors (Hosan & Shaikh, 2020) is the indication of pore refinement which also helped in reducing the shrinkage of those concretes.

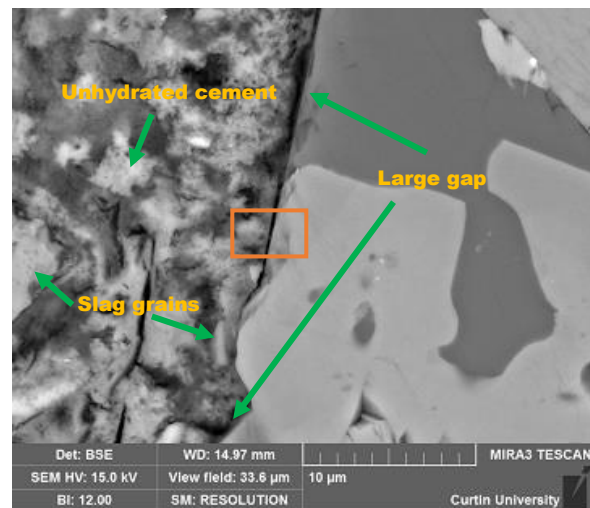
### ***7.3.3 Microstructural modifications***

The addition of 1% NC improved the compressive strength, durability properties and reduced the drying shrinkage of HVS and HVS-FA concretes. The pore filling effect of NC and formation of additional hydration products through pozzolanic reaction of NC, BFS and FA in the matrix and the densification of ITZ around the aggregates of those concretes are believed to be the reason for such improvement. Microstructure of matrix and the ITZ of all concretes

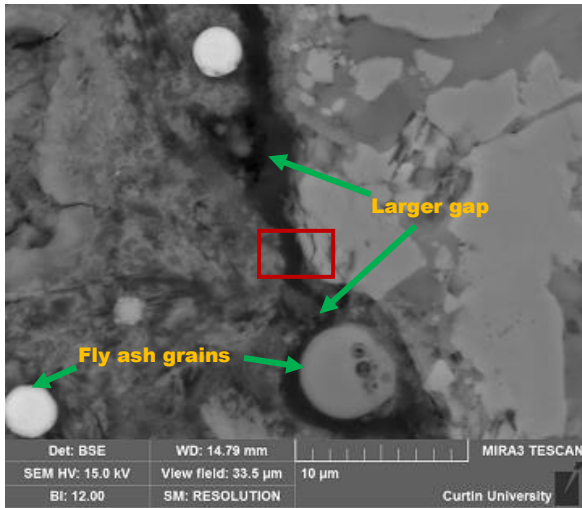
in this study is studied and their SEM images and EDS spectrums are shown in **Fig. 7.10**. It can be seen in the figure that the microstructure of matrix of HVS and HVS-FA concretes (Fig. 7.10b-c) are relatively porous than that of concrete OPC concrete (Fig. 7.10a). The ITZ around the aggregate in those concretes is also porous than that of conventional OPC concrete. This can be attributed to the slow pozzolanic reaction of FA and BFS in those concretes. This observation is also consistent with the measured compressive strength, durability properties and shrinkage results. However, the same concretes containing 1% NC show significant improvement in the microstructure of the matrix and the ITZ area as can be seen when the SEM images in **Fig. 7.10d-e** are compared with the images in **Fig. 7.10b-c** and also contributed to improve the modulus and hardness and reduce the thickness of ITZ (Hosan et al., 2020). It can be seen that the microstructure of the paste matrix of concrete containing 69% BFS is significantly densified due to addition of 1% NC with very few cracks in the matrix as well as compact ITZ zone (**Fig. 7.10d**) resemble the results of similar study of HVS composites with NC (Balcikanli et al., 2020). Similar observation is also valid for HVS-FA concrete containing combined FA and BFS content of 69% and 1% NC. However, presence of unreacted fly ash particles can be seen in the matrix as well as few voids (**Fig. 7.10e**). Hairline cracks can also be seen in ITZ area but the ITZ zone is more compact than that observed in the HVS-FA concrete (**Fig. 7.10c**).



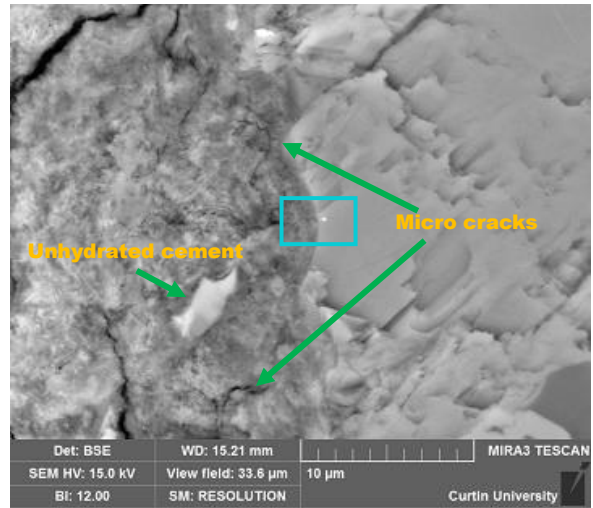
a) OPC



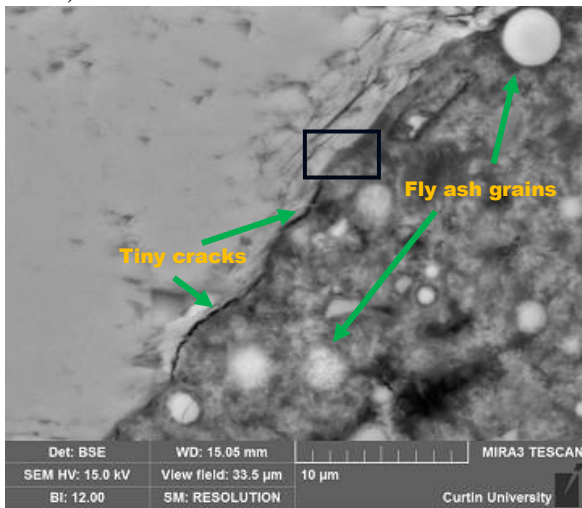
b) 70BFS



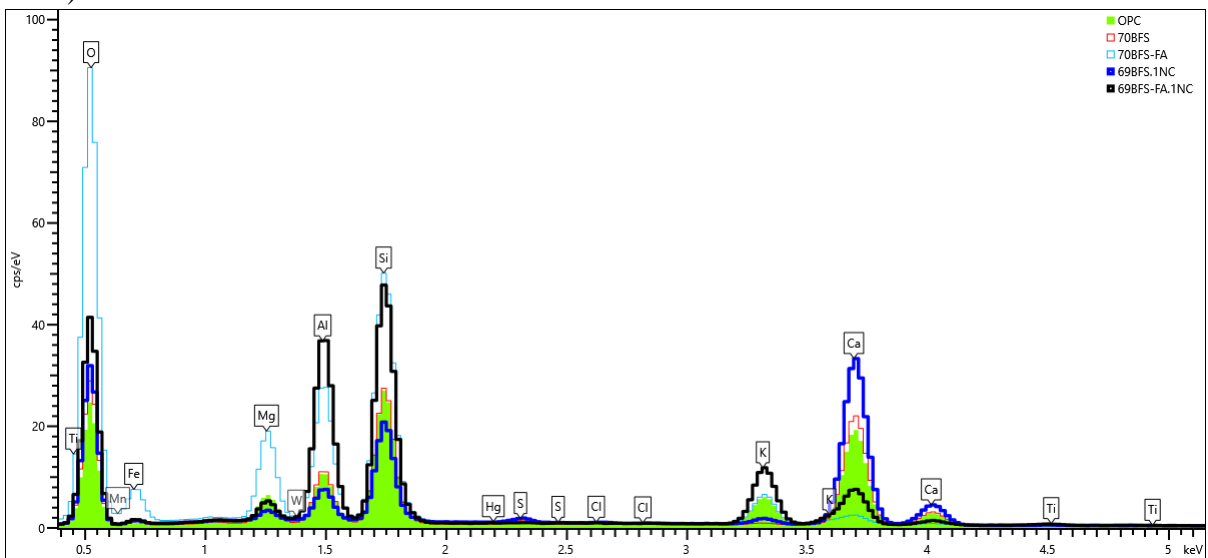
c) 70BFS-FA



d) 69BFS.1NC



e) 69BFS-FA.1NC



f) EDS spectrum of different concrete mixes at ITZ.

**Fig. 7.10** SEM images and EDS spectrum of different concrete mixes with and without nano- $\text{CaCO}_3$  addition after 28 days of curing.

It can also be seen from the comparison of EDS (**Fig. 7.10f**) traces taken in the ITZ of all concrete mixes that both HVS and HVS-FA concretes having higher traces of oxygen than OPC concrete, particularly in HVS-FA concrete which is a confirmation of more permeable voids between the aggregates and binder paste interface of that individual concrete mix. Nevertheless, an addition of 1% nano-CaCO<sub>3</sub> in both HVS and HVS-FA mixes significantly reduces the oxygen traces and exhibited similar or even lower oxygen traces indication of higher degree of dense microstructures. Besides, an increase amount of Ca traces in those concretes is also noteworthy due to the nano-CaCO<sub>3</sub> addition in the system that point out the development of new C-S-H gel. Overall, it is clear from the microstructural investigation that nano-CaCO<sub>3</sub> addition densified the matrix and formed a denser and compacted aggregate and binder paste interface subsequently formed a concrete with higher strengths and durability. It would be worthy to mention that EDS traces of the ITZ of different concrete mixes were measured accurately with similar area of ITZ for all concrete mixes and comparison made between them to identify the differences of the spectrums found in the analysis (Hosan & Shaikh, 2020).

#### **7.4 Summary**

This chapter presents comparable and even better compressive strength and durability properties of environmentally friendly concrete with 54% lower carbon footprint that containing 70% less OPC. Based on the results and discussions of high volume slag and high volume slag-fly ash blended concrete containing nano-CaCO<sub>3</sub>, the following conclusions can be drawn:

- ◆ The Compressive strength of high volume slag containing 69% blast furnace slag improved significantly by 43% at 3 days of concrete age due to the addition of 1% nano-CaCO<sub>3</sub> compare to their control concrete without nano-CaCO<sub>3</sub> and exceeds the compressive strengths of OPC concrete at 7days and maintained superior strengths in the later ages.
- ◆ The addition of 1% nano-CaCO<sub>3</sub> increased the compressive strengths of high volume slag-fly ash blended concrete containing 48.5% blast furnace slag and 20.5% fly ash by 28% at 3 days of concrete age than their control concrete with no nano-CaCO<sub>3</sub> and surpasses the compressive strengths of control OPC concrete at 28 days of age and showed similar long term compressive strengths.

- ◆ Addition of 1% nano-CaCO<sub>3</sub> reduced water absorption of HVS and HVS-FA concrete by 1% and 10% respectively after 28 days of curing. However, greater reduction observed after 90 days of curing in both concretes and exhibited comparable sorptivity to control OPC concrete.
- ◆ Significant reduction of volume of permeable voids of HVS concrete containing 69% BFS and HVS-FA concrete containing 69% BFS-FA observed due to the addition of 1% nano-CaCO<sub>3</sub> by about 18% and 21% respectively than their control HVS and HVS-FA concrete after 28 days of curing and showed lower permeable voids than the OPC concrete and reduction was greater in 90 days of curing.
- ◆ Exceptional resistance against chloride ion permeability measured in HVS and HVS-FA concrete with and without nano-CaCO<sub>3</sub> addition after 28 days and 90 days of curing. Inclusion of 1% nano-CaCO<sub>3</sub> also reduced the charge passed by 14% and 22% of HVS concrete and by 39% and 45% of HVS-FA concrete than their respective control concrete after 28 and 90 days of curing respectively.
- ◆ Addition of 1% nano-CaCO<sub>3</sub> remarkably lowered the early drying shrinkage of HVS and HVS-FA concrete and maintained shrinkage strain well below in later ages of HVS-FA concrete than control OPC concrete. However, the strain reduction gap between control OPC concrete and HVS concrete containing 60% BFS and 1% nano-CaCO<sub>3</sub> was narrowing down in later ages.
- ◆ Microstructural investigation confirmed a higher degree of compacted ITZ of HVS and HVS-FA concrete due to the addition of 1% NC than the concrete without NC and possessed a similar or even better interfacial bond between aggregates and binder paste than conventional concrete.



## 7.5 References

- Aghaeipour, A. and M. Madhkhan, Effect of ground granulated blast furnace slag (GGBFS) on RCCP durability. *Construction and Building Materials*, 2017. **141**: p. 533-541.
- Aly, T. and J.G. Sanjayan, Mechanism of early age shrinkage of concretes. *Materials and Structures*, 2008. 42(4): p. 461.
- ASTM C1202, Standard Test Method for Electrical Indication of Concrete's Ability to Resist Chloride Ion Penetration. 2019.
- ASTM C157, Standard Test Method for Length Change of Hardened Hydraulic-Cement Mortar and Concrete. 2017.
- ASTM C1585, Standard Test Method for Measurement of Rate of Absorption of Water by Hydraulic-Cement Concretes. 2013.
- ASTM C642, Standard Test Method for Density, Absorption, and Voids in Hardened Concrete. 2013.
- ASTM C873, Standard Test Method for Compressive Strength of Concrete Cylinders Cast in Place in Cylindrical Molds. 2015.
- Balcikanli Bankir, M., et al., Effect of n-CaCO<sub>3</sub> on fresh, hardened properties and acid resistance of granulated blast furnace slag added mortar. *Journal of Building Engineering*, 2020. 29: p. 101209.
- Benhelal, E., et al., Global strategies and potentials to curb CO<sub>2</sub> emissions in cement industry. *Journal of Cleaner Production*, 2013. **51**(Supplement C): p. 142-161.
- Bentz, D.P., Activation energies of high-volume fly ash ternary blends: Hydration and setting. *Cement and Concrete Composites*, 2014. **53**: p. 214-223.
- Bentz, D.P., et al., Fine limestone additions to regulate setting in high volume fly ash mixtures. *Cement and Concrete Composites*, 2012. **34**(1): p. 11-17.
- Damtoft, J.S., et al., Sustainable development and climate change initiatives. *Cement and Concrete Research*, 2008. **38**(2): p. 115-127.
- De Weerd, K., et al., Synergy between fly ash and limestone powder in ternary cements. *Cement and Concrete Composites*, 2011. **41**: p. 279-291.

Demirboğa, R., İ. Türkmen, and M.B. Karakoç, Relationship between ultrasonic velocity and compressive strength for high-volume mineral-admixed concrete. *Cement and Concrete Research*, 2004. **34**(12): p. 2329-2336.

Du, S., Wu, J., AlShareedah, O. and Shi, X. (2019) Nanotechnology in cement based materials: A review of durability, modeling and advanced characterization. *Nanomaterials*.

Duran Atış, C. and C. Bilim, Wet and dry cured compressive strength of concrete containing ground granulated blast-furnace slag. *Building and Environment*, 2007. **42**(8): p. 3060-3065.

Duran-Herrera, A., et al., Self-compacting concretes using fly ash and fine limestone powder: Shrinkage and surface electrical resistivity of equivalent mortars. *Construction and Building Materials*, 2019. **199**: p. 50-62.

Elchalakani, M., T. Aly, and E. Abu-Aisheh, Sustainable concrete with high volume GGBFS to build Masdar City in the UAE. *Case Studies in Construction Materials*, 2014. **1**: p. 10-24.

Georgescu, M. and N. Saca, Properties of blended cement with limestone filler and fly ash content. *Scientific Bulletin*, 2009. **71**: p. 1454-2331.

Gesoğlu, M. and E. Özbay, Effects of mineral admixtures on fresh and hardened properties of self-compacting concretes: binary, ternary and quaternary systems. *Materials and Structures*, 2007. **40**(9): p. 923-937.

Güneyisi, E. and M. Gesoğlu, A study on durability properties of high-performance concretes incorporating high replacement levels of slag. *Materials and Structures*, 2008. **41**(3): p. 479-493.

Hosan, A. and F.U.A. Shaikh, Influence of nano-CaCO<sub>3</sub> addition on the compressive strength and microstructure of high volume slag and high volume slag-fly ash blended pastes. *Journal of Building Engineering*, 2020. **27**: p. 100929.

Hosan, A., et al., Nano- and micro-scale characterisation of interfacial transition zone (ITZ) of high volume slag and slag-fly ash blended concretes containing nano SiO<sub>2</sub> and nano CaCO<sub>3</sub>. *Construction and Building Materials*, 2020: p. 121311.

Hosan, A. and F.U.A. Shaikh, Influence of nano silica on compressive strength, durability, and microstructure of high-volume slag and high-volume slag–fly ash blended concretes. *Structural Concrete*. <https://doi.org/10.1002/suco.202000251>

Kuder, K., et al., Mechanical properties of self consolidating concrete blended with high volumes of fly ash and slag. *Construction and Building Materials*, 2012. **34**: p. 285-295.

Malhotra, V.M., Introduction: Sustainable development and concrete technology, ACI Board Group on Sustainable Development. ACI Concrete International, 2002. **24(7)**: p. 22.

Mehta, P.K., Reducing the environmental impact of concrete. ACI Concrete International, 2001. **23(10)**: p. 61-66.

Meng, T., Y. Yu, and Z. Wang, Effect of nano-CaCO<sub>3</sub> slurry on the mechanical properties and micro-structure of concrete with and without fly ash. *Composites Part B: Engineering*, 2017. **117**: p. 124-129.

Oner, A. and S. Akyuz, An experimental study on optimum usage of GGBS for the compressive strength of concrete. *Cement and Concrete Composites*, 2007. **29(6)**: p. 505-514.

Pera, J., S. Husson, and B. Guilhot, Influence of finely ground limestone on cement hydration. *Cement and Concrete Composites*, 1999. **21**: p. 99-105.

Sato, T. and F. Diallo, Seeding effect of nano-CaCO<sub>3</sub> on the hydration of tricalcium silicate. *Journal of the Transportation Research Board*, 2010. **2141**: p. 61-67.

Shaikh, F.U.A. and S.W.M. Supit, Chloride induced corrosion durability of high volume fly ash concretes containing nano particles. *Construction and Building Materials*, 2015. **99**: p. 208-225.

Shaikh, F.U.A. and S.W.M. Supit, Mechanical and durability properties of high volume fly ash (HVFA) concrete containing calcium carbonate (CaCO<sub>3</sub>) nanoparticles. *Construction and Building Materials*, 2014. **70(Supplement C)**: p. 309-321.

Supit, S.W.M. and F.U.A. Shaikh, Effect of Nano-CaCO<sub>3</sub> on Compressive Strength Development of High Volume Fly Ash Mortars and Concretes. *Journal of Advanced Concrete Technology*, 2014. **12(6)**: p. 178.

Tharakan, J.L.P., D. Macdonald, and X. Liang, Technological, economic and financial prospects of carbon dioxide capture in the cement industry. *Energy Policy* 2013. **61**: p. 1377-1387.

Vishwakarma, V., et al., Enhancing antimicrobial properties of fly ash mortars specimens through nanophase modification. *Materials Today: Proceedings*, 2016. **3(6)**: p. 1389-1397.

Wainwright, P.J. and N. Rey, The influence of ground granulated blastfurnace slag (GGBS) additions and time delay on the bleeding of concrete. *Cement and Concrete Composites*, 2000. **22**(4): p. 253-257.

Won, J.-P., et al., Shrinkage and durability characteristics of eco-friendly fireproof high-strength concrete. *Construction and Building Materials*, 2013. 40: p. 753-762.

Zhang MH, Islam J (2012) Use of nano-silica to reduce setting time and increase early strength of concretes with high volume fly ash or slag. *Constr Build Mater* 29:573–580

Zhao, Y., J. Gong, and S. Zhao, Experimental study on shrinkage of HPC containing fly ash and ground granulated blast-furnace slag. *Construction and Building Materials*, 2017. 155: p. 145-153.37.

*All reasonable efforts have been made to acknowledge the authors of the copyright material. It would be highly appreciated if I can hear from any authors has been ignored or incorrectly acknowledged.*

## **Chapter 8: Chloride induced corrosion and chloride diffusion of HVS and HVS-FA concretes containing nano silica and nano calcium carbonate**

---

This chapter evaluates the effect of addition of optimum content of nano silica and nano calcium carbonate on the chloride induced corrosion and chloride diffusion of the high volume slag (HVS) and high volume slag-fly ash (HVS-FA) concretes. This chloride induced corrosion test was conducted by collecting corrosion rate and concrete resistivity of those concrete sample every week in a 3.5 days wet in a 3.5% NaCl solution and 3.5 days dry cycle. Chloride diffusion test was performed in a 50 mm discs of those concrete samples after 28 days of curing and then placed them in a container containing sodium chloride solution with a concentration of  $165 \pm 1$  m/L for 60 days. Moreover, service life prediction of those HVS and HVS-FA concretes sample were calculated based on the chloride diffusion data are also demonstrated in this chapter.

### **8.1 Overview**

Ordinary Portland cement (OPC) is considered to be the most common binder in concrete and cement based composites. Worldwide production of OPC in 2019 was 4.2 billion metric tons compared to 3.27 billion metric tons in 2010 and expected to be 4.83 billion metric tons in 2030 (Zementwerke, 2013). The life span of reinforced concrete structures largely depends on the durability properties of concrete and OPC concrete is a proven longer durable material in a non-aggressive environment. However, in contact with seawater, underground construction and chemical exposure lead to deterioration of OPC concrete due to its heterogeneous porous properties severely affecting the service life of the structures (Association, 2002; Mehta, 1991; Val & Stewart, 2003).

---

The content of this chapter has been written based on the paper submitted in the following journal.

Hosan, A. and F.U.A. Shaikh, Effect of nano materials on chloride induced corrosion and service life of high volume slag and high volume slag-fly ash blended concretes. *Journal of Materials in Civil Engineering* . (Under review).

To reduce the corrosion of reinforced concrete structures and to improve the durability, high-performance concrete with low water binder ratio and more concrete cover are required (Australia, 2018) which eventually increase the cost of the structures. Moreover, OPC production is highly energy-intensive and contributes roughly 7% of global CO<sub>2</sub> emission into the atmosphere which cause climate change (Benhelal et al., 2013; Mehta, 2001). To reduce the environmental impact caused by cement production and to extend the service life of concrete structures in the marine environment, the use of several supplementary cementitious materials (SCM) such as blast furnace slag (BFS), fly ash (FA), silica fume (SF), metakaolin, etc. as partial replacement of OPC in concrete production is widely practiced. BFS and FA are extensively used by researchers to partially substitute cement in a large volume and found similar mechanical and durability properties of OPC concrete (Elchalakani et al., 2014; Hooton, 2000; Rashad, 2015; Siddique, 2004). Furthermore, concrete structures made with partial replacement of BFS and FA showed a better resistance against corrosion and longer service life even with higher volume replacement of OPC with SCM (Güneyisi & Gesoğlu, 2008; McNally & Sheils, 2012; Heede et al., 2017). Osborne (1999) reported that concrete with 70% cement replacement by BFS showed the lowest chloride attack in a fully submersed condition in seawater. Another study (Pal et al., 2002) found higher corrosion resistance of concrete containing 70% BFS and the resistivity is increased with the increasing amount of BFS. Yean and Kim (2005) also reported higher corrosion resistance of concrete samples when 55% cement is replaced by BFS compared to reference concrete. Lower corrosion rate is observed in concretes containing 50% and 70% slag compared to control concrete. Additionally, a number of studies with 50% reduction of cement with slag and fly ash reported in lower chloride ion penetration and chloride diffusion coefficient (Berndt, 2009; Dhir et al., 1996; Jau & Tsay, 1998; Ramezaniyanpour & Malhotra, 1995; Sengul & Tasdemir, 2009). Similarly, higher chloride resistance and extended service life of concrete structures containing 30%, 40%, and 60% FA are also reported in recent studies (Nath et al., 2018; Shaikh & Supit, 2015). Nevertheless, higher volume (>50%) replacement of OPC by BFS, FA, SF, and their blended mix showed few challenges of low early age strengths, longer setting time, higher shrinkage, and vigorous carbonation (Kuder et al., 2012; Oner & Akyuz, 2007; Şahmaran et al., 2008; Younsi et al., 2011).

In recent times, using a small amount of nano materials such as nano-CaCO<sub>3</sub> (NC) and nano-SiO<sub>2</sub> (NS) along with partial replacement of BFS and FA gained popularity in green concrete development as nano materials has a significant positive effect on the properties of concrete

such as influence in the improvement of early strength as well as later strength by stimulating the hydration reactions and boost the durability properties due to their huge specific surface area, exceptionally tiny particle size and micro- and nano-pores filling (Güneyisi et al., 2015; Hou et al., 2013; Kawashima et al., 2013). Zhang et al. (2012) reported an accelerated pozzolanic activity and increased compressive strengths of mortars containing 50% slag with the addition of 2% NS. It is reported that the addition of 2% NS in concretes containing 50% slag reduced initial and final setting times, significant improved in early age compressive strengths and reduction in chloride-ion permeability (Zhang & Islam, 2012). Liu et al. (2016) also found an enhanced pozzolanic activity with the addition of 3% NS in paste containing 30% slag as partial replacement of OPC and reported improved compressive strengths and reduced total porosity of 30% and 40% slag replaced mortar specimens with the inclusion of 3% NS. Nazari and Riahi (2011) reported improved early age hydration, increased split tensile strengths and reduced pore volume of concrete specimens containing 45% slag with the addition of 3% NS. Rashad et al. (2018) reported higher compressive strengths of pastes containing 65% slag with the inclusion of 1-4% NS and found an increasing trend of compressive strengths with the increasing dosage of NS. Additionally, Zhang and Islam (2012) assessed that the addition of 1% NS in paste samples containing 50% FA accelerated the hydration of FA particles and increased the compressive strengths of mortars containing 50% FA. They also found that 2% NS inclusion in concrete containing 50% FA reduced the initial and final setting time. Similar results such as the accelerated pozzolanic activity of FA particles, improved compressive strengths, and lower volume of porosity also reported in another study in which 4% NS was added with 50% FA replaced concrete (Li, 2004). Shaikh et al. (2015 & 2014) reported improved workability, compressive strengths, durability properties and microstructure of 60% FA replaced concrete, mortars, and pastes with the inclusion of 2% NS. However, the BFS and FA replacement in all the above studies are within 60% cement replacement even there is a strong demand for the higher volume of replacement from the perspective of corrosion control and CO<sub>2</sub> reduction into the atmosphere.

Recently authors (Hosan & Shaikh, 2020; Shaikh & Hosan, 2019) studied the addition of 1-4% NC and NS on the compressive strength and microstructure of HVS and HVS and FA blended pastes and observed improved compressive strengths of HVS pastes containing 70-90% BFS and HVS and FA blended paste containing 70% BFS-FA as partial replacement of OPC. They also observed that NS and NC inclusion resulted in a denser microstructure with the formation of additional calcium silicate hydrate (CSH) gels and about 70-80% reduction in carbon

footprint of blended cement pastes. This paper extends the above encouraging results to corrosion durability and the long term compressive strength development of HVS and HVS-FA concretes where the effects of NS and NC on compressive strength development and chloride induced corrosion durability of above green concretes over one year are presented. In addition the effects of NS and NC on chloride diffusion and damage resistance of above HVS and HVS-FA concretes are also presented in this paper along with the extension of predicted service life of above green concretes due to the addition of NS and NC.

## **8.2 Experimental Program**

### ***8.2.1 Materials***

The ordinary Portland cement (OPC) used in this study fully complies with the requirements of Australian Standard AS 3972 for general purpose cement (AS 3972-1997). The blast furnace slag (BFS) is locally supplied and class F fly ash (FA) is provided by a coal-fired power plant in Australia which also confirm the Australian standards (AS 3582.1-1198; AS 3582.2-2001). All coarse and fine aggregates used in this study met the required Australian standard (AS2758.1:2014). Aggregates are soaked in water for at least 24 hours and exposed to open air to achieve saturated and surface dry (SSD) condition. Dry nano-CaCO<sub>3</sub> (NC) and nano-SiO<sub>2</sub> (NS) powders are purchased from commercial nano materials manufacturers. Tap water from concrete laboratory is used in all mixes and a naphthalene sulphonate based superplasticizer (SP) is used to maintain the workability of concrete mixes. Physical properties and chemical compositions of all cementitious materials are shown in **Table 5.1** and **Figs. 3.2, 4.1-4.2** show the X-ray diffraction (XRD) analysis results of OPC, BFS, FA, NC, and NS. It can be seen by comparing the XRD results that the NS is highly amorphous compared to the NC. Among OPC, BFS, and FA, BFS is more amorphous with amorphous content of 95.7% compared to 67.8% amorphous content of FA and 24 % amorphous content of OPC based on quantitative XRD analysis results.

### ***8.2.2 Mix design and sample preparation***

All the concrete mixes were designed with a total binder quantity of 400 kg/m<sup>3</sup> and a constant water/binder ratio of 0.4. However, superplasticizer was used when needed to maintain the workability of concrete mixes with a target slump range of 100-125 mm. Coarse and fine aggregates mass and ratios were also kept constant in all mixes. **Table 5.2** shows the mix proportions and the measured slump of all mixes. It can be seen from the dosage of



superplasticizers in **Table 5.2** that the required dosage of superplasticizers increased with increase in BFS and nano materials to maintain the target slump for a workable concrete mix. A designated ID was given for each mix considering binder name and amount present on the mixes. For example, 69BFS.1NC means a mix containing 69% BFS and 30% OPC with the inclusion of 1% NC of the total binder. The amount of BFS, BFS-FA, and nano materials dosage used in Table 2 were selected from the results of the authors previous investigation with paste samples (Hosan & Shaikh, 2020; Shaikh & Hosan, 2019), where 1% NC and 2-3% NS addition in HVS pastes containing 70-80% BFS and combined BFS and FA content of 70% exhibited highest compressive strengths among various nano materials contents of 1-4% and BFS and combined BFS and FA contents of 70-90%.

Concrete mixes were prepared in a pan mixer at ambient temperature. First, all the dry ingredients such as cement, coarse aggregates, fine aggregates, and SCM (in case of HVS and HVS-FA mixes) were mixed for 4-5 minutes. Next, water was added and again mixed for around 2-3 minutes until a homogenous mix was obtained. Besides, NC and NS were dispersed in water containing superplasticizer by mixing the nano materials powder with partial water and superplasticizers required for the concrete mixes (depending on the percentage of nano materials inclusion). The NS or NC was then dispersed ultrasonically by an ultrasonic mixer shown in **Fig. 4.4** with 100% amplitude and at maximum cycle for 45 minutes for 1% NC, 60 minutes and 75 minutes for 2 % and 3 % of NS, respectively (Hosan & Shaikh, 2020; Shaikh & Hosan,2019). The solutions containing dispersed nano materials were added to the dry mixed ingredients of concretes containing nano materials together with remaining water and added slowly into the concrete mixes while the pan mixer was running to ensure proper dispersion of both NC and NS particles into the concrete mixes. Additional superplasticizer was added to attain the target slump for all mixes as shown in **Fig. 8.1**.

Standard cylindrical specimens with a diameter of 100 mm and a height of 200 mm were cast for compressive strengths and durability properties such as chloride diffusion and chloride ion penetration. For each concrete mix, two 100 x100x400 mm square cross-sectional rectangular beam were cast to conduct the accelerated corrosion test. A deformed 12 mm diameter 360 mm long bar was placed in the bottom centre of each beam with an effective clear cover of 20 mm of all concrete mixes. Steel bars were cleaned and accurately weighed before an electrical cable connected at one side of the bars and then placed in the beam. All the specimens were compacted in a vibrating table with three layers for cylindrical samples and two layers for beam samples. All the specimens were demoulded after 24 hours of casting and then cured in water

tank at room temperature for 28 days for accelerated corrosion test, chloride diffusion and chloride ion penetration tests. Compressive strength specimens were cured until the required test ages.

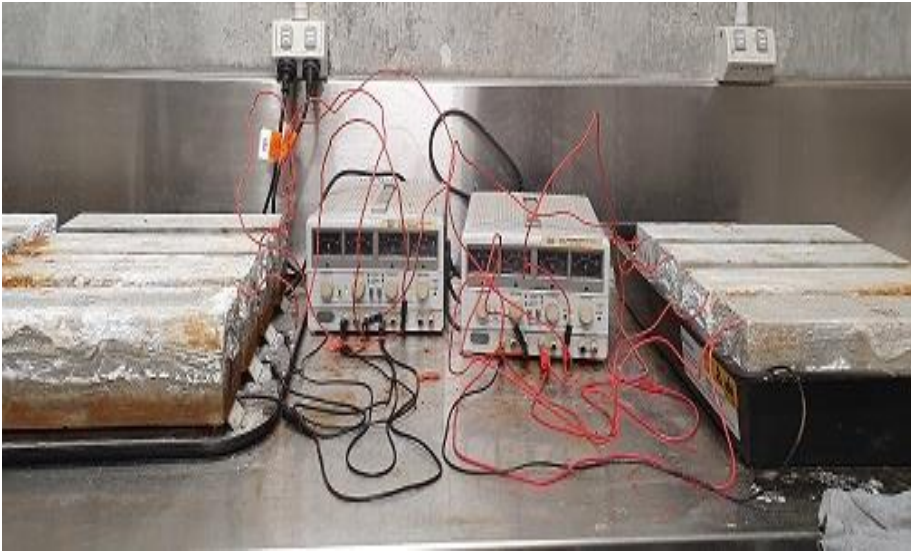


**Fig. 8.1** Slump test of a concrete mix

### ***8.2.3 Experimental methods***

#### ***8.2.3.1 Compressive strength***

Compressive strength was measured according to ASTM C873 (2015) standard with a loading rate of 0.33 MPa/s until failure at 7, 28, 90, 180, and 365 days of all mixes. Diameters of the cylinders were measured and sulphur capped at least 4 hours prior to the test. Compressive strengths were calculated as the maximum crushing load divided by the average cross-sectional area of the specimens. For each test age, at least three specimens were tested and the average value of three was reported in this study.



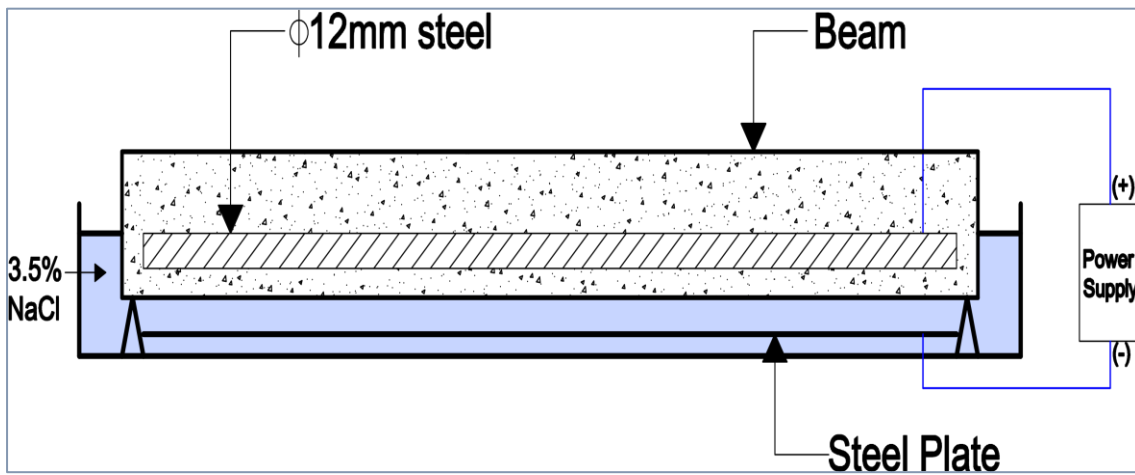
(a)



(b)



(c)



(d)

**Fig. 8.2** Chloride induced accelerated corrosion test of concrete mixes (a) test setup (b) applied voltage (c) typical data collection (d) schematic diagram (Not to scale)

### 8.2.3.2 Accelerated corrosion test

Chloride induced corrosion of steel in concrete is a slow process and often accelerated corrosion technique is used by many researchers to accelerate the corrosion of steel in the concrete. In this study vary low DC potential was applied to each specimen. Corrosion of steel bar was accelerated by applying constant low anodic potential of 3V between steel bar as an anode and steel plate as a cathode. One reinforced concrete beam from each mix was placed in a tray filled with 3.5% sodium chloride (NaCl) solution which sat on two chairs ensuring the beam partially submersed in the solution maintaining the water level above 10 mm of the steel bar placed inside the beam. Another beam of each mix was kept in a dry tray also sitting on two chairs ensuring the steel plate (cathode) exactly under the beam. A repeated “3.5 days wet” and “3.5 days dry” cycle was applied to stimulate the tide environment and to ensure oxygen availability. The NaCl solution was removed every fortnight and refilled with a newly prepared solution and continued for 52 weeks (one year). The photographs and schematic diagram of the corrosion test is shown in **Figs. 8.2a-b** and **d**. In a particular day of every week, samples were taken out from the tray and corrosion rate and concrete resistivity were recorded with an iCOR™ measuring device following the ASTM C876 (2015) standard as shown in **Fig. 8.2c**. After 52 weeks of collecting the corrosion rate and concrete resistivity data, one sample of each mix were cut in the middle to test the chloride penetration depth into the samples by the colorimetric process by spraying silver nitrate ( $\text{AgNO}_3$ ) solution on the cut surface (Otsuki et al., 1993). Both specimens of each mix were then crushed out and the corroded steel bars were recovered from the crushed specimens, removed the rust and cleaned according to ASTM G1 standard. The measured weight of each bar is compared with the initial weight of each bar recorded before steel bars placed in the beam prior to casting of the specimens. According to the ASTM G1, the actual mass of rust per unit surface area was calculated by using the Eq. (1).

$$M_{ac} = \frac{W_i - W_f}{\pi DL} \quad (1)$$

Where,  $M_{ac}$  = actual mass of rust per unit surface area of the bar ( $\text{g}/\text{cm}^2$ ),  $W_i$  = initial weight of the bar before corrosion (g),  $W_f$  = weight after corrosion (g) for a given duration of induced corrosion (T),  $D$  = diameter of the rebar (cm),  $L$  = length of the rebar sample (cm).

### 8.2.3.3 Chloride diffusion

To study the chloride penetration and chloride diffusion coefficient of all the concrete mixes with and without nano materials addition including the control OPC concrete, three 50 mm thick samples were cut excluding top and bottom parts from the 100 mm x 200 mm cylinder after 28 days of curing. One sample was used to determine the initial chloride content ( $C_i$ ) of each mix and the remaining samples were used for chloride ponding test. Test specimens were coated with epoxy paint except one flat side to allow chloride ion penetration in one direction into the concrete specimens. Samples were then placed in a container containing sodium chloride solution with a concentration of  $165 \pm 1$  m/L for 60 days. After that the samples were removed from the exposure liquid and then rinse with tap water and dried for 24 hours in the laboratory at ambient temperature following the ASTM C1556 -11a standard. Powder samples were collected from a depth ranging from 1 mm to 16 mm parallel to the flat exposed surface by using a profile grinder. The acid soluble chloride concentration of the samples was then measured by using a potentiometric titration method and the average of the two samples was calculated from two identical samples of each mix. The values of surface chloride concentration ( $C_s$ ) and chloride diffusion coefficients ( $D_a$ ) for each sample were determined by fitting Eq. (2) from the measured chloride contents of each layer by using non-linear regression analysis using Fick's second law of diffusion (Fick, 1995) for one-dimensional diffusion.

$$C(x, t) = C_s - (C_s - C_i) \operatorname{erf} \left[ \frac{x}{\sqrt{4D_a t}} \right] \quad (2)$$

Where,

$C(x, t)$  = the chloride concentration at a depth  $x$  and exposure time  $t$  (mass %),  $C_s$  = the chloride concentration at the surface of the samples (mass %),  $C_i$  = initial chloride concentration of the concrete prior to the submersion in the exposure liquid (mass %),  $\operatorname{erf}$  = the error function,  $x$  = depth below the exposure surface (m),  $D_a$  = the chloride diffusion coefficient ( $\text{m}^2/\text{s}$ ) and  $t$  = the exposure time (seconds).

### 8.2.3.4 Service life assessment

The service life of concrete structures against marine environment is determined by models based on Fick's second law of diffusion and has been widely used by other researchers (Cao & Liana, 2000; Thomas, 2008; Riding, 2007). A model (Thomas, 2008; Riding, 2007) is used to calculate the service life of different concrete mixes in this study by using the values of  $D_t$  and

$C_s$  at any time  $t$ . The model accounts for the time-dependent reduction in the diffusion coefficient of concrete by using the Eq. (3).

$$D_t = D_{28} \left(\frac{28}{t}\right)^m + D_{ult} \left(1 - \left(\frac{28}{t}\right)^m\right) \quad (3)$$

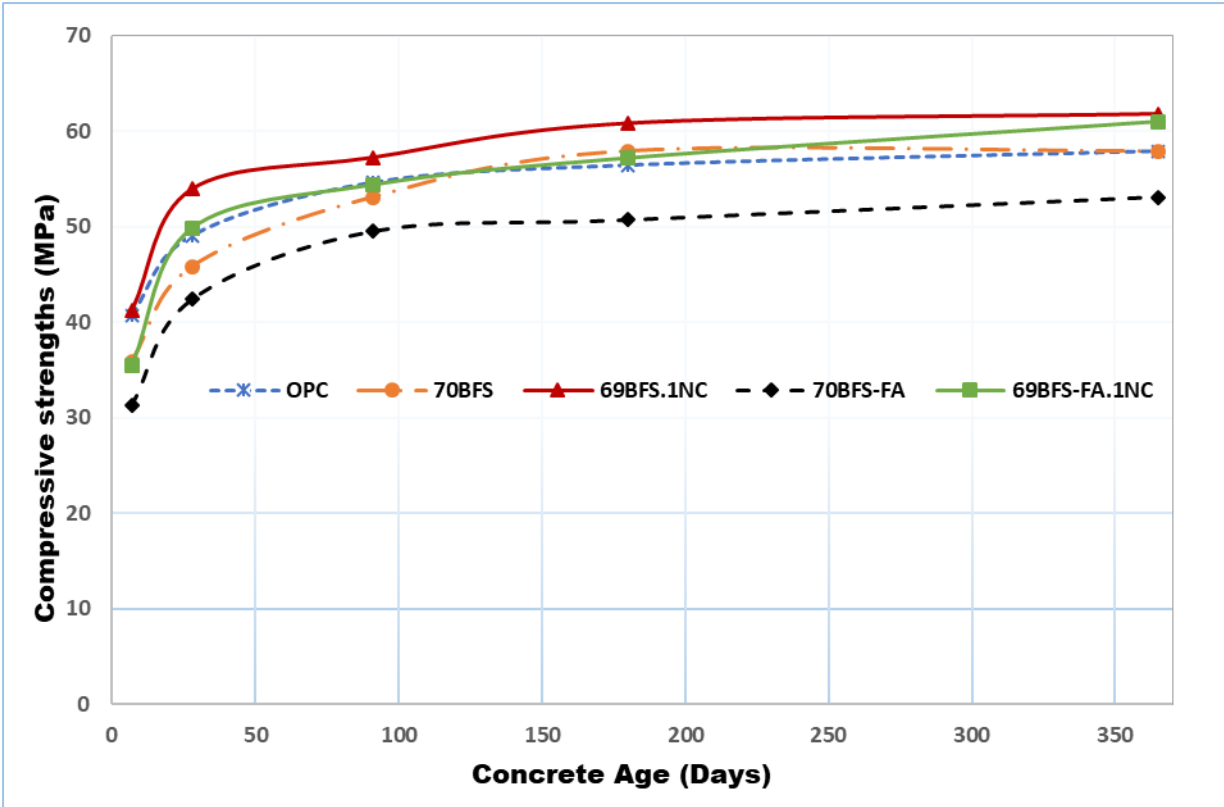
Where,  $D_t$  = chloride diffusion coefficient ( $m^2/s$ ) at time  $t$  (days),  $D_{28}$  = chloride diffusion coefficient at 28 days ( $m^2/s$ ), and  $D_{ult}$  = ultimate chloride diffusion coefficient ( $m^2/s$ ). The values of  $D_{ult}$  and  $m$  are calculated from the mixture proportions and  $D_{ult}$  is assumed to be the chloride diffusion coefficient at 100 years and calculated from the Eq. (4).

$$D_{ult} = D_{28} \left(\frac{28}{36500}\right)^m \quad (4)$$

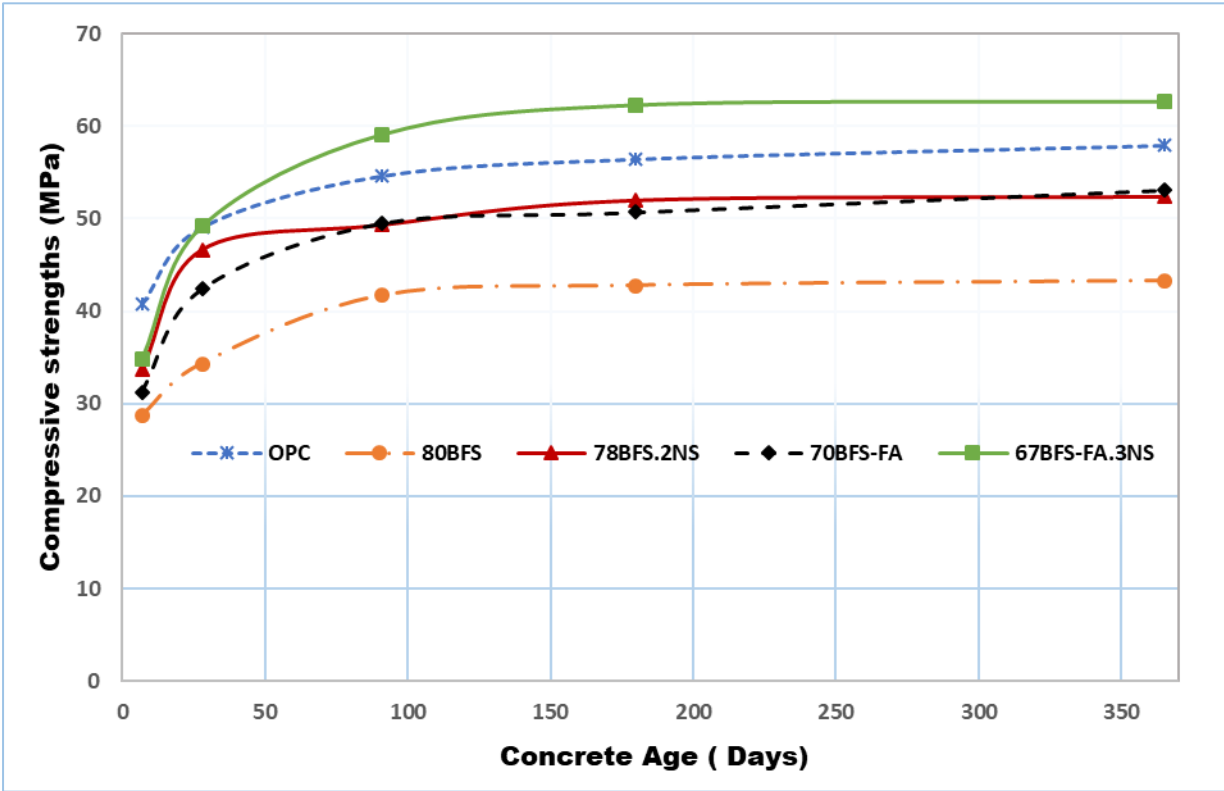
Where,  $D_{28}$  is considered the early age chloride diffusion coefficient calculated by using Fick's second law Eq. (2) and the value of  $m$  is influence by the percentage of BFS and FA present in the concrete mixes which controls the rate of decrease of the diffusion coefficient with time. The value of  $m$  is calculated by using the following Eq. (5).

$$m = 0.26 + 0.4 \left(\frac{FA}{50} + \frac{SG}{70}\right) \quad (5)$$

Where,  $m$  = diffusion decay constant, FA= percentage of fly ash and SG = percentage of slag of the total cementitious materials in the mix. The values of  $m$  should not exceed 0.6 prescribed by the model. Hence the value of  $m$  is considered to 0.26 for OPC mix and 0.6 for all other HVS and HVS-FA mixes with and without nano materials. The model also assumes a constant chloride content at the surface of the samples  $C_s = 0.8\%$  for a tidal exposure. By using the Eq. (3-5), the values of  $D_t$  calculated and  $C_i$  that were also measured from the experiments were substituted in the Eq. (1) to calculate the chloride concentration at the clear cover depth of reinforcement ( $x$ ). Repeated number of attempts have taken for different sets of  $D_t$  and  $t$  until the chloride concentration at cover depth  $C_t$  reached at the assumed critical chloride level  $C_{cr}$  ( $C_t = C_{cr}$ ). In this study,  $C_{cr}$  is assumed to be 0.05% and 0.1% w/w of concrete considering the higher volume of BFS and FA presence in the mixes (Cao & Liana, 2000). The life span of different concrete mixes was estimated for the cover depth of reinforcement ranging from 20 mm to 100 mm.

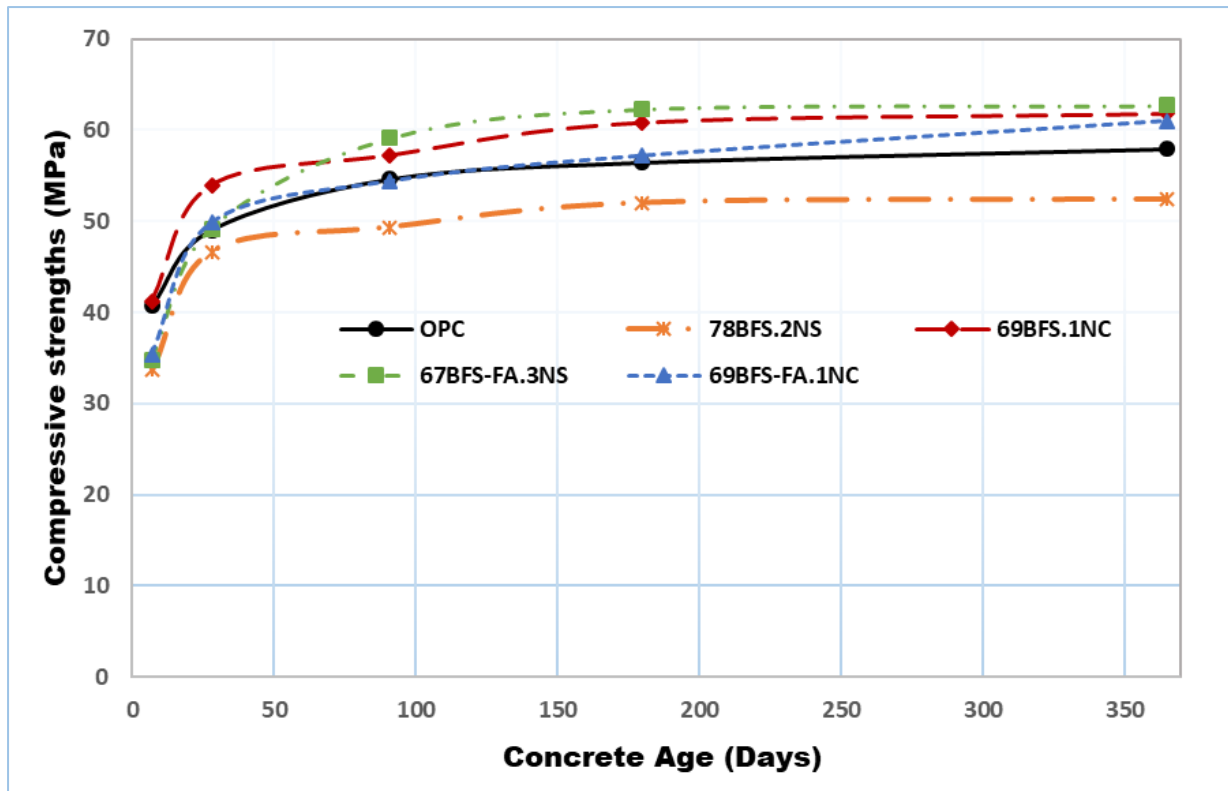


(a) Compressive strengths of control OPC, HVS and HVS-FA concrete with and without nano-CaCO<sub>3</sub>



(b) Compressive strengths of control OPC, HVS and HVS-FA concrete with and without nano-SiO<sub>2</sub>





(c) Comparison of compressive strengths of concretes containing nano materials with control OPC concrete.

**Fig. 8.3** Average compressive strengths of different concrete mixes at various ages with and without nano materials.

## 8.3 Results and discussions

### 8.3.1 Compressive strengths

#### 8.3.1.1 Effect of nano calcium carbonate

Compressive strength development over one year of control OPC, HVS, and HVS-FA concretes with and without NC addition is shown in **Fig. 8.3a**. It can be seen that the HVS concrete containing 70% BFS and HVS-FA concrete containing combined BFS and FA content of 70% without NC show significant lower compressive strengths at early age (7 days) than the control OPC concrete. However, the HVS concrete containing 70% BFS showed similar compressive strength at later ages to the OPC concrete. It can also be seen that 1% NC addition in both HVS and HVS-FA concretes increased the early age strength at 7 days and 28 days significantly than their respective control concretes without NC. The HVS concrete containing 69% BFS and 1% NC showed comparatively better performance at early age than the HVS-FA concrete containing 69% BFS-FA and 1% NC. Additionally, concrete mix 69BFS.1NC

displayed superior compressive strength than the OPC concrete throughout the period up to 365 days. On the other hand, concrete mix 69BFS-FA.1NC exhibited similar compressive strengths to the OPC concrete up to 90 days followed by continued strength gain at later ages and surpasses the OPC concrete's strength significantly due to the pozzolanic activity of FA in the mixes. The compressive strengths of 69BFS.1NC were 15% and 18% higher than the counterpart 70BFS concrete at 7 days and 28 days respectively, while concrete mix 69BFS-FA.1NC gained 13% and 18% more strengths than 70BFS-FA concrete, respectively. However, the compressive strength improvement of 69BFS-FA.1NC concrete at 90, 180, and 365 days were 10%, 13%, and 15%, respectively than its counterpart 70BFS-FA concrete, while the strength improvement of 69BFS.1NC were 8%, 5%, and 8% at 90, 180, and 365 days, respectively than their control concrete without NC addition. It is understandable that the presence of FA in the concrete mixes enhanced the development of the strengths at late ages due to its slow pozzolanic reaction.

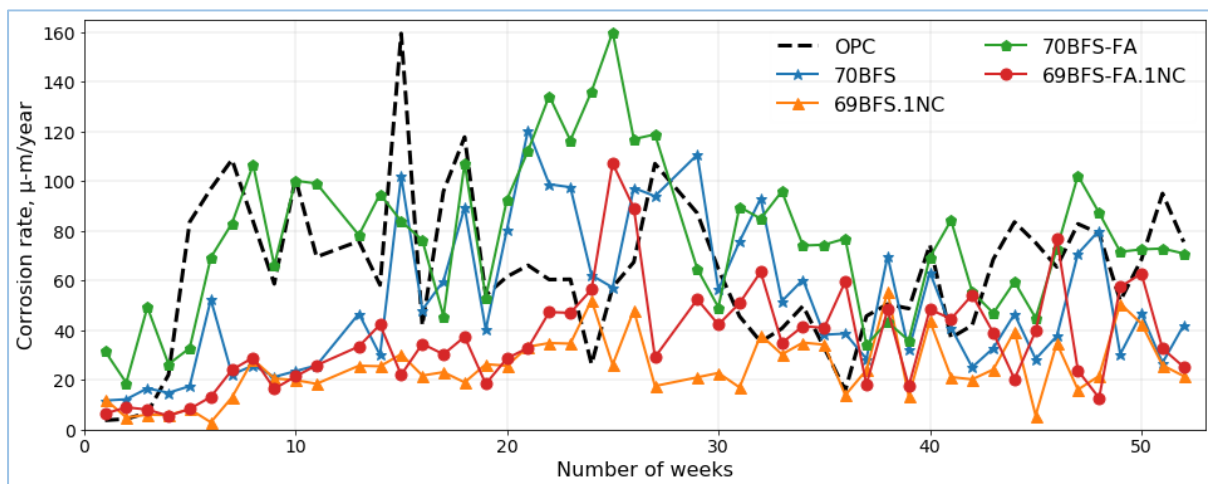
#### ***8.3.1.2 Effect of nano silica***

**Fig. 8.3b** shows the compressive strengths development of OPC concrete, HVS, and HVS-FA concretes with and without NS addition. It can be witnessed that the incorporation of NS improved the compressive strengths of both HVS and HVS-FA concretes than their corresponding control concretes at early age as well as later ages. The gain of compressive strength of 78BFS.2NS concrete was 17% and 36% at 7 days and 28 days respectively while the improvement of strength of 67BFS-FA.3NS concrete was 11% and 16% at 7 days and 28 days, respectively than their respective control concrete. Besides, the gain in compressive strength of 78BFS.2NS concrete at 91, 180, and 365 days was 18%, 22%, and 21%, respectively while the gain of strength of 67BFS-FA.3NS was 19%, 23%, and 18% respectively. Hence, it is clear that the improvement of compressive strength of both HVS and HVS-FA concretes were similar throughout the period up to 365 days due to the addition of NS dosage. However, the compressive strength of 78BFS.2NS concrete was marginally lower than the control OPC concrete. On the other hand, 67BFS-FA.3NS concrete exhibited higher compressive strengths than the OPC concrete in later ages and comparable strengths at early ages.

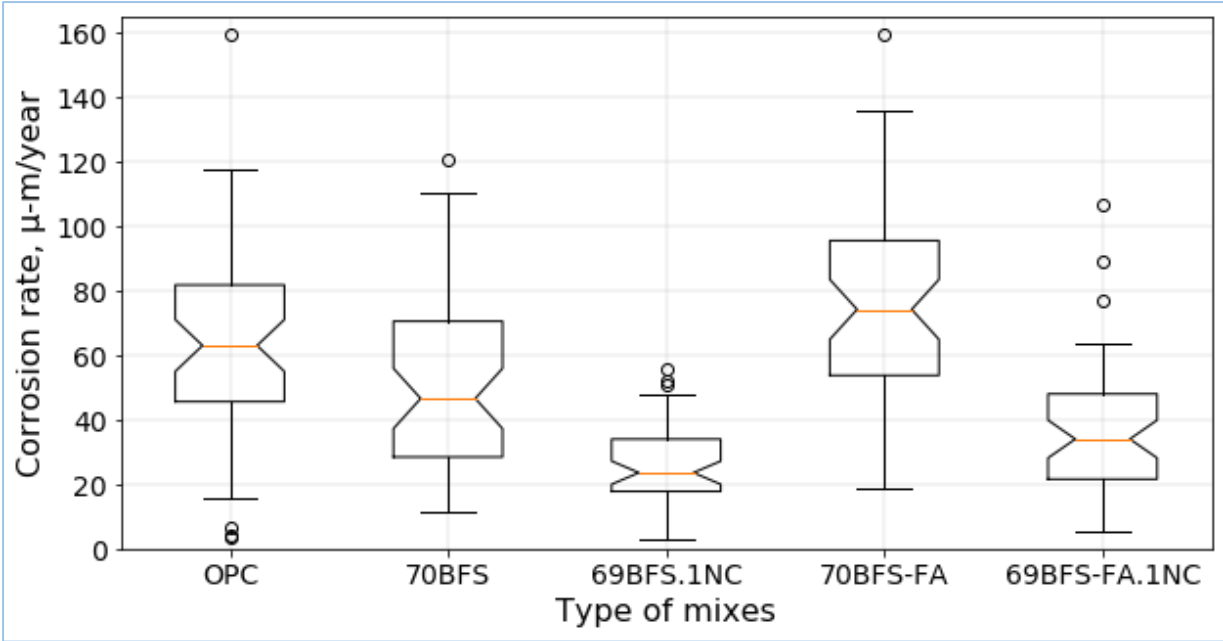
#### ***8.3.1.3 Comparison of concretes with nano materials***

Comparison of compressive strengths development of HVS and HVS-FA concretes containing nano materials along with OPC concrete is shown in **Fig. 8.3c**. The design of concrete structures is basically based on the 28 days compressive strengths of concrete mixes. It can be

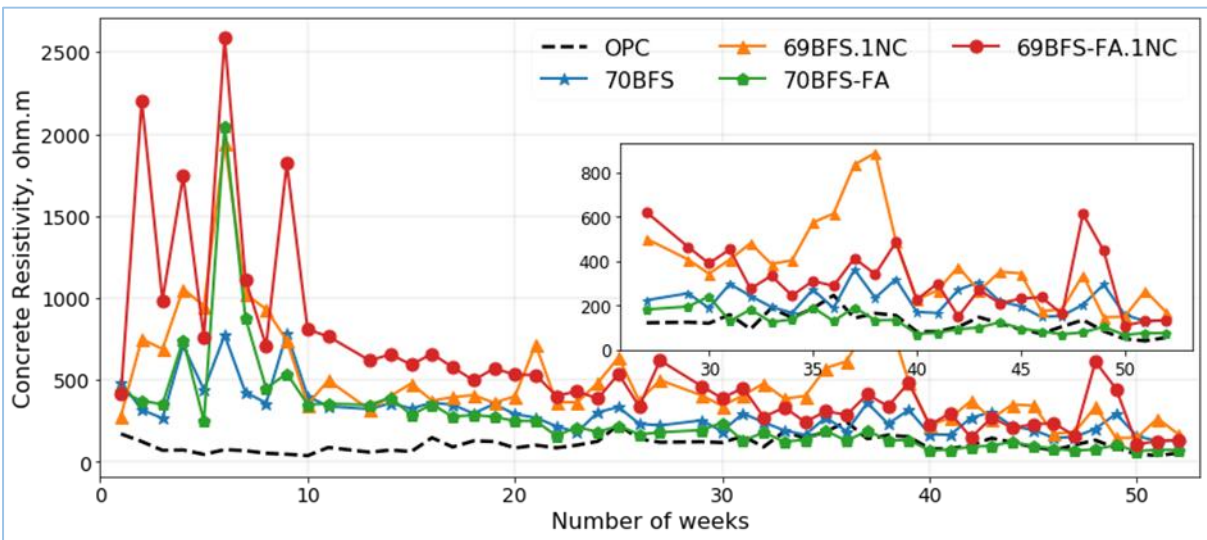
observed that the 28 days compressive strengths of all HVS and HVS-FA concretes containing NS and NC exhibited similar or better compressive strengths than control OPC concrete except the 78BFS.2NS concrete mix. It can also be seen that all HVS and HVS-FA concretes except 78BFS.2NS performed better than the control OPC concrete at later ages. Nevertheless, the 7 days compressive strengths of above concretes were lower than the control OPC concrete except for 69BFS.1NC mix which showed similar strengths to OPC. It is worth to note that the addition of 1% NC in HVS concrete containing 69% BFS and 3% NS in HVS-FA concrete containing combined FA and BFS content of 67% played an outstanding role in enhancing the hydration of high volume slag and high volume slag-fly ash blended mixes, respectively. Considering the 28 days compressive strength the 69BFS.1NC concrete mix outperformed all mixes containing nano materials and control OPC concrete. It can also be seen that the NS and NC addition accelerate the hydration process especially at early ages by forming new CSH gels, reducing the capillary pores, and increasing the degree of compactness of the matrix, hence increases the compressive strengths (Hosan & Shaikh, 2020; Shaikh & Hosan, 2019).



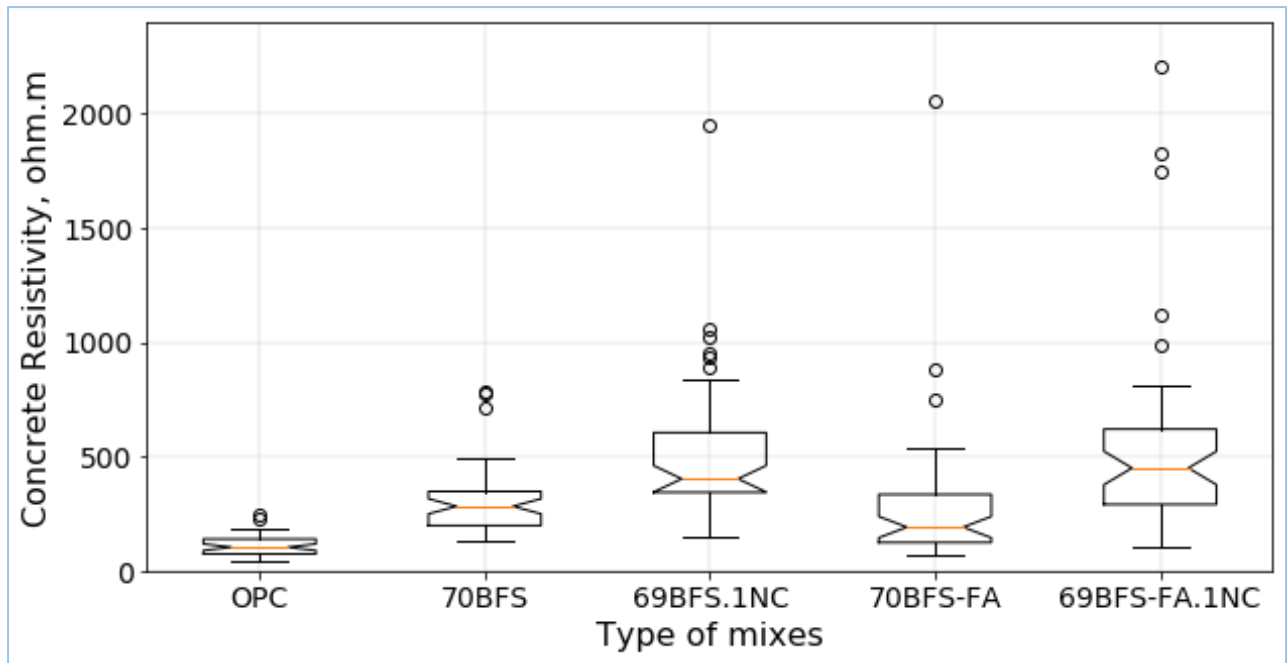
(a) Corrosion rate of different concrete mixes with and without nano-CaCO<sub>3</sub>



(b) Box-Whisker plot of corrosion rate of concrete mixes with and without nano-CaCO<sub>3</sub>



(c) Concrete resistivity of concrete mixes with and without nano-CaCO<sub>3</sub>



(d) Box-whisker plot of concrete resistivity of concrete mixes with and without nano- $\text{CaCO}_3$

**Fig. 8.4** Corrosion rate and concrete resistivity of OPC, HVS and HVS-FA concrete with and without nano- $\text{CaCO}_3$  addition.

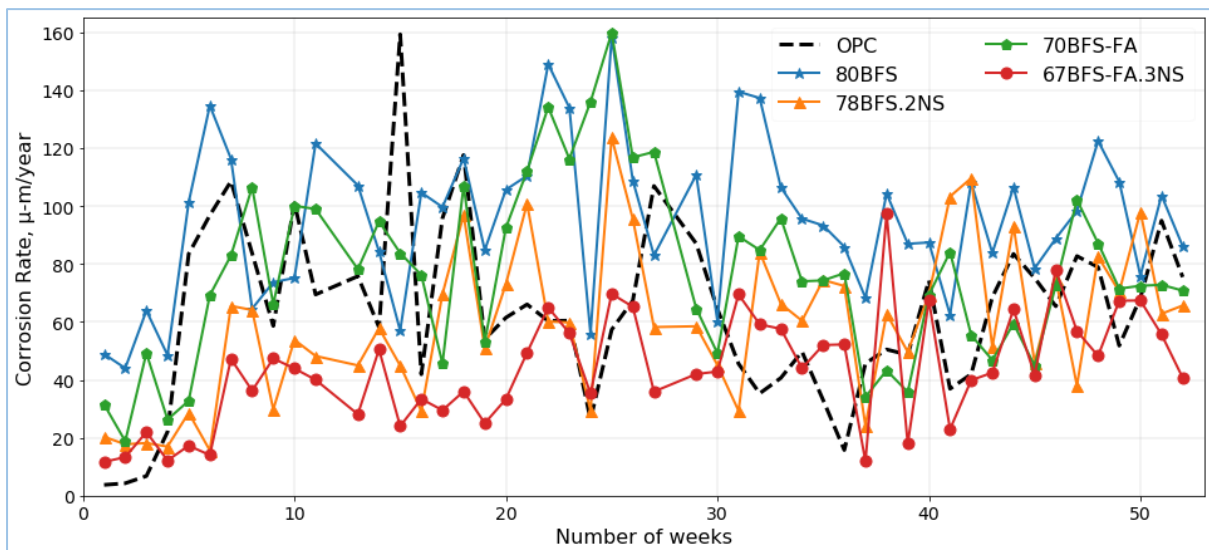
### 8.3.2 Chloride induced corrosion

#### 8.3.2.1 Effect of nano calcium carbonate

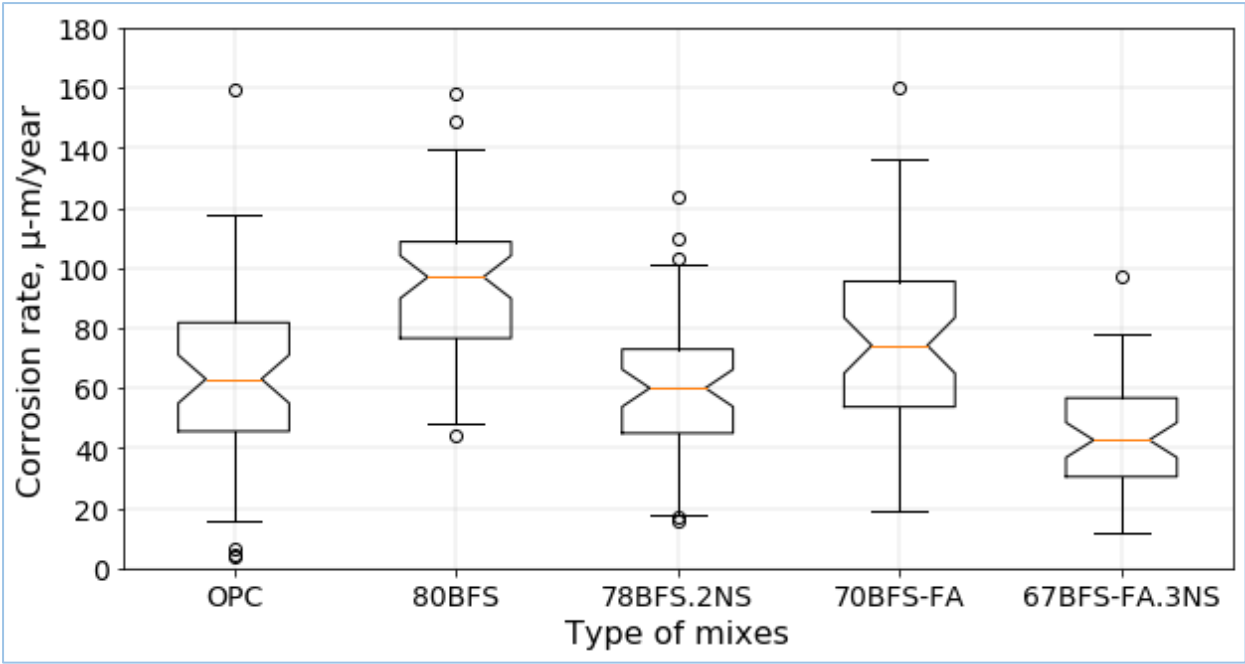
Corrosion rate and concrete resistivity of HVS and HVS-FA concretes with and without NC inclusion along with control OPC concrete for a period of 52 weeks of accelerated chloride corrosion are presented in **Figs. 8.4a-d**. It can be seen in **Figs. 8.4a-b** that the corrosion rate of HVS concrete mix containing 70% BFS showed lower corrosion rate than the OPC concrete for the whole one year of corrosion test, similar result is published in a past study (Pal et al., 2002). However, the HVS-FA concrete containing combined BFS and FA content of 70% exhibited slightly higher corrosion rate than the OPC concrete. The addition of 1% NC in both HVS and HVS-FA mixes reduced the corrosion rate dramatically from the very first week up to the end of the test of 52 weeks. The reduction was more pronounced in concrete mix 69BFS.1NC than the concrete mix 69BFS-FA.1NC which can be observed from the box whisker plot in Fig. 8b.

On the other hand, the effect of NC addition on the concrete resistivity of HVS and HVS-FA concretes can be seen in **Figs. 8.4c-d** with an inset in concrete resistivity from week 25 to week

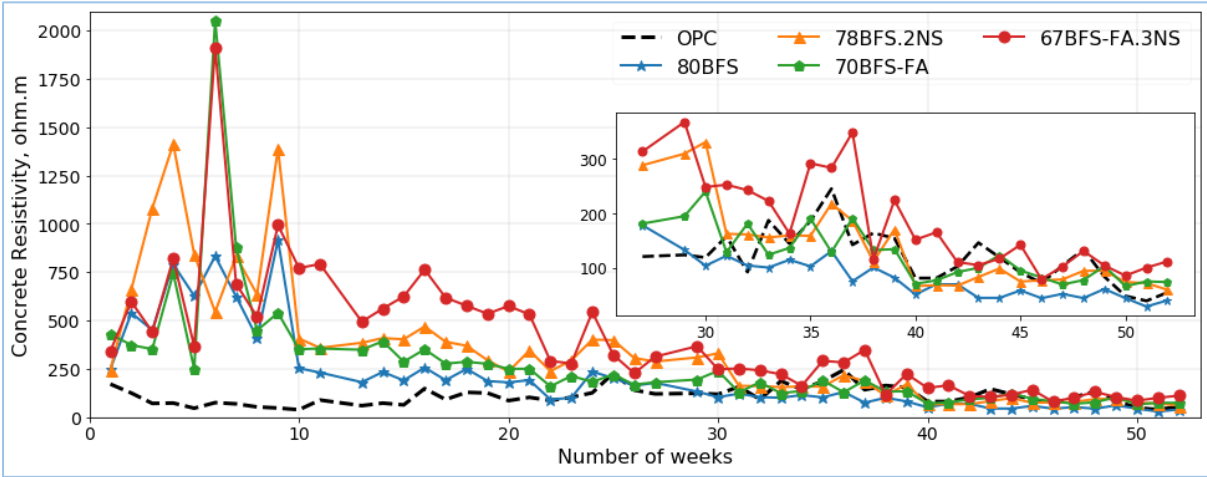
52 showing in **Fig. 8.4c**. Surprisingly, both HVS and HVS-FA concretes showed better resistivity than the OPC concrete up to 32 weeks and the HVS-FA concrete containing 70% BFS-FA blend had similar resistivity to OPC mix (**Fig. 8.4c**). Similar to corrosion rate, the NC addition in both HVS and HVS-FA concretes promotes concrete resistivity overwhelmingly from the first week of test and kept continued up to 52 weeks of the test. It can also be seen that the concrete mix 69BFS-FA.1NC exhibited better resistivity than the 69BFS.1NC concrete at early stage of corrosion test followed by almost similar concrete resistivity, the observation is consistent with the corrosion rate results. The better concrete resistivity of those concretes containing NC than their counterparts without NC can be interpreted to the formation of additional hydration products e.g., CSH through pozzolanic reaction and enhanced hydration reaction due to the presence of NC due to continuous wet-dry cycle as well as pores filling effect of nano NC.



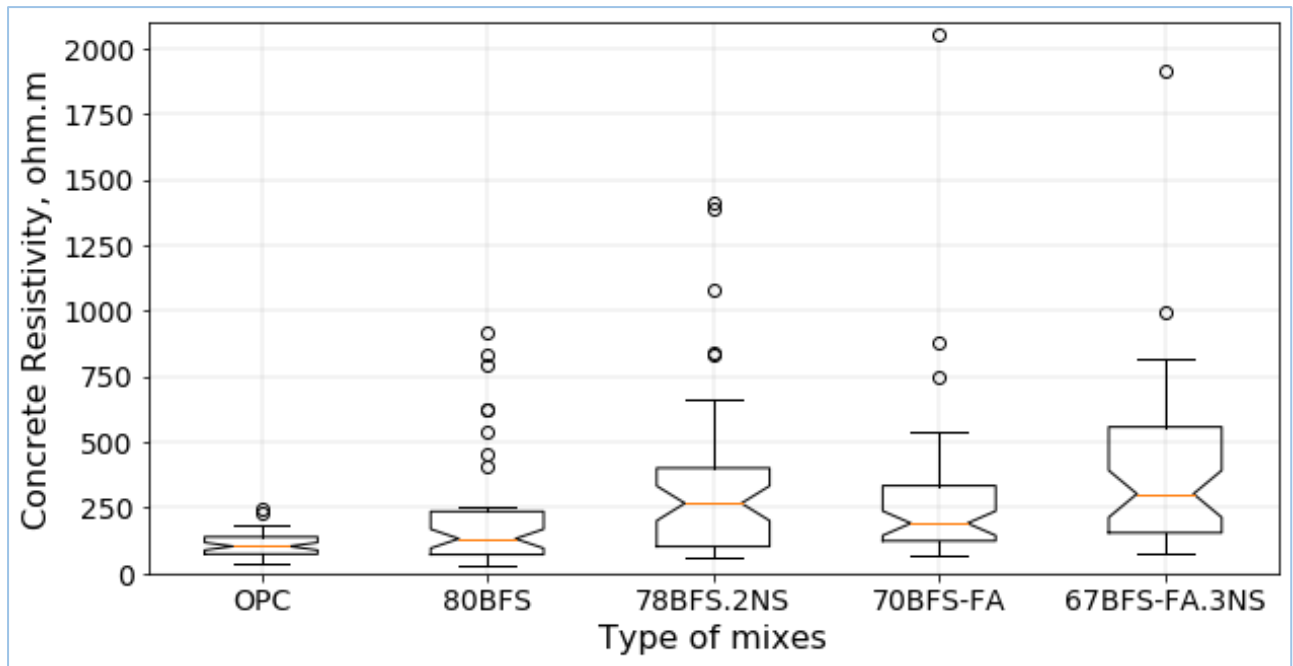
(a) Corrosion rate of OPC, HVS and HVS-FA concrete with and without nano-SiO<sub>2</sub> inclusion



(b) Box-whisker plot of corrosion rate data of OPC, HVS and HVS-FA concrete with and without nano-SiO<sub>2</sub>



(c) Concrete resistivity of OPC, HVS and HVS-FA concretes with and without nano-SiO<sub>2</sub> inclusion



(d) Box-whisker plot of concrete resistivity of different concrete mixes with and without nano-SiO<sub>2</sub> inclusion

**Fig. 8.5** Corrosion rate and concrete resistivity of different concrete mixes with and without nano-SiO<sub>2</sub>

### 8.3.2.2 Effect of nano silica

**Figs. 8.5a-d** present the corrosion rate and concrete resistivity of HVS and HVS-FA concretes with and without NS addition exposed to accelerated corrosion regime for 52 weeks. In contrast to the 70BFS concrete mix (discussed in section 8.3.2.1.), the corrosion rate of HVS concrete containing 80% BFS is significantly higher than the OPC and slightly higher than the 70BFS-FA concrete which can be seen in **Fig. 8.5b**. However, the addition of 2% NS in 80BFS concrete reduced the rate of corrosion considerably and maintain lower corrosion rate than the control OPC concrete up to 18 weeks of corrosion test and then exhibited similar corrosion at later ages which can be observed in box whisker plot in **Fig. 8.5b**. Similarly, the 3% NS addition in HVS-FA concrete control the corrosion of reinforcement and showed lower corrosion than the OPC concrete up to 30 weeks followed by similar corrosion in rest of the weeks. However, the average corrosion rate of 67BFS-FA.3NS concrete is considerably lower than the ordinary concrete which can be witnessed from **Fig. 8.5b**.



The effect of NS inclusion on the concrete resistivity of HVS and HVS-FA concretes is demonstrated in **Figs. 8.5c-d** with an inset picture from 25 weeks in **Fig. 8.5c**. It can be seen that both HVS and HVS-FA concretes exhibited higher resistivity than the OPC concrete up to 31 weeks of test and then lowered down to the rest of the time of the test. Likewise, NS addition in both HVS and HVS-FA concretes improved the concrete resistivity significantly up to 30<sup>th</sup> week and then showed similar resistivity to OPC concrete up to 52 weeks. This could be due to accelerated hydration of NS in early ages.

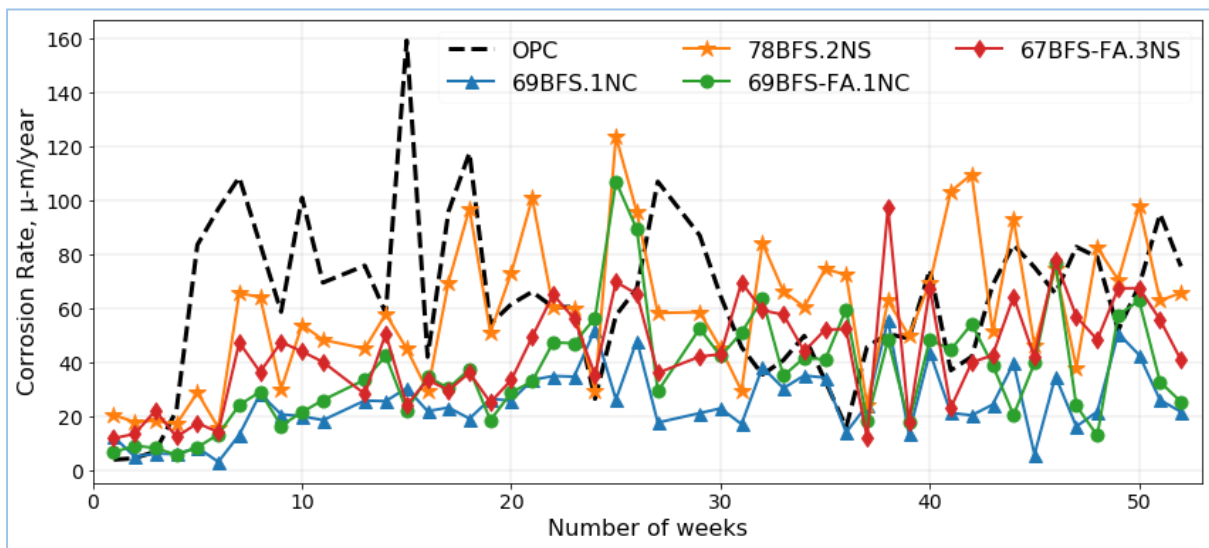


**Fig. 8.6** Comparison of corrosion rates of HVS and HVS-FA concrete mixes with nano materials

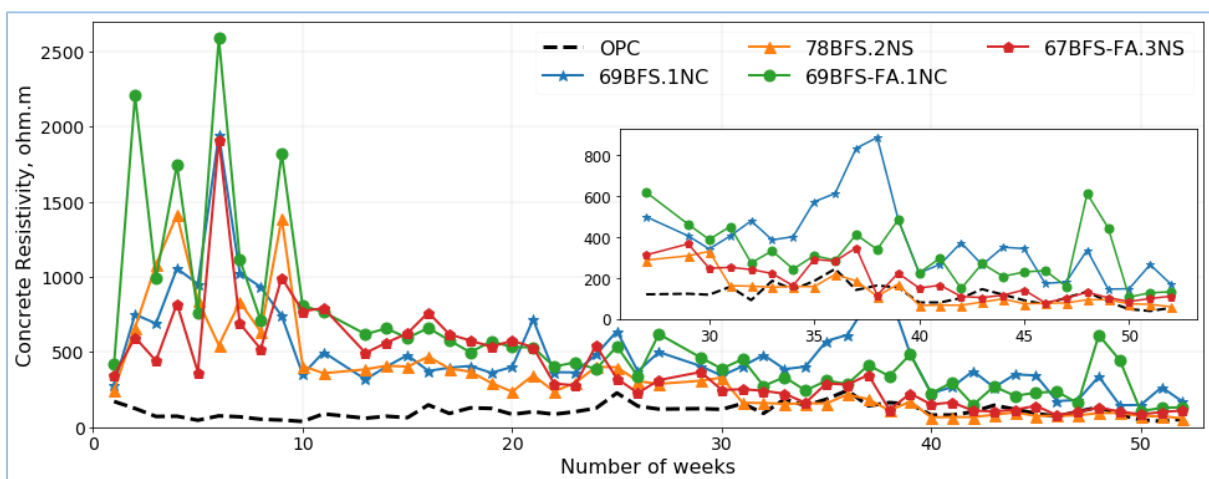


**Fig. 8.7** Comparison of concrete resistivity of OPC, HVS and HVS-FA concrete with nano materials

### 8.3.2.3 Performance against corrosion of concretes containing nano materials

**Fig. 8.6** shows the comparison of corrosion rate among all HVS and HVS-FA concretes containing nano materials along with control OPC concrete. As discussed earlier that the addition of NC and NS lowered the corrosion rate of HVS and HVS-FA concretes. Among them the mixes with NC inclusion showed comparatively better performance against corrosion than the mixes with NS addition even with a required higher dosage of NS recommended in the earlier study (Faiz Uddin Ahmed Shaikh & Hosan, 2019). This demonstrates that NS's effect on the hydration of high volume (>60%) supplementary cementitious materials diminished with time. Among both mixes with NC, the 69BFS.1NC mix displayed comparatively superior performance against corrosion and revealed a similar contribution to the compressive strengths discussed earlier in section.

In the case of concrete resistivity, significant improvement is showed by all HVS and HVS-FA concretes up to the 30<sup>th</sup> week due to the addition of NC and NS. However, the resistivity of mixes with NS is weakened yet exhibited similar or in some cases better resistivity than the OPC concrete as can be seen in the inset of **Fig. 8.7**. Among both HVS and HVS-FA concretes with NC, the 69BFS.1NC again showed extremely greater resistivity than all concrete mixes used in this study. This could be the reason for additional hydration products fill the larger capillary pores and formed a compact micro-structure (Hosan & Shaikh, 2020).

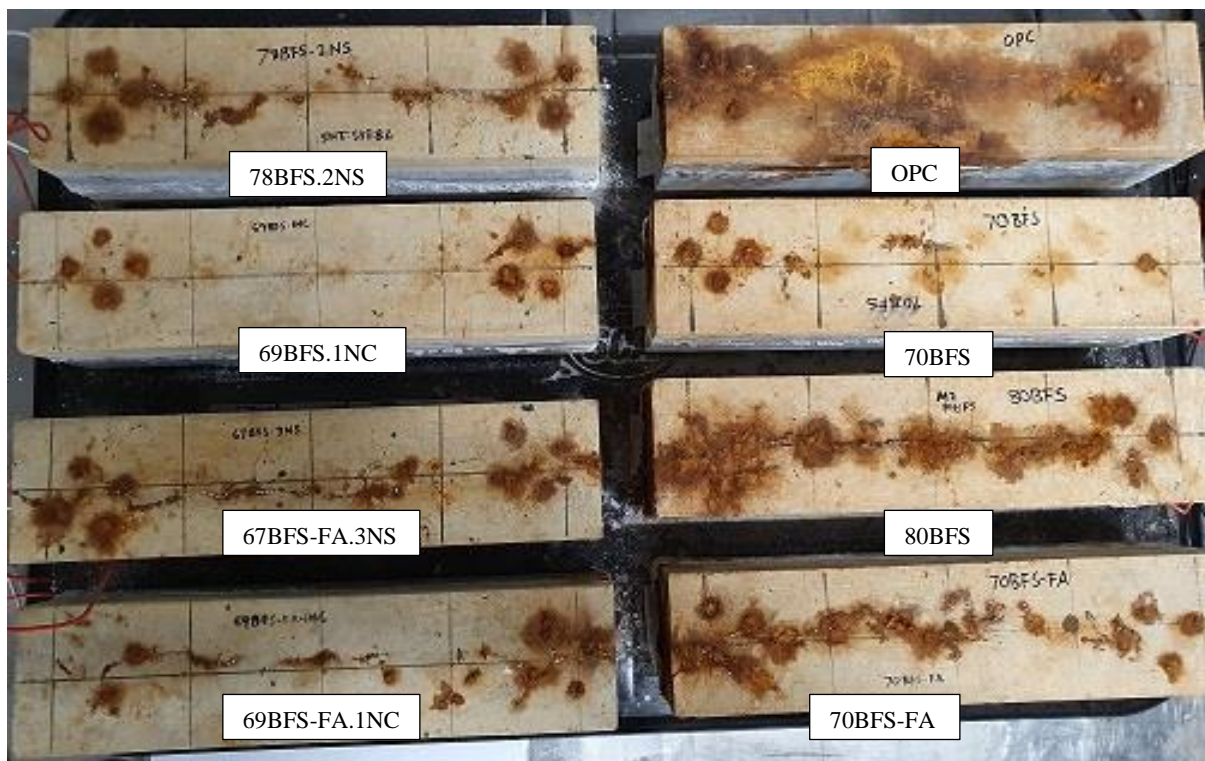
**Table 8.1** Mass loss of rebar of different concrete mixes after 52 weeks of accelerated corrosion test

Mix ID	Average initial mass (g)	Average final mass (g)	Average mass loss (g)	Actual mass loss (g/cm <sup>2</sup> )	Percentage of mass loss (%)	Week at first crack observed
OPC	307	255.5	51.5	3.8	16.8	7 <sup>th</sup>
70BFS	309.2	296	13.2	0.97	4.25	32 <sup>th</sup>
69BFS.1NC	306.9	299.5	7.4	0.54	2.40	38 <sup>th</sup>
80BFS	307.3	258.1	49.2	3.62	16.0	18 <sup>th</sup>
78BFS.2NS	310	290.1	19.9	1.47	6.45	23 <sup>rd</sup>
70BFS-FA	307.6	286.8	20.8	1.53	6.76	22 <sup>th</sup>
69BFS-FA.1NC	305.8	296.3	9.5	0.70	3.09	26 <sup>th</sup>
67BFS-FA.3NS	306.2	295.6	10.6	0.78	3.45	25 <sup>th</sup>

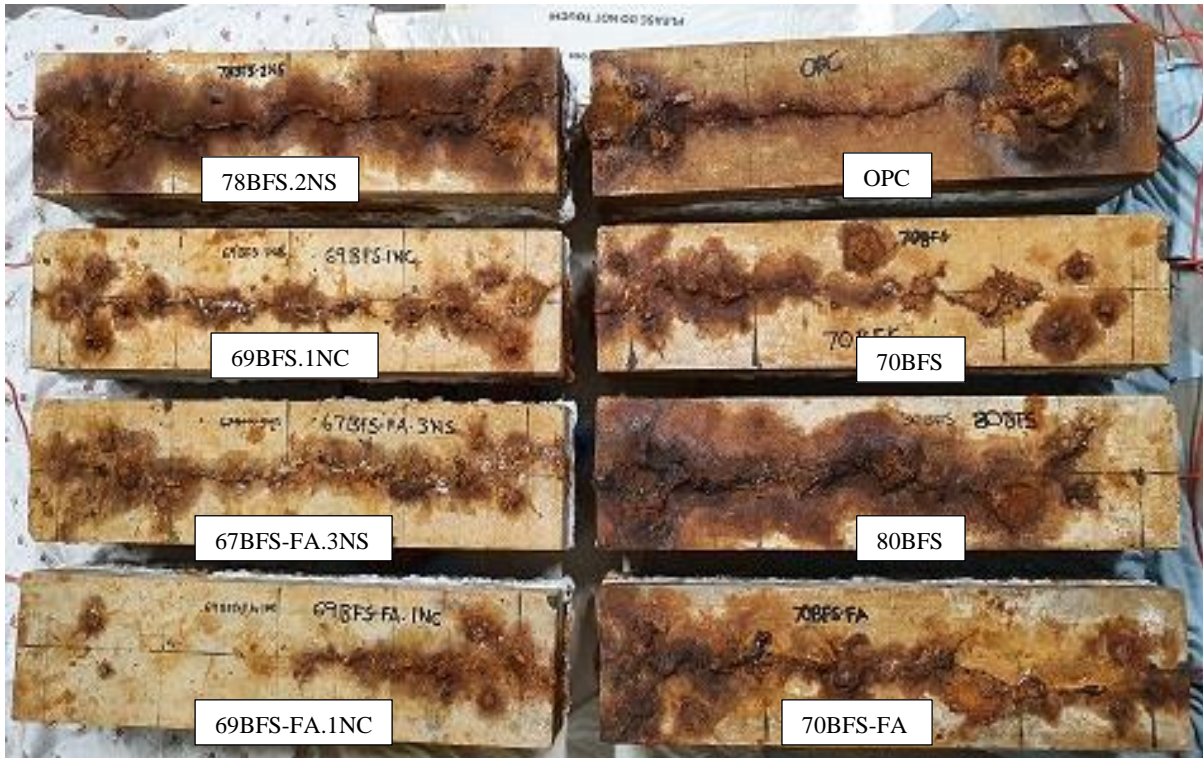
### 8.3.2.4 Visual Observation

#### 8.3.2.4.1 Corrosion induced cracking

**Figs. 8.8a-b** present the corrosion induced cracking of control OPC, HVS, and HVS-FA concretes with and without NC and NS addition after 26 weeks and 52 weeks of accelerated corrosion test. **Table 8.1** shows the first corrosion induced crack observed in different concrete mixes due to the corrosion of the reinforcement. Corrosion crack was first observed in OPC concrete at 7<sup>th</sup> week of accelerated corrosion test. Among all HVS and HVS-FA concrete without nano materials, first crack is formed in 80BFS, 70BFS and 70BFS-FA concretes at 18<sup>th</sup>, 32<sup>nd</sup> and 22<sup>nd</sup> week, respectively resembles the corrosion rate and concrete resistivity results. Moreover, the addition of NC and NS in HVS and HVS-FA concretes extends the time of first crack such as from 32<sup>nd</sup> to 38<sup>th</sup> for 69BFS.1NC concrete, from 22<sup>nd</sup> to 26<sup>th</sup> for 69BFS-FA.1NC concrete, from 18<sup>th</sup> to 23<sup>rd</sup> for 78BFS.2NS concrete and from 22<sup>nd</sup> to 25<sup>th</sup> for 67BFS.3NS concrete. It is also interesting to note that the first crack in both mixes with NC inclusion appeared last in this study. It can be seen that the cracks formation is directly related to the corrosion rate and concrete resistivity of their respective concrete mixes.

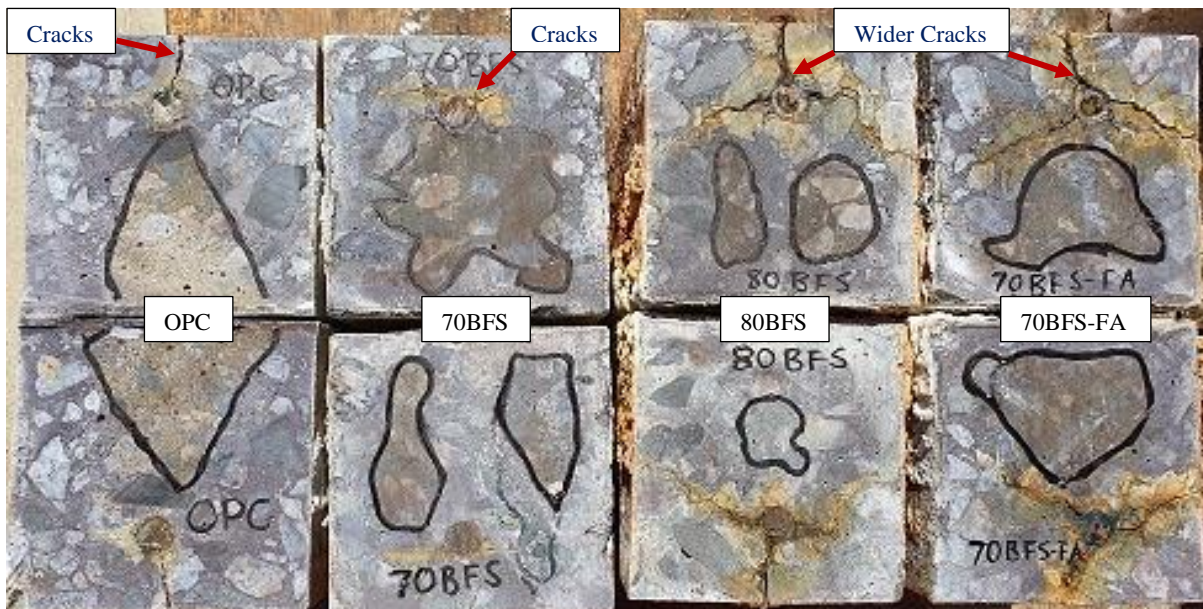


(a)

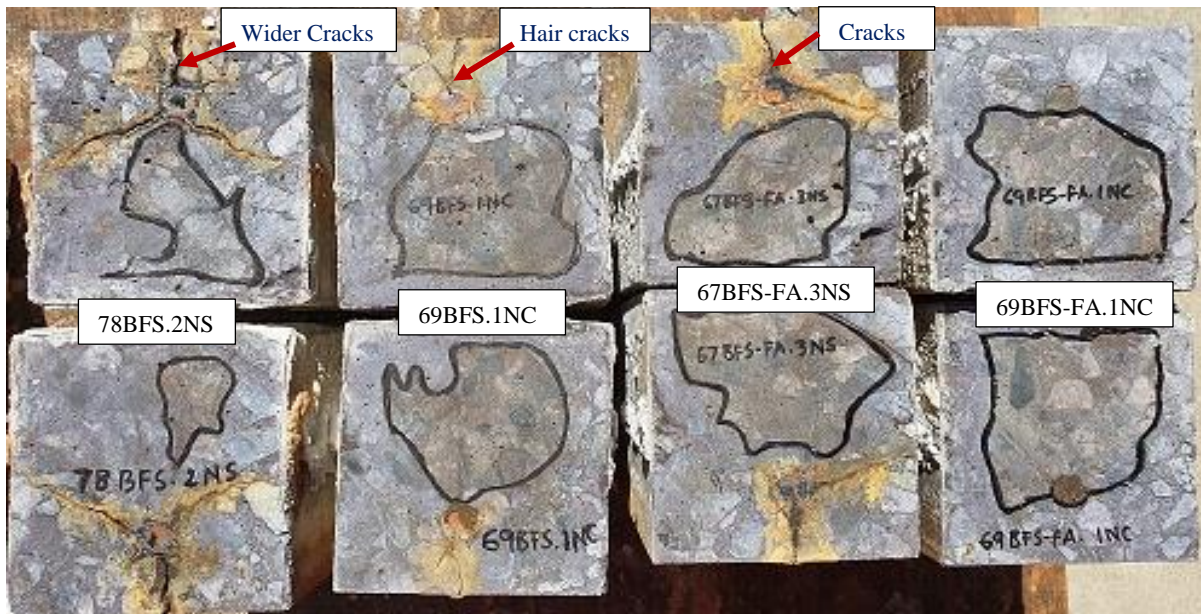


(b)

**Fig. 8.8** Concrete samples after (a) 26 weeks and (b) 52 weeks of accelerated corrosion test



(a) Chloride penetration of control OPC, HVS and HVS-FA samples after 52 weeks of accelerated corrosion test



(b) Chloride penetration of HVS and HVS-FA samples containing nano-SiO<sub>2</sub> and nano-CaCO<sub>3</sub> after 52 weeks of accelerated corrosion test

**Fig. 8.9** Chloride penetration of OPC, HVS and HVS-FA concrete mixes with and without nano materials addition

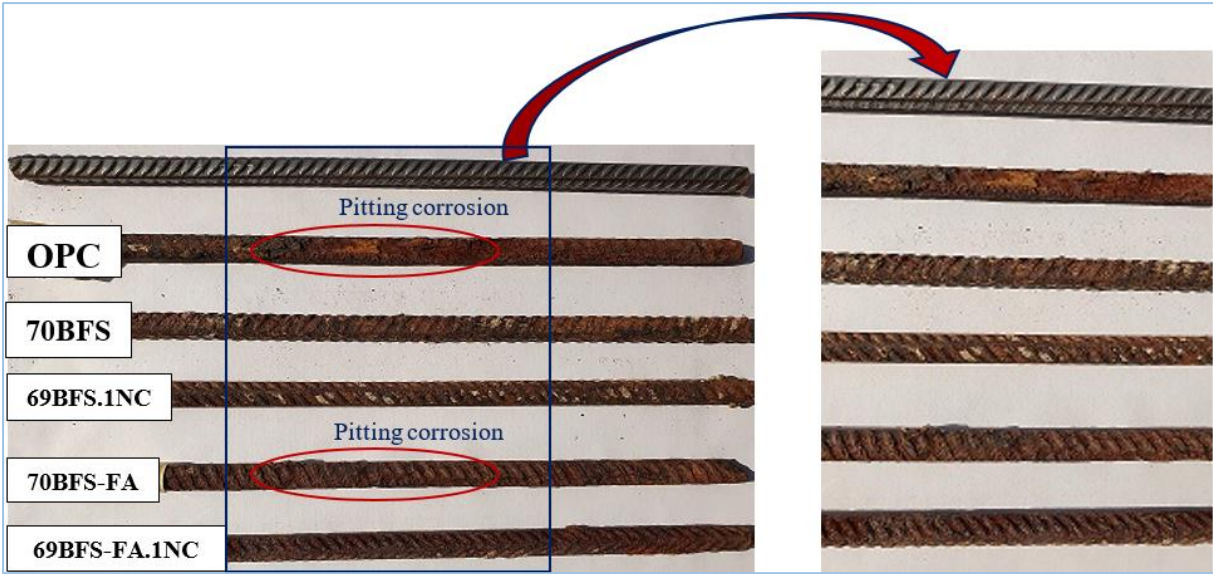
#### 8.3.2.4.2 Chloride penetration depth and cracks width

After 52 weeks of accelerated corrosion test, one sample from each concrete mix was cut in the middle and then sprayed with silver nitrate solution to observe the colour changes due to the chloride penetration into the samples. **Figs. 8.9a-b** show the concrete samples with and without nano materials inclusion after colour change due to chloride penetration. It can be seen from **Fig. 8.9a** that chloride penetration depth of HVS and HVS-FA concretes is generally bigger than the control OPC concrete, except the 70BFS concrete specimen whose chloride penetration depth is very similar to the control OPC concrete specimen. However, the chloride penetration depth is reduced due to the addition of NC and NS into the HVS, and HVS-FA concretes which can be seen in **Fig. 8.9b**. Among all HVS and HVS-FA samples with nano materials addition, as expected samples with NC showed smaller penetration depth than the OPC and HVS and HVS-FA concretes containing NS. Opposing to the above discussion, the 69BFS-FA.1NC showed lower chloride penetration depth and surprisingly, 67BFS-FA.3NS had similar chloride penetration depth of 69BFS-FA.1NC concrete mix.

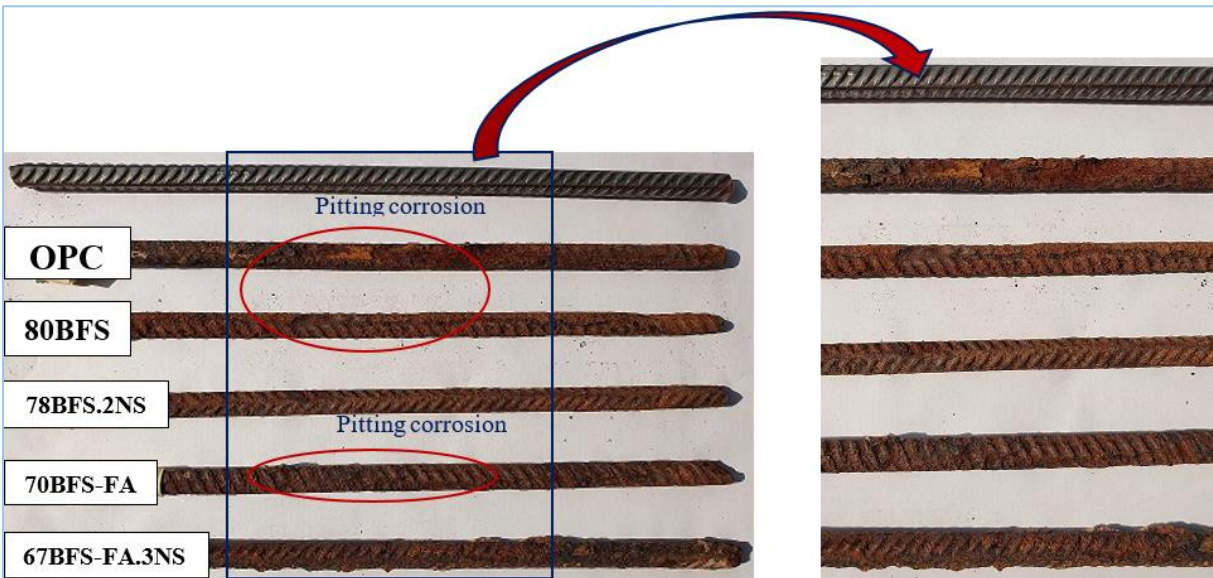
On the other hand, crack formed due to the corrosion of steel can also be seen in **Figs. 8.9a-b**. It is clear that among all control samples the 70BFS had fewer and narrower crack whereas the 80BFS and 70BFS-FA concretes had wider cracks. It is also noticeable that NC and NS addition limit the width of the cracks presumably due to lower corrosion rate than their corresponding control concretes. Similar to the chloride penetration depth result, there are no crack formed in the 69BFS-FA.1NC concrete while there are few hair cracks observed in this concrete. However, the NS inclusion in the HVS concrete did not show any noticeable improvement but a reasonable advancement can be seen in the HVS-FA mix in terms of smaller width of the cracks.

#### **8.3.2.4.3 Corrosion of reinforcement**

Corrosion of steel bars in all concretes specimens exposed to chloride induced corrosion for 52 weeks along with a non-corroded steel bar before the test is shown in **Figs. 8.10a-b**. It is clear from the images that the steel bar in the OPC had higher overall corrosion and pitting corrosion in some locations. The HVS and HVS-FA concrete specimens also show signs of corrosion in the rebar specially in 70BFS-FA sample where pitting corrosion can also be seen. However, the NC inclusion showed a significant improvement with no visible pitting corrosion in both 69BFS.1NC and 69BFS-FA.1NC specimens. On the other hand, the 80BFS sample showed slightly higher corrosion of steel than 70BFS-FA samples shown in **Fig. 8.10b**. Nevertheless, NS addition in both samples improved resistance against corrosion with a lower degree of deterioration of steel bar than their counterpart concretes without NS addition. The actual mass loss of rebar used in different concrete mixes can be seen in **Table 8.1** which is directly related to the deterioration of the steel reinforcement discussed above. Control OPC concrete specimen had greater actual mass loss with 3.8 g/cm<sup>2</sup> (16.8%) compared to 0.97 (4.25%), 3.62 (16%), and 1.53 g/cm<sup>2</sup> (6.76%) in 70BFS, 80BFS and 70BFS-FA concretes, respectively. The inclusion of NC and NS had a significant impact on reducing the deterioration of rebar in HVS and HVS-FA concretes with a much lower level of actual mass loss than their corresponding concretes without nano materials addition such as reducing from 4.25% to 2.40% in 69BFS.1NC, 16% to 6.45% in 78BFS.2NS, 6.76% to 3.09% in 69BFS-FA.1NC and 6.67% to 3.45% in 67BFS-FA.3NS concrete mixes. The 78BFS.2NS concrete had a higher degree of reduction of mass loss, but still show a greater percentage of mass loss among all the concrete mixes containing nano materials. Overall, from the above discussion of visual observation, it is clear that nano materials addition in HVS and HVS-FA concretes reduced the corrosion of steel bar.

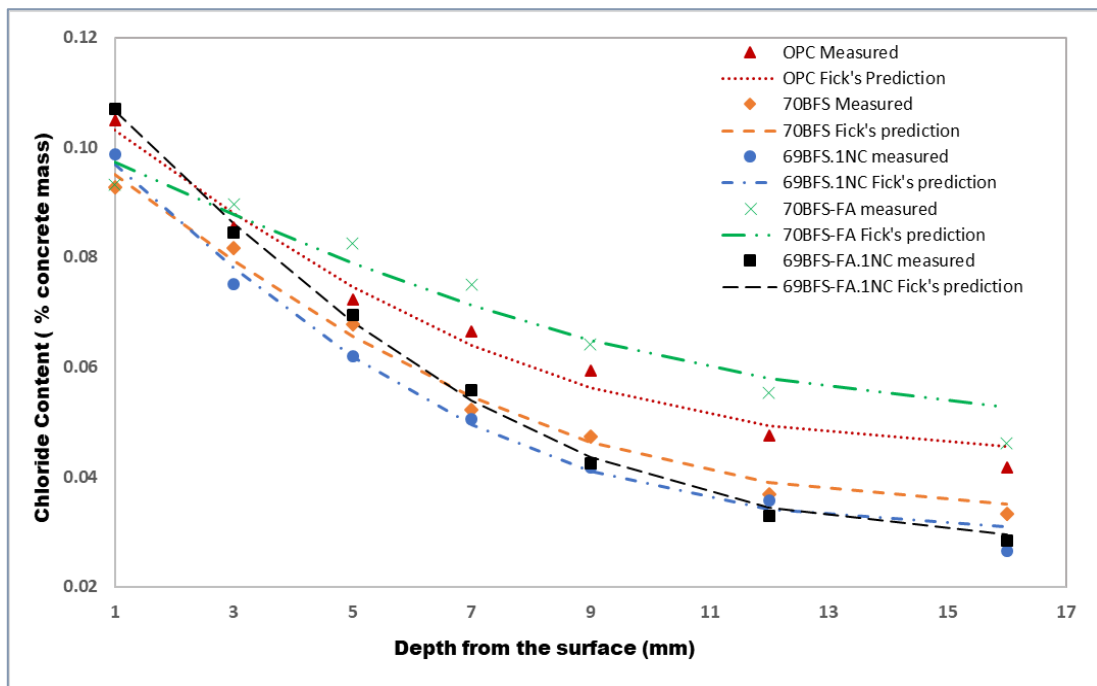


(a)

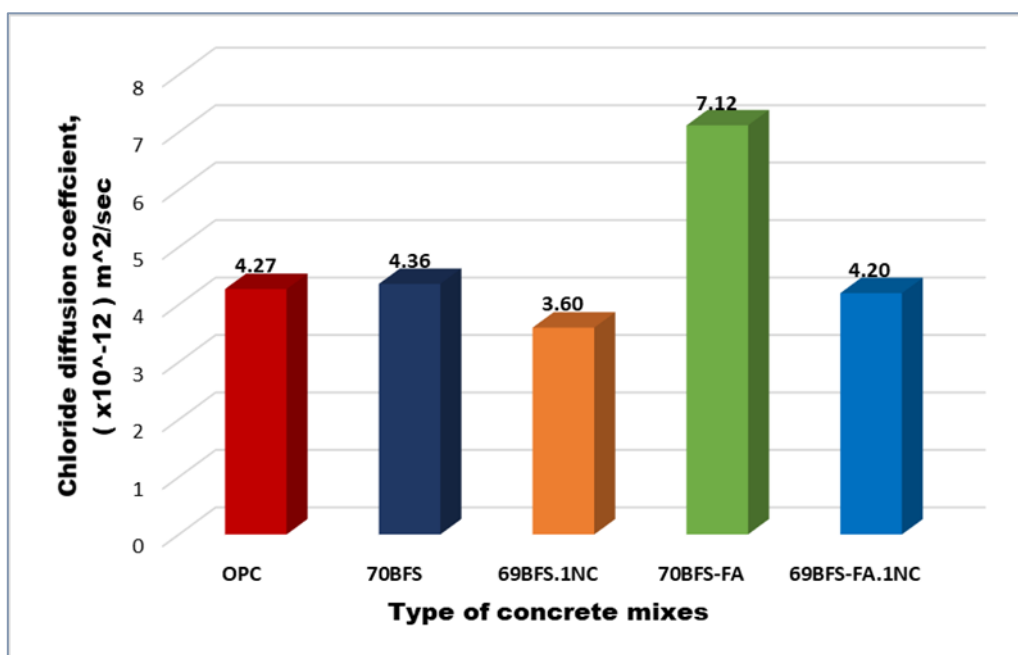


(b)

**Fig. 8.10** Deterioration of rebars of control OPC concrete and HVS and HVS-FA concrete with and without (a) nano-CaCO<sub>3</sub> (b) nano-SiO<sub>2</sub> inclusion



(a)



(b)

**Fig. 8.11** (a) Acid soluble chloride content and (b) chloride diffusion coefficient of control OPC and HVS, HVS-FA concrete with and without nano- $\text{CaCO}_3$  inclusion

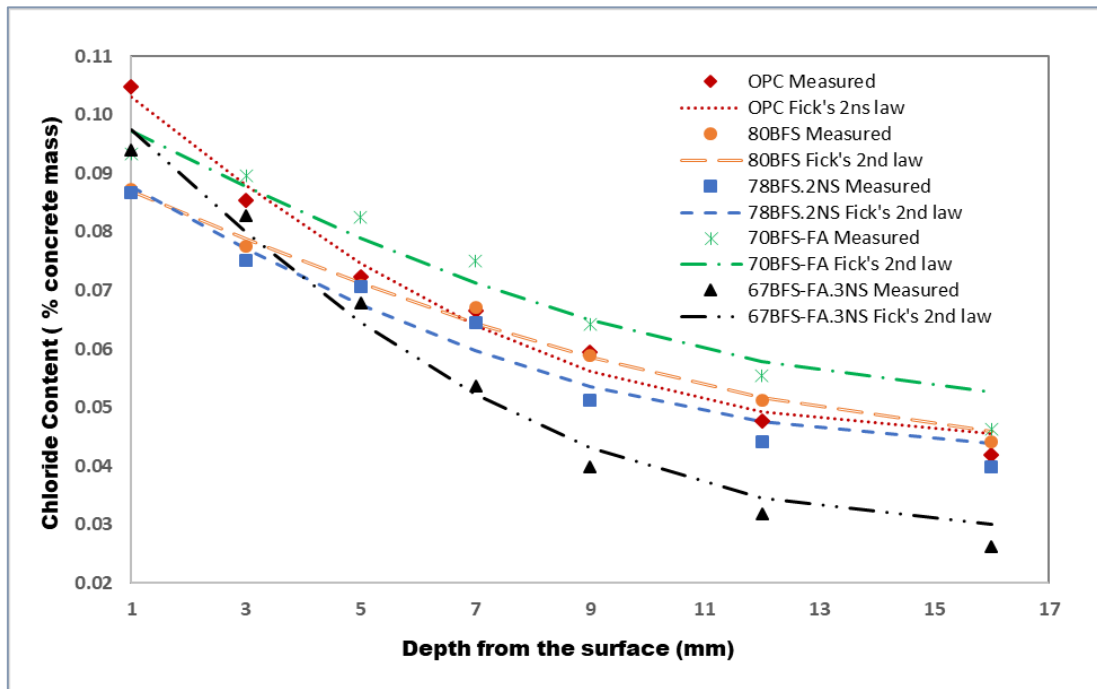


### **8.3.3 Chloride diffusion**

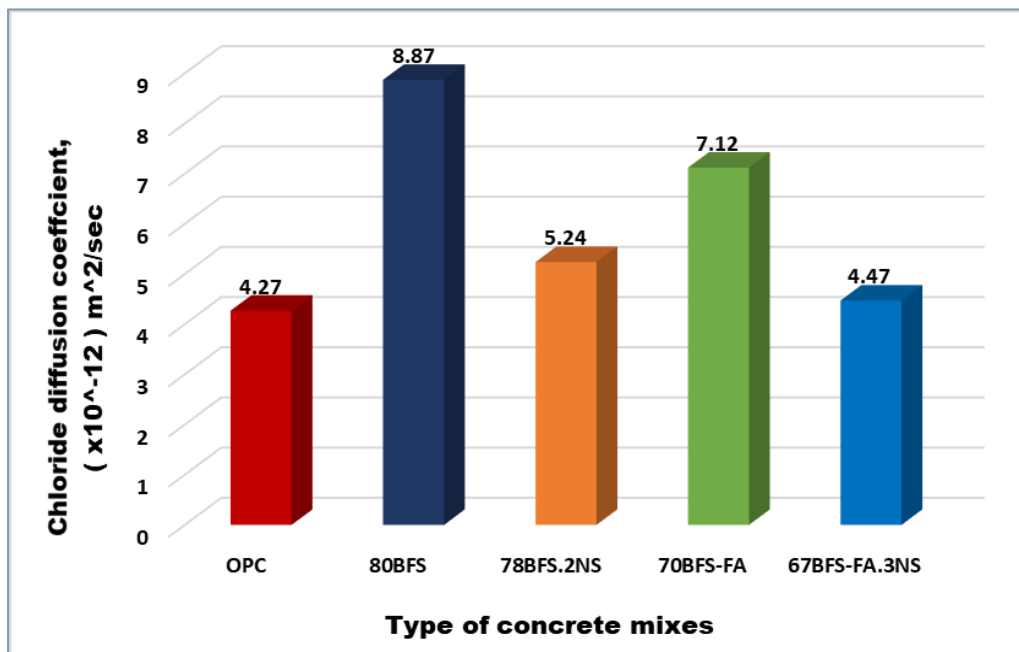
#### **8.3.3.1 Effect of nano calcium carbonate**

The acid soluble chloride content of different HVS and HVS-FA concretes with and without NC dosage along with control OPC concrete after 60 days exposure in NaCl solution is shown in **Figs. 8.11a-b**. The effect of 1% NC dosage in both HVS and HVS-FA concretes can be seen with a significantly lower concentration of chloride ion content with the increase in depth of the sample than that of the control OPC, HVS and HVS-FA concrete (Fig. 8.11a). It is also evident that the surface chloride content of HVS and HVS-FA concrete with NC were much higher than their counterpart control concretes. Based on the experimental data, it is evident that HVS and HVS-FA concrete containing NC exhibited greater resistance to chloride penetration due to the enhanced pozzolanic reaction of a higher volume of slag and fly ash after 28 days of curing. It can also be comprehended that experimental data were in good agreement with the predicted profiles derived from Fick's second law.

The effect of NC addition in chloride diffusion coefficients of different concrete mixes can be seen in Fig. 8.11b. It can be witnessed that the HVS and HVS-FA concretes with NC showed greater resistance to chloride diffusion by reducing chloride diffusion coefficient from  $4.36 \times 10^{-12} \text{ m}^2/\text{s}$  to  $3.6 \times 10^{-12} \text{ m}^2/\text{s}$  (17.4% reduction) and from  $7.12 \times 10^{-12} \text{ m}^2/\text{s}$  to  $4.2 \times 10^{-12} \text{ m}^2/\text{s}$  (41% reduction) of 69BFS.1NC and 69BFS-FA.1NC, respectively and showed better resistance than OPC concrete ( $4.27 \times 10^{-12} \text{ m}^2/\text{s}$ ). Contrasting to the previous study, the chloride diffusion coefficient of 70BFS and 70BFS-FA concretes are higher than OPC concrete though the replacement of slag and fly ash were up to 60% in past studies (Berndt, 2009; Dhir et al., 1996; Nath et al., 2018; Shaikh & Supit, 2015). Hence, it is clear that the chloride diffusion coefficient is increased with the increasing content of slag and fly ash when the replacement level is above 60%. This could be the cause of higher porosity and lower compactness of concrete samples due to the slow hydration of slag and fly ash particles when replacement level is more than 60% (Hosan & Shaikh, 2020). However, based on the results in this study, it can be seen that the NC addition is an effective way to reduce the chloride diffusion into the higher volume replacement of slag and slag-fly ash blended concretes.



(a)



(b)

**Fig. 8.12** (a) Acid soluble chloride content and (b) chloride diffusion coefficient of different concrete mixes with and without nano-SiO<sub>2</sub> addition.

### **8.3.3.2 Effect of nano silica**

**Fig. 8.12a** shows the percent of chloride content with the depth of the different HVS and HVS-FA concretes with and without NS addition as well as control OPC concrete after 60 days of exposure to NaCl solution. It can be seen that the chloride concentration of mixes containing NS is reduced with increase in depth than their corresponding control concretes and even than control OPC concrete. However, the reduction is more pronounced in HVS-FA concrete due to the NS inclusion than the HVS concrete could be the reason of 80% replacement of cement by BFS resulting lower degree of compactness and higher porosity which bear a resemblance to the results of the compressive strengths of the study. On the other hand, similar to the compressive strengths and corrosion results, the 67BFS.3NS concrete exhibited greater resistance to chloride penetration also showed a good correlation with the predicted profile derived from Fick's second law.

The chloride diffusion coefficient values of different concrete samples with and without NS addition are shown in **Fig. 8.12b**. It is evident that from the diffusion coefficient of 70BFS and 80BFS concretes that concrete with higher slag replacement (>60%) exhibited higher value of chloride diffusion coefficient. It can also be observed from the results that the concrete containing NS achieved greater resistance to chloride diffusion than their counterpart HVS and HVS-FA concretes. Furthermore, the inclusion of NS reduced the chloride diffusion coefficient of HVS and HVS-FA concrete by 41% and 37%, respectively. However, both mixes exhibited higher chloride diffusion coefficients than the ordinary control concrete.

### **8.3.3.3 Comparison of concretes containing nano materials**

The comparison of chloride diffusion coefficients of concrete mixes containing nano materials is presented in **Fig. 8.13**. It can be seen from the chloride diffusion coefficient data that the mixes with NC inclusion showed lower chloride diffusion coefficient than the mixes containing NS and the control OPC concrete. On the other hand, the 67BFS.3NS concrete exhibited comparable chloride diffusion coefficient while 78BFS.2NS had a 22% higher value of chloride diffusion coefficient to that of OPC concrete. This results also support the results of effects of NS and NC on compressive strengths and corrosion test of the respective concrete mixes. Among all concretes containing nano materials, the 69BFS.1NC showed greater resistance against chloride diffusion with about 15.7% lower value than the OPC concrete. Additionally, both HVS-FA mixes containing nano materials also showed considerably comparable resistance against chloride diffusion and consistent with the outcome of compressive strength and corrosion test results.

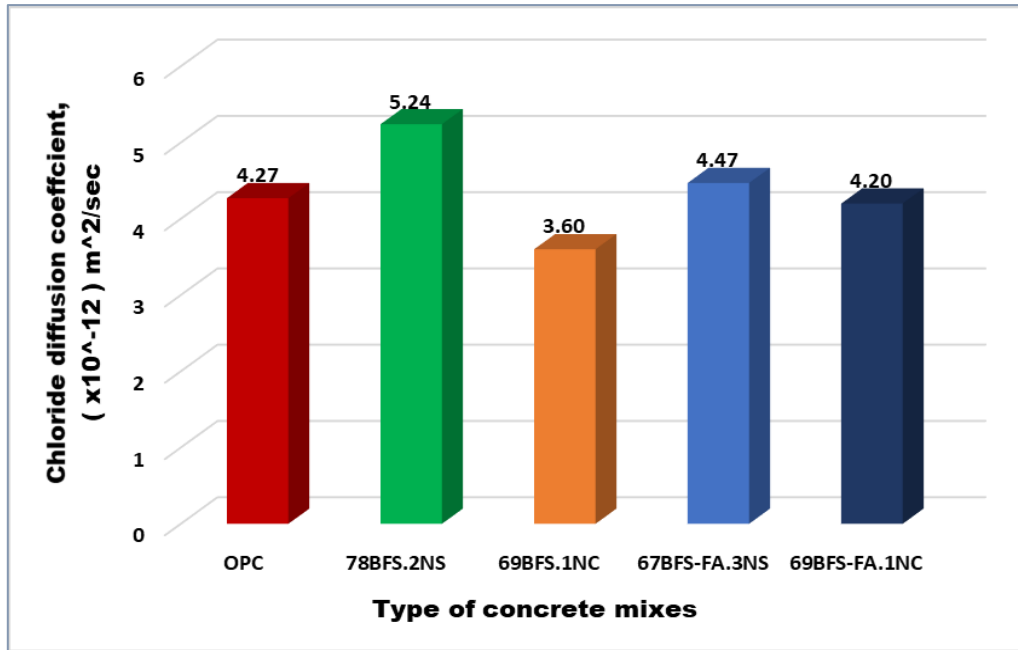
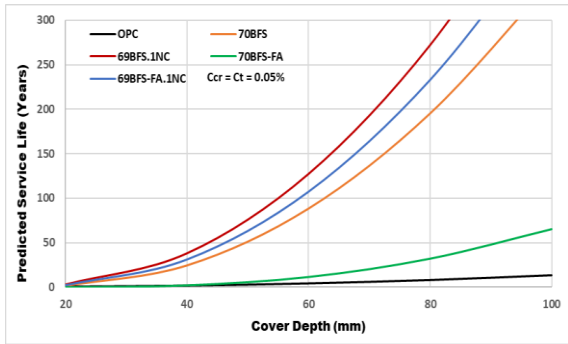


**Fig. 8.13** Comparison of chloride diffusion coefficient of control OPC and HVS, HVS-FA concretes containing nano-CaCO<sub>3</sub> and nano-SiO<sub>2</sub>

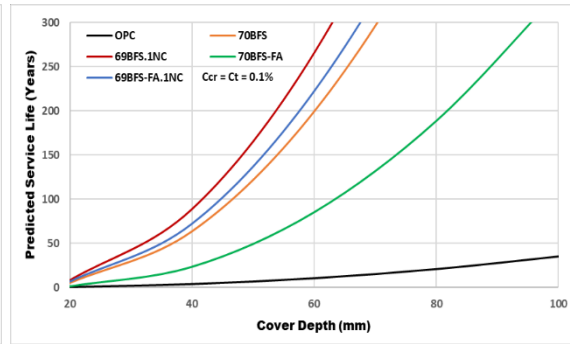
### 8.3.4 Service life

#### 8.3.4.1 Influence of nano calcium carbonate

The service life of different HVS, and HVS-FA concretes with and without NC including ordinary concrete in terms of various depths of clear cover predicted by model outlined in section 8.2.3.4. is presented in **Figs. 8.14a-b**. It can be seen from the graphs that the addition of 1% NC in both HVS and HVS-FA concretes increase the service life of both concrete mixes significantly than their corresponding control concretes. However, it is also evident that the service life of both HVS and HVS-FA concretes is much longer than the control concrete without NC addition for a similar clear cover of reinforcement and is more pronounced in 70BFS concrete. The effect of 1% NC addition in service life is more prominent in HVS-FA concrete with a higher increase ratio yet HVS concrete displayed longer service life for any depth of clear cover than the HVS-FA concrete. It can also be observed that by doubling the critical chloride level ( $C_{cr}$ ) from 0.05% to 0.1% the service life of a concrete mix is increased by more than 100% due to the addition of 1% NC. However, the increase in service life of HVS and HVS-FA concretes is higher than that of samples containing NC due to the rise of the critical chloride levels. Nevertheless, the total length of the service life of HVS and HVS-FA concretes containing NC is always higher than other concrete mixes investigated in this study for any particular depth of clear cover.

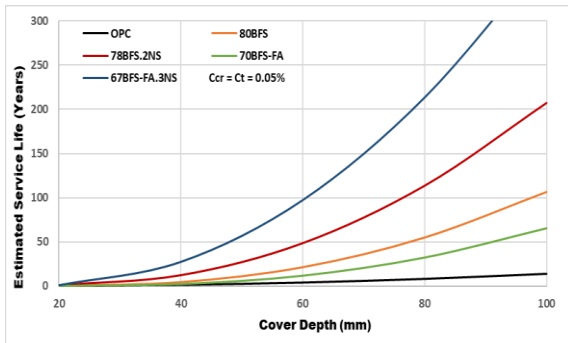


(a)

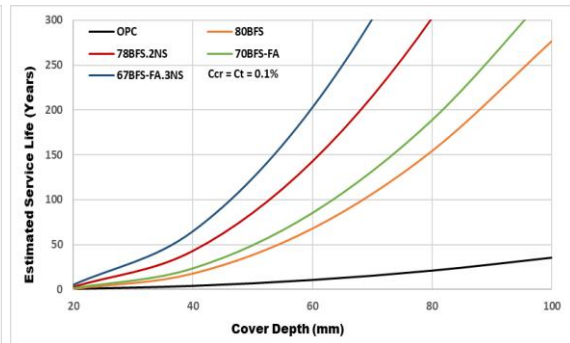


(b)

**Fig. 8.14** Estimated service life span of different concrete mixtures with and without nano- $\text{CaCO}_3$  when (a)  $C_t = 0.05\%$  (b)  $C_t = 0.1\%$

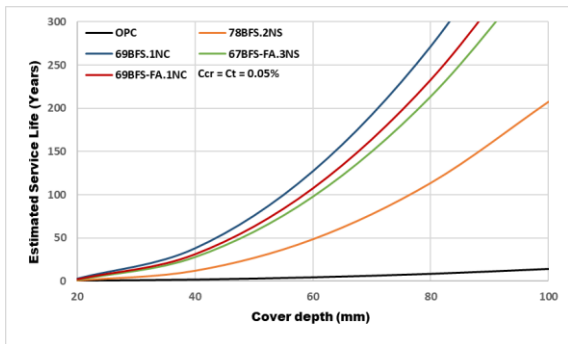


(a)

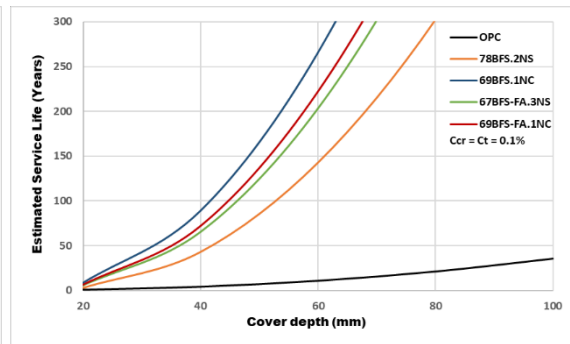


(b)

**Fig. 8.15** Estimated service life span of different concrete mixtures with and without nano- $\text{SiO}_2$  when (a)  $C_t = 0.05\%$  (b)  $C_t = 0.1\%$



(a)



(b)

**Fig. 8.16** Comparison of service life span of different concrete mixtures with the addition of nano- $\text{CaCO}_3$  and nano- $\text{SiO}_2$  along with control OPC concrete when (a)  $C_t = 0.05\%$  (b)  $C_t = 0.1\%$

#### **8.3.4.2 Influence of nano silica**

The predicted service life of different concrete mixes with and without NS addition for a number of clear cover of reinforcement is shown in **Figs. 8.15a-b** with the assumption defined in section 8.2.3.4. and is compared with control OPC concrete. The effect of NS inclusion in the HVS and HVS-FA concretes is clearly evident from the graphs with longer service life than their counterpart concretes without NS for any depth of clear cover. Surprisingly, the concrete mix containing 80% BFS showed longer service life than the 70BFS-FA and OPC concretes when critical chloride level is 0.05% contrasting to the values of chloride diffusion coefficient. However, by doubling the  $C_{cr}$  value from 0.05% to 0.1%, the required clear cover depth is decreased for a particular service life of concrete mix and it is more definite in the mixes containing NS. Comparing both HVS and HVS-FA concretes containing NS, the 3% addition of NS into BFS-FA concrete exhibited longer service life than 2% NS in HVS concrete. Nonetheless, both HVS and HVS-FA concretes revealed a significant increase in service life than all control mixes including OPC concrete due to the addition of NS.

#### **8.3.4.3 Influence comparison between nano materials**

**Figs. 8.16a-b** present the variations of predicted service life based on the assumptions made by the model described in section 8.2.3.4. of concrete mixes containing NC and NS as well as control OPC concrete. Once again concrete mix 69BFS.1NC revealed an extremely longer predicted service life than any other mix containing nano materials including OPC concrete. Furthermore, the HVS-FA concrete containing NC and NS exhibited almost similar service life for a particular clear cover of reinforcement. Besides, consistent with the earlier results the concrete mix 78BFS.2NS also slightly underperformed in the service life than other mixes containing nano materials. The effects of an increase of critical chloride level  $C_{cr}$  for all HVS and HVS-FA concretes containing nano materials can be observed in **Table 8.2** for a particular cover depth. It can be seen that for 50 mm clear cover, the estimated service life of mixes containing nano materials is almost doubled for critical chloride level increased from 0.05% to 0.1% which is also evident for 75 mm clear cover depth of reinforcement. It is clearly revealed that concrete with NC performed extremely well in terms of service life for a similar grade of concrete in the marine environment than concrete mixes containing NS. However, the service life of both HVS and HVS-FA concretes is increased considerably than the control OPC concrete in the marine environment due to the NS addition. This is also another confirmation of the greater level of compactness of concrete mixes caused by enhanced hydration of high

volume of supplementary cementitious materials present in those mixes as a result of the addition of nano materials (NC and NS).

**Table 8.2** Chloride diffusion coefficient and service life of different concrete mixes

Mix ID	Cl diffusion coefficient, $D_a$ ( $\times 10^{-12} \text{m}^2/\text{s}$ )	Estimated service life at cover depth of 50 mm, years		Estimated service life at cover depth of 75 mm, years	
		Ccr = 0.05%	Ccr = 0.10%	Ccr = 0.05%	Ccr = 0.10%
OPC	4.27	3	7	7	18
70BFS	4.36	51	122	164	351
69BFS.1NC	3.60	76	164	230	458
80BFS	8.87	11	39	45	130
78BFS.2NS	5.24	27	85	94	257
70BFS-FA	7.12	6	49	26	158
69BFS-FA.1NC	4.20	63	136	197	387
67BFS-FA.3NS	4.47	57	125	180	358

#### 8.4 Summary

This chapter investigated the effect of nano calcium carbonate (NC) and nano silica (NS) on the early and later age compressive strengths, corrosion rate and concrete resistivity against corrosion, chloride diffusion and service life of high volume slag (HVS) and high volume slag-fly ash (HVS-FA) concretes. Based on the experimental results found in this research, the following calculations can be made.

- ✚ Addition of 1% NC in both HVS and HVS-FA concretes increased the compressive strengths significantly in early and later ages than their corresponding control concretes without NC. Both concrete exhibited higher compressive strengths than control OPC concrete in all curing ages up to 365 days.
- ✚ Improvement in compressive strength of HVS and HVS-FA concretes is observed than their counterpart control concretes in all ages due to the addition of 2-3% NS. However, concrete mix 78BFS.2NS showed marginally lower while 67BFS.3NS displayed superior compressive strengths than control OPC concrete.
- ✚ Noteworthy reduction of corrosion rate is observed in both HVS and HVS-FA concretes from first week to 52 weeks due to the addition of 1% NC than their respective control concretes and OPC concrete. Improvement of concrete resistivity is also found in HVS and HVS-FA concretes containing NC than their respective control concretes and control OPC concrete.
- ✚ Considerable reduction of corrosion rate and improvement of concrete resistivity are observed in the HVS and HVS-FA concretes in early weeks of tests and then showed

similar trend of control OPC concrete due to the inclusion of NS in both HVS and HVS-FA concretes.

- ✚ HVS and HVS-FA concretes with NC revealed lower corrosion induced damage, chloride penetration depth and mass loss of rebar than the HVS and HVS-FA concretes containing NS after the chloride induced corrosion test and presented superior performance than the control OPC concrete.
- ✚ Both HVS and HVS-FA concrete mixes with NC inclusion showed significantly greater resistance against chloride diffusion and lower chloride diffusion coefficient values than the OPC concrete. On the other hand, concrete mix 67BFS.3NS revealed higher resistance against chloride penetration and similar chloride diffusion coefficient to that of OPC concrete while 78BFS.2NS showed comparatively poorer performance against chloride diffusion.
- ✚ Service life of both HVS and HVS-FA concretes is almost doubled due to the inclusion of NC and NS than their respective control concretes for similar clear cover to the reinforcing steel. However, once again concrete mix 78BFS.2NS slightly underperformed than other concrete mixes containing nano materials.



## 8.5 References

- Alonso, M. C., Garcia Calvo, J. L., Sanchez, M., & Fernandez, A. (2012). Ternary mixes with high mineral additions contents and corrosion related properties. *Materials and Corrosion*, 63(12), 1078-1086.
- Association, P. C. (2002). Types and causes of concrete deterioration. Portland Cement Association: Skokie, IL, USA.
- ASTM G1 Standard Practice for Preparing, Cleaning, and Evaluating Corrosion Test Specimens.
- ASTM, Standard Test Method for Compressive Strength of Concrete Cylinders Cast in Place in Cylindrical Molds. 2015.
- ASTM, Standard Test Method for Corrosion Potentials of Uncoated Reinforcing Steel in Concrete.
- ASTM, Standard Test Method for Determining the Apparent Chloride Diffusion Coefficient of Cementitious Mixtures by Bulk Diffusion.
- Australia, S. (2018). Concrete structures. In AS 3600:2018 (pp. 259): Standard Australia.
- Australia, S., Aggregates and rock for engineering purposes Concrete aggregates, in AS 2758.1:2014 2014, Standards Australia.
- Australia, S., Portland and blended cements, in AS 3972-1997. 1997, Standard Australia.
- Australia, S., Supplementary cementitious materials for use with portland and blended cement Fly ash, in AS 3582.1-1998 1998, Standards Australia.
- Australia, S., Supplementary cementitious materials for use with portland and blended cement Slag - Ground granulated iron blast-furnace, in AS 3582.2-2001 2001, Standard Australia.
- Benhelal, E., Zahedi, G., Shamsaei, E., & Bahadori, A. (2013). Global strategies and potentials to curb CO<sub>2</sub> emissions in cement industry. *Journal of Cleaner Production*, 51(Supplement C), 142-161.
- Berndt, M. L. (2009). Properties of sustainable concrete containing fly ash, slag and recycled concrete aggregate. *Construction and Building Materials*, 23(7), 2606-2613.
- Cao, H.T. and B. Liana, Fly Ash Concrete In Marine Environments. CSIRO Research Report Bre, 2000.
- Dhir, R. K., El-Mohr, M. A. K., & Dyer, T. D. (1996). Chloride binding in GGBS concrete. *Cement and Concrete Research*, 26(12), 1767-1773.
- El-Chabib, H., & Syed, A. (2013). Properties of Self-Consolidating Concrete made with High volume of Supplementary Cementitious Materials. *Materials in Civil Engineering*, 25(11), 1579-1586.
- Elchalakani, M., Aly, T., & Abu-Aisheh, E. (2014). Sustainable concrete with high volume GGBFS to build Masdar City in the UAE. *Case Studies in Construction Materials*, 1, 10-24.

- Fick, A., On liquid diffusion. *Journal of Membrane Science*, 1995. 100(1): p. 33-38.
- Güneyisi, E., & Gesoğlu, M. (2008). A study on durability properties of high-performance concretes incorporating high replacement levels of slag. *Materials and Structures*, 41(3), 479-493.
- Güneyisi, E., Gesoglu, M., Al-Goody, A., & İpek, S. (2015). Fresh and rheological behavior of nano-silica and fly ash blended self-compacting concrete. *Construction and Building Materials*, 95, 29-44.
- Hooton, R. D. (2000). Canadian use of ground granulated blast-furnace slag as a supplementary cementing material for enhanced performance of concrete. *Canadian Journal of Civil Engineering*, 27(4), 754-760.
- Hosan, A., & Shaikh, F. U. A. (2020). Influence of nano-CaCO<sub>3</sub> addition on the compressive strength and microstructure of high volume slag and high volume slag-fly ash blended pastes. *Journal of Building Engineering*, 27, 100929.
- Hou, P.-k., Kawashima, S., Wang, K.-j., Corr, D. J., Qian, J.-s., & Shah, S. P. (2013). Effects of colloidal nanosilica on rheological and mechanical properties of fly ash–cement mortar. *Cement and Concrete Composites*, 35(1), 12-22.
- Jau, W. C., & Tsay, D. S. (1998). A study of the basic engineering properties of slag cement concrete and its resistance to seawater corrosion. *Cement and Concrete Research*, 28(10), 1363-1371.
- Jeong, Y., Park, H., Jun, Y., Jeong, J.-H., & Oh, J. E. (2015). Microstructural verification of the strength performance of ternary blended cement systems with high volumes of fly ash and GGBFS. *Construction and Building Materials*, 95, 96-107.
- Kawashima, S., Hou, P., Corr, D. J., & Shah, S. P. (2013). Modification of cement-based materials with nanoparticles. *Cement and Concrete Composites*, 36(Supplement C), 8-15.
- Kuder, K., Lehman, D., Berman, J., Hannesson, G., & Shogren, R. (2012). Mechanical properties of self consolidating concrete blended with high volumes of fly ash and slag. *Construction and Building Materials*, 34, 285-295.
- Li, G. (2004). Properties of high-volume fly ash concrete incorporating nano-SiO<sub>2</sub>. *Cement and Concrete Research*, 34(6), 1043-1049.
- Liu, M., Zhou, Z., Zhang, X., Yang, X., & Cheng, X. (2016). The synergistic effect of nano-silica with blast furnace slag in cement based materials. *Construction and Building Materials*, 126, 624-631.
- McNally, C., & Sheils, E. (2012). Probability-based assessment of the durability characteristics of concretes manufactured using CEM II and GGBS binders. *Construction and Building Materials*, 30, 22-29.
- Mehta, P. K. (1991). *Concrete in the Marine Environment*. London: CRC Press.
- Mehta, P. K. (2001). Reducing the environmental impact of concrete. *ACI Concrete International*, 23(10), 61-66.

- Nath, P., Sarker, P. K., & Biswas, W. K. (2018). Effect of fly ash on the service life, carbon footprint and embodied energy of high strength concrete in the marine environment. *Energy and Buildings*, 158, 1694-1702.
- Nazari, A., & Riahi, S. (2011). Splitting tensile strength of concrete using ground granulated blast furnace slag and SiO<sub>2</sub> nanoparticles as binder. *Energy and Buildings*, 43(4), 864-872.
- Oner, A., & Akyuz, S. (2007). An experimental study on optimum usage of GGBS for the compressive strength of concrete. *Cement and Concrete Composites*, 29(6), 505-514.
- Osborne, G. J. (1999). Durability of Portland blast-furnace slag cement concrete. *Cement and Concrete Composites*, 21(1), 11-21.
- Otsuki, N., S. Nagataki, and K. Nakashita, Evaluation of the AgNO<sub>3</sub> solution spray method for measurement of chloride penetration into hardened cementitious matrix materials. *Construction and Building Materials*, 1993. 7(4): p. 195-201.
- Pal, S. C., Mukherjee, A., & Pathak, S. R. (2002). Corrosion behavior of reinforcement in slag concrete. *ACI Materials Journal*, 99(6), 521-527.
- Ramezani-pour, A., & Malhotra, V. (1995). Effect of curing on the compressive strength, resistance to chloride-ion penetration and porosity of concretes incorporating slag, fly ash or silica fume. *Cement and Concrete Composites*, 17(2), 125-133.
- Rashad, A. M. (2015). An investigation of high-volume fly ash concrete blended with slag subjected to elevated temperatures. *Journal of Cleaner Production*, 93(Supplement C), 47-55.
- Rashad, A. M., El-Nouhy, H. A., & Zeedan, S. R. (2018). An Investigation on HVS Paste Modified with Nano-SiO<sub>2</sub> Imperilled to Elevated Temperatures. *Arabian Journal for Science and Engineering*, 43(10), 5165-5177.
- Riding, K.A., Early age concrete thermal stress measurement and modeling. 2007.
- Şahmaran, M., Keskin, S. B., Ozerkan, G., & Yaman, I. O. (2008). Self-healing of mechanically-loaded self consolidating concretes with high volumes of fly ash. *Cement and Concrete Composites*, 30(10), 872-879.
- Sengul, O., & Tasdemir, M. A. (2009). Compressive strength and rapid chloride permeability of concretes with ground fly ash and slag. *Journal of Materials in Civil Engineering*, 21(9), 494-501.
- Shaikh, F. U. A., & Hosan, A. (2019). Effect of nano silica on compressive strength and microstructures of high volume blast furnace slag and high volume blast furnace slag-fly ash blended pastes. *Sustainable Materials and Technologies*, 20, e00111.
- Shaikh, F. U. A., & Supit, S. W. M. (2015). Chloride induced corrosion durability of high volume fly ash concretes containing nano particles. *Construction and Building Materials*, 99, 208-225.
- Shaikh, F. U. A., Supit, S. W. M., & Sarker, P. K. (2014). A study on the effect of nano silica on compressive strength of high volume fly ash mortars and concretes. *Materials & Design*, 60(Supplement C), 433-442.

- Siddique, R. (2004). Performance characteristics of high-volume Class F fly ash concrete. *Cement and Concrete Research*, 34(3), 487-493.
- Thomas, M.D.A., et al., Performance of slag concrete in marine environment. *ACI Materials Journal*, 2008. 105(6): p. 628-634.
- Val, D. V., & Stewart, M. G. (2003). Life-cycle cost analysis of reinforced concrete structures in marine environments. *Structural Safety*, 25(4), 343-362
- Van den Heede, P., De Keersmaecker, M., Elia, A., Adriaens, A., & De Belie, N. (2017). Service life and global warming potential of chloride exposed concrete with high volumes of fly ash. *Cement and Concrete Composites*, 80, 210-223.
- Yeau, K. Y., & Kim, E. K. (2005). An experimental study on corrosion resistance of concrete with ground granulate blast-furnace slag. *Cement and Concrete Research*, 35(7), 1391-1399.
- Younsi, A., Turcry, P., Rozière, E., Aït-Mokhtar, A., & Loukili, A. (2011). Performance-based design and carbonation of concrete with high fly ash content. *Cement and Concrete Composites*, 33(10), 993-1000.
- Zementwerke, V. D. (2013). Global cement production from 1990 to 2030. Retrieved from <https://www.statista.com/statistics/373845/global-cement-production-forecast/>. Statista Research Department
- Zhang, M.-H., & Islam, J. (2012). Use of nano-silica to reduce setting time and increase early strength of concretes with high volume of fly ash or slag. *Construction and Building Materials*, 29, 573-580.
- Zhang, M.-H., Islam, J., & Peethamparan, S. (2012). Use of nano-silica to increase early strength and reduce setting time of concretes with high volumes of slag. *Cement and Concrete Composites*, 34(5), 650-662.

*All reasonable efforts have been made to acknowledge the authors of the copyright material. It would be highly appreciated if I can hear from any authors has been ignored or incorrectly acknowledged.*

## Chapter 9: Research findings and future recommendations

---

### 9.1 Review of the study

This research was conducted to study the effects of addition of nano silica (NS) and nano calcium carbonate (NC) on durability properties of high volume slag (HVS) and high volume slag-fly ash (HVS-FA) concretes. To accomplish the objectives, an optimum combination of NS or NC, blast furnace slag (BFS) and fly ash (FA) as a partial replacement of ordinary Portland cement were determined based on the 28 days compressive strengths of different mix proportions of HVS and HVS-FA pastes containing slag and slag-fly ash blends from 60% ~ 90% in the first part of the study. Microstructural investigation through mercury intrusion porosimetry (MIP), thermogravimetric analysis (TGA), x-ray diffraction analysis (XRD), scanning electron microscopy (SEM) and energy dispersive x-ray spectroscopy (EDS) of those HVS and HVS-FA pastes exhibited higher 28 days compressive strengths than the control have been studied to select the optimum content of materials for the next part of this research. In the second part of this research, the effects of optimum content of NS and NC on the early age and long term compressive strengths up to 180 days of HVS and HVS-FA concretes were examined. Durability related properties such as sorptivity, volume of permeable voids, rapid chloride permeability, drying shrinkage, chloride induced corrosion and chloride diffusion of HVS and HVS-FA concretes containing optimum content of NS or NC were also evaluated. Moreover, microstructural changes of interfacial transition zone (ITZ) of those HVS and HVS-FA concretes containing NS or NC were investigated through nanoindentation, SEM and EDS analysis and compared with the ordinary concrete and HVS and HVS-FA concretes without nano materials.

### 9.2 Main research findings

The following research findings can be summarised as the main achievements of this study on the effects of nano silica and nano calcium carbonate on the HVS and HVS-FA concretes.

#### *9.2.1 Effect of nano materials on high volume slag and high volume slag-fly ash blended pastes*

1. Compressive strengths of HVS paste containing 70%, 80% and 90% BFS improved by 9-25%, 11-29% and 17-41% due to the addition of 1-4% NS while the improvement were 8-24%, 1-16% and 2-20%, respectively with the 1-4% NC inclusion.

2. Addition of 1-4% NS in the HVS-FA paste containing blended mix of 49% BFS and 21% FA improved by 1-59% approximately and increased with the increasing content of NS. On the other hand, 16-24% improvement observed due to the addition of 1-4% NC in the same mix and maintained higher compressive strengths than control OPC paste. However, HVS-FA paste containing 80% BFS-FA (56% BFS and 24% FA) always had lower compressive strengths than control OPC paste even after NS or NC addition.
3. Large and medium capillary pores of HVS paste containing 70% and 80% BFS reduced significantly due to the addition of NS while NC addition reduced larger capillary pores only. Moreover, HVS-FA paste containing 70% BFS-FA blend showed a significant decrease in gel pores and medium capillary pores due to the addition of both NS and NC.
4. Reduction of  $\text{Ca}(\text{OH})_2$  in both HVS and HVS-FA paste exhibited due to the addition of NS and NC confirmed in thermogravimetric (TGA) analysis.
5. Slight reduction of intensity of calcium hydroxide peaks observed in both HVS and HVS-FA paste due to the addition of NS and NC found in XRD analysis. Moreover, increased content of ettringite (E), calcium silicate hydrate (C-S-H), calcium aluminate hydrate (C-A-H) and calcium carbonate are found due to the addition of NC in all HVS and HVS-FA pastes.
6. Incorporation of NS and NC densified the internal microstructure due to the early accelerated hydration and formation of new element revealed in SEM images and EDS trace analysis.
7. The optimum combination of NS/NC, 70-80% replaced BFS or BFS-FA composites could reduce the  $\text{CO}_2$  emission into the atmosphere by approximately 66-76% while maintaining similar or even better compressive strengths than control OPC concrete and create a sustainable green composites.
8. The 2% NS addition with 78% BFS in a HVS composites and 3% NS addition with 67% BFS-FA in a HVS-FA composites showed a best performance among all other mixes. On the other hand, 1% NC addition in both HVS and HVS-FA paste containing 69% BFS and 69% BFS-FA blended mix exhibited superior properties than other mixes containing NC.

### ***9.2.2 Effect of nano materials on durability properties and compressive strength development of high volume slag and high volume slag-fly ash blended concretes***

1. Significant improvement of compressive strengths of HVS concrete containing 78% BFS by 34% and 36% at 3 days and 28 days, respectively observed due to the addition of 2% NS and showed comparable strengths to control OPC concrete in the later ages. On the other hand, 3% NS addition into the HVS-FA concrete containing 67% BFS-FA blended mix improved compressive strengths by 45% at 3 days and exhibited significantly higher compressive strengths than control OPC concrete in all concrete ages.
2. Inclusion of 1% NC increased the compressive strengths of HVS concrete containing 69% BFS by 43% at 3 day than their corresponding control concrete without NC and exceed the strength of OPC concrete at 7 days of age and exhibited significantly higher compressive strength at later ages while HVS-FA concrete containing 69% BFS-FA blended mix showed 28% increased at 3 days and surpasses the strength of control OPC concrete at 28 days and displayed similar compressive strengths up to 180 days.
3. Substantial reduction of water absorption by around 27% and 36% of HVS concrete of 78% BFS due to 2% NS addition and by around 38% and 37% of HVS-FA concrete of 67% BFS-FA blended mix due to the 3% NS addition observed after 28 and 90 days of curing respectively. In addition, HVS concrete presented equivalent and HVS-FA concrete showed superior sorptivity values of those of OPC concrete in both ages due to the inclusion of 2% and 3% NS respectively. Correspondingly, around 1% and 10% drop of water absorption observed in HVS and HVS-FA concrete respectively, after 28 days of curing and reduction were greater after 90 days of curing in both HVS and HVS-FA concretes.
4. Marginal reduction of volume of permeable voids of HVS concrete by around 14% and 10% after 28 days and 90 days of curing respectively witnessed due to the 2% NS addition than their corresponding control concrete. However, VPV values were lower than control OPC concrete. Surprisingly, huge VPV reduction experimented by around 23% after 28 days of HVS-FA concrete and were considerably lower than traditional OPC concrete. Remarkably, a greater reduction of VPV found due to 1% NC addition of HVS and HVS-FA concrete by around 18% and 21% respectively than their control concrete without NC inclusion after 28 days of curing and reduction were further more on the samples of 90 days curing of both concretes.

5. Resistance against chloride ion penetration were significant in case of both HVS and HVS-FA concrete with or without NS addition than the control OPC concrete after both curing age. Reductions were around 47% after 28 days and 90 days of curing for HVS concrete while around 36% reduction detected after 90 days of curing of HVS-FA concrete. Meanwhile, around 14% and 22% of HVS concrete and by 39% and 45% of HVS-FA concrete reduction of passing charge experienced after 28 days and 90 days respectively due to the 1% NC inclusion. Furthermore, all HVS and HVS-FA concrete samples containing NS or NC showed very low category of passing charge according to ASTM standard.
6. Extraordinary resistance against drying shrinkage at early age showed by both HVS and HVS-FA concrete containing NS or NC and shrinkage strain were remarkably lesser than the OPC concrete in later ages of HVS-FA concrete of both nano materials. However, HVS concrete containing NS or NC did not performed well in later ages in terms controlling shrinkage though shrinkage were lower or similar to that of OPC concrete.
7. Considerable decrease of corrosion and improvement of concrete resistivity were observed in the HVS and HVS-FA concrete containing NS in the early weeks of corrosion monitoring up to 26 weeks and then exposed similar to that of control OPC concrete up to 52 weeks of observations. However, reduction of corrosion rate were noteworthy in case of HVS and HVS-FA concrete containing 1% NC from beginning to up to 52 weeks of observation. In addition, development of concrete resistivity against corrosion were also apparent in both HVS and HVS-FA concrete due to the addition of NC than their corresponding control concrete without NC and OPC concrete.
8. Both HVS and HVS-FA concrete containing 1% NC displayed significantly lower damage due to the corrosion of reinforcement, depth of chloride penetration and mass loss of reinforcement than the concrete with NS and exhibited exceedingly superior performance than the traditional OPC concrete.
9. Tremendous resistance against chloride diffusion and approximately 17% and 41% lower diffusion coefficient than the corresponding control concrete were found in the HVS and HVS-FA concrete respectively, due to the inclusion of 1% NC. On the other hand, NS addition into the HVS-FA concrete resulted higher resistance against chloride penetration and similar diffusion coefficient to that of OPC concrete despite the fact that HVS concrete did not performed well against chloride diffusion.



10. Service life of all HVS and HVS-FA concretes were almost doubled due to the addition of nano materials except HVS concrete containing 78% BFS which was slightly underachieved than other HVS and HVS-FA concrete with NS or NC.
11. The addition of NS and/or NC improved the ITZ of HVS and HVS-FA concretes exhibited higher modulus and hardness than their corresponding control concrete and OPC concrete. The width of the ITZ were reduced due to the inclusion of NS or NC by formation of new and additional C-S-H and filling the pores of the composites.
12. A higher degree of dense and compacted ITZ of HVS and HVS-FA concretes containing NS or NC than the HVS and HVS-FA concrete without nano materials and even OPC concretes observed through higher magnified SEM images and higher peaks of Ca and Si found in EDS analysis indicating additional C-S-H gel in the concrete composites.

### **9.3 Recommendations for future study**

From the above concluded remarks, it is obvious that NS or NC addition enhanced the improvement of the early strengths as well later age strengths of HVS and HVS-FA concrete. Moreover, NS and NC addition helped to improve the durability properties and micro structural changes to make denser microstructure of HVS and HVS-FA concretes. However, some recommendations for future study on this topic are added as follows:

- In this study, effect of an individual nano materials such NS or NC on the properties of HVS and HVS-FA concretes have been studied. It is recommended to study the combine effect of NS and NC as it is evident that NS enhanced the hydration properties while NC mostly works as a filler of the very fine pores of the composites. Moreover, to reduce the production cost of the concrete, effect of micro calcium carbonate (2 -4 microns) can be studied as individually and/or as a blended material with NS and NC.
- In this study only the compressive strengths at early and later ages were evaluated as mechanical properties of HVS and HVS-FA concretes. Other mechanical properties such as Elastic modulus, flexural strengths, tensile strengths etc. should be investigated to authenticate the outcome of this study.
- Other durability properties such as carbonation, alkali silica reaction (ASR), sulphate resistance etc. which have not been investigated in this research due to the limited time and resources should also be studied in future.

- Though there are few evidence available that ultra-sonication process provides a proper dispersion of nano materials, it is necessary to study the effect of colloidal nano materials on the properties of HVS and HVS-FA concretes.
- Sustainability analysis such cost and environmental impact of these HVS and HVS-FA concretes need to be analysed to validate the importance of the alternative sources of binding materials to reduce the use of cement and save the earth.

## **APPENDICES**

## APPENDIX A: Experimental Images



**Fig. A.1** Compression test of a typical concrete cylinder



**Fig. A.2** Failure pattern of control concretes (left) and concrete with nano materials (right) after compression test



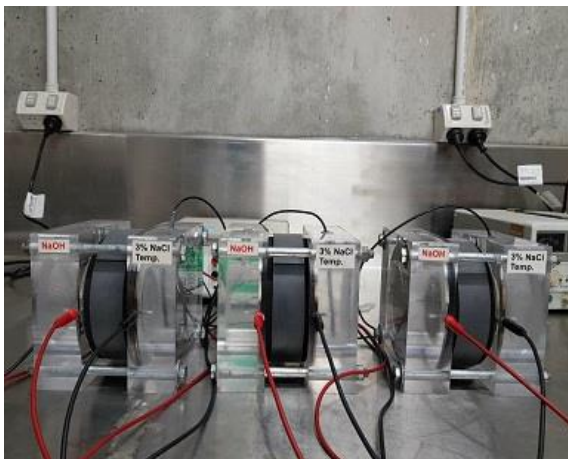
**Fig. A.3** Cutting concrete cylinders in 50 mm discs



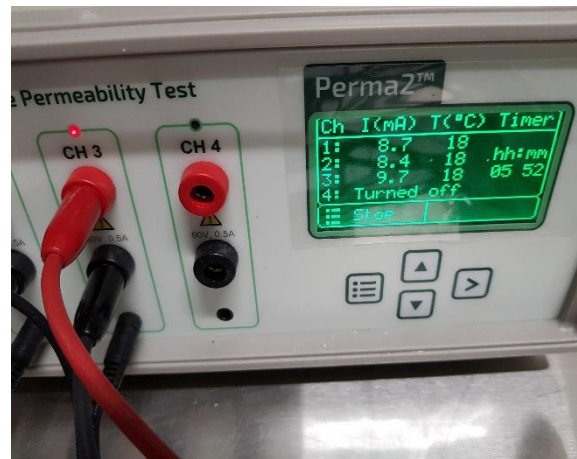
**Fig. A.4** Sorptivity test of concrete



(a)



(b)



(c)

**Fig. A.5** RCPT test of concrete (a) Vacuum desiccator (b) Test cells (c) Data logging



**Fig. A.6** Boiling samples in a water bath for VPV test

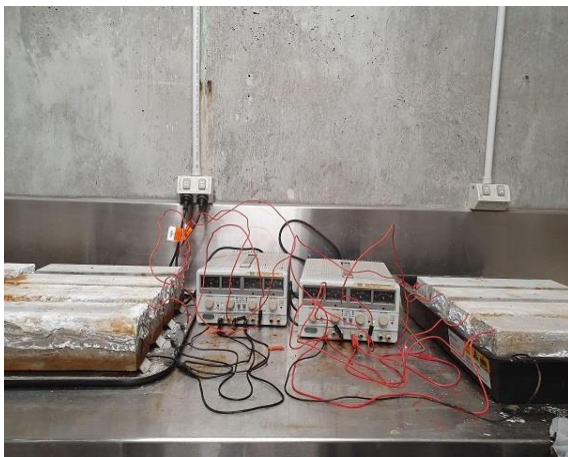


**Fig. A.7** (a) Test setup (b) Data collection of Corrosion test of concrete samples

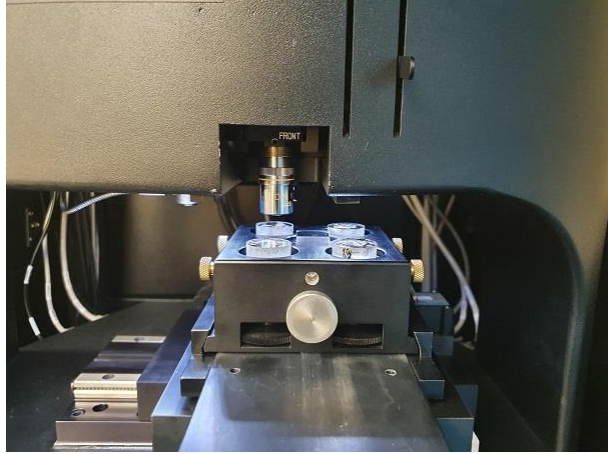


**Fig. A.8** Nano Indentation test of concrete samples



## APPENDIX B: Test Results Analysis

**Table B.1** Compressive strengths of control HVS and HVS-FA paste

<b>Binder's Composition</b>	<b>Mix ID</b>	<b>Avg. Compressive strengths, MPa</b>	<b>Standard Deviation</b>
<b>100% OPC</b>	OPC	42.80	3.06
<b>60% BFS</b>	60BFS	44.40	4.69
<b>70% BFS</b>	70BFS	42.70	3.88
<b>80% BFS</b>	80BFS	38.89	1.16
<b>90% BFS</b>	90BFS	26.85	3.26
<b>60% FA</b>	60FA	23.72	1.21
<b>70% FA</b>	70FA	17.25	0.67
<b>80% FA</b>	80FA	12.80	0.41
<b>90% FA</b>	90FA	6.77	0.47
<b>60%BFS</b>	60BFS	44.40	4.69
<b>60% BFS-FA</b>	42BFS18FA	49.89	2.27
	36BFS24FA	46.87	2.93
	30BFS30FA	44.72	4.72
<b>70% BFS</b>	70BFS	42.70	3.88
<b>70% BFS-FA</b>	49BFS21FA	36.69	1.71
	42BFS28FA	33.88	2.24
	35BFS35FA	36.52	2.79
<b>80% BFS</b>	80BFS	38.89	1.16
<b>80% BFS-FA</b>	56BFS24FA	31.78	2.42
	48BFS32FA	28.32	0.88
	40BFS40FA	30.33	2.54
<b>90% BFS</b>	90BFS	26.85	3.26
<b>90% BFS-FA</b>	63BFS27FA	23.73	1.76
	54BFS36FA	21.29	1.38
	45BFS45FA	20.01	0.77

**Table B.2** Compressive strengths of HVS and HVS-FA paste containing NS

<b>Binder's Composition</b>	<b>Mix ID</b>	<b>Avg. Compressive strengths, MPa</b>	<b>Standard Deviation</b>
<b>100% OPC</b>	OPC	42.8	3.06
<b>30%OPC+70%BFS</b>	70BFS	42.70	3.88
<b>1-4% NS addition</b>	69BFS1NS	46.46	4.49
	68BFS2NS	46.44	5.46
	67BFS3NS	42.09	4.05
	66BFS4NS	52.82	3.31
<b>20%OPC+80%BFS</b>	80BFS	38.89	1.16
<b>1-4% NS addition</b>	79BFS1NS	43.75	3.24
	78BFS2NS	49.99	2.92
	77BFS3NS	43.21	3.25
	76BFS4NS	47.72	2.32
<b>10%OPC+90%BFS</b>	90BFS	26.85	3.26
<b>1-4% NS addition</b>	89BFS1NS	31.44	2.00
	88BFS2NS	31.78	1.74
	87BFS3NS	33.10	1.06
	86BFS4NS	37.78	1.19
<b>30%OPC+49%BFS+21%FA</b>	49BFS21FA	36.69	1.71
<b>1-4% NS addition</b>	49BFS20FA1NS	38.39	1.75
	49BFS19FA2NS	44.69	2.75
	49BFS18FA3NS	52.06	1.56
	49BFS17FA4NS	60.47	4.89
<b>20%OPC+56%BFS+24%FA</b>	56BFS24FA	31.78	2.42
<b>1-4% NS addition</b>	56BFS23FA1NS	33.41	1.77
	56BFS22FA2NS	38.51	1.90
	56BFS21FA3NS	37.99	1.51
	56BFS20FA4NS	36.10	1.65

**Table B.3** Compressive strengths of HVS and HVS-FA paste containing NC

<b>Binder's Composition</b>	<b>Mix ID</b>	<b>Avg. Compressive strengths, MPa</b>	<b>Standard Deviation</b>
<b>100% OPC</b>	OPC	42.8	3.06
<b>30%OPC+70%BFS</b>	70BFS	42.70	3.88
<b>1-4% NC addition</b>	69BFS1NC	50.54	2.13
	68BFS2NC	50.97	3.62
	67BFS3NC	46.33	1.26
	66BFS4NC	53.1	2.68
<b>20%OPC+80%BFS</b>	80BFS	38.89	1.16
<b>1-4% NC addition</b>	79BFS1NC	38.98	4.35
	78BFS2NC	41.89	3.05
	77BFS3NC	45.32	1.78
	76BFS4NC	46.66	3.24
<b>10%OPC+90%BFS</b>	90BFS	26.85	3.26
<b>1-4% NC addition</b>	89BFS1NC	27.80	1.12
	88BFS2NC	29.02	2.23
	87BFS3NC	28.33	1.22
	86BFS4NC	32.36	1.16
<b>30%OPC+49%BFS+21%FA</b>	49BFS21FA	36.69	1.71
<b>1-4% NC addition</b>	49BFS20FA1NC	43.39	2.3
	49BFS19FA2NC	43.08	1.92
	49BFS18FA3NC	42.95	1.48
	49BFS17FA4NC	45.45	1.92
<b>20%OPC+56%BFS+24%FA</b>	56BFS24FA	31.78	2.42
<b>1-4% NC addition</b>	56BFS23FA1NC	37.83	2.68
	56BFS22FA2NC	27.03	0.44
	56BFS21FA3NC	31.99	2.37
	56BFS20FA4NC	34.69	1.55

**Table B.4** Compressive strengths of control OPC concrete at different age

Days	No	Load, KN	Compressive Strength, MPa	Average Compressive strength, MPa	Standard Deviation
3	1	295.68	37.78	38.73	0.8
	2	308.28	39.32		
	3	305.75	39.09		
7	1	326.82	41.74	40.73	0.9
	2	313.89	40.05		
	3	316.45	40.39		
28	1	391.86	49.92	49.05	1.7
	2	370.18	47.09		
	3	392.79	50.14		
56	1	422.56	53.84	52.80	0.9
	2	408.21	52.05		
	3	411.57	52.52		
91	1	429.21	54.79	54.62	0.2
	2	428.93	54.71		
	3	425.19	54.36		
180	1	455.66	58.04	56.44	1.4
	2	436.16	55.50		
	3	438.05	55.77		

**Table B.5** Compressive strengths of 70BFS concrete at different age

Days	No	Load, KN	Compressive Strength, MPa	Average Compressive strength, MPa	Standard Deviation
3	1	170	21.67	22.04	0.4
	2	176.53	22.47		
	3	172.21	21.98		
7	1	276.74	35.31	35.86	0.5
	2	285.63	36.41		
	3	281.02	35.84		
28	1	373.88	47.78	45.78	2.4
	2	363.58	46.39		
	3	338.8	43.16		
56	1	406.17	51.74	51.59	1.1
	2	413.19	52.64		
	3	395.19	50.41		
91	1	429.49	54.75	53.06	1.5
	2	411.09	52.41		
	3	407.17	52.01		
180	1	447.27	57.07	57.88	0.9
	2	453.38	57.76		
	3	461.85	58.80		

**Table B.6** Compressive strengths of 80BFS concrete at different age

<b>Days</b>	<b>No</b>	<b>Load, KN</b>	<b>Compressive Strength, MPa</b>	<b>Average Compressive strength, MPa</b>	<b>Standard Deviation</b>
<b>3</b>	1	165.66	21.17	21.05	0.3
	2	166.87	21.27		
	3	161.87	20.72		
<b>7</b>	1	217.59	27.73	28.73	0.9
	2	228.83	29.21		
	3	229.46	29.26		
<b>28</b>	1	249.54	31.82	34.32	2.3
	2	285.41	36.26		
	3	273.76	34.87		
<b>56</b>	1	325.44	41.54	40.29	1.1
	2	309.57	39.55		
	3	311.78	39.77		
<b>91</b>	1	338.13	43.18	41.69	1.3
	2	323.52	41.28		
	3	318.11	40.60		
<b>180</b>	1	321.95	41.16	42.78	1.9
	2	331.38	42.29		
	3	351.95	44.89		

**Table B.7** Compressive strengths of 70BFS-FA concrete at different age

<b>Days</b>	<b>No</b>	<b>Load, KN</b>	<b>Compressive Strength, MPa</b>	<b>Average Compressive strength, MPa</b>	<b>Standard Deviation</b>
<b>3</b>	1	165.34	21.06	20.79	0.8
	2	167.68	21.40		
	3	156.12	19.91		
<b>7</b>	1	252.38	32.28	31.28	1.1
	2	246.52	31.46		
	3	235.61	30.09		
<b>28</b>	1	321.83	41.09	42.38	1.4
	2	343.97	43.83		
	3	331.51	42.22		
<b>56</b>	1	330.67	42.12	44.25	1.9
	2	352.96	44.84		
	3	359.42	45.79		
<b>91</b>	1	381.17	48.56	49.51	1.8
	2	379.17	48.36		
	3	405.09	51.60		
<b>180</b>	1	389.54	49.66	50.71	1.3
	2	395.45	50.36		
	3	408.08	52.10		

**Table B.8** Compressive strengths of 78BFS.2NS concrete at different age

<b>Days</b>	<b>No</b>	<b>Load, KN</b>	<b>Compressive Strength, MPa</b>	<b>Average Compressive strength, MPa</b>	<b>Standard Deviation</b>
<b>3</b>	1	217.84	27.86	28.18	1.1
	2	213.86	27.32		
	3	230.02	29.35		
<b>7</b>	1	261.37	33.40	33.65	1.1
	2	273.43	34.88		
	3	255.99	32.67		
<b>28</b>	1	359.90	46.02	46.65	1.5
	2	356.29	45.56		
	3	378.93	48.36		
<b>56</b>	1	391.11	49.89	47.17	2.6
	2	351.28	44.75		
	3	366.7	46.88		
<b>91</b>	1	393.65	50.23	49.33	1.2
	2	376.29	48.03		
	3	389.17	49.73		
<b>180</b>	1	403.86	51.72	51.99	1.1
	2	415.99	53.22		
	3	399.16	51.03		

**Table B.9** Compressive strengths of 69BFS.1NC concrete at different age

<b>Days</b>	<b>No</b>	<b>Load, KN</b>	<b>Compressive Strength, MPa</b>	<b>Average Compressive strength, MPa</b>	<b>Standard Deviation</b>
<b>3</b>	1	239.26	30.49	31.59	1.2
	2	257.52	32.89		
	3	245.31	31.38		
<b>7</b>	1	313.32	40.06	41.22	1.8
	2	339.61	43.29		
	3	315.97	40.32		
<b>28</b>	1	417.51	53.39	53.94	1.3
	2	434.73	55.37		
	3	416.44	53.05		
<b>56</b>	1	443.45	56.72	56.13	0.6
	2	438.25	56.05		
	3	436.23	55.62		
<b>91</b>	1	438.41	55.89	57.23	1.9
	2	441.86	56.39		
	3	465.45	59.42		
<b>180</b>	1	453.92	57.89	60.80	2.5
	2	485.57	62.01		
	3	489.27	62.51		

**Table B.10** Compressive strengths of 67BFS-FA.3NS concrete at different age

<b>Days</b>	<b>No</b>	<b>Load, KN</b>	<b>Compressive Strength, MPa</b>	<b>Average Compressive strength, MPa</b>	<b>Standard Deviation</b>
<b>3</b>	1	230.56	29.41	30.11	0.8
	2	241.85	30.92		
	3	235.56	30.01		
<b>7</b>	1	264.06	33.74	34.81	0.9
	2	275.11	35.18		
	3	277.91	35.51		
<b>28</b>	1	390.76	49.77	49.19	1.4
	2	372.93	47.61		
	3	393.82	50.19		
<b>56</b>	1	462.48	58.91	57.35	1.6
	2	450.18	57.47		
	3	437.15	55.67		
<b>91</b>	1	471.75	60.41	59.10	2.6
	2	439.17	56.11		
	3	476.1	60.76		
<b>180</b>	1	490.68	62.76	62.29	1.2
	2	495.22	63.22		
	3	489.17	60.90		

**Table B.11** Compressive strengths of 69BFS-FA.1NC concrete at different age

<b>Days</b>	<b>No</b>	<b>Load, KN</b>	<b>Compressive Strength, MPa</b>	<b>Average Compressive strength, MPa</b>	<b>Standard Deviation</b>
<b>3</b>	1	208.98	26.61	26.65	0.0
	2	208.93	26.67		
	3	208.98	26.67		
<b>7</b>	1	275.79	35.18	35.41	0.8
	2	272.67	34.79		
	3	284.34	36.25		
<b>28</b>	1	389.56	49.71	49.81	1.5
	2	378.89	48.35		
	3	402.96	51.37		
<b>56</b>	1	399.11	51.11	51.93	1.0
	2	415.49	52.98		
	3	405.44	51.69		
<b>91</b>	1	434.18	55.49	54.36	1.0
	2	422.97	54.03		
	3	418.17	53.55		
<b>180</b>	1	440.39	56.17	57.15	1.2
	2	445.62	56.75		
	3	457.65	58.52		

**Table B.12** Shrinkage calculation of control OPC concrete at different age

Days	Sample	Reading (mm)					Avg.		
7	1	1.598	1.599	1.598	1.598	1.599	1.5984		
	2	2.623	2.623	2.623	2.622	2.622	2.6226		
	3	1.763	1.763	1.762	1.762	1.762	1.7624		
Days	Sample	Reading (mm)			Avg. mm	Difference mm		Avg. diff/gauge L *10 <sup>-6</sup> (microstrain)	
14	1	1.544	1.544	1.544	1.544	0.0544	217.6	237	
	2	2.566	2.566	2.566	2.566	0.0566	226.4		
	3	1.696	1.696	1.696	1.696	0.0664	265.6		
21	1	1.544	1.544	1.544	1.544	0.0544	217.6	255	
	2	2.559	2.559	2.558	2.558	0.0639	255.7		
	3	1.690	1.690	1.689	1.689	0.0727	290.9		
28	1	1.536	1.536	1.536	1.536	0.0624	249.6	284	
	2	2.547	2.546	2.546	2.546	0.0762	305.0		
	3	1.688	1.688	1.688	1.688	0.0744	297.6		
35	1	1.532	1.532	1.532	1.532	0.0664	265.6	293	
	2	2.545	2.545	2.544	2.544	0.0779	311.7		
	3	1.687	1.687	1.686	1.686	0.0757	302.9		
56	1	1.518	1.518	1.518	1.518	0.0804	321.6	341	
	2	2.536	2.536	2.536	2.536	0.0866	346.4		
	3	1.674	1.674	1.674	1.674	0.0884	353.6		
91	1	1.506	1.506	1.506	1.506	0.0924	369.6	381	
	2	2.528	2.527	2.527	2.527	0.0952	381.0		
	3	1.664	1.664	1.664	1.664	0.0984	393.6		
120	1	1.504	1.504	1.503	1.503	0.0947	378.9	400	
	2	2.52	2.52	2.52	2.52	0.1026	410.4		
	3	1.66	1.66	1.66	1.66	0.1024	409.6		
150	1	1.502	1.502	1.502	1.502	0.0964	385.6	417	
	2	2.512	2.511	2.511	2.511	0.1112	445.0		
	3	1.657	1.657	1.657	1.657	0.1054	421.6		
180	1	1.502	1.502	1.502	1.502	0.0964	385.6	419	
	2	2.511	2.511	2.511	2.511	0.1116	446.4		
	3	1.656	1.656	1.656	1.656	0.1064	425.6		
210	1	1.5	1.5	1.5	1.5	0.0984	393.6	424	
	2	2.511	2.51	2.51	2.510	0.1122	449.0		
	3	1.655	1.655	1.655	1.655	0.1074	429.6		
240	1	1.496	1.495	1.495	1.495	0.1030	412.2	445	
	2	2.504	2.504	2.504	2.504	0.1186	474.4		
	3	1.65	1.65	1.65	1.65	0.1124	449.6		
270	1	1.495	1.495	1.495	1.495	0.1034	413.6	447	
	2	2.503	2.503	2.503	2.503	0.1196	478.4		
	3	1.65	1.65	1.65	1.65	0.1124	449.6		



300	1	1.495	1.495	1.495	1.495	0.1034	413.6	447
	2	2.503	2.503	2.503	2.503	0.1196	478.4	
	3	1.65	1.65	1.65	1.65	0.1124	449.6	
330	1	1.495	1.495	1.495	1.495	0.1034	413.6	447
	2	2.503	2.503	2.503	2.503	0.1196	478.4	
	3	1.65	1.65	1.65	1.65	0.1124	449.6	
365	1	1.495	1.495	1.495	1.495	0.1034	413.6	447
	2	2.503	2.503	2.503	2.503	0.1196	478.4	
	3	1.65	1.65	1.65	1.65	0.1124	449.6	

**Table B.13** Shrinkage calculation of 70BFS concrete at different age

Days	Sample	Reading (mm)					Avg.		
7	1	0.364	0.363	0.362	0.362	0.361	0.3624		
	2	1.098	1.098	1.097	1.096	1.095	1.0968		
	3	0.647	0.647	0.646	0.646	0.646	0.6464		
Days	Sample	Reading (mm)				Avg.	Difference		Avg. diff/gauge L
					mm	mm	*10 <sup>-6</sup>	*10 <sup>-6</sup>	(microstrain)
14	1	0.280	0.280	0.279	0.2797	0.0827	330.9	255	
	2	1.044	1.044	1.043	1.0437	0.0531	212.5		
	3	0.591	0.591	0.591	0.5910	0.0554	221.6		
21	1	0.279	0.279	0.279	0.2790	0.0834	333.6	282	
	2	1.032	1.032	1.032	1.0320	0.0648	259.2		
	3	0.583	0.583	0.583	0.5830	0.0634	253.6		
28	1	0.266	0.266	0.266	0.2660	0.0964	385.6	312	
	2	1.027	1.026	1.026	1.0263	0.0705	281.9		
	3	0.579	0.579	0.579	0.5790	0.0674	269.6		
35	1	0.264	0.264	0.263	0.2637	0.0987	394.9	318	
	2	1.025	1.025	1.024	1.0247	0.0721	288.5		
	3	0.579	0.579	0.579	0.5790	0.0674	269.6		
56	1	0.254	0.254	0.254	0.2540	0.1084	433.6	364	
	2	1.002	1.002	1.002	1.0020	0.0948	379.2		
	3	0.577	0.576	0.576	0.5763	0.0701	280.3		
91	1	0.246	0.245	0.245	0.2453	0.1171	468.3	397	
	2	0.999	0.998	0.998	0.9983	0.0985	393.9		
	3	0.565	0.564	0.563	0.5640	0.0824	329.6		
120	1	0.24	0.239	0.239	0.2393	0.1231	492.3	410	
	2	0.997	0.997	0.997	0.9970	0.0998	399.2		
	3	0.562	0.562	0.562	0.5620	0.0844	337.6		
150	1	0.234	0.234	0.233	0.2337	0.1287	514.9	428	
	2	0.992	0.991	0.991	0.9913	0.1055	421.9		
	3	0.56	0.559	0.559	0.5593	0.0871	348.3		

180	1	0.232	0.231	0.231	0.2313	0.1311	524.3	443
	2	0.987	0.987	0.986	0.9867	0.1101	440.5	
	3	0.555	0.555	0.555	0.5550	0.0914	365.6	
210	1	0.231	0.231	0.231	0.2310	0.1314	525.6	455
	2	0.98	0.98	0.979	0.9797	0.1171	468.5	
	3	0.554	0.554	0.554	0.5540	0.0924	369.6	
240	1	0.228	0.228	0.227	0.2277	0.1347	538.9	463
	2	0.979	0.978	0.977	0.9780	0.1188	475.2	
	3	0.553	0.553	0.553	0.5530	0.0934	373.6	
270	1	0.224	0.223	0.223	0.2233	0.1391	556.3	470
	2	0.977	0.977	0.977	0.9770	0.1198	479.2	
	3	0.553	0.553	0.552	0.5527	0.0937	374.9	
300	1	0.224	0.223	0.223	0.2233	0.1391	556.3	471
	2	0.977	0.977	0.977	0.9770	0.1198	479.2	
	3	0.552	0.552	0.552	0.5520	0.0944	377.6	
330	1	0.223	0.222	0.222	0.2223	0.1401	560.3	480
	2	0.974	0.974	0.974	0.9740	0.1228	491.2	
	3	0.55	0.549	0.549	0.5493	0.0971	388.3	
365	1	0.221	0.221	0.221	0.2210	0.1414	565.6	484
	2	0.973	0.972	0.972	0.9723	0.1245	497.9	
	3	0.55	0.549	0.549	0.5493	0.0971	388.3	

**Table B.14** Shrinkage calculation of 80BFS concrete at different age

Days	Sample	Reading (mm)					Avg.		
7	1	1.535	1.535	1.534	1.534	1.533	1.5342		
	2	1.936	1.936	1.935	1.935	1.934	1.9352		
	3	2.354	2.353	2.352	2.352	2.351	2.3524		
Days	Sample	Reading (mm)				Avg. mm	Difference mm		Avg. diff/gauge L *10 <sup>-6</sup> (microstrain)
14	1	1.464	1.464	1.464	1.4640	0.0702	280.8		
	2	1.862	1.862	1.861	1.8617	0.0735	294.1		
	3	2.315	2.314	2.314	2.3143	0.0381	152.3		
21	1	1.456	1.456	1.455	1.4557	0.0785	314.1		
	2	1.841	1.841	1.840	1.8407	0.0945	378.1		
	3	2.305	2.305	2.305	2.3050	0.0474	189.6		
28	1	1.447	1.446	1.446	1.4463	0.0879	351.5		
	2	1.799	1.799	1.799	1.7990	0.1362	544.8		
	3	2.27	2.27	2.27	2.2700	0.0824	329.6		
35	1	1.433	1.433	1.432	1.4327	0.1015	406.1		
	2	1.782	1.782	1.782	1.7820	0.1532	612.8		
	3	2.257	2.257	2.256	2.2567	0.0957	382.9		

<b>56</b>	1	1.428	1.428	1.428	1.4280	0.1062	424.8	494
	2	1.779	1.779	1.779	1.7790	0.1562	624.8	
	3	2.245	2.244	2.244	2.2443	0.1081	432.3	
<b>91</b>	1	1.417	1.416	1.416	1.4163	0.1179	471.5	536
	2	1.763	1.763	1.762	1.7627	0.1725	690.1	
	3	2.241	2.241	2.24	2.2407	0.1117	446.9	
<b>120</b>	1	1.409	1.408	1.407	1.4080	0.1262	504.8	558
	2	1.758	1.758	1.757	1.7577	0.1775	710.1	
	3	2.238	2.238	2.238	2.2380	0.1144	457.6	
<b>150</b>	1	1.403	1.403	1.403	1.4030	0.1312	524.8	583
	2	1.758	1.758	1.758	1.7580	0.1772	708.8	
	3	2.224	2.224	2.223	2.2237	0.1287	514.9	
<b>180</b>	1	1.4	1.4	1.4	1.4000	0.1342	536.8	595
	2	1.756	1.756	1.755	1.7557	0.1795	718.1	
	3	2.22	2.22	2.22	2.2200	0.1324	529.6	
<b>210</b>	1	1.396	1.396	1.396	1.3960	0.1382	552.8	613
	2	1.752	1.752	1.752	1.7520	0.1832	732.8	
	3	2.214	2.214	2.214	2.2140	0.1384	553.6	
<b>240</b>	1	1.391	1.39	1.39	1.3903	0.1439	575.5	630
	2	1.746	1.746	1.746	1.7460	0.1892	756.8	
	3	2.213	2.213	2.213	2.2130	0.1394	557.6	
<b>270</b>	1	1.389	1.388	1.388	1.3883	0.1459	583.5	643
	2	1.741	1.741	1.741	1.7410	0.1942	776.8	
	3	2.21	2.21	2.21	2.2100	0.1424	569.6	
<b>300</b>	1	1.389	1.388	1.388	1.3883	0.1459	583.5	644
	2	1.741	1.741	1.74	1.7407	0.1945	778.1	
	3	2.21	2.21	2.21	2.2100	0.1424	569.6	
<b>330</b>	1	1.386	1.386	1.386	1.3860	0.1482	592.8	663
	2	1.738	1.738	1.737	1.7377	0.1975	790.1	
	3	2.201	2.201	2.201	2.2010	0.1514	605.6	
<b>365</b>	1	1.384	1.384	1.383	1.3837	0.1505	602.1	675
	2	1.736	1.736	1.735	1.7357	0.1995	798.1	
	3	2.197	2.196	2.195	2.1960	0.1564	625.6	

**Table B.15** Shrinkage calculation of 70BFS-FA concrete at different age

Days	Sample	Reading (mm)					Avg.		
7	1	1.151	1.151	1.15	1.149	1.149	1.15		
	2	1.196	1.195	1.195	1.194	1.194	1.1948		
	3	1.569	1.569	1.568	1.567	1.566	1.5678		
Days	Sample	Reading (mm)			Avg. mm	Difference mm		*10 <sup>-6</sup>	Avg. diff/gauge L *10 <sup>-6</sup> (microstrain)
14	1	1.083	1.083	1.082	1.0827	0.0673	269.3	293	
	2	1.118	1.118	1.117	1.1177	0.0771	308.5		
	3	1.493	1.493	1.492	1.4927	0.0751	300.5		
21	1	1.067	1.066	1.066	1.0663	0.0837	334.7	346	
	2	1.11	1.11	1.109	1.1097	0.0851	340.5		
	3	1.477	1.477	1.477	1.4770	0.0908	363.2		
28	1	1.058	1.058	1.058	1.0580	0.0920	368.0	383	
	2	1.098	1.098	1.098	1.0980	0.0968	387.2		
	3	1.469	1.469	1.469	1.4690	0.0988	395.2		
35	1	1.054	1.054	1.054	1.0540	0.0960	384.0	410	
	2	1.09	1.09	1.09	1.0900	0.1048	419.2		
	3	1.461	1.461	1.461	1.4610	0.1068	427.2		
56	1	1.052	1.052	1.052	1.0520	0.0980	392.0	427	
	2	1.084	1.084	1.084	1.0840	0.1108	443.2		
	3	1.456	1.456	1.456	1.4560	0.1118	447.2		
91	1	1.049	1.049	1.05	1.0493	0.1007	402.7	439	
	2	1.081	1.081	1.081	1.0810	0.1138	455.2		
	3	1.453	1.453	1.452	1.4527	0.1151	460.5		
120	1	1.034	1.034	1.034	1.0340	0.1160	464.0	485	
	2	1.063	1.063	1.063	1.0630	0.1318	527.2		
	3	1.452	1.452	1.452	1.4520	0.1158	463.2		
150	1	1.026	1.026	1.026	1.0260	0.1240	496.0	520	
	2	1.051	1.051	1.05	1.0507	0.1441	576.5		
	3	1.446	1.446	1.446	1.4460	0.1218	487.2		
180	1	1.025	1.025	1.025	1.0250	0.1250	500.0	527	
	2	1.049	1.049	1.049	1.0490	0.1458	583.2		
	3	1.444	1.444	1.443	1.4437	0.1241	496.5		
210	1	1.014	1.014	1.014	1.0140	0.1360	544.0	558	
	2	1.044	1.044	1.043	1.0437	0.1511	604.5		
	3	1.437	1.437	1.436	1.4367	0.1311	524.5		
240	1	1.012	1.011	1.011	1.0113	0.1387	554.7	570	
	2	1.042	1.041	1.041	1.0413	0.1535	613.9		
	3	1.433	1.432	1.432	1.4323	0.1355	541.9		
270	1	1.009	1.009	1.009	1.0090	0.1410	564.0	578	
	2	1.04	1.04	1.04	1.0400	0.1548	619.2		
	3	1.43	1.43	1.43	1.4300	0.1378	551.2		

300	1	1.009	1.009	1.009	1.0090	0.1410	564.0	578
	2	1.04	1.04	1.04	1.0400	0.1548	619.2	
	3	1.43	1.43	1.43	1.4300	0.1378	551.2	
330	1	1.007	1.007	1.006	1.0067	0.1433	573.3	588
	2	1.037	1.037	1.037	1.0370	0.1578	631.2	
	3	1.428	1.428	1.427	1.4277	0.1401	560.5	
365	1	1.007	1.007	1.006	1.0067	0.1433	573.3	594
	2	1.035	1.035	1.035	1.0350	0.1598	639.2	
	3	1.426	1.426	1.425	1.4257	0.1421	568.5	

**Table B.16** Shrinkage calculation of 78BFS.2NS concrete at different age

Days	Sample	Reading (mm)					Avg.		
7	1	1.095	1.094	1.093	1.092	1.092	1.0932		
	2	0.978	0.977	0.977	0.977	0.976	0.977		
	3	0.378	0.377	0.376	0.376	0.375	0.3764		
Days	Sample	Reading (mm)				Avg.	Difference		Avg. diff/gauge L
					mm	mm	*10 <sup>-6</sup>	*10 <sup>-6</sup> (microstrain)	
14	1	1.065	1.065	1.065	1.0650	0.0282	112.8	115	
	2	0.943	0.942	0.942	0.9423	0.0347	138.7		
	3	0.354	0.353	0.352	0.3530	0.0234	93.6		
21	1	1.062	1.062	1.062	1.0620	0.0312	124.8	143	
	2	0.938	0.938	0.937	0.9377	0.0393	157.3		
	3	0.34	0.34	0.339	0.3397	0.0367	146.9		
28	1	1.041	1.04	1.04	1.0403	0.0529	211.5	207	
	2	0.92	0.92	0.92	0.9200	0.0570	228.0		
	3	0.332	0.331	0.33	0.3310	0.0454	181.6		
35	1	1.035	1.035	1.034	1.0347	0.0585	234.1	228	
	2	0.913	0.913	0.913	0.9130	0.0640	256.0		
	3	0.328	0.328	0.328	0.3280	0.0484	193.6		
56	1	1.016	1.016	1.015	1.0157	0.0775	310.1	299	
	2	0.895	0.895	0.895	0.8950	0.0820	328.0		
	3	0.312	0.312	0.312	0.3120	0.0644	257.6		
91	1	1.002	1.001	1.001	1.0013	0.0919	367.5	342	
	2	0.885	0.884	0.884	0.8843	0.0927	370.7		
	3	0.305	0.304	0.304	0.3043	0.0721	288.3		
120	1	0.986	0.986	0.985	0.9857	0.1075	430.1	407	
	2	0.867	0.867	0.867	0.8670	0.1100	440.0		
	3	0.289	0.289	0.289	0.2890	0.0874	349.6		
150	1	0.983	0.982	0.982	0.9823	0.1109	443.5	424	
	2	0.862	0.862	0.861	0.8617	0.1153	461.3		
	3	0.285	0.285	0.284	0.2847	0.0917	366.9		

180	1	0.978	0.978	0.977	0.9777	0.1155	462.1	435
	2	0.86	0.859	0.859	0.8593	0.1177	470.7	
	3	0.283	0.283	0.283	0.2830	0.0934	373.6	
210	1	0.974	0.974	0.974	0.9740	0.1192	476.8	447
	2	0.855	0.855	0.855	0.8550	0.1220	488.0	
	3	0.283	0.282	0.281	0.2820	0.0944	377.6	
240	1	0.972	0.972	0.972	0.9720	0.1212	484.8	457
	2	0.853	0.853	0.853	0.8530	0.1240	496.0	
	3	0.279	0.279	0.279	0.2790	0.0974	389.6	
270	1	0.972	0.972	0.971	0.9717	0.1215	486.1	474
	2	0.846	0.846	0.845	0.8457	0.1313	525.3	
	3	0.274	0.274	0.273	0.2737	0.1027	410.9	
300	1	0.969	0.969	0.969	0.9690	0.1242	496.8	478
	2	0.846	0.846	0.845	0.8457	0.1313	525.3	
	3	0.274	0.274	0.273	0.2737	0.1027	410.9	
330	1	0.969	0.969	0.969	0.9690	0.1242	496.8	489
	2	0.846	0.846	0.846	0.8460	0.1310	524.0	
	3	0.265	0.265	0.264	0.2647	0.1117	446.9	
365	1	0.969	0.969	0.969	0.9690	0.1242	496.8	489
	2	0.846	0.846	0.846	0.8460	0.1310	524.0	
	3	0.265	0.265	0.265	0.2650	0.1114	445.6	

**Table B.17** Shrinkage calculation of 69BFS.1NC concrete at different age

Days	Sample	Reading (mm)					Avg.		
7	1	1.711	1.711	1.71	1.71	1.71	1.7104		
	2	0.512	0.512	0.511	0.511	0.511	0.5114		
	3	0.21	0.21	0.21	0.21	0.21	0.21		
Days	Sample	Reading (mm)				Avg. mm	Difference mm		Avg. diff/gauge L *10 <sup>-6</sup> (microstrain)
14	1	1.688	1.688	1.688	1.6880	0.0224	89.6		
	2	0.504	0.504	0.503	0.5037	0.0077	30.9	72	
	3	0.186	0.186	0.186	0.1860	0.0240	96.0		
21	1	1.667	1.667	1.667	1.6670	0.0434	173.6		
	2	0.476	0.476	0.476	0.4760	0.0354	141.6	153	
	3	0.174	0.174	0.174	0.1740	0.0360	144.0		
28	1	1.66	1.66	1.66	1.6600	0.0504	201.6		
	2	0.467	0.467	0.466	0.4667	0.0447	178.9	184	
	3	0.167	0.167	0.167	0.1670	0.0430	172.0		
35	1	1.648	1.648	1.648	1.6480	0.0624	249.6		
	2	0.457	0.457	0.456	0.4567	0.0547	218.9	226	
	3	0.158	0.158	0.158	0.1580	0.0520	208.0		

<b>56</b>	1	1.632	1.632	1.632	1.6320	0.0784	313.6	294
	2	0.444	0.439	0.439	0.4407	0.0707	282.9	
	3	0.139	0.138	0.138	0.1383	0.0717	286.7	
<b>91</b>	1	1.623	1.623	1.623	1.6230	0.0874	349.6	335
	2	0.427	0.427	0.426	0.4267	0.0847	338.9	
	3	0.131	0.131	0.131	0.1310	0.0790	316.0	
<b>120</b>	1	1.616	1.616	1.616	1.6160	0.0944	377.6	371
	2	0.416	0.415	0.415	0.4153	0.0961	384.3	
	3	0.122	0.122	0.122	0.1220	0.0880	352.0	
<b>150</b>	1	1.615	1.615	1.614	1.6147	0.0957	382.9	382
	2	0.413	0.413	0.413	0.4130	0.0984	393.6	
	3	0.119	0.118	0.117	0.1180	0.0920	368.0	
<b>180</b>	1	1.609	1.609	1.609	1.6090	0.1014	405.6	398
	2	0.409	0.409	0.409	0.4090	0.1024	409.6	
	3	0.116	0.115	0.115	0.1153	0.0947	378.7	
<b>210</b>	1	1.607	1.606	1.605	1.6060	0.1044	417.6	417
	2	0.405	0.405	0.405	0.4050	0.1064	425.6	
	3	0.108	0.108	0.108	0.1080	0.1020	408.0	
<b>240</b>	1	1.603	1.602	1.602	1.6023	0.1081	432.3	431
	2	0.4	0.4	0.399	0.3997	0.1117	446.9	
	3	0.107	0.106	0.106	0.1063	0.1037	414.7	
<b>270</b>	1	1.599	1.599	1.598	1.5987	0.1117	446.9	442
	2	0.399	0.399	0.398	0.3987	0.1127	450.9	
	3	0.104	0.103	0.103	0.1033	0.1067	426.7	
<b>300</b>	1	1.596	1.596	1.595	1.5957	0.1147	458.9	450
	2	0.399	0.398	0.398	0.3983	0.1131	452.3	
	3	0.1	0.1	0.1	0.1000	0.1100	440.0	
<b>330</b>	1	1.596	1.596	1.596	1.5960	0.1144	457.6	450
	2	0.399	0.399	0.399	0.3990	0.1124	449.6	
	3	0.099	0.099	0.099	0.0990	0.1110	444.0	
<b>365</b>	1	1.596	1.596	1.596	1.5960	0.1144	457.6	451
	2	0.399	0.399	0.399	0.3990	0.1124	449.6	
	3	0.099	0.099	0.098	0.0987	0.1113	445.3	

**Table B.18** Shrinkage calculation of 67BFS-FA.3NS concrete at different age

Days	Sample	Reading (mm)					Avg.	
7		0.722	0.722	0.721	0.72	0.719	0.7208	
		0.858	0.857	0.856	0.856	0.854	0.8562	
		-0.02	-0.02	-0.03	-0.04	-0.04	-0.03	
Days	Sample	Reading (mm)			Avg. mm	Difference mm *10 <sup>-6</sup>		Avg. diff/gauge L *10 <sup>-6</sup> (microstrain)
14	1	0.677	0.676	0.676	0.6763	0.0445	177.9	139
	2	0.814	0.813	0.812	0.8130	0.0432	172.8	
	3	-0.046	-0.046	-0.047	-0.0463	0.0163	65.3	
21	1	0.667	0.667	0.666	0.6667	0.0541	216.5	167
	2	0.81	0.809	0.809	0.8093	0.0469	187.5	
	3	-0.054	-0.054	-0.055	-0.0543	0.0243	97.3	
28	1	0.662	0.662	0.661	0.6617	0.0591	236.5	227
	2	0.789	0.788	0.788	0.7883	0.0679	271.5	
	3	-0.073	-0.073	-0.073	-0.0730	0.0430	172.0	
35	1	0.658	0.658	0.658	0.6580	0.0628	251.2	240
	2	0.785	0.785	0.784	0.7847	0.0715	286.1	
	3	-0.075	-0.075	-0.076	-0.0753	0.0453	181.3	
56	1	0.643	0.643	0.643	0.6430	0.0778	311.2	290
	2	0.774	0.773	0.773	0.7733	0.0829	331.5	
	3	-0.087	-0.087	-0.087	-0.0870	0.0570	228.0	
91	1	0.638	0.638	0.638	0.6380	0.0828	331.2	325
	2	0.755	0.754	0.753	0.7540	0.1022	408.8	
	3	-0.089	-0.089	-0.089	-0.0890	0.0590	236.0	
120	1	0.632	0.632	0.631	0.6317	0.0891	356.5	366
	2	0.74	0.74	0.739	0.7397	0.1165	466.1	
	3	-0.099	-0.099	-0.099	-0.0990	0.0690	276.0	
150	1	0.629	0.628	0.628	0.6283	0.0925	369.9	380
	2	0.736	0.736	0.735	0.7357	0.1205	482.1	
	3	-0.102	-0.102	-0.103	-0.1023	0.0723	289.3	
180	1	0.629	0.628	0.628	0.6283	0.0925	369.9	391
	2	0.734	0.733	0.733	0.7333	0.1229	491.5	
	3	-0.108	-0.108	-0.108	-0.1080	0.0780	312.0	
210	1	0.629	0.628	0.628	0.6283	0.0925	369.9	399
	2	0.73	0.73	0.73	0.7300	0.1262	504.8	
	3	-0.11	-0.11	-0.111	-0.1103	0.0803	321.3	
240	1	0.629	0.628	0.628	0.6283	0.0925	369.9	404
	2	0.727	0.727	0.726	0.7267	0.1295	518.1	
	3	-0.111	-0.111	-0.111	-0.1110	0.0810	324.0	
270	1	0.629	0.628	0.628	0.6283	0.0925	369.9	415
	2	0.725	0.724	0.723	0.7240	0.1322	528.8	
	3	-0.116	-0.116	-0.117	-0.1163	0.0863	345.3	



<b>300</b>	1	0.629	0.628	0.628	0.6283	0.0925	369.9	421
	2	0.72	0.72	0.72	0.7200	0.1362	544.8	
	3	-0.117	-0.117	-0.117	-0.1170	0.0870	348.0	
<b>330</b>	1	0.629	0.628	0.628	0.6283	0.0925	369.9	421
	2	0.72	0.72	0.72	0.7200	0.1362	544.8	
	3	-0.118	-0.117	-0.117	-0.1173	0.0873	349.3	
<b>365</b>	1	0.629	0.628	0.628	0.6283	0.0925	369.9	421
	2	0.72	0.72	0.72	0.7200	0.1362	544.8	
	3	-0.117	-0.117	-0.117	-0.1170	0.0870	348.0	

**Table B.19** Shrinkage calculation of 69BFS-FA.1NC concrete at different age

Days	Sample	Reading (mm)					Avg.		Avg. diff/gauge L
<b>7</b>	1.059	1.059	1.059	1.058	1.058	1.0586	1.059	99	
	1.575	1.574	1.574	1.573	1.573	1.5738	1.575		
	2.467	2.467	2.467	2.466	2.465	2.4664	2.467		
Days	Sample	Reading (mm)				Avg. mm	Difference mm		Avg. diff/gauge L *10 <sup>-6</sup> (microstrain)
<b>14</b>	1	1.029	1.029	1.029	1.0290	0.0296	118.4	99	
	2	1.55	1.55	1.549	1.5497	0.0241	96.5		
	3	2.446	2.446	2.445	2.4457	0.0207	82.9		
<b>21</b>	1	1.023	1.023	1.022	1.0227	0.0359	143.7	135	
	2	1.533	1.533	1.533	1.5330	0.0408	163.2		
	3	2.442	2.442	2.441	2.4417	0.0247	98.9		
<b>28</b>	1	1.016	1.016	1.015	1.0157	0.0429	171.7	158	
	2	1.528	1.528	1.527	1.5277	0.0461	184.5		
	3	2.437	2.437	2.437	2.4370	0.0294	117.6		
<b>35</b>	1	1.01	1.009	1.009	1.0093	0.0493	197.1	180	
	2	1.521	1.521	1.52	1.5207	0.0531	212.5		
	3	2.434	2.434	2.433	2.4337	0.0327	130.9		
<b>56</b>	1	1.000	0.999	0.999	0.9993	0.0593	237.1	239	
	2	1.503	1.502	1.502	1.5023	0.0715	285.9		
	3	2.418	2.418	2.418	2.4180	0.0484	193.6		
<b>91</b>	1	0.993	0.993	0.993	0.9930	0.0656	262.4	257	
	2	1.501	1.501	1.5	1.5007	0.0731	292.5		
	3	2.413	2.412	2.412	2.4123	0.0541	216.3		
<b>120</b>	1	0.987	0.987	0.986	0.9867	0.0719	287.7	283	
	2	1.491	1.491	1.49	1.4907	0.0831	332.5		
	3	2.409	2.409	2.409	2.4090	0.0574	229.6		
<b>150</b>	1	0.985	0.985	0.984	0.9847	0.0739	295.7	290	
	2	1.489	1.488	1.488	1.4883	0.0855	341.9		
	3	2.408	2.408	2.408	2.4080	0.0584	233.6		

<b>180</b>	1	0.984	0.983	0.983	0.9833	0.0753	301.1	296
	2	1.486	1.486	1.485	1.4857	0.0881	352.5	
	3	2.408	2.408	2.408	2.4080	0.0584	233.6	
<b>210</b>	1	0.976	0.976	0.975	0.9757	0.0829	331.7	320
	2	1.482	1.482	1.481	1.4817	0.0921	368.5	
	3	2.402	2.402	2.401	2.4017	0.0647	258.9	
<b>240</b>	1	0.972	0.972	0.971	0.9717	0.0869	347.7	329
	2	1.479	1.479	1.478	1.4787	0.0951	380.5	
	3	2.402	2.402	2.401	2.4017	0.0647	258.9	
<b>270</b>	1	0.97	0.97	0.969	0.9697	0.0889	355.7	338
	2	1.475	1.475	1.474	1.4747	0.0991	396.5	
	3	2.401	2.401	2.401	2.4010	0.0654	261.6	
<b>300</b>	1	0.968	0.967	0.967	0.9673	0.0913	365.1	343
	2	1.474	1.474	1.473	1.4737	0.1001	400.5	
	3	2.401	2.4	2.4	2.4003	0.0661	264.3	
<b>330</b>	1	0.966	0.966	0.966	0.9660	0.0926	370.4	358
	2	1.472	1.472	1.472	1.4720	0.1018	407.2	
	3	2.392	2.392	2.392	2.3920	0.0744	297.6	
<b>365</b>	1	0.964	0.964	0.963	0.9637	0.0949	379.7	362
	2	1.472	1.472	1.472	1.4720	0.1018	407.2	
	3	2.392	2.392	2.392	2.3920	0.0744	297.6	

**Table B.20** Water absorption of control OPC concrete at 28 days

Time (Sec)	SQRT Time	Mass of Sample 1 (gm)	Mass of Sample 2 (gm)	Avg. Mass Change (gm)	Exposed Area (mm <sup>2</sup> )	Absorption (mm)
0	0	966.81	976.09	0	7823.86	0
60	7.74596669	967.97	977.3	1.185		0.151
300	17.3205081	969.08	978.36	2.27		0.290
600	24.4948974	970.03	979.17	3.15		0.402
1200	34.6410162	971.38	980.3	4.39		0.561
1800	42.4264069	972.26	981.21	5.285		0.675
3600	60	974.47	983.17	7.37		0.941
7200	84.8528137	977.43	985.89	10.21		1.304
10800	103.923048	979.78	988.18	12.53		1.601
14400	120	981.76	990.13	14.495		1.852
18000	134.164079	983.53	991.92	16.275		2.080
21600	146.969385	985.13	993.55	17.89		2.286

**Table B.21** Water absorption of control OPC concrete at 90 days

Time (Sec)	SQRT Time	Mass of Sample 1 (gm)	Mass of Sample 2 (gm)	Avg. Mass Change (gm)	Exposed Area (mm <sup>2</sup> )	Absorption (mm)
0	0	932.7	992.7	0	7828.95	0
60	7.74596669	933.55	993.35	0.75		0.096
300	17.3205081	934.8	993.9	1.65		0.211
600	24.4948974	935.35	994.05	2		0.256
1200	34.6410162	936.6	994.8	3		0.383
1800	42.4264069	937.15	995.15	3.45		0.441
3600	60	939.7	997	5.65		0.722
7200	84.8528137	942.8	999.75	8.575		1.096
10800	103.923048	946.2	1001.7	11.25		1.438
14400	120	948.45	1003.25	13.15		1.681
18000	134.164079	950.2	1004.7	14.75		1.885
21600	146.969385	951.75	1005.75	16.05		2.051

**Table B.22** Water absorption of 70BFS concrete at 28 days

Time (Sec)	SQRT Time	Mass of Sample 1 (gm)	Mass of Sample 2 (gm)	Avg. Mass Change (gm)	Exposed Area (mm <sup>2</sup> )	Absorption (mm)
0	0	924.9	962.2		7750.25	0
60	7.74596669	927.1	964.9	2.45		0.32
300	17.3205081	929.7	967.5	5.05		0.65
600	24.4948974	931.1	969.1	6.55		0.85
1200	34.6410162	933	972.2	9.05		1.17
1800	42.4264069	934.3	975.2	11.2		1.45
3600	60	936.8	977.6	13.65		1.76
7200	84.8528137	939.8	979.3	16		2.06
10800	103.923048	942	981.5	18.2		2.35
14400	120	943.7	982.7	19.65		2.54
18000	134.164079	945.1	983.7	20.85		2.69
21600	146.969385	946	984.7	21.8		2.81

**Table B.23** Water absorption of 70BFS concrete at 90 days

Time (Sec)	SQRT Time	Mass of Sample 1 (gm)	Mass of Sample 2 (gm)	Avg. Mass Change (gm)	Exposed Area (mm <sup>2</sup> )	Absorption (mm)
0	0	964	938.4		7805.59	0
60	7.74596669	966.1	940.3	2		0.26
300	17.3205081	968.3	942.2	4.05		0.52
600	24.4948974	969.7	943.6	5.45		0.70
1200	34.6410162	971.2	945	6.9		0.88
1800	42.4264069	972.5	946.5	8.3		1.06
3600	60	974.6	948.8	10.5		1.35
7200	84.8528137	977.5	952.1	13.6		1.74
10800	103.923048	979.5	954.8	15.95		2.04
14400	120	981.2	957.1	17.95		2.30
18000	134.164079	982.5	958.9	19.5		2.50
21600	146.969385	983.9	960.9	21.2		2.72

**Table B.24** Water absorption of 80BFS concrete at 28 days

Time (Sec)	SQRT Time	Mass of Sample 1 (gm)	Mass of Sample 2 (gm)	Avg. Mass Change (gm)	Exposed Area (mm <sup>2</sup> )	Absorption (mm)
0	0	909.6	940.8		7771.76	0
60	7.74596669	912.1	943.4	2.55		0.33
300	17.3205081	915.8	947.3	6.35		0.82
600	24.4948974	918.4	949.7	8.85		1.14
1200	34.6410162	921.2	952.4	11.6		1.49
1800	42.4264069	923.1	954	13.35		1.72
3600	60	926.6	957.3	16.75		2.16
7200	84.8528137	930.8	961.1	20.75		2.67
10800	103.923048	933.3	963.2	23.05		2.97
14400	120	935	964.7	24.65		3.17
18000	134.164079	936.1	966	25.85		3.33
21600	146.969385	937	966.9	26.75		3.44

**Table B.25** Water absorption of 80BFS concrete at 90 days

Time (Sec)	SQRT Time	Mass of Sample 1 (gm)	Mass of Sample 2 (gm)	Avg. Mass Change (gm)	Exposed Area (mm <sup>2</sup> )	Absorption (mm)
0	0	923.1	905.2		7815.16	0
60	7.74596669	925.05	907.24	1.995		0.26
300	17.3205081	927.68	910.08	4.73		0.61
600	24.4948974	929.92	912.52	7.07		0.90
1200	34.6410162	932.16	914.76	9.31		1.19
1800	42.4264069	933.4	915.8	10.45		1.34
3600	60	937.14	919.24	14.04		1.80
7200	84.8528137	942.08	923.68	18.73		2.40
10800	103.923048	944.82	926.02	21.27		2.72
14400	120	946.26	927.66	22.81		2.92
18000	134.164079	947.3	928.6	23.8		3.05
21600	146.969385	948.04	929.34	24.54		3.14

**Table B.26** Water absorption of 70BFS-FA concrete at 28 days

Time (Sec)	SQRT Time	Mass of Sample 1 (gm)	Mass of Sample 2 (gm)	Avg. Mass Change (gm)	Exposed Area (mm <sup>2</sup> )	Absorption (mm)
0	0	930.1	1005		7771.73	0
60	7.74596669	931.9	1007.5	2.15		0.28
300	17.3205081	934.5	1010.5	4.95		0.64
600	24.4948974	936.2	1012.6	6.85		0.88
1200	34.6410162	938.4	1014.7	9		1.16
1800	42.4264069	939.8	1016.3	10.5		1.35
3600	60	942.5	1019.1	13.25		1.70
7200	84.8528137	946	1022.4	16.65		2.14
10800	103.923048	948.5	1024.7	19.05		2.45
14400	120	950.3	1026.1	20.65		2.66
18000	134.164079	951.5	1027.1	21.75		2.80
21600	146.969385	952.2	1028	22.55		2.90

**Table B.27** Water absorption of 70BFS-FA concrete at 90 days

Time (Sec)	SQRT Time	Mass of Sample 1 (gm)	Mass of Sample 2 (gm)	Avg. Mass Change (gm)	Exposed Area (mm <sup>2</sup> )	Absorption (mm)
0	0	936.2	941.5		7819.62	0.00
60	7.74596669	937.6	943.2	1.55		0.20
300	17.3205081	940.2	945.4	3.95		0.51
600	24.4948974	941.2	946.4	4.95		0.63
1200	34.6410162	943.4	948.1	6.9		0.88
1800	42.4264069	944.4	948.8	7.75		0.99
3600	60	947.4	951.5	10.6		1.36
7200	84.8528137	951.1	954.9	14.15		1.81
10800	103.923048	953.2	957.1	16.3		2.08
14400	120	954.9	958.3	17.75		2.27
18000	134.164079	956.2	959.5	19		2.43
21600	146.969385	957.1	960.2	19.8		2.53

**Table B.28** Water absorption of 69BFS.1NC concrete at 28 days

Time (Sec)	SQRT Time	Mass of Sample 1 (gm)	Mass of Sample 2 (gm)	Avg. Mass Change (gm)	Exposed Area (mm <sup>2</sup> )	Absorption (mm)
0	0	966.7	875.1		7817.89	0
60	7.74596669	968.6	877.3	2.05		0.26
300	17.3205081	970.4	879.5	4.05		0.52
600	24.4948974	971.6	881.9	5.85		0.75
1200	34.6410162	973.2	882.7	7.05		0.90
1800	42.4264069	974.2	884	8.2		1.05
3600	60	976.7	886.9	10.9		1.39
7200	84.8528137	979.6	890.7	14.25		1.82
10800	103.923048	982	893.7	16.95		2.17
14400	120	983.6	895.6	18.7		2.39
18000	134.164079	984.7	897.1	20		2.56
21600	146.969385	985.7	898.1	21		2.69

**Table B.29** Water absorption of 69BFS.1NC concrete at 90 days

Time (Sec)	SQRT Time	Mass of Sample 1 (gm)	Mass of Sample 2 (gm)	Avg. Mass Change (gm)	Exposed Area (mm <sup>2</sup> )	Absorption (mm)
0	0	905.8	893.4		7756.11	0
60	7.74596669	906.9	894.6	1.15		0.15
300	17.3205081	908.2	895.9	2.45		0.32
600	24.4948974	909.9	897.1	3.9		0.50
1200	34.6410162	911.5	899.4	5.85		0.75
1800	42.4264069	912.8	901.1	7.35		0.95
3600	60	914.3	903.1	9.1		1.17
7200	84.8528137	916.1	905.3	11.1		1.43
10800	103.923048	919.3	908.5	14.3		1.84
14400	120	920.7	909.7	15.6		2.01
18000	134.164079	921.7	910.9	16.7		2.15
21600	146.969385	922.9	912	17.85		2.30

**Table B.30** Water absorption of 78BFS.2NS concrete at 28 days

Time (Sec)	SQRT Time	Mass of Sample 1 (gm)	Mass of Sample 2 (gm)	Avg. Mass Change (gm)	Exposed Area (mm <sup>2</sup> )	Absorption (mm)
0	0	944.9	874.8		7786.58	0
60	7.74596669	946.3	876.7	1.65		0.21
300	17.3205081	948.5	879.2	4		0.51
600	24.4948974	949.8	880.8	5.45		0.70
1200	34.6410162	951.5	882.6	7.2		0.92
1800	42.4264069	952.5	883.9	8.35		1.07
3600	60	954.7	886.9	10.95		1.41
7200	84.8528137	957.3	890	13.8		1.77
10800	103.923048	959.3	892	15.8		2.03
14400	120	960.7	893.5	17.25		2.22
18000	134.164079	962	894.7	18.5		2.38
21600	146.969385	963.2	895.7	19.6		2.52

**Table B.31** Water absorption of 78BFS.2NS concrete at 90 days

Time (Sec)	SQRT Time	Mass of Sample 1 (gm)	Mass of Sample 2 (gm)	Avg. Mass Change (gm)	Exposed Area (mm <sup>2</sup> )	Absorption (mm)
0	0	902.2	929.3		7771.82	0.00
60	7.74596669	904.2	930.3	1.5		0.19
300	17.3205081	906.7	932.9	4.05		0.52
600	24.4948974	907.9	934.3	5.35		0.69
1200	34.6410162	910.1	936.1	7.35		0.95
1800	42.4264069	911.2	936.9	8.3		1.07
3600	60	913.4	938.8	10.35		1.33
7200	84.8528137	916.2	940.4	12.55		1.61
10800	103.923048	918	941.5	14		1.80
14400	120	919.2	942.4	15.05		1.94
18000	134.164079	920.1	943.1	15.85		2.04
21600	146.969385	920.7	943.6	16.4		2.11

**Table B.32** Water absorption of 69BFS-FA.1NC concrete at 28 days

Time (Sec)	SQRT Time	Mass of Sample 1 (gm)	Mass of Sample 2 (gm)	Avg. Mass Change (gm)	Exposed Area (mm <sup>2</sup> )	Absorption (mm)
0	0	939.9	958.2		7838.31	0
60	7.74596669	943.1	960.3	2.65		0.34
300	17.3205081	945.7	962.3	4.95		0.63
600	24.4948974	947.3	963.5	6.35		0.81
1200	34.6410162	949.3	964.8	8		1.02
1800	42.4264069	950.5	965.9	9.15		1.17
3600	60	953.2	968	11.55		1.47
7200	84.8528137	956.8	970.7	14.7		1.88
10800	103.923048	959.4	972.5	16.9		2.16
14400	120	961.4	974.1	18.7		2.39
18000	134.164079	963	975.5	20.2		2.58
21600	146.969385	964.1	976.4	21.2		2.70



**Table B.33** Water absorption of 69BFS-FA.1NC concrete at 90 days

Time (Sec)	SQRT Time	Mass of Sample 1 (gm)	Mass of Sample 2 (gm)	Avg. Mass Change (gm)	Exposed Area (mm <sup>2</sup> )	Absorption (mm)
0	0	928.5	962.9		7785.80	0
60	7.74596669	930.3	964.3	1.6		0.21
300	17.3205081	932	966.8	3.7		0.48
600	24.4948974	933.2	967.8	4.8		0.62
1200	34.6410162	934.6	969.1	6.15		0.79
1800	42.4264069	935.7	970.2	7.25		0.93
3600	60	936.8	972.1	8.75		1.12
7200	84.8528137	939.4	974.8	11.4		1.46
10800	103.923048	942.7	976.6	13.95		1.79
14400	120	944.1	978.5	15.6		2.00
18000	134.164079	945.8	979.2	16.8		2.16
21600	146.969385	946.4	980.4	17.7		2.27

**Table B.34** Water absorption of 67BFS-FA.3NS concretes at 28 days

Time (Sec)	SQRT Time	Mass of Sample 1 (gm)	Mass of Sample 2 (gm)	Avg. Mass Change (gm)	Exposed Area (mm <sup>2</sup> )	Absorption (mm)
0	0	917.8	952.5		7786.58	0
60	7.74596669	919.2	954.1	1.5		0.19
300	17.3205081	921.1	955.9	3.35		0.43
600	24.4948974	922.5	957.1	4.65		0.60
1200	34.6410162	923.6	958.4	5.85		0.75
1800	42.4264069	925.5	960.2	7.7		0.99
3600	60	926.5	961	8.6		1.10
7200	84.8528137	928.8	963	10.75		1.38
10800	103.923048	930.2	964.2	12.05		1.55
14400	120	931.4	964.9	13		1.67
18000	134.164079	932.2	965.6	13.75		1.77
21600	146.969385	933.1	966.1	14.45		1.86

**Table B.35** Water absorption of 67BFS-FA.3NS concrete at 90 days

Time (Sec)	SQRT Time	Mass of Sample 1 (gm)	Mass of Sample 2 (gm)	Avg. Mass Change (gm)	Exposed Area (mm <sup>2</sup> )	Absorption (mm)
0	0	950.4	923.1		7758.06	0
60	7.74596669	952.1	924.1	1.35		0.17
300	17.3205081	953.9	925.8	3.1		0.40
600	24.4948974	955.3	926.7	4.25		0.55
1200	34.6410162	956.7	927.6	5.4		0.70
1800	42.4264069	957.8	928.4	6.35		0.82
3600	60	959.9	929.8	8.1		1.04
7200	84.8528137	962	930.8	9.65		1.24
10800	103.923048	963.6	931.6	10.85		1.40
14400	120	964.4	932.6	11.75		1.51
18000	134.164079	965.4	932.8	12.35		1.59
21600	146.969385	966	933.7	13.1		1.69

**Table B.36** Volume of Permeable voids of different HVS and HVS-FA concretes after 28 days

OPC											
Sample	Oven dry wt (gm)	Wt after immersion (gm)	Wt after boiling (gm)	Wt under water (gm)	Absorption after immersion	Absorption after boiling	Avg. Absorption after immersion	Bulk Density (dry)	Apparent Density	Permeable voids (%)	Avg. Permeable Voids (%)
1	960.2	1005.5	1006	595.2	4.72	4.79	4.93	2.34	2.63	11.19	11.61
2	934.9	981.8	982.5	577.4	5.02	5.09		2.31	2.62	11.75	
3	927.8	974.8	975.6	573.9	5.07	5.15		2.31	2.62	11.90	
70BFS											
Sample	Oven dry wt (gm)	Wt after immersion (gm)	Wt after boiling (gm)	Wt under water (gm)	Absorption after immersion	Absorption after boiling	Avg. Absorption after immersion	Bulk Density (dry)	Apparent Density	Permeable voids (%)	Avg. Permeable Voids (%)
1	929.5	984.6	985.8	575.70	5.93	6.06	6.06	2.27	2.63	13.73	13.95
2	903.8	960.2	961.2	561.00	6.24	6.35		2.26	2.64	14.34	
3	933.7	989.7	990.6	577.30	6.00	6.09		2.26	2.62	13.77	

80BFS											
Sample	Oven dry wt (gm)	Wt after immersion (gm)	Wt after boiling (gm)	Wt under water (gm)	Absorption after immersion	Absorption after boiling	Avg. Absorption after immersion	Bulk Density (dry)	Apparent Density	Permeable voids (%)	Avg. Permeable Voids (%)
1	932.9	988.3	989.2	582.7	5.94	6.03	6.27	2.29	2.66	13.85	14.48
2	916.6	978.8	979.5	570.5	6.79	6.86		2.24	2.65	15.38	
3	945.3	1002.7	1003.4	594.9	6.07	6.15		2.31	2.70	14.22	
70BFS-FA											
Sample	Oven dry wt (gm)	Wt after immersion (gm)	Wt after boiling (gm)	Wt under water (gm)	Absorption after immersion	Absorption after boiling	Avg. Absorption after immersion	Bulk Density (dry)	Apparent Density	Permeable voids (%)	Avg. Permeable Voids (%)
1	955.4	1005.6	1007.5	595.8	5.25	5.45	5.50	2.32	2.66	12.65	12.94
2	922.8	974.2	975.5	571	5.57	5.71		2.28	2.62	13.03	
3	929.8	982.7	983.5	574.9	5.69	5.78		2.28	2.62	13.14	

**Table B.37** Volume of Permeable voids of different HVS and HVS-FA concretes after 90 days

OPC											
Sample	Oven dry wt (gm)	Wt after immersion (gm)	Wt after boiling (gm)	Wt under water (gm)	Absorption after immersion	Absorption after boiling	Avg. Absorption after immersion	Bulk Density (dry)	Apparent Density	Permeable voids (%)	Avg. Permeable Voids (%)
1	893.44	931.44	932.61	551.90	4.25	4.38	4.50	2.35	2.62	10.29	10.79
2	901.95	944.74	945.86	555.00	4.74	4.87		2.31	2.60	11.23	
3	878.97	919.72	921.23	541.50	4.64	4.81		2.31	2.60	11.13	
4	904.67	944.12	945.27	559.60	4.36	4.49		2.35	2.62	10.53	
70BFS											
Sample	Oven dry wt (gm)	Wt after immersion (gm)	Wt after boiling (gm)	Wt under water (gm)	Absorption after immersion	Absorption after boiling	Avg. Absorption after	Bulk Density (dry)	Apparent Density	Permeable voids (%)	Avg. Permeable Voids (%)
1	979.45	1021.97	1023.87	602.20	4.34	4.54	4.21	2.32	2.60	10.53	10.06
2	923.04	961.79	962.44	560.80	4.20	4.27		2.30	2.55	9.81	
3	987.79	1029.13	1030.81	605.80	4.19	4.36		2.32	2.59	10.12	
4	949.82	988.89	989.83	580.00	4.11	4.21		2.32	2.57	9.76	

80BFS											
Sample	Oven dry wt (gm)	Wt after immersion (gm)	Wt after boiling (gm)	Wt under water (gm)	Absorption after immersion	Absorption after boiling	Avg. Absorption after immersion	Bulk Density (dry)	Apparent Density	Permeable voids (%)	Avg. Permeable Voids (%)
1	934.56	977.18	977.58	574.3	4.56	4.60	4.80	2.32	2.59	10.67	11.22
2	909.17	956.34	957.07	560.2	5.19	5.27		2.29	2.61	12.07	
3	933.78	978.41	978.67	571.2	4.78	4.81		2.29	2.58	11.02	
4	919.96	963.05	964.08	567.6	4.68	4.80		2.32	2.61	11.13	
70BFS-FA											
Sample	Oven dry wt (gm)	Wt after immersion (gm)	Wt after boiling (gm)	Wt under water (gm)	Absorption after immersion	Absorption after boiling	Avg. Absorption after immersion	Bulk Density (dry)	Apparent Density	Permeable voids (%)	Avg. Permeable Voids (%)
1	921.75	958.17	959.24	562	3.95	4.07	3.79	2.32	2.56	9.44	9.10
2	911.78	946.87	947.66	555.5	3.85	3.94		2.33	2.56	9.15	
3	927.28	962.03	962.69	564.6	3.75	3.82		2.33	2.56	8.89	
4	988.23	1024.12	1025.63	605.8	3.63	3.78		2.35	2.58	8.91	

**Table B.38** Volume of Permeable voids of different HVS and HVS-FA concretes containing nano materials after 28 days

78BFS.2NS											
Sample	Oven dry wt (gm)	Wt after immersion (gm)	Wt after boiling (gm)	Wt under water (gm)	Absorption after immersion	Absorption after boiling	Avg. Absorption after immersion	Bulk Density (dry)	Apparent Density	Permeable voids (%)	Avg. Permeable Voids (%)
1	898.8	947.10	950.00	554.60	5.37	5.70	5.25	2.27	2.61	12.95	12.50
2	921.8	967.80	969.10	573.40	4.99	5.13		2.33	2.65	11.95	
3	918.4	968.00	969.00	567.20	5.40	5.51		2.29	2.62	12.59	
69BFS.1NC											
Sample	Oven dry wt (gm)	Wt after immersion (gm)	Wt after boiling (gm)	Wt under water (gm)	Absorption after immersion	Absorption after boiling	Avg. Absorption after immersion	Bulk Density (dry)	Apparent Density	Permeable voids (%)	Avg. Permeable Voids (%)
1	937.9	979.8	980.8	579	4.47	4.57	4.89	2.33	2.61	10.68	11.38
2	887.7	933.7	933.9	546.2	5.18	5.20		2.29	2.60	11.92	
3	903.2	948.5	948.6	555.40	5.02	5.03		2.30	2.60	11.55	

67BFS-FA.3NS											
Sample	Oven dry wt (gm)	Wt after immersion (gm)	Wt after boiling (gm)	Wt under water (gm)	Absorption after immersion	Absorption after boiling	Avg. Absorption after immersion	Bulk Density (dry)	Apparent Density	Permeable voids (%)	Avg. Permeable Voids (%)
1	914.8	954.9	955.7	563.8	4.38	4.47	4.21	2.33	2.61	10.44	9.94
2	943.8	982.8	983.5	579.1	4.13	4.21		2.33	2.59	9.82	
3	908.6	945.9	946.1	554.2	4.11	4.13		2.32	2.56	9.57	
69BFS-FA.1NC											
Sample	Oven dry wt (gm)	Wt after immersion (gm)	Wt after boiling (gm)	Wt under water (gm)	Absorption after immersion	Absorption after boiling	Avg. Absorption after immersion	Bulk Density (dry)	Apparent Density	Permeable voids (%)	Avg. Permeable Voids (%)
1	918.7	957.8	958.3	559.5	4.26	4.31	4.36	2.30	2.56	9.93	10.22
2	922.7	962.7	963.3	561.5	4.34	4.40		2.30	2.55	10.10	
3	883.5	923.1	924.3	539.9	4.48	4.62		2.30	2.57	10.61	

**Table B.39** Volume of Permeable voids of different HVS and HVS-FA concretes containing nano materials after 90 day

78BFS.2NS											
Sample	Oven dry wt (gm)	Wt after immersion (gm)	Wt after boiling (gm)	Wt under water (gm)	Absorption after immersion	Absorption after boiling	Avg. Absorption after immersion	Bulk Density (dry)	Apparent Density	Permeable voids (%)	Avg. Permeable Voids (%)
1	955.2	992.40	993.30	579.50	3.89	3.99	4.29	2.31	2.54	9.21	10.07
2	974.3	1015.90	1017.00	589.60	4.27	4.38		2.28	2.53	9.99	
3	926.1	967.00	968.10	561.40	4.42	4.54		2.28	2.54	10.33	
4	928.5	971.10	972.70	561.90	4.59	4.76		2.26	2.53	10.76	
69BFS.1NC											
Sample	Oven dry wt (gm)	Wt after immersion (gm)	Wt after boiling (gm)	Wt under water (gm)	Absorption after immersion	Absorption after boiling	Avg. Absorption after	Bulk Density (dry)	Apparent Density	Permeable voids (%)	Avg. Permeable Voids (%)
1	945.6	983.3	985.4	570.8	3.99	4.21	3.99	2.28	2.52	9.60	9.44
2	929.1	966.1	966.7	557.8	3.98	4.05		2.27	2.50	9.20	
3	937.5	972.2	974.2	568.50	3.70	3.91		2.31	2.54	9.05	
4	890.7	928.8	930	534.4	4.28	4.41		2.25	2.50	9.93	

67BFS-FA.3NS											
Sample	Oven dry wt (gm)	Wt after immersion (gm)	Wt after boiling (gm)	Wt under water (gm)	Absorption after immersion	Absorption after boiling	Avg. Absorption after immersion	Bulk Density (dry)	Apparent Density	Permeable voids (%)	Avg. Permeable Voids (%)
1	942.3	977.2	978.7	574.9	3.70	3.86	3.80	2.33	2.56	9.01	9.08
2	875.4	909.7	910.5	530.8	3.92	4.01		2.31	2.54	9.24	
3	943.6	979.8	980.9	574.6	3.84	3.95		2.32	2.56	9.18	
4	899	932.8	933.6	544.6	3.76	3.85		2.31	2.54	8.89	
69BFS-FA.1NC											
Sample	Oven dry wt (gm)	Wt after immersion (gm)	Wt after boiling (gm)	Wt under water (gm)	Absorption after immersion	Absorption after boiling	Avg. Absorption after immersion	Bulk Density (dry)	Apparent Density	Permeable voids (%)	Avg. Permeable Voids (%)
1	910.5	946.5	947.1	552.1	3.95	4.02	3.75	2.31	2.54	9.27	8.95
2	949.9	985	986	576.5	3.70	3.80		2.32	2.54	8.82	
3	940.1	972.6	974.2	575.4	3.46	3.63		2.36	2.58	8.55	
4	884.8	919.4	920.2	534.9	3.91	4.00		2.30	2.53	9.19	

**Table B.40** Rapid chloride penetration data of different HVS and HVS-FA concretes with and without nano materials after 28 days

Mix ID	Sample No.	Charge Passed (Coulombs)	Average Charge Passed (Coulombs)	Standard Deviation
OPC	1	1309	1280.33	35.23
	2	1241		
	3	1291		
70BFS	1	241	238.33	12.22
	2	225		
	3	249		
80BFS	1	203	219.67	17.01
	2	237		
	3	219		
70BFA	1	249	241.33	7.51
	2	234		
	3	241		
78BFS.2NS	1	105	116.33	11.50
	2	128		
	3	116		
69BFS.1NC	1	204	204.33	14.50
	2	190		
	3	219		

67BFS-FA.3NS	1	226	225.67	2.52
	2	228		
	3	223		
69BFS-FA.1NC	1	175	146.33	25.79
	2	139		
	3	125		

**Table B.41** Rapid chloride penetration data of different HVS and HVS-FA concretes with and without nano materials after 90 days

Mix ID	Sample No.	Charge Passed (Coulombs)	Average Charge Passed (Coulombs)	Standard Deviation
OPC	1	1189	1121.67	59.16
	2	1098		
	3	1078		
70BFS	1	221	222.67	5.69
	2	229		
	3	218		
80BFS	1	187	198.00	11.00
	2	198		
	3	209		
70BFA	1	216	222.00	6.00
	2	222		
	3	228		
78BFS.2NS	1	102	106.67	4.51
	2	111		
	3	107		
69BFS.1NC	1	178	174.67	6.66
	2	167		
	3	179		
67BFS-FA.3NS	1	130	143.00	12.12
	2	154		
	3	145		
69BFS-FA.1NC	1	99	121.00	20.30
	2	139		
	3	125		

**Table B.42** Corrosion rate and concrete resistivity of different HVS and HVS-FA concretes with and without NC

<b>Average Corrosion Rate, <math>\mu\text{m}/\text{year}</math></b>					
Mix Week	OPC	70BFS	69BFS.1NC	70BFS-FA	69BFS-FA.1NC
1	3.75	11.7	12.27	31.52	6.45
2	4.3	12.2	4.90	18.83	8.97
3	6.8	16.62	6.00	49.23	8.08
4	22.07	14.82	5.85	26.32	5.53
5	83.5	17.5	8.25	32.77	8.32
6	96.85	52.33	2.95	69.23	13.17
7	108.58	22.13	12.98	82.97	24.03
8	83.72	25.8	28.22	106.53	28.98
9	58.63	21.2	20.57	66.07	16.38
10	101	23.52	19.93	100.10	21.40
11	69.48	25.83	18.43	99.00	25.87
13	75.8	46.65	25.70	78.23	33.45
14	58.17	30.02	25.48	94.73	42.25
15	159.33	101.88	30.33	83.80	22.03
16	41.92	48.17	21.75	76.22	34.52
17	95.85	59.82	23.12	45.67	30.30
18	117.67	89.37	19.00	107.10	37.35
19	54.07	40.13	26.33	53.17	18.38
20	61.5	80.5	25.67	92.50	28.67
21	66.07	120.5	33.32	112.17	32.88
22	60.35	98.67	34.83	134.17	47.27
23	60.45	97.5	34.58	116.33	46.97
24	26.33	62.1	52.10	136.00	56.33
25	57.33	57.17	26.10	159.82	107.02
26	67.37	97.23	48.00	116.83	89.17
27	106.97	93.88	17.53	118.73	29.12
29	87.05	110.57	21.03	64.65	52.40
30	64.5	56.33	22.80	49.18	42.23
31	45.58	75.68	16.97	89.57	50.85
32	35.33	93.02	38.05	84.83	63.47
33	40.68	51.63	30.28	95.82	34.88
34	49.73	60.33	35.00	74.03	41.62
35	33.02	38.17	34.18	74.35	40.92
36	15.78	38.63	13.87	76.83	59.58
37	45.67	28.48	23.98	34.13	18.18
38	50.5	69.78	55.48	43.28	48.23
39	48.68	32.05	13.43	35.83	17.55
40	74.33	63.28	43.67	69.33	48.37
41	36.93	41	21.15	84.17	44.52



42	41.97	25.08	20.22	55.45	54.17
43	68.57	32.8	24.20	46.83	38.90
44	83.5	46.48	39.60	59.45	20.33
45	75.17	28.4	5.68	44.90	39.63
46	65.43	37.6	34.73	72.67	76.90
47	82.75	70.79	16.08	102.17	23.78
48	78.93	80.07	21.60	87.17	12.73
49	51.83	30.3	50.65	71.50	57.37
50	68.33	46.7	42.63	72.50	62.80
51	94.98	26.9	25.90	72.83	32.60
52	75.5	41.98	21.52	70.83	25.22

<b>Average Concrete resistivity, ohm.m</b>					
Mix	OPC	70BFS	69BFS.1NC	70BFS-FA	69BFS-FA.1NC
Week					
1	171.5	489	283.17	430.33	418.33
2	125.17	318.33	750.50	373.33	2205.33
3	71.67	267.5	689.83	352.33	987.67
4	73.5	711.5	1055.67	744.67	1744.33
5	46.67	440.17	953.00	250.17	757.17
6	75.67	774.5	1947.00	2052.17	2585.50
7	69.33	425.17	1025.00	880.83	1116.33
8	53.33	360.67	932.83	449.50	709.33
9	47.83	786.83	740.17	539.67	1821.67
10	38.83	400.67	351.83	351.67	808.17
11	89	340	498.50	355.50	766.50
13	60	323	318.00	349.17	619.00
14	73.17	359.5	403.00	393.00	657.33
15	63.83	326.5	479.50	287.33	593.67
16	148.5	361.83	374.50	351.33	660.50
17	91.83	349.33	396.00	277.17	578.00
18	128.83	296.33	407.83	286.83	498.67
19	125.33	353.67	362.00	276.33	570.83
20	86	292.17	401.00	250.33	533.33
21	103	270.83	716.33	250.83	531.33
22	86.67	218.17	366.67	159.67	403.17
23	103.17	182.17	364.33	213.67	431.50
24	126.5	303.5	483.17	183.17	386.50
25	228	335.5	638.50	220.67	537.83
26	140.5	233.17	371.67	168.67	338.83
27	120.83	223.33	500.00	181.17	619.83
29	123.83	254.17	406.67	194.83	463.33
30	119	187.5	342.67	240.00	389.17
31	157.83	296.5	406.00	128.83	452.33

32	92.5	242.17	480.00	181.17	274.67
33	187.17	192.67	386.83	124.00	333.33
34	144.5	166.17	403.00	136.67	244.17
35	186	271.33	573.50	190.33	310.00
36	245.17	187.33	614.33	129.00	287.50
37	142.33	362	835.00	191.00	412.83
38	164	233.5	887.50	132.67	340.17
39	154.33	317.83	488.50	134.33	485.00
40	81.17	170.33	225.33	70.83	225.83
41	81.33	165.33	267.67	77.17	298.17
42	102.67	269.67	373.33	92.33	149.33
43	146.17	305.33	265.00	100.17	271.00
44	119.33	217.17	351.67	123.50	208.67
45	91.67	196.17	344.00	95.33	230.17
46	72.33	147.5	174.00	82.33	237.00
47	104	153	181.50	69.50	160.00
48	133.83	202.5	337.00	77.67	612.67
49	83.83	294.33	146.33	103.33	446.33
50	48.5	158.17	148.17	66.50	107.50
51	39.5	127.83	266.17	75.17	128.50
52	54.83	132.5	169.50	74.00	133.50

**Table B.43** Corrosion rate and concrete resistivity of different HVS and HVS-FA concretes with and without NS

<b>Average Corrosion Rate, <math>\mu\text{m}/\text{year}</math></b>					
Mix	OPC	80BFS	78BFS.2NS	70BFS-FA	67BFS-FA.3NS
Week					
1	3.75	48.93	20.33	31.52	11.68
2	4.3	44.03	17.77	18.83	13.33
3	6.8	63.92	18.20	49.23	21.98
4	22.07	48.53	16.97	26.32	12.18
5	83.5	101.35	28.63	32.77	17.30
6	96.85	134.72	15.63	69.23	14.02
7	108.58	116.33	65.55	82.97	47.25
8	83.72	64.58	64.12	106.53	36.27
9	58.63	73.73	29.78	66.07	47.40
10	101	75.20	53.83	100.10	43.93
11	69.48	121.62	48.25	99.00	40.03
13	75.8	107.17	45.00	78.23	28.13
14	58.17	84.33	57.85	94.73	50.50
15	159.33	57.00	44.97	83.80	24.03
16	41.92	104.70	29.23	76.22	33.42
17	95.85	99.67	69.63	45.67	29.52

18	117.67	116.53	96.95	107.10	36.02
19	54.07	84.83	50.92	53.17	25.02
20	61.5	105.67	73.13	92.50	33.37
21	66.07	110.50	100.90	112.17	49.40
22	60.35	149.00	60.17	134.17	65.00
23	60.45	134.00	59.83	116.33	56.13
24	26.33	55.95	29.35	136.00	35.27
25	57.33	158.38	123.73	159.82	69.70
26	67.37	108.85	95.60	116.83	65.25
27	106.97	83.00	58.23	118.73	35.95
29	87.05	110.80	58.52	64.65	42.02
30	64.5	60.33	45.13	49.18	42.88
31	45.58	139.50	29.33	89.57	69.52
32	35.33	137.33	84.17	84.83	59.17
33	40.68	106.50	66.25	95.82	57.62
34	49.73	95.67	60.42	74.03	44.00
35	33.02	93.33	74.50	74.35	52.03
36	15.78	85.98	72.43	76.83	52.25
37	45.67	68.33	24.17	34.13	11.87
38	50.5	104.33	62.83	43.28	97.33
39	48.68	87.00	49.68	35.83	17.92
40	74.33	87.45	69.50	69.33	67.43
41	36.93	62.50	103.33	84.17	22.98
42	41.97	108.17	109.67	55.45	39.88
43	68.57	83.83	51.33	46.83	42.50
44	83.5	106.50	93.17	59.45	64.33
45	75.17	78.50	46.00	44.90	41.73
46	65.43	88.83	74.83	72.67	77.90
47	82.75	98.33	38.00	102.17	56.88
48	78.93	122.50	82.57	87.17	48.27
49	51.83	108.45	70.42	71.50	67.33
50	68.33	75.97	98.02	72.50	67.42
51	94.98	103.67	62.83	72.83	55.67
52	75.5	86.17	65.67	70.83	40.73

<b>Average Concrete resistivity, ohm.m</b>					
Mix	OPC	80BFS	78BFS.2NS	70BFS-FA	67BFS-FA.3NS
Week					
1	171.5	250.00	245.33	430.33	342.83
2	125.17	539.33	661.83	373.33	597.50
3	71.67	451.33	1081.33	352.33	441.67
4	73.5	791.67	1413.33	744.67	821.00
5	46.67	627.67	843.50	250.17	366.67
6	75.67	833.17	545.00	2052.17	1913.17

7	69.33	624.67	833.00	880.83	690.33
8	53.33	411.00	635.33	449.50	519.67
9	47.83	916.67	1389.00	539.67	993.67
10	38.83	253.50	407.33	351.67	771.67
11	89	231.17	359.00	355.50	792.67
13	60	181.33	385.17	349.17	494.17
14	73.17	234.33	409.17	393.00	562.00
15	63.83	190.33	403.17	287.33	624.83
16	148.5	257.00	469.50	351.33	763.33
17	91.83	191.50	390.17	277.17	618.50
18	128.83	250.33	369.83	286.83	576.67
19	125.33	187.17	294.83	276.33	535.33
20	86	180.33	236.50	250.33	575.33
21	103	192.17	345.33	250.83	532.00
22	86.67	92.00	238.67	159.67	291.33
23	103.17	100.50	293.83	213.67	278.17
24	126.5	236.00	401.50	183.17	544.33
25	228	202.33	399.33	220.67	323.33
26	140.5	163.00	306.33	168.67	227.67
27	120.83	178.17	288.17	181.17	313.33
29	123.83	133.00	309.33	194.83	367.50
30	119	104.00	330.67	240.00	248.33
31	157.83	122.17	162.50	128.83	252.50
32	92.5	104.33	161.33	181.17	242.50
33	187.17	100.67	155.67	124.00	222.67
34	144.5	114.83	159.67	136.67	162.83
35	186	102.83	158.83	190.33	291.83
36	245.17	130.67	217.83	129.00	283.33
37	142.33	75.50	186.50	191.00	348.50
38	164	100.83	111.67	132.67	116.17
39	154.33	82.00	170.83	134.33	224.00
40	81.17	51.33	66.50	70.83	151.67
41	81.33	70.00	68.33	77.17	165.33
42	102.67	69.83	67.50	92.33	110.50
43	146.17	45.00	83.33	100.17	105.17
44	119.33	45.00	98.83	123.50	116.83
45	91.67	58.67	75.00	95.33	142.33
46	72.33	44.50	77.17	82.33	79.33
47	104	52.33	78.83	69.50	102.50
48	133.83	44.67	94.50	77.67	131.00
49	83.83	61.33	94.83	103.33	104.33
50	48.5	44.50	74.00	66.50	85.83
51	39.5	29.17	72.17	75.17	100.50
52	54.83	40.50	59.83	74.00	111.83

**Table B.44** Average chloride content of different HVS and HVS-FA concretes with and without NC

Mix	OPC	70BFS	69BFS.1NC	70BFS-FA	69BFS-FA.1NC
Depth, mm					
1	0.116118	0.092796	0.098725	0.093227	0.106931
3	0.09544	0.081732	0.075045	0.089547	0.084539
5	0.072266	0.067828	0.061883	0.082424	0.069541
7	0.066456	0.052161	0.050495	0.07494	0.055786
9	0.059346	0.047334	0.041789	0.064169	0.042492
12	0.047603	0.036744	0.035724	0.055367	0.032849
16	0.041802	0.033322	0.026547	0.046196	0.028343

**Table B.45** Average chloride content of different HVS and HVS-FA concretes with and without NS

Mix	OPC	80BFS	78BFS.2NS	70BFS-FA	67BFS-FA.3NS
Depth, mm					
1	0.116118	0.087243	0.08676	0.093227	0.093965
3	0.09543985	0.0774705	0.07517	0.089547	0.08283
5	0.072266	0.0708075	0.070595	0.082424	0.067815
7	0.066456	0.0670235	0.06447	0.07494	0.0535685
9	0.0593455	0.0588445	0.051166	0.064169	0.0398675
12	0.047603	0.0512955	0.0441425	0.0553665	0.03181275
16	0.041802	0.0441285	0.03981185	0.0461955	0.0262497

## APPENDIX C: Attribution of Research Outputs

### **Journal Articles: 1-2 & 4-6**

1. Shaikh, F.U.A. and A. Hosan, Effect of nano silica on compressive strength and microstructures of high volume blast furnace slag and high volume blast furnace slag-fly ash blended pastes. *Sustainable Materials and Technologies*, 2019. **20**: p. e00111.
2. Hosan, A. and F.U.A. Shaikh, Influence of nano-CaCO<sub>3</sub> addition on the compressive strength and microstructure of high volume slag and high volume slag-fly ash blended pastes. *Journal of Building Engineering*, 2020. **27**: p. 100929.
4. Hosan, A. and F.U.A. Shaikh, Influence of nano silica on compressive strength, durability, and microstructure of high-volume slag and high-volume slag-fly ash blended concretes. *Structural Concrete*. <https://doi.org/10.1002/suco.202000251>.
5. Hosan, A. and F.U.A. Shaikh, Compressive strength development and durability properties of high volume slag and slag-fly ash blended concretes containing nano-CaCO<sub>3</sub>. *Journal of Materials Research and Technology*. (Under review)
6. Hosan, A. and F.U.A. Shaikh, Effect of nano materials on chloride induced corrosion and service life of high volume slag and high volume slag-fly ash blended concretes. *Materials and Structures*, 2020. (Under review).

### **Authors and full affiliations:**

Md Anwar Hosan, PhD student, School of Civil and Mechanical Engineering, Curtin University, WA

Dr Faiz Uddin Ahmed Shaikh, Associate Professor, School of Civil and Mechanical Engineering, Curtin University, WA

Co-author attribution: Associate Professor Faiz Uddin Ahmed Shaikh,

Article Number	Literature review	Experimental design/idea	Data collection	Data analysis	Discussion	Paper writing
1		√			√	√
2		√			√	√
4		√			√	√
5		√			√	√
6		√			√	√

I acknowledge that these represent my contribution to the above research output.

(Signature)

**Journal Article: 3**

Hosan, A., et al., Nano- and micro-scale characterization of interfacial transition zone (ITZ) of high volume slag and slag-fly ash blended concretes containing nano SiO<sub>2</sub> and nano CaCO<sub>3</sub>. *Construction and Building Materials*, 2020: p. 121311.

**Authors and full affiliations:**

Md Anwar Hosan, PhD student, School of Civil and Mechanical Engineering, Curtin University, WA

Dr Faiz Uddin Ahmed Shaikh, Associate Professor, School of Civil and Mechanical Engineering, Curtin University, WA

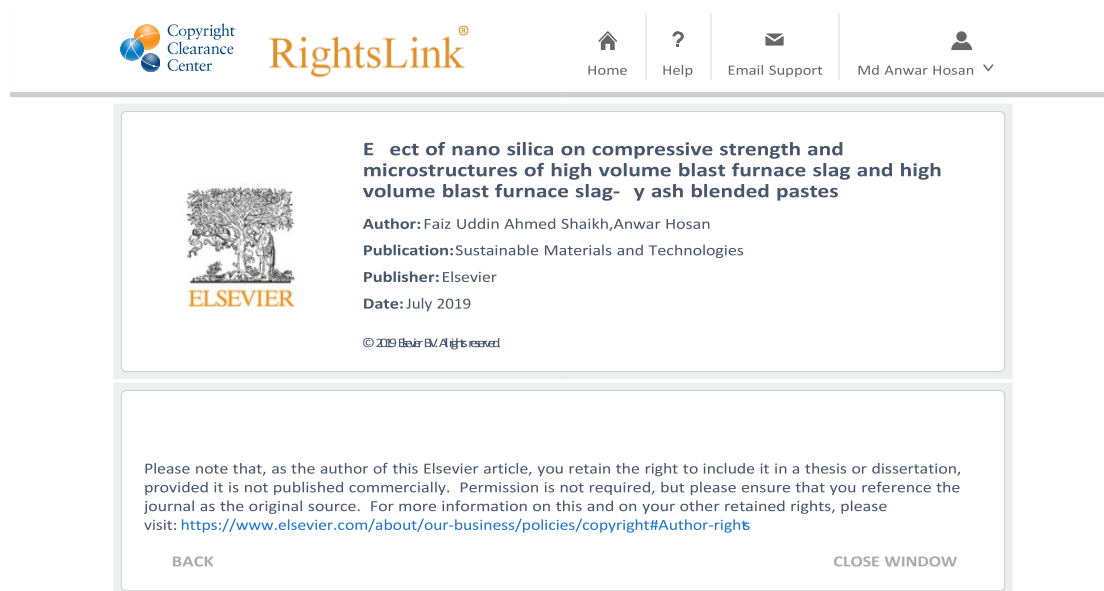
Dr Prabir Sarker, Associate Professor, School of Civil and Mechanical Engineering, Curtin University, WA

Dr Farhad Aslani, Senior Lecturer, School of Civil, Environmental and Mining Engineering, University of Western Australia, WA

Name of Co-author	Literature review	Experimental design/idea	Data collection	Data analysis	Discussion	Paper writing
Faiz Uddin Ahmed Shaikh		√		√	√	√
I acknowledge that these represent my contribution to the above research output.  (Signature)						
Prabir Sarker					√	√
I acknowledge that these represent my contribution to the above research output.  (Signature)						
Farhad Aslani					√	√
I acknowledge that these represent my contribution to the above research output.  (Signature)						


## APPENDIX D: Copyright Permission

1. Shaikh, F.U.A. and A. Hosan, Effect of nano silica on compressive strength and microstructures of high volume blast furnace slag and high volume blast furnace slag-fly ash blended pastes. *Sustainable Materials and Technologies*, 2019. **20**: p. e00111.



The screenshot shows the Elsevier RightsLink interface. At the top, there is a navigation bar with the Copyright Clearance Center logo, the RightsLink logo, and a user profile for Md Anwar Hosan. Below the navigation bar, the article title is displayed: "Effect of nano silica on compressive strength and microstructures of high volume blast furnace slag and high volume blast furnace slag-fly ash blended pastes". The author is listed as Faiz Uddin Ahmed Shaikh, Anwar Hosan. The publication is "Sustainable Materials and Technologies" and the publisher is Elsevier. The date is July 2019. A copyright notice states "© 2019 Elsevier B.V. All rights reserved." Below the article information, there is a disclaimer: "Please note that, as the author of this Elsevier article, you retain the right to include it in a thesis or dissertation, provided it is not published commercially. Permission is not required, but please ensure that you reference the journal as the original source. For more information on this and on your other retained rights, please visit: <https://www.elsevier.com/about/our-business/policies/copyright#Author-rights>". At the bottom of the disclaimer, there are buttons for "BACK" and "CLOSE WINDOW".

2. Hosan, A. and F.U.A. Shaikh, Influence of nano-CaCO<sub>3</sub> addition on the compressive strength and microstructure of high volume slag and high volume slag-fly ash blended pastes. *Journal of Building Engineering*, 2020. **27**: p. 100929.



The screenshot shows the Elsevier RightsLink interface. At the top, there is a navigation bar with the Copyright Clearance Center logo, the RightsLink logo, and a user profile for Md Anwar Hosan. Below the navigation bar, the article title is displayed: "Influence of nano-CaCO<sub>3</sub> addition on the compressive strength and microstructure of high volume slag and high volume slag-fly ash blended pastes". The author is listed as Anwar Hosan, Faiz Uddin Ahmed Shaikh. The publication is "Journal of Building Engineering" and the publisher is Elsevier. The date is January 2020. A copyright notice states "© 2019 Elsevier B.V. All rights reserved." Below the article information, there is a disclaimer: "Please note that, as the author of this Elsevier article, you retain the right to include it in a thesis or dissertation, provided it is not published commercially. Permission is not required, but please ensure that you reference the journal as the original source. For more information on this and on your other retained rights, please visit: <https://www.elsevier.com/about/our-business/policies/copyright#Author-rights>". At the bottom of the disclaimer, there are buttons for "BACK" and "CLOSE WINDOW".



3. Hosan, A., et al., Nano- and micro-scale characterisation of interfacial transition zone (ITZ) of high volume slag and slag-fly ash blended concretes containing nano SiO<sub>2</sub> and nano CaCO<sub>3</sub>. *Construction and Building Materials*, 2020: p. 121311.

HomeHelpEmail SupportMd Anwar Hosan ▾

---



**Nano- and micro-scale characterisation of interfacial transition zone (ITZ) of high volume slag and slag-fly ash blended concretes containing nano SiO<sub>2</sub> and nano CaCO<sub>3</sub>**

**Author:** Anwar Hosan, Faiz Uddin Ahmed Shaikh, Prabir Sarker, Farhad Aslani

**Publication:** Construction and Building Materials

**Publisher:** Elsevier

**Date:** Available online 3 November 2020

© 2020 Elsevier Ltd. All rights reserved.

Please note that, as the author of this Elsevier article, you retain the right to include it in a thesis or dissertation, provided it is not published commercially. Permission is not required, but please ensure that you reference the journal as the original source. For more information on this and on your other retained rights, please visit: <https://www.elsevier.com/about/our-business/policies/copyright#Author-rights>

BACK

CLOSE WINDOW

4. Hosan, A. and F.U.A. Shaikh, Influence of nano silica on compressive strength, durability, and microstructure of high-volume slag and high-volume slag–fly ash blended concretes. *Structural Concrete*. <https://doi.org/10.1002/suco.202000251>.

12/17/2020

RightsLink Printable License

**JOHN WILEY AND SONS LICENSE  
TERMS AND CONDITIONS**

Dec 17, 2020

---

This Agreement between Shaikh Ahmed ("You") and John Wiley and Sons ("John Wiley and Sons") consists of your license details and the terms and conditions provided by John Wiley and Sons and Copyright Clearance Center.

License Number 4971220241069

License date Dec 17, 2020

Licensed Content Publisher John Wiley and Sons

Licensed Content Publication Structural Concrete

Licensed Content Title Influence of nano silica on compressive strength, durability, and microstructure of high-volume slag and high-volume slag–fly ash blended concretes

Licensed Content Author Anwar Hosan, Faiz Uddin Ahmed Shaikh

Licensed Content Date Sep 21, 2020

Licensed Content Volume 0

Licensed Content Issue 0

Licensed Content Pages 14

5. Hosan, A. and F.U.A. Shaikh, Compressive strength development and durability properties of high volume slag and slag-fly ash blended concretes containing nano-CaCO<sub>3</sub>. *Journal of Materials Research and Technology*. <https://doi.org/10.1016/j.jmrt.2021.01.001>

3/24/2021

Rightslink® by Copyright Clearance Center



RightsLink®



Home

Help

Email Support

Md Anwar Hosan ▾



**Compressive strength development and durability properties of high volume slag and slag-fly ash blended concretes containing nano-CaCO<sub>3</sub>**

**Author:** Anwar Hosan, Faiz Uddin Ahmed Shaikh

**Publication:** Journal of Materials Research and Technology

**Publisher:** Elsevier

**Date:** January–February 2021

© 2021 The Author(s). Published by Elsevier B.V.

**Journal Author Rights**

Please note that, as the author of this Elsevier article, you retain the right to include it in a thesis or dissertation, provided it is not published commercially. Permission is not required, but please ensure that you reference the journal as the original source. For more information on this and on your other retained rights, please visit: <https://www.elsevier.com/about/our-business/policies/copyright#Author-rights>

BACK

CLOSE WINDOW

© 2021 Copyright - All Rights Reserved | [Copyright Clearance Center, Inc.](#) | [Privacy statement](#) | [Terms and Conditions](#)  
Comments? We would like to hear from you. E-mail us at [customer-care@copyright.com](mailto:customer-care@copyright.com)